Modelling, Control, and Handling Quality Analysis of the Flying-V

Master of Science Thesis

Simon van Overeem

Delft University of Technology

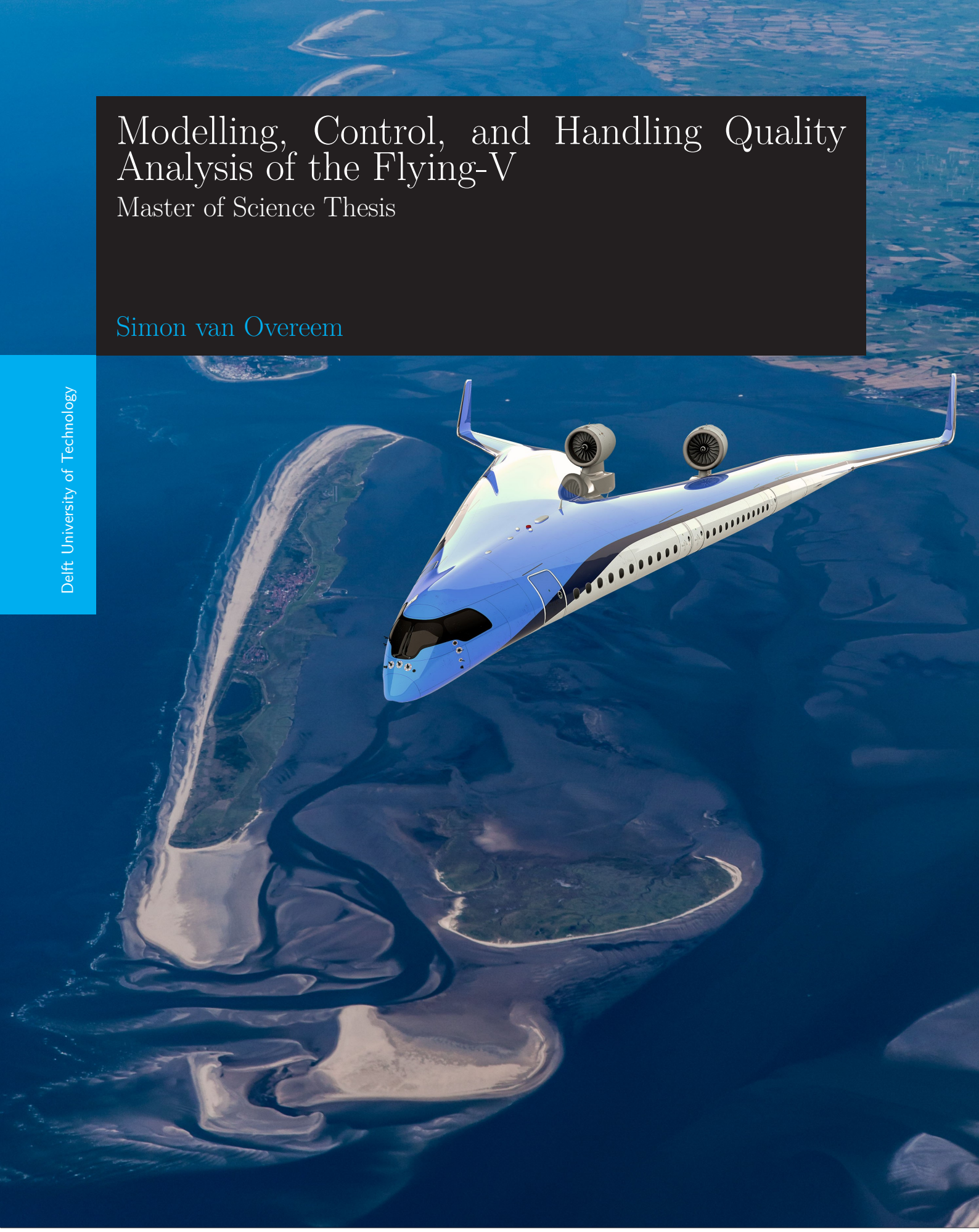

TU Delft Delft University of Technology

Challenge the future

Modelling, Control, and Handling Quality Analysis of the Flying-V

Master of Science Thesis

by

Simon van Overeem

to obtain the degree of Master of Science
at the Delft University of Technology,
to be defended publicly on Wednesday January 12, 2022 at 14:00.

Student Number:	4442423	
Project Duration:	November 16, 2020 - January 12, 2022	
Thesis Committee:	Dr. Guido de Croon	TU Delft, chair
	Dr. Ir. Erik-Jan van Kampen	TU Delft, supervisor
	Dr. X. (Sherry) Wang	TU Delft, supervisor
	Dr. Ir. Roelof Vos	TU Delft, examiner

Cover page adopted from TU Delft Flying-V website.[1]

[1] https://www.tudelft.nl/lr/flying-v

TU Delft Delft University of Technology

Preface

After more than a year of full-time research, this work wraps up my time at TU Delft. My study period at the faculty of Aerospace Engineering has been truly an incredible experience that I will remember for the rest of my life.

First of all, I would like to express my gratitude to my thesis supervisors Dr. ir. Erik-Jan van Kampen and Dr. Xuerui (Sherry) Wang for their continuous support and regular meetings during my thesis. I would also like to thank my parents and brother for their unconditional support during my studies. Besides that, because this thesis was performed during the Covid-19 pandemic, I have mainly worked from home. Therefore, I would also like to thank my roommates and girlfriend for giving me some additional motivation from time to time. Finally, I want to thank my study friends for the great time we have had during our studies.

Simon van Overeem
Den Haag, January 2022

Abstract

Over the last five decades, the majority of commercial aircraft consisted of the traditional tube-and-wing configuration. This traditional configuration is approaching a fuel efficiency asymptote. Besides that, with the increasing number of passengers and cargo transported by air every year, and environmental impact as an important factor in aircraft design, there is a necessity for a solution that is able to boost aircraft efficiency. Currently, the faculty of Aerospace Engineering at TU Delft is working on a promising aircraft configuration, namely the Flying-V. This is a specific type of flying wing that is tailless, V-shaped, and consists of two cylindrical pressurised cabins located in the leading edge of the wing. Wind tunnel experiments show that the aircraft is longitudinally statically stable up to an angle of attack of 20°, after that pitch break occurs. Besides that, research performed on the aerodynamic coefficients obtained using the Vortex Lattice Method and results from the maiden flight test of a scale model of the aircraft conclude that the Dutch roll mode is unstable. Therefore, this research defines a set of key stability and handling quality requirements based on civil aviation authorities combined with military standards for cruise- and approach conditions. These key requirements are consequently assessed with a simulation model of the aircraft using aerodynamic coefficients obtained from the Vortex Lattice Method and wind tunnel experiments. In an attempt to make the key stability and handling quality characteristics of the TU Delft Flying-V adhere to the defined requirements, this thesis aims to contribute to this research field by designing a nonlinear Incremental Nonlinear Dynamic Inversion (INDI) flight control system that is applied to the simulation model of the aircraft. Finally, the performance of the aircraft using this flight control system is assessed and proposals for aerodynamic design changes and control layout design changes are given.

Contents

List of Figures

List of Tables

1

Introduction

This chapter introduces the Master of Science thesis report: "Modelling, Control, and Handling Quality Analysis of the Flying-V". This thesis is written at the Control & Simulation department of the faculty of Aerospace Engineering at Delft University of Technology. The introduction presents a motivation for the research as presented in section 1.1. Besides that, the research objectives and research questions are presented in section 1.2. Furthermore, section 1.3 elaborates on the scope of this research. Finally, section 1.4 presents the outline of the report.

1.1. Research Motivation

Over the last five decades, the majority of commercial aircraft consisted of the traditional tube-and-wing configuration. This conventional design has obtained significant efficiency gains of 100% over the years [Martinez-Val et al., 2010]. However, the Airbus A350 and Boeing 787 represent an asymptote regarding aircraft efficiency. Besides that, considerable growth in the number of passengers and cargo transported by air is predicted [Faggiano, F. et al., 2017]. Furthermore, since the reduction of aircraft noise and environmental impact become more important factors in aircraft design, there is a necessity for a solution that is able to boost the efficiency for the increasing number of passengers and cargo, while reducing noise and environmental impact [Martinez-Val, R., 2007]. One course of action to overcome the existing challenges in aviation is the design of an innovative aircraft configuration. One of the most promising aircraft configurations for future operations is the flying wing in all its different settings such as the Blended-Wing-Body (BWB), C-Wing, and Tail-less aircraft. Flying wings have the potential to significantly increase efficiency, resulting in less pollution, and reduce noise levels during landing and take-off [Martinez-Val, R., 2007].

The Flying-V is a specific type of flying wing that is tailless, V-shaped, and consists of two cylindrical pressurised cabins located in the leading edge of the wing. The aircraft is shown in Figure 1.1 [Flying-V Website, 2020]. The design of a Flying-V aircraft concept contains several benefits compared to conventional tube-and-wing aircraft. The main advantage of this type of aircraft is the reduction of wetted area and frictional drag since one structure integrates the structural function of accommodating payload and aerodynamic function of providing lift [Okonkwo and Smith, 2016]. Furthermore, this type of aircraft suffers less from interference drag due to the smooth shape of the configuration. Additionally, the reduced wetted area per unit of useful volume results in a reduction of the zero-lift drag [Zhenli et al., 2019]. Therefore, this type of aircraft can achieve a higher lift-to-drag ratio compared to conventional aircraft and hence has a reduced fuel burn and takeoff weight [Benad, J., 2015, Liebeck, 2004]. Research on the aerodynamic advantages of the Flying-V presents that the aircraft can have aerodynamic efficiency gains ranging from 10% to 25% compared to conventional tube-and-wing aircraft of similar size and weight while reducing the noise level due to the location of the engines on top of the wing [Benad, J., 2015, Faggiano, F. et al., 2017].

Currently, the main design challenges of the Flying-V are centred on two different aspects. The first design challenge entails modelling and assessment of the stability and handling qualities of this

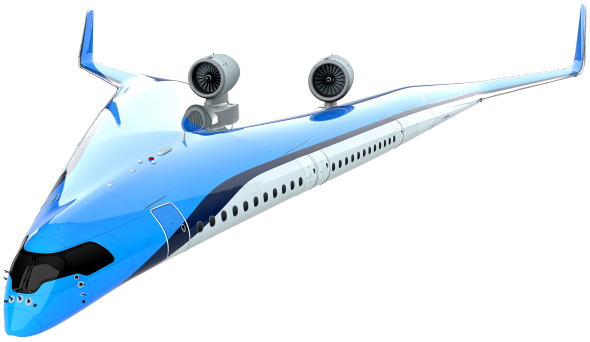

Figure 1.1: The Flying-V Aircraft [Flying-V Website, 2020].

novel aircraft design for certification and qualification purposes. The second design challenge entails the design of a flight control system that can be used to improve the stability and handling qualities, and allows the Flying-V to follow a specific tracking task.

1.1.1. Stability & Handling Qualities

Previous research is conducted on the stability and handling qualities of the full-size aircraft by designing a six degrees-of-freedom flight dynamic toolbox using aerodynamic coefficients obtained from the Vortex Lattice Method and inertia estimations obtained using a lumped mass method. A stability and handling quality assessment is performed using military standards and requirements obtained from the European Aviation Safety Agency (EASA). The main limitation of previous research is the use of linearised aerodynamic data, meaning that the aerodynamic model is not able to accurately describe the corners of the flight envelope and that deviation from the linearisation points results in inaccurate estimations. Previous research concludes that the Dutch roll mode is unstable and that the lateral-directional controllability of the aircraft is limited in the case of One Engine Inoperative (OEI) at low speeds [Cappuyns, T., 2019]. The unstable Dutch roll behaviour obtained from previous research was confirmed during a flight test with a small scale model of the aircraft[1] and is also in coherence with previous research on the undesirable lateral-directional behaviour of flying wings [Ammar, S. et al., 2017, Humphreys-Jennings, C. et al., 2020]. In preparation for this flight test, Wind Tunnel Experiments have been performed on a half-span small scale model of the Flying-V. These experiments focus on the longitudinal flight characteristics of the Flying-V small scale model for which the centre of gravity range is determined (1.32 m - 1.40 m from the nose of the aircraft) to guarantee trimmability of the aircraft at approach speeds and high angles of attack. Besides that, former research reveals that the Flying-V shows longitudinal unstable behaviour in case the angle of attack is larger than 20° [Palermo, M. et al., 2020, Viet, R., 2019]. This longitudinal unstable behaviour is also captured in an aerodynamic model obtained from Wind Tunnel Experiments to perform aerodynamic model identification of the Flying-V half-span small scale model. Due to limitations of the experiments, the aerodynamic model obtained from these experiments only considers the longitudinal static aerodynamic coefficients [Garcia, A.R., 2019].

Regarding stability and handling qualities, this thesis consists of two contributions to research related to the Flying-V aircraft. First of all, this study integrates the aerodynamic models that can be obtained from the Vortex Lattice Method and Wind Tunnel Experiments into a rigid six degrees-of-freedom flight dynamic simulation model that is able to capture the undesired behaviour of the Flying-V obtained from previous research, such as the unstable Dutch roll mode and longitudinal unstable behaviour. Secondly, this research aims to assess the most essential stability and handling qualities of the Flying-V during cruise and approach conditions for several centre of gravity locations using the flight dynamic simulation model.

[1] https://www.tudelft.nl/en/2020/tu-delft/successful-maiden-flight-for-the-tu-delft-flying-v

1.1.2. Flight Control System Design

The previous research discussed in section 1.1.1 shows that the Flying-V contains several stability issues. After analysing the stability and handling qualities of the Flying-V, it is possible to give a quantifiable measure to the extend up to which the aircraft adheres to the stability and handling qualities defined by military standards [Anonymous, 1980]. After that it is possible to design a Flight Control System that can be used to improve the stability and handling qualities. Besides that, the Flight Control System can be used to make the Flying-V follow a specific tracking task.

A couple of decades ago, almost all Flight Control Systems (FCS) for aircraft were designed using classical (linear) control techniques [Balas, G.J., 2003]. Even though the systems involved with aircraft control are nonlinear, it is still possible to apply a linear controller to this system by making the key assumption that the linear controller is only applied to a small range within the complete flight envelope [Slotine, J.E. et al., 1991]. This requires the design of multiple linear controllers to cover the complete flight envelope and construct a gain schedule by interpolating the gains with respect to the flight condition. This procedure is very time consuming, expensive, and is not flexible regarding design changes [Adams, R.J. et al., 1993]. Furthermore, during the design of a linear controller, it is necessary to assume that the parameters of the aircraft model are well known, which is not always the case. In case a linear controller is based on inaccurate model parameters, it may exhibit performance degradation or instability [Slotine, J.E. et al., 1991].

To overcome the shortcomings of linear controllers, several nonlinear control methods have emerged over the past years. One of the most popular of these control methodologies is known as Nonlinear Dynamic Inversion (NDI). The theory of NDI originates from research performed by Brockett and Krener on the extension of linear control studies to the nonlinear case [Brockett, R.W., 1978, Krener, A.J., 1999]. NDI makes use of an accurate model of the system to entirely or partially cancel nonlinearities using feedback and exact state transformations. These transformations transform the nonlinear system dynamics into a linear system over the desired region of interest. Consequently, it is possible to apply conventional linear control techniques to achieve the desired closed-loop dynamics [Acquatella, P. et al., 2012].

The disadvantage of NDI-based control laws is the necessity for accurate knowledge of the nonlinear system dynamics [Acquatella, P. et al., 2012]. This requirement is almost impossible to meet in reality due to model simplifications, computational errors, and external disturbances [Wang, X. et al., 2019]. In an attempt to increase the robustness of the NDI controller, the controller is combined with linear robust control techniques such as structural singular value (μ) analysis [Reiner, J. et al., 1996] and $\mathcal{H}_\infty$ synthesis [Spillman, M. et al., 1996]. However, these control techniques often treat known nonlinear time-varying dynamics as uncertainties. This results in control systems that are either marginal or very conservative in performance and stability robustness [Hodel, A. et al., 2008].

Incremental Nonlinear Dynamic Inversion (INDI) is a sensor-based control method. Therefore, this control method requires less model information and can therefore improve the system robustness against model uncertainties [Wang, X. et al., 2019]. This is especially useful for the control system design of the Flying-V. As the simulation model that will be designed consists of several assumptions such as rigid body and zero wind. Besides that, aerodynamic coefficients contain a certain degree of uncertainty, which are consequently introduced into the simulation model as well.

Regarding flight control system design, this thesis consists of two contributions to research related to the Flying-V aircraft. First of all, this thesis designs an Incremental Nonlinear Dynamic Inversion (INDI) controller to improve the stability and handling qualities of the Flying-V. Secondly, the robustness of the controller is assessed by analysing the effects of aerodynamic uncertainty on the tracking error of the aircraft aiming to follow a reference trajectory.

1.2. Research Question

From section 1.1 it is possible to conclude that the Flying-V offers a solution to some of the main existing challenges in aviation. However, the aircraft also comes with its own challenges regarding stability and handling qualities. In an attempt to make the key stability and handling quality characteristics of the Flying-V adhere to the regulations set by certification authorities, this thesis aims to contribute to this research field by designing a flight control system that can be applied to a simulation model of the

aircraft. For this purpose, the following research question is formulated:

> How can the Flying-V adhere to the key stability and handling qualities, set by certification authorities, by developing a flight control system applied to a six degree-of-freedom rigid simulation model of the aircraft?

To answer this research question, several sub-questions have been formulated to give the research a clearly defined direction and to divide the research work into several work-packages. Therefore, the following sub-questions are formulated:

1. What are the stability and handling qualities of the Flying-V?
   - How can the stability and handling qualities of the Flying-V be assessed?
   - What are the stability and handling qualities characteristics of the Flying-V aircraft?
2. How can a simulation model of the Flying-V aircraft be obtained?
   - What are the specific elements of a simulation model of the Flying-V?
   - What uncertainty sources are present in the simulation model of the Flying-V?
   - What is the validity of the simulation model of the Flying-V?
3. How do the stability and handling qualities of the Flying-V aircraft change after applying a flight control system?
   - What types of flight control systems are applicable to the aircraft and can contribute to improved stability and handling qualities of the aircraft?
   - How does the performance of the aircraft change using a flight control system?
4. What kind of design changes can further improve the stability and handling qualities of the aircraft?
   - How can additional requirements on the flight control system design improve the stability and handling qualities?
   - How can additional requirements on the aircraft aerodynamic design and control surface layout design improve the stability and handling qualities?

The main contribution of the research focuses on the development of a flight control system that can be applied to a simulation model of the Flying-V aircraft to improve the key stability and handling qualities of the aircraft. This also presents the novelty of this research, as mainly a longitudinal static stability analysis has been performed on the aircraft and no flight control system implementation and analysis has been done yet. It follows that one sub-objective of this research is to develop a six degree-of-freedom simulation model of the rigid aircraft that can be used to analyse the static and dynamic, longitudinal and lateral-directional stability and handling qualities. The second sub-objective consists of the assessment of the key stability and handling qualities performance of the simulation model with respect to the requirements set by certification authorities. The third sub-objective is to develop a flight control system that can be applied to the simulation model. The final sub-objective is to evaluate the performance of the flight control system, iterate where necessary, and deliver any additional aerodynamic design and control surface layout design requirements that may originate from a control point of view. This final sub-objective increases the feasibility of the development of a full-scale Flying-V aircraft in the future.

1.3. Research Scope

Analysing the different research questions in section 1.2 it is possible to distinguish three different fundamental components of this research, namely the stability and handling qualities, the Flying-V simulation model, and the flight control system. Additionally, these three components are connected

through an iterative process as can be observed in fig. 1.2. In this figure, it is possible to observe that after performing simulations using the aircraft simulation model, it is possible to assess the stability and handling qualities of the aircraft. The conclusions obtained from this assessment lead to requirements for the flight controller that can be applied to the simulation model. Consequently, it is possible to run a new set of simulations and assess the stability and handling qualities. In case the set of key stability and handling quality requirements are met, it is possible to assess additional stability and handling quality requirements in future research to even further improve the performance of the aircraft. To define the scope of the research, the work that is done on the stability and handling qualities, aircraft simulation model, and flight control system, is discussed in section 1.3.1, section 1.3.2, and section 1.3.3 respectively.

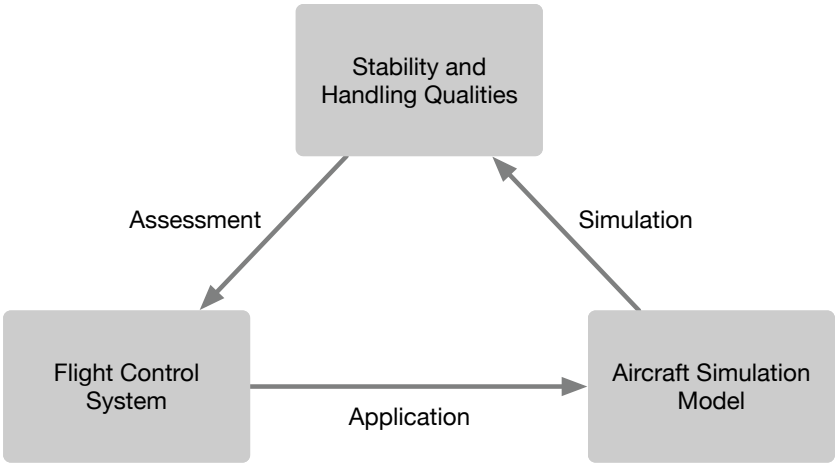

Figure 1.2: Iteration cycle of fundamental components

1.3.1. Stability and Handling Qualities Scope

The stability and handling qualities aspect of the research is used to define a metric that can be used to assess the performance of the aircraft. Within the scope of this research, it is not possible to assess all stability and handling quality requirements that can be obtained from aviation certification authorities for the complete flight envelope of the aircraft. Therefore it is decided to base the stability and handling quality analysis on the eigenmodes of the Flying-V and the Control Anticipation Parameter. Namely, from previous research it is obtained that the Dutch roll mode is unstable. Besides that, the longitudinal unstable behaviour may deteriorate longitudinal handling qualities. Therefore it is decided to analyse the Control Anticipation Parameter.

1.3.2. Aircraft Simulation Model Scope

The aircraft simulation model aspect of the research is used to design a platform that can be used for the assessment of the stability and handling quality requirements and consequently for the application of the flight control system. To scope this part of the research, it is decided to focus on the design of a simulation model that involves the full-scale aircraft, while assuming a rigid body, meaning that no aeroelastic effects are taken into account. Besides that, no system identification will be performed to obtain the aerodynamic forces and moments of the aircraft. Instead, the coefficients obtained in previous research using the Vortex Lattice Method and Wind Tunnel Experiments are combined to design an aerodynamic model that is able to capture the undesired behaviour obtained from previous research. Finally, the simulation model will not include any pilot-in-the-loop simulation components, as this research is focused on the control system design.

1.3.3. Flight Control System Scope

The flight control system design aspect of this research is used to improve the behaviour of the aircraft such that the aircraft can adhere to the key stability and handling quality requirements. Many control

techniques can be applied to the Flying-V. However, the focus of this research is on the application of a nonlinear controller to the system. It is consequently possible to assess whether the controlled aircraft is able to adhere to the stability and handling qualities. Besides that, the robustness of the controller to uncertainty is assessed.

1.4. Thesis Layout

In part I, two scientific papers are presented that discuss the research performed during this thesis. The first scientific paper elaborates on the design of the flight dynamic simulation model, and the stability and handling quality analysis. The second scientific paper discusses the application of the flight control system to the Flying-V. After that, part II presents the literature study of this thesis. Furthermore, part III elaborates on additional derivations and results. Finally, conclusions and recommendations are given in chapter 8.

I

Scientific Papers

Modelling and Handling Quality Assessment of the Flying-V Aircraft

Simon van Overeem*
Delft University of Technology, The Netherlands, 2629 HS Delft

Considerable growth in the number of passengers and cargo transported by air is predicted. Besides that, aircraft noise and climate impact become increasingly important factors in aircraft design. These existing challenges in aviation boost interest in the design of innovative aircraft configurations. One of these configurations is a V-shaped flying wing named the Flying-V. This work aims at developing a flight dynamic simulation model of the Flying-V based on aerodynamic data obtained from the Vortex Lattice Method and wind tunnel experiments. The simulation model is used to assess the stability and handling qualities for certification and qualification purposes. Prior work has shown an assessment of the stability and handling qualities based on a linear aerodynamic model. However, to capture the longitudinal undesired behaviour of the Flying-V it is necessary to use a nonlinear aerodynamic model. Therefore, this paper illustrates how a flight dynamic simulation model, based on combined aerodynamic data from the Vortex Lattice Method and wind tunnel experiments, is used for certification and qualification purposes. The stability and handling qualities are assessed by analysing the aircraft dynamic modes and analysing nonlinear system handling qualities based on linearisation for both the cruise and approach condition.

I. Introduction

Over the last five decades, the majority of commercial aircraft consisted of the traditional tube-and-wing configuration. This conventional design has obtained significant efficiency gains of 100% over the years [1]. However, the Airbus A350 and Boeing 787 represent an asymptote regarding aircraft efficiency. Besides that, considerable growth in the number of passengers and cargo transported by air is predicted [2]. Furthermore, since the reduction of aircraft noise and environmental impact become more important factors in aircraft design, there is a necessity for a solution that is able to boost the efficiency for the increasing number of passengers and cargo, while reducing noise and environmental impact [3]. One course of action to overcome the existing challenges in aviation is the design of an innovative aircraft configuration. One of the most promising aircraft configurations for future operations is the flying wing in all its different settings such as the Blended-Wing-Body (BWB), C-Wing, and Tail-less aircraft. Flying wings have the potential to significantly increase efficiency, resulting in less pollution, and reduce noise levels during landing and take-off [3].

The Flying-V is a specific type of flying wing that is tailless, V-shaped, and consists of two cylindrical pressurised cabins located in the leading edge of the wing. The design of a Flying-V aircraft concept contains several benefits compared to conventional tube-and-wing aircraft. The main advantage of this type of aircraft is the reduction of wetted area and frictional drag since one structure integrates the structural function of accommodating payload and aerodynamic function of providing lift [4]. Furthermore, this type of aircraft suffers less from interference drag due to the smooth shape of the configuration. Additionally, the reduced wetted area per unit of useful volume results in a reduction of the zero-lift drag [5]. Therefore, this type of aircraft can achieve a higher lift-to-drag ratio compared to conventional aircraft and hence has a reduced fuel burn and takeoff weight [6, 7]. Research on the aerodynamic advantages of the Flying-V presents that the aircraft can have aerodynamic efficiency gains ranging from 10% to 25% compared to conventional tube-and-wing aircraft of similar size and weight while reducing the noise level due to the location of the engines on top of the wing [2, 7]. The preliminary design of the Flying-V is shown in Fig. 1.

Currently, the two main Flying-V design challenges are centred on modelling and assessment of the stability and handling qualities of this novel aircraft design for certification and qualification purposes. Previous research is conducted on the stability and handling qualities of the full-size aircraft by designing a six degrees-of-freedom flight dynamic toolbox using aerodynamic coefficients obtained from the Vortex Lattice Method and inertia estimations obtained using a lumped mass method. A stability and handling quality assessment is performed using military standards and requirements obtained from the European Aviation Safety Agency (EASA). The main limitation of previous research

*Graduate Student, Faculty of Aerospace Engineering at Delft University of Technology, s.vanovereem@student.tudelft.nl

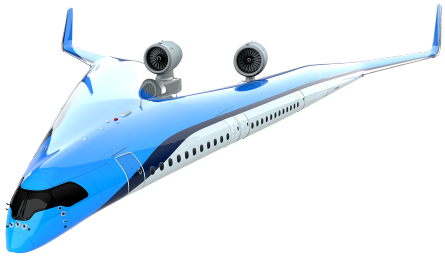

Fig. 1 The Flying-V aircraft.*

is the use of linearised aerodynamic data, meaning that the aerodynamic model is not able to accurately describe the corners of the flight envelope and that deviation from the linearisation points results in inaccurate estimations. Previous research concludes that the Dutch roll mode is unstable and that the lateral-directional controllability of the aircraft is limited in the case of One Engine Inoperative (OEI) at low speeds [8]. The unstable Dutch roll behaviour obtained from previous research was confirmed during a flight test with a small scale model of the aircraft* and is also in coherence with previous research on the undesirable lateral-directional behaviour of flying wings [9, 10]. In preparation for this flight test, wind tunnel experiments have been performed on a half-span small scale model of the Flying-V. These experiments focus on the longitudinal flight characteristics of the Flying-V small scale model for which the centre of gravity range is determined (1.32 m - 1.40 m from the nose of the aircraft) to guarantee trimmability of the aircraft at approach speeds and high angles of attack. Besides that, the Flying-V shows longitudinal unstable behaviour in case the angle of attack is larger than 20° [11, 12]. This longitudinal unstable behaviour is also captured in an aerodynamic model obtained from wind tunnel experiments to perform aerodynamic model identification of the Flying-V half-span small scale model. Due to limitations of the experiments, the aerodynamic model obtained from these experiments only considers the longitudinal static aerodynamic coefficients [13].

This study consists of two contributions to research related to the Flying-V aircraft. First of all, this study integrates the aerodynamic models that are obtained from the Vortex Lattice Method and wind tunnel experiments into a rigid six degrees-of-freedom flight dynamic simulation model that is able to capture the undesired behaviour of the Flying-V revealed by previous research, such as the unstable Dutch roll mode and longitudinal unstable behaviour. Secondly, this research aims to assess the most essential stability and handling qualities of the Flying-V during cruise and approach conditions for several centre of gravity locations using the flight dynamic simulation model.

The rest of this paper is structured as follows. Section II elaborates on the essential stability and handling qualities assessed using the flight dynamic simulation model. Besides that, the flight dynamic simulation model design is discussed including combining the aerodynamic models obtained from the Vortex Lattice Method and wind tunnel experiments. In section III, the results of the assessment of the essential stability and handling qualities of the Flying-V are shown. Finally, conclusions are discussed in section IV and recommendations for further research are given in section V.

II. Methodology

In this section, the methodology to assess the stability and handling qualities of the Flying-V is discussed in section II.A. After that, section II.B elaborates on the design of the flight dynamic simulation model.

A. Stability and Handling Quality Assessment

In this section, the key stability and handling quality requirements for certification and qualification purposes are discussed. In section II.A.1, the trimmability of the Flying-V is discussed. After that, section II.A.2 elaborates on the responses of the eigenmodes. Finally, section II.A.3 discusses the handling qualities.

*https://www.tudelft.nl/en/2020/tu-delft/successful-maiden-flight-for-the-tu-delft-flying-v

1. Trim

The requirements for aircraft trim are obtained from EASA CS25.161 (Trim) [14]. Trim requirements can be subdivided into longitudinal and lateral-directional requirements. These requirements are discussed below for the cruise phase and approach phase.

Longitudinal Trim

During the approach phase, the aircraft must have the ability to be trimmed within the normal range of approach speeds with power settings corresponding to a glidepath angle of 3° for the most unfavourable combination of centre of gravity position and weight approved for landing [14].

During the cruise phase, the aircraft must have the ability to be trimmed at any airspeed ranging between 1.3 times the stall speed and the maximum operating limit speed with the landing gear and wing-flaps retracted [14].

Based on the availability of aerodynamic data, the longitudinal trimmability of the aircraft is assessed for Ma = 0.2 during approach and Ma = 0.85 during cruise. Furthermore, the most forward and aft centre of gravity locations are considered (29.372 m and 31.714 m from the nose respectively). It is expected that the longitudinal trimmability of the aircraft is mainly demanding for low airspeeds [15]. Due to limited research on the aerodynamic effects of extending the landing gear of the Flying-V, an approach phase with landing gear retracted is considered.

Lateral-Directional Trim

The aircraft must have the ability to maintain lateral-directional trim with the most adverse lateral displacement of the centre of gravity at any airspeed ranging between 1.3 times the stall speed and the maximum operating limit speed [14]. During the analysis of the Flying-V, it is assumed that the centre of gravity is located in the plane of symmetry of the aircraft. Therefore, lateral-directional trim is not considered for this research.

2. Modes Response

Because civil aviation authorities do not provide quantifiable requirements for the longitudinal and lateral-directional modes of an aircraft, it is decided to use military (quantifiable) requirements to assess the dynamic modes of the Flying-V [16]. To use these military standards, it is necessary to identify the aircraft class and prevailing flight conditions. According to these standards, aircraft can be divided into several classes namely: Class I (small light aircraft), Class II (medium weight, low to medium manoeuvrability aircraft), Class III (large, heavy, low to medium manoeuvrability aircraft), and Class IV (high manoeuvrability aircraft) [17, 18]. Besides that, flight phases can be divided into several categories. Category A consists of non-terminal flight phases that require rapid manoeuvring, precision tracking, or precise flight path control such as ground attacks, aerobatics, and close formation flight. Category B consists of non-terminal flight phases that require gradual manoeuvring, less precise tracking and accurate flight path control such as climb, cruise, and loiter. Category C consists of terminal flight phases that require gradual manoeuvring and precision flight path control such as takeoff, approach, and landing [17, 18]. Based on these classes and flight phases the Flying-V can be considered a Class III aircraft with prevailing flight phases in Category B and Category C.

To identify the ability of the aircraft to complete the mission for which it is designed, three levels of flying qualities can be defined that indicate the severity of the pilot workload during the execution of a specific flight phase. In case the flying qualities of an aircraft are rated Level 1, the flying qualities are adequate for the mission flight phase. Furthermore, Level 2 flying qualities correspond to adequacy for the mission flight phase, but with an increase in pilot workload and, or, degradation in mission effectiveness. Finally, Level 3 flying qualities describe degraded flying qualities, but such that the aircraft can be controlled with inadequate mission effectiveness and high pilot workload [17, 18]. To assess the modes it is first necessary to linearise the equations of motion such that specific parameters such as the damping ratio, natural frequency, and characteristic time constants can be determined. These parameters are used to compare the characteristics of the Flying-V with military standards. Consequently, it is possible to give a quantifiable measure for the flying qualities of the aircraft. The specific modes are discussed below.

Short-Period Mode

The short-period motion is an oscillating pitch rate response. This motion is fast and is the transient response of an elevator input. Therefore, to have a sufficient tracking of a reference signal, the short-period must be well damped to reach a steady state pitch condition quickly [19]. To assess the short period mode, it is necessary to determine the damping ratio of this mode and compare it with military standards [17, 18].

Phugoid Mode

The phugoid is a slow pitch angle response. During a phugoid motion, the aircraft follows a sinusoidal path, while interchanging potential energy with kinetic energy [19]. In general, the phugoid dynamics are considered acceptable in case the mode is stable and the damping ratio adheres to the limits set by military standards [17, 18].

Dutch Roll Mode

The Dutch roll is a yawing and simultaneously rolling motion that originates from a sideslip deviation that induces a yawing motion. Aerodynamic coupling results in the rolling of the aircraft. The vertical tail surface of a conventional aircraft has the largest contribution in dampening the motion [19]. The Dutch roll mode can be considered as a short-period mode in the lateral direction and has therefore an important influence on lateral-directional handling qualities. It is therefore assessed using the damping ratio and frequency of the mode [17, 18].

Aperiodic Roll Mode

The aperiodic roll mode represents the quick response of the roll rate to a roll control input. In case the roll control input is removed, the roll rate should return to zero [19]. The aperiodic roll mode can be assessed by determining the characteristic time constant (T_r) and comparing it with military standards [17, 18].

Spiral Mode

The spiral mode is a slowly developing turning flight when the aircraft spirals down. In case this motion is stable, the aircraft returns to wings level flight after a roll input (either a roll disturbance or pilot input) is applied to the aircraft. In case this motion is unstable, the roll angle slowly increases [19]. In case the spiral mode is stable, it is always acceptable irrespective of its time constant. Because this mode generally involves slow dynamic behaviour, it is not a very critical mode, unless the mode is very unstable. For this reason, the minimum acceptable degrees of instability are quantified in terms of the spiral time constant (T_s), which is a function of the time to double bank angle (T_2) during an uncontrolled departure from straight and level flight [17, 18].

3. Handling Qualities

The handling qualities of an aircraft are considered as a description of the adequacy of the short term dynamic response to controls during the execution of a flight task [17]. The main focus of the handling qualities discussed in this research involves quantitative handling qualities as these quantitative methods do not require pilot-in-the-loop experiments. However, it needs to be noted that potential future pilot-in-the-loop experiments are taken into account while analysing the handling qualities. The handling quality assessed for this research consist of the Control Anticipation Parameter (CAP). This is a measure of manoeuvrability of the aircraft. In case the CAP is too high, the aircraft's response is faster than would be expected by the pilot resulting in understeering. On the other hand, in case the CAP is too low, the aircraft's response is sluggish, which results in oversteering [8].

B. Flight Dynamic Simulation Model Design

In this section, the simulation model design is discussed. In section II.B.1 the frames of reference used during the simulation are discussed. After that, section II.B.2 elaborates on the dynamic and kinematic equations. Furthermore, in section II.B.3 the aerodynamic model is discussed. Also, section II.B.4 shows the methodology for verification and validation of the simulation model. Finally, section II.B.5 elaborates on the assumptions and limitations of the simulation model.

1. Frames of Reference

Before the stability and handling qualities of the aircraft can be analysed, it is necessary to define two coordinate frames. First of all, it is necessary to define the vehicle-carried normal Earth reference frame ($\mathcal{E}$-frame). This frame has the $X_{\mathcal{E}}$-axis directed to the north and the $Y_{\mathcal{E}}$-axis directed 90 degrees to the right of the $X_{\mathcal{E}}$-axis (to the east). In case it is assumed that the Earth is spherical, the $Z_{\mathcal{E}}$-axis is pointed in the direction of the centre of the Earth. However, for this analysis it is assumed that the Earth is a flat plate. Therefore, the $Z_{\mathcal{E}}$-axis points downwards, and the vehicle-carried normal Earth reference frame is an inertial frame. Besides that, the body fixed reference frame can be defined (the $\mathcal{B}$-frame). For this frame, the $X_{\mathcal{B}}$-axis is located in the plane of symmetry and points forward. The $Z_{\mathcal{B}}$-axis is also located in the symmetry plane and points downwards. Finally, the $Y_{\mathcal{B}}$-axis completes the right-handed coordinate system

and points perpendicular to both the $X_{\mathcal{B}}$-axis and the $Z_{\mathcal{B}}$-axis. The two frames can be observed in Fig. 2.

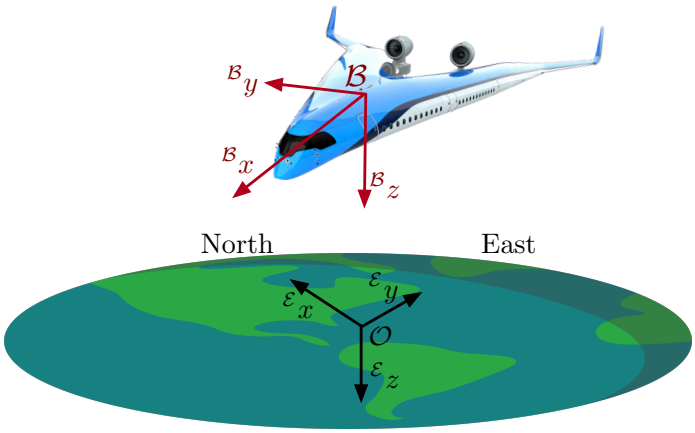

Fig. 2 Frames of reference.

2. Dynamics and Kinematics

After derivation of the equations of motion it is possible to obtain the dynamic equations as shown in Eq. (1). The states of this system consist of the velocity in body-frame components (${}^{\mathcal{B}}\boldsymbol{v}$) and the angular velocity of the body-frame with respect to the Earth-frame in body-frame components (${}^{\mathcal{B}}\boldsymbol{\omega}_{\mathcal{B}/\mathcal{E}}$). Besides that, the angular velocity matrix and inertia matrix are shown (${}^{\mathcal{B}}\Omega_{\mathcal{B}/\mathcal{E}}$ and J respectively). Finally, the force and moments consist of the forces due to gravity (${}^{\mathcal{B}}\boldsymbol{F}_{\text{grav}}$), aerodynamic forces (${}^{\mathcal{B}}\boldsymbol{F}_{\text{aero}}$), the thrust force (${}^{\mathcal{B}}\boldsymbol{F}_{\text{thrust}}$), aerodynamic moments (${}^{\mathcal{B}}\boldsymbol{M}_{\text{aero}}$), moments due to thrust (${}^{\mathcal{B}}\boldsymbol{M}_{\text{thrust}}$), and moments due to a shift in the centre of gravity (${}^{\mathcal{B}}\boldsymbol{M}_{\text{cg}}$). The moments induced by the centre of gravity shift can be obtained using Eq. (2) [20]. This equation shows that the moment due to a centre of gravity shift can be obtained by first subtracting the centre of gravity position ($\boldsymbol{p}_{\text{cg}}$) from the reference position around which the aerodynamic forces and moments are calculated ($\boldsymbol{p}_{\text{ref}}$). Consequently, a cross product with the aerodynamic forces results in the moment induced by the centre of gravity shift.

$$\begin{bmatrix} {}^{\mathcal{B}}\dot{\boldsymbol{v}} \\ {}^{\mathcal{B}}\dot{\boldsymbol{\omega}}_{\mathcal{B}/\mathcal{E}} \end{bmatrix} = \begin{bmatrix} -{}^{\mathcal{B}}\Omega_{\mathcal{B}/\mathcal{E}} & 0 \\ 0 & -J^{-1}{}^{\mathcal{B}}\Omega_{\mathcal{B}/\mathcal{E}}J \end{bmatrix} \begin{bmatrix} {}^{\mathcal{B}}\boldsymbol{v} \\ {}^{\mathcal{B}}\boldsymbol{\omega}_{\mathcal{B}/\mathcal{E}} \end{bmatrix} + \begin{bmatrix} \frac{{}^{\mathcal{B}}\boldsymbol{F}_{\text{grav}}}{m} + \frac{{}^{\mathcal{B}}\boldsymbol{F}_{\text{aero}}}{m} + \frac{{}^{\mathcal{B}}\boldsymbol{F}_{\text{thrust}}}{m} \\ J^{-1}\left({}^{\mathcal{B}}\boldsymbol{M}_{\text{aero}} + {}^{\mathcal{B}}\boldsymbol{M}_{\text{thrust}} + {}^{\mathcal{B}}\boldsymbol{M}_{\text{cg}}\right) \end{bmatrix} \tag{1}$$

$${}^{\mathcal{B}}\boldsymbol{M}_{\text{cg}} = (\boldsymbol{p}_{\text{ref}} - \boldsymbol{p}_{\text{cg}}) \times {}^{\mathcal{B}}\boldsymbol{F}_{\text{aero}} \tag{2}$$

It is consequently also possible to derive the kinematic equations as can be observed in Eq. (3). In this equation, the roll, pitch, and yaw angles are shown (ϕ, θ, and ψ respectively) together with the roll, pitch, and yaw rates (p, q, and r respectively).

$$\begin{bmatrix} \dot{\phi} \\ \dot{\theta} \\ \dot{\psi} \end{bmatrix} = \begin{bmatrix} 1 & \sin\phi\tan\theta & \cos\phi\tan\theta \\ 0 & \cos\phi & -\sin\phi \\ 0 & \frac{\sin\phi}{\cos\theta} & \frac{\cos\phi}{\cos\theta} \end{bmatrix} \begin{bmatrix} p \\ q \\ r \end{bmatrix}_{\mathcal{B}} \tag{3}$$

To estimate the components of the inertia matrix, the lumped mass method is used. The general idea of this method is to consider the power plant and landing gear as point masses. The rest of the aircraft is divided into lumped masses placed at half chord locations. The lumped masses are divided over point masses equally spaced from the root of the wing to the tip. The spacing is considered to be good enough such that the moment of inertia around each specific point mass is negligible. In the inertia matrix, the coefficients J_{xy} and J_{yz} can be set to zero as the Flying-V is assumed to be a mass-symmetrical vehicle [8].

3. Aerodynamic Model

The undesired behaviour of the Flying-V consists of unstable Dutch roll motion and longitudinal instability for angles of attack larger than 20°. The unstable Dutch roll is obtained from a stability and handling quality analysis using aerodynamic coefficients obtained from the Vortex Lattice Method [8]. Besides that, the longitudinal unstable behaviour of the aircraft was observed during wind tunnel experiments [11, 12] and captured in an aerodynamic model obtained from these wind tunnel experiments [13]. Therefore, this section elaborates on the aerodynamic models obtained from the Vortex Lattice Method and wind tunnel experiments. After that, the methodology used to combine these aerodynamic models into a single aerodynamic model that is able to capture both the unstable Dutch roll and longitudinal instability for angles of attack larger than 20° is discussed.

Vortex Lattice Method

To define the aerodynamic coefficients using the Vortex Lattice Method, the aerodynamic geometry of the aircraft defined in previous work [2] is translated into a panel model that can be used for the aerodynamic estimations. Using this panel method it is possible to compute the lift and induced drag of the aircraft while omitting the thickness and viscosity. The output consists of the aerodynamic coefficients for specific Mach numbers [8]. The aerodynamic model is validated using a comparative analysis of the lift coefficient and pitching moment coefficient obtained from the Vortex Lattice Method with wind tunnel tests performed by [11].

The aerodynamic model obtained from the Vortex Lattice Method also consists of several limitations. First of all, the aerodynamic data is linear, meaning that this model is not able to accurately display the corners of the flight envelope due to nonlinearities. This also means that deviation from the linearisation points results in inaccurate estimations. The model is considered valid for angles of attack ranging between -5° up to 15°. Besides that, frictional drag [21], ground effect, compressibility, and aeroelasticity effects are not taken into account. Also, the atmospheric model does not include wind, turbulence, nor wind shear. Finally, the landing gear and fairing of the Flying-V are not modelled [8]. Due to these limitations, the aerodynamic model obtained from the Vortex Lattice Method cannot be used to model the unstable longitudinal behaviour of the Flying-V. Besides that, the dynamic behaviour of the aircraft may change compared to a real flight due to the components not included into the aerodynamic model.

Wind Tunnel Experiments

To obtain an aerodynamic model from wind tunnel experiments, a 1/22 scaled half-span model of the Flying-V is used (shown in Fig. 3). During these experiments, several independent variables (the angle of attack, wind speed, and elevon deflections) are altered to determine the aerodynamic coefficients (dependent variables). During the identification process, the independent variables are assumed to be not contaminated with noise, while the dependent variables are contaminated with uniformly distributed noise. The measurements are considered accurate enough for angles of attack ranging from -10° up to 30° and airspeeds ranging between 12m/s up to 30m/s. Due to high uncertainties, the lateral force coefficient (C_Y) could not be identified [13].

For the wind tunnel model, it is necessary to take into account that only the half-span clean wing configuration is modelled without landing gear, fairing, nor engines. This results in limited fidelity of this model with respect to the full aircraft configuration. Furthermore, no winglets including rudders are added to the wind tunnel model. For this reason, using this model limits the user to accurately simulate the lateral-directional dynamics of the aircraft. Besides that, outside the fidelity bounds, no measurements were taken during the construction of the aerodynamic model meaning that extrapolating outside this convex hull results in new, unmodeled effects that affect the validity of the model [13]. Due to these limitations, the aerodynamic model obtained from wind tunnel experiments cannot be used to model the lateral-directional dynamics of the Flying-V (including the unstable Dutch roll mode). Besides that, the use of a scaled model that does not include landing gear, fairing, engines, nor winglets affects the dynamic behaviour of the small-scale Flying-V compared to the full-scale aircraft.

Aerodynamic Model Discrepancies

The aerodynamic models obtained from the Vortex Lattice Method (VLM) and wind tunnel experiments (WTE) are different on several aspects that need to be mentioned before the aerodynamic models can be combined into a single aerodynamic model that is able to capture the undesired behaviour obtained from previous research. First of all, the VLM model is a linear model, whereas the WTE model is a nonlinear model. Besides that, the VLM model is based on the full-scale aircraft, whereas the WTE model is based on a small-scale aircraft. Also, the control surface layout of the full-scale aircraft is different from the small-scale aircraft. Namely, the full-scale aircraft consists of an inboard elevon (used for pitch control), an outboard elevon (used for pitch and roll control), and a rudder integrated into the winglet

(used for yaw control). The small-scale aircraft consists of three elevons that can be used for both pitch and roll control, and no winglets nor rudders. The geometrical differences are visible in Fig. 3.

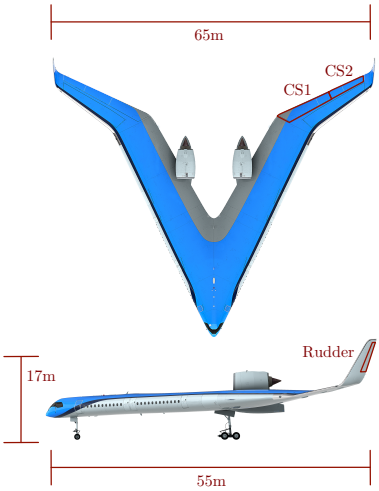

(a) Full-scale Flying-V used for Vortex Lattice Method (landing gear not included for analysis).*

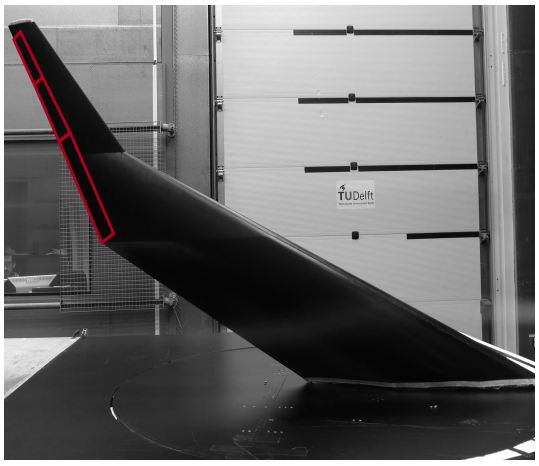

(b) Small-scale Flying-V used for wind tunnel experiments [12].

Fig. 3 Flying-V aircraft used for aerodynamic models.

Aerodynamic Model Design

To design a flight dynamic simulation model that is able to capture the unstable Dutch roll and unstable longitudinal behaviour of the Flying-V it is necessary to combine the aerodynamic model obtained from the Vortex Lattice Method with the aerodynamic model obtained from the wind tunnel experiments. To combine the VLM aerodynamic model and the WTE aerodynamic model, the VLM model is used as the baseline model. This means that the Flying-V model used for this analysis consists of an inboard elevon, outboard elevon, and rudder integrated into the winglet (shown in Fig. 3). After that, elements from the WTE model are implemented into the VLM model, such that the combined model is able to capture the unstable Dutch roll and longitudinal instability obtained from previous research [8, 11, 12]. Therefore, this research combines the coefficients that are relevant for modelling the longitudinal instability. These are the longitudinal force coefficient (C_X), directional force coefficient (C_Z), and pitch moment coefficient (C_M). The remaining coefficients consist of the lateral force coefficient (C_Y), roll moment coefficient (C_L), and yaw moment coefficient (C_N). For these coefficients, the coefficients obtained from the VLM model are used. Besides that, the aerodynamic coefficients are determined for the approach- and cruise condition (Ma = 0.2 and Ma = 0.85 respectively) for angles of attack ranging between $-5°$ and $30°$. Additionally, due to the significant difference in control surface layout between the two models, deflections are kept equal to zero. Essentially, this means that the aerodynamic model combination entails combining the contribution of the angle of attack to the coefficients: C_X, C_Z, and C_M.

Both aerodynamic models operate in different airspeed regimes due to the difference in aircraft size. Therefore it is necessary to scale the airspeed according to Dynamic or Froude scaling. This scaling method can be used for scaled aircraft models that are capable of simulating the relative motions of a larger full-scale aircraft [22]. After scaling the airspeed, it is possible to compare the aerodynamic coefficients for different angles of attack as shown in Fig. 4.

This figure shows that the aerodynamic coefficients of the VLM and WTE are of the same magnitude, but that the VLM model is not able to capture the longitudinal instability that becomes apparent at 20 degrees angle of attack. Therefore, the WTE curves are vertically translated to match the VLM curve at $\alpha = 15°$. The discontinuity that originates from this operation is resolved by interpolating the datapoints using the shape-preserving piecewise cubic interpolating polynomial function "pchip". This function makes use of splines, where each spline is a third-degree polynomial with specified derivatives at the interpolation points[†]. This results in a combined aerodynamic model, where the coefficients for angles of attack ranging between -5° up to 15° are obtained from the VLM model and the coefficients for angles of attack ranging between 15° up to 30° are obtained from the WTE model. Based on the aerodynamic model

[†] https://www.mathworks.com/help/matlab/ref/pchip.html#bvjbz1m-2

obtained from the combination of the VLM model and WTE model, it is concluded that the aerodynamic model does not contain any zero-lift drag (C_{D_0}), decreasing the fidelity of the model. Due to limited analysis on the zero-lift drag of a full scale model of the Flying-V it is decided to use the zero-lift drag from the Airbus A350-900 (the aircraft used as a reference for the design of the Flying-V) and add this to the aerodynamic model of the Flying-V. This results into a zero-lift drag of 0.027 during cruise and 0.057 during approach [23]. The combined aerodynamic model is shown in Fig. 5, where it is visible that the longitudinal unstable behaviour is captured by the combined aerodynamic model.

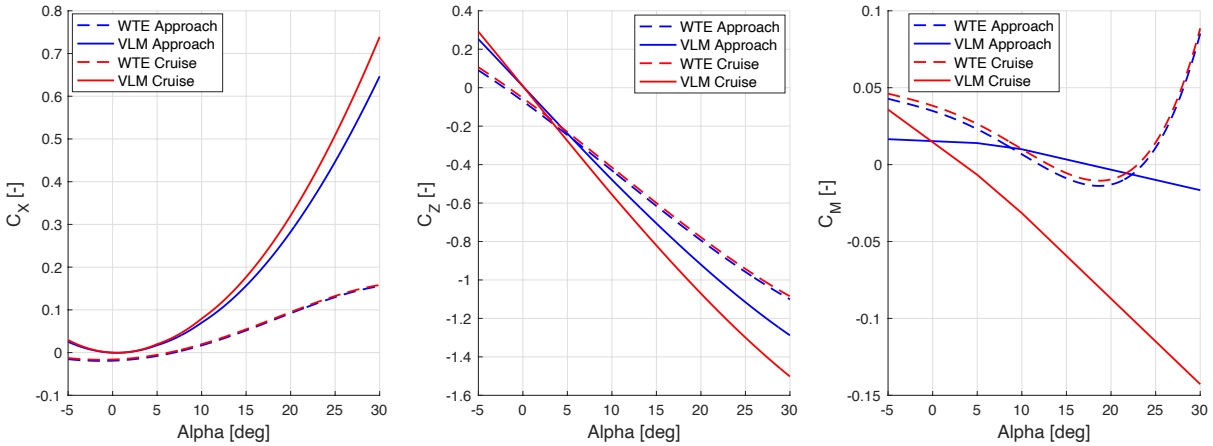

Fig. 4 Aerodynamic model curves from VLM and WTE for approach and cruise phase.

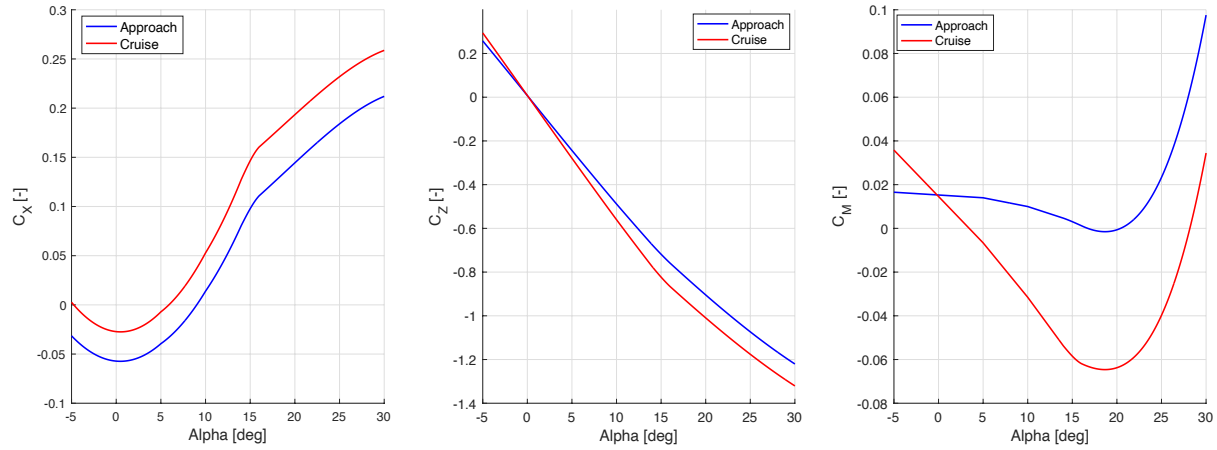

Fig. 5 Aerodynamic model obtained from combining VLM with WTE.

4. Verification and Validation

Before the simulation model to analyse the stability and handling qualities of the Flying-V can be used, it is first necessary to perform verification and validation on the model. This section first elaborates on the methodology used to verify the simulation model. After that, the validation methodology is discussed.

Simulation Model Verification

Before it is possible to analyse the simulation model results it is necessary to perform verification on the aerodynamic model and linearisation of the equations of motion. As mentioned in section II.A.2 it is necessary to linearise the equations of motion to determine specific parameters such as the damping ratio, natural frequency, and characteristic time constants to compare these with military standards.

For the verification of the aerodynamic model it is essential to analyse whether the aerodynamic model is implemented

correctly, and whether interpolation between datapoints is performed appropriately. The aerodynamic coefficients can be determined using linear interpolation between a set of data points arranged in a grid. Verification of the aerodynamic model is performed by two researchers using the same set of data points to obtain an aerodynamic model of the Flying-V. Consequently, the aerodynamic model results are compared for different inputs to obtain a range for which it can be guaranteed that a verified aerodynamic model is used.

To verify the results obtained from the linearised equations of motion, the response of the Flying-V to an input on the control surfaces is analysed and compared with the response of the nonlinear equations of motion. Small control surface inputs result in small deviations from the linearisation point. Therefore the response of the linearised simulation model is expected to be approximately equal to the response of the nonlinear simulation model. This comparative analysis is used to determine whether the linearisation is implemented correctly.

Simulation Model Validation

Validation of the simulation model of the Flying-V is ideally accomplished by comparison of accurately predicted aerodynamic responses of the aircraft from the simulation model with experimental tests [24]. However, using the flight test data from the maiden flight test[‡] for validation purposes is considered unreliable. This is because the flight test involves a small scale model, whereas the simulation model considers a full scale model. Therefore, it is necessary to apply Dynamic scaling to one of the models. This is however not possible due to a discrepancy between the mass distribution of the the full scale model and small scale model [13]. Besides that, Reynolds number effects will be present due to discrepancies between the airflow over the small scale model and full scale model [13]. Validation is therefore performed by first analysing the thrust setting during cruise. The thrust setting of an aircraft during cruise ranges between 20% and 30% of the maximum available thrust[§]. Besides that, it can be obtained that the thrust setting of the Airbus A350-900 is approximately 33.3% of the maximum available thrust[¶].

Furthermore, the simulation model results should be comparable with the results obtained from previous research [8, 11–13]. Therefore, the second validation analysis implies a comparative analysis between the eigenmodes obtained from the simulation model and previous research.

5. Assumptions and Limitations

During the design of the flight dynamic simulation model, several assumptions and therefore accompanying limitations have to be taken into account.

First of all, during the construction of the combined aerodynamic model, it is assumed that only the angle of attack makes a non-linear contribution to the force and moment coefficients. In reality, it is likely that other components (such as the control surfaces) also show nonlinear behaviour at high angles of attack. Therefore, it is expected that the fidelity of the contribution of these components to the forces and moments is limited.

Secondly, because the VLM model and WTE model both operate in different speed regimes due to the difference in aircraft size, it is necessary to apply Dynamic or Froude scaling. To apply this scaling method, the relative density factor and the relative moment of inertia of the small-scale model must be the same as in the full-scale aircraft [13]. This is not the case for the Flying-V and therefore results in inaccuracies of the combined aerodynamic model.

Moreover, because the VLM model is used as the baseline model, the combined aerodynamic model of the Flying-V does not contain frictional drag. It is not possible to obtain an accurate estimate of the frictional drag from the WTE model due to scaling. Frictional drag is therefore added to the combined aerodynamic model using data obtained from the Airbus A350-900.

In case the duration of the flight is short, the influence of the Earth's curvature and angular velocity is negligible. Therefore, the Earth can be assumed to be flat and the Coriolis acceleration and centripetal acceleration can be neglected. In case the period of the flight is large (in the order of hours), this introduces large errors that influence the accuracy of the simulation [25].

During the simulation zero wind and a perfect atmosphere is assumed that corresponds to the International Standard Atmosphere. Additional wind results in the fact that the kinematic velocity of the vehicle is different from the aerodynamic velocity. Wind conditions result in changing aerodynamic forces and moments acting on the aircraft, influencing the dynamic response of the vehicle.

Finally, because the Earth is not perfectly spherical with constant mass distribution, the gravity vector is not constant

[‡] https://www.tudelft.nl/en/2020/tu-delft/successful-maiden-flight-for-the-tu-delft-flying-v

[§] https://howthingsfly.si.edu/ask-an-explainer/i-assume-jet-engine-reaches-maximum-thrust-take-and-lift-cruising-elevation-and-red

[¶] https://www.airbus.com/aircraft/passenger-aircraft/a350xwb-family/a350-900.html

with respect to different locations on Earth. In reality, the gravity vector changes in direction and magnitude throughout the flight of the aircraft resulting in changing dynamic responses.

III. Results and Discussions

In this section, the results obtained from the flight dynamic simulation model are displayed and discussed. Section III.A shows the trim results. After that, the eigenmodes are discussed in section III.B. Furthermore, section III.C elaborates in the handling qualities results. Finally, the results from the verification and validation are shown in section III.D.

A. Trim

To assess the trimmability of the aircraft, for the cruise and approach phase, it is assumed that the aircraft is in a steady symmetric flight. Therefore the deflections of the rudders used for yaw control (δ_{CS3}) are set to zero. The trim algorithm aims at minimising the cost function shown in Eq. (4). In this equation, W_* represents the weight of each parameter of the cost function. The weights are determined iteratively and shown in Table 1. Besides that, $\dot{u}$, $\dot{w}$, and $\dot{q}$ are the time derivatives of the forward velocity component, vertical velocity component, and pitch rate respectively. Furthermore, V represents the airspeed, a represents the speed of sound, and γ is the flight path angle. As inputs, the trim function uses the forward velocity component (u), vertical velocity component (w), pitch angle (θ), elevon deflection angle of both the inboard and outboard elevons ($\delta_{CS1}/\delta_{CS2}$), and thrust setting ($T$). Consequently, the trim algorithm minimises the cost function using the MATLAB® function "fminsearch". This algorithm can be used to find the minimum of unconstrained multivariable functions using the Nelder-Mead simplex algorithm[‖]. The trim algorithm has three different stopping criteria. First of all, the trim algorithm stops in case the current function value differs by less than 10^{-9} from the previous function value. Besides that, the trim algorithm stops in case the current inputs differ from the previous inputs by less than 10^{-9}. In case these two criteria are not met, the trim algorithm stops in case the number of trim function evaluations exceeds 1,000,000.

$$J(\dot{u}, \dot{w}, \dot{q}, V, \gamma) = W_u \dot{u}^2 + W_w \dot{w}^2 + W_q \dot{q}^2 + W_V \left(\frac{V - V_{\text{ref}}}{a}\right)^2 + W_\gamma (\gamma - \gamma_{\text{ref}}) \tag{4}$$

Table 1 Weights for cost function.

Parameter	W_u	W_w	W_q	W_V	W_γ
Weight	100	1	100	100	1

The trim conditions for both the approach and cruise phase can be observed in Table 2. During approach, moving the centre of gravity forward leads to an increased angle of attack, control surface deflection, and thrust setting. Besides that, the flight path angle is equal to $\gamma = -3°$ as indicated by the requirements discussed in Section II.A.1. During cruise, moving the centre of gravity forward also leads to an increased angle of attack and control surface deflection, whereas the thrust setting remains similar.

The observed trends are due to the induced pitch down moment in case the centre of gravity is moved forward. To counteract this pitch down moment an increased (upwards) elevon deflection is required, which leads to a necessity to increase the lift force. This additional lift force can be obtained by increasing the angle of attack. It is expected that the thrust force mainly increases during approach due to a more significant angle of attack increase (3.4° during approach compared to 1.0° during cruise) and the larger air density during approach conditions. The results obtained from the trim conditions show the same trends as discussed in former research on the longitudinal flying qualities of blended-wing-body aircraft [26].

B. Modes Response

To analyse the eigenmodes of the aircraft, it is necessary to linearise the equations of motion such that the eigenvalues from a state-space system can be obtained. Therefore, nonlinear equations of motion are analytically linearised at the

[‖] https://www.mathworks.com/help/matlab/ref/fminsearch.html

Table 2 Trim Results

Flight Condition	Forward CG		Aft CG	
Approach (Ma = 0.2)	u	$64.1\frac{m}{s}$	u	$65.4\frac{m}{s}$
	w	$24.5\frac{m}{s}$	w	$20.7\frac{m}{s}$
	α	$20.9°$	α	$17.5°$
	θ	$17.9°$	θ	$14.5°$
	$\delta_{CS1}/\delta_{CS2}$	$20.2°$	$\delta_{CS1}/\delta_{CS2}$	$3.9°$
	T	$175642.8N$	T	$109867.0N$
Cruise (Ma = 0.85)	u	$248.8\frac{m}{s}$	u	$249.3\frac{m}{s}$
	w	$31.1\frac{m}{s}$	w	$26.8\frac{m}{s}$
	α	$7.1°$	α	$6.1°$
	θ	$7.1°$	θ	$6.1°$
	$\delta_{CS1}/\delta_{CS2}$	$8.0°$	$\delta_{CS1}/\delta_{CS2}$	$2.6°$
	T	$124199.7N$	T	$124377.6N$

trim conditions. In Section III.B.1, the eigenvalues obtained from the state-space system are discussed. Besides that, each eigenmode and the corresponding flying qualities are discussed below in Section III.B.2 - Section III.B.6.

1. Eigenvalue Analysis

After linearising the nonlinear equations of motion, it is possible to obtain the eigenvalues from the state-space system. The eigenvalues for each trim condition can be observed in Figure 6 and Figure 7. Furthermore, the natural frequency and damping ratio of each eigenmode for the different flight conditions are shown in Table 3.

First of all, the eigenvalues of the Flying-V during approach, shown in Figure 6, can be analysed. This figure shows how changing the centre of gravity location affects the location of the eigenvalues. Figure 6 shows that during approach, the short period mode and aperiodic roll mode are stable, whereas the phugoid mode, Dutch roll mode, and spiral mode are unstable. Furthermore, shifting the centre of gravity aft changes the location of the eigenvalues. First of all, for the oscillatory modes, the magnitude of the imaginary part of each eigenvalue decreases when moving the centre of gravity aft. Furthermore, the short period mode and aperiodic roll mode shift to a location closer to the imaginary axis. Besides that, the phugoid mode shifts further into the right half-plane. Finally, the Dutch roll mode and spiral mode (both located in the right half-plane) shift to a location closer to the imaginary axis.

Secondly, the eigenvalues of the Flying-V during cruise, shown in Figure 7, can be analysed. During cruise, the short period mode, phugoid mode, and aperiodic roll mode are stable, whereas the spiral mode is unstable. The Dutch roll mode is unstable at the forward centre of gravity location but stable at the aft centre of gravity location. During cruise the effect of shifting the centre of gravity aft is similar to approach. First of all, the magnitude of the imaginary part of each eigenvalue also decreases when moving the centre of gravity aft. Besides that, the short period mode, phugoid mode, and aperiodic roll mode shift to a location closer to the imaginary axis. Finally, the Dutch roll mode and spiral mode shift to the left. For the Dutch roll mode, this results in a stable mode during cruise at the aft centre of gravity location.

The results obtained from the eigenvalues are also shown in Table 3. This table shows the damping ratio and undamped natural frequency of each eigenmode. Moving the centre of gravity aft shows an increased short period damping ratio and decreased short period undamped natural frequency. Besides that, for the phugoid mode, shifting the centre of gravity aft results in a larger magnitude of the damping ratio in case the mode is unstable. The damping ratio decreases in case the mode is stable. The undamped natural frequency decreases when the centre of gravity is moved aft. The results obtained from Table 3 cohere with previous research on the handling qualities of a blended-wing-body aircraft [27]. Besides that, the results shown in Fig. 6, Fig. 7 show that the longitudinal stability deteriorates when moving the centre of gravity aft [27].

Looking at the Dutch roll mode, it can be observed that shifting the centre of gravity aft leads to larger magnitude of the damping ratio during approach. Besides that, during cruise, shifting the centre of gravity aft leads to a stable Dutch roll mode. Furthermore, the undamped natural frequency decreases when moving the centre of gravity aft. The

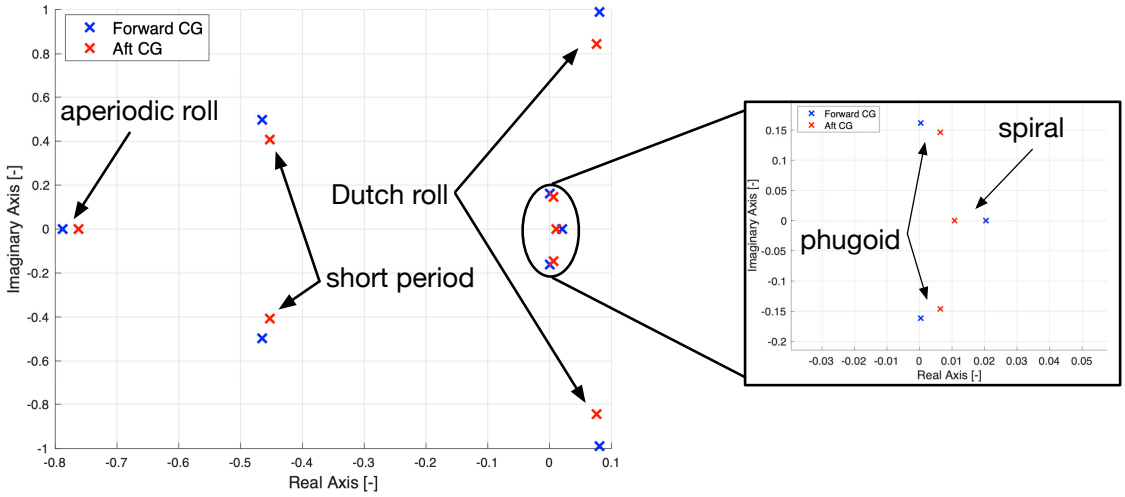

Fig. 6 Eigenvalues of the Flying-V during approach at forward and aft centre of gravity location.

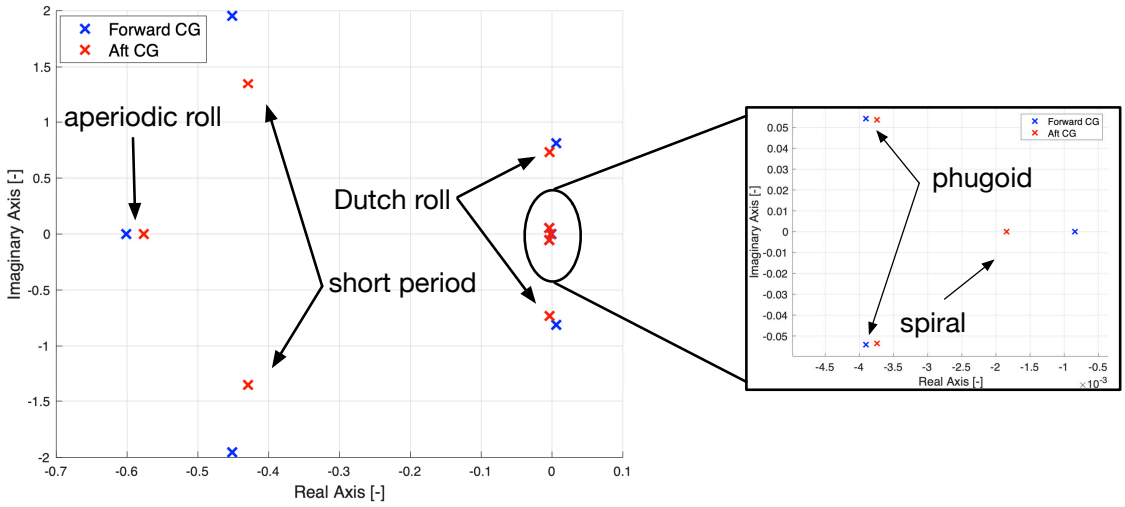

Fig. 7 Eigenvalues of the Flying-V during cruise at forward and aft centre of gravity location.

eigenvalues in Fig. 6 and Fig. 7 show that moving the centre of gravity aft moves the poles to the left. This is in contrast to former research that describes the deterioration of stability when moving the centre of gravity aft [27, 28].

Finally, the aperiodic roll mode and spiral mode are critically damped non-oscillatory modes and are therefore not considered in Table 3. However, looking at the aperiodic roll and spiral mode eigenvalues shown in 6 and Fig. 7, it can be observed that the magnitude eigenvalue increases when the centre of gravity is moved forward. This leads to a faster mode when moving the centre or gravity forward.

2. Short-period Mode

Section III.B.1 shows that the eigenvalues of the short-period mode consist of a negative real component during approach as well as cruise, meaning that this mode is stable. To analyse the flying quality level of the aircraft, it is necessary to determine the damping ratio of the short-period mode (ς_{sp}). The damping ratios and the requirements from military standards [18] can be observed in Table 4. It can be observed that the damping ratio during cruise is lower compared to approach. This decrease in damping ratio originates from the low air density at the cruise altitude of the

Table 3 Damping ratio and natural frequency for eigenmodes of the Flying-V.

Eigenmodes	Approach (Ma = 0.2)				Cruise (Ma = 0.85)			
	Forward		Aft		Forward		Aft	
	ς	ω	ς	ω	ς	ω	ς	ω
Short Period	0.683	0.681	0.744	0.609	0.225	2.01	0.303	1.41
Phugoid	$-2.31 \cdot 10^{-3}$	0.161	$-4.37 \cdot 10^{-2}$	0.146	$7.19 \cdot 10^{-2}$	$5.43 \cdot 10^{-2}$	$6.97 \cdot 10^{-2}$	$5.37 \cdot 10^{-2}$
Dutch Roll	$-8.14 \cdot 10^{-2}$	0.992	$-8.97 \cdot 10^{-2}$	0.848	$-7.38 \cdot 10^{-3}$	0.811	$4.68 \cdot 10^{-3}$	0.732
Aperiodic Roll	-	-	-	-	-	-	-	-
Spiral	-	-	-	-	-	-	-	-

Flying-V.

Table 4 shows that the short period mode of the Flying-V has Level 1 flying qualities at the approach condition and cruise condition at the aft centre of gravity location. Furthermore, the Flying-V shows Level 2 flying qualities at the forward centre of gravity location during cruise.

Table 4 Short-period flying qualities of the Flying-V.

	Approach (Ma = 0.2)		Cruise (Ma = 0.85)	
Forward CG	$\varsigma_{sp} = 6.83 \cdot 10^{-1}$		$\varsigma_{sp} = 2.25 \cdot 10^{-1}$	
Aft CG	$\varsigma_{sp} = 7.44 \cdot 10^{-1}$		$\varsigma_{sp} = 3.03 \cdot 10^{-1}$	
Short-period requirements	Level 1:	$0.5 < \varsigma_{sp} < 1.3$	Level 1:	$0.3 < \varsigma_{sp} < 2.0$
	Level 2:	$0.35 < \varsigma_{sp} < 2.0$	Level 2:	$0.2 < \varsigma_{sp} < 2.0$
	Level 3:	$\varsigma_{sp} > 0.25$	Level 3:	$\varsigma_{sp} > 0.1$

3. Phugoid Mode

Section III.B.1 shows that the real part of the eigenvalues of the phugoid mode are positive during approach and negative during cruise. This implies that the phugoid is unstable during approach. To analyse the flying quality level of the aircraft it is necessary to determine the damping ratio (ς_{ph}), and in case the phugoid is unstable, the period of the mode (T_{ph}). Using Table 5, these parameters can be compared with the military standards [18]. Table 5 shows that due to the small period of the unstable phugoid, the flying qualities during approach cannot be quantified by military standards. During cruise, the phugoid mode shows Level 1 flying qualities.

Table 5 Phugoid flying qualities of the Flying-V.

	Approach (Ma = 0.2)		Cruise (Ma = 0.85)	
Forward CG	Unstable but $T_{ph} = 39.0s$		$\varsigma_{ph} = 7.19 \cdot 10^{-2}$	
Aft CG	Unstable but $T_{ph} = 43.0s$		$\varsigma_{ph} = 6.97 \cdot 10^{-2}$	
Phugoid requirements	Level 1:	$\varsigma_{ph} > 0.04$	Level 1:	$\varsigma_{ph} > 0.04$
	Level 2:	$\varsigma_{ph} > 0$	Level 2:	$\varsigma_{ph} > 0$
	Level 3:	Unstable but $T_{ph} > 55s$	Level 3:	Unstable but $T_{ph} > 55s$

4. Dutch Roll Mode

In Section III.B.1, the eigenvalues from the Dutch roll mode show that the Dutch roll is unstable during approach, whereas the mode is stable when moving the centre of gravity aft during cruise. To analyse the flying quality level

of the aircraft it is necessary to determine damping ratio (ς_d) and undamped natural frequency of the motion (ω_d). The parameters obtained from military standards [18] and the simulation model can be observed in Table 6. This table shows that the flying quality level of an unstable Dutch roll mode cannot be quantified by military standards. Besides that, the Dutch roll mode during cruise at the aft centre of gravity location shows Level 3 flying qualities.

Table 6 Dutch roll flying qualities of the Flying-V.

	Approach (Ma = 0.2)				Cruise (Ma = 0.85)			
Forward CG	Unstable				Unstable			
Aft CG	Unstable				$\varsigma_d = 4.68 \cdot 10^{-3}$	$\varsigma_d\omega_d = 3.43 \cdot 10^{-3}$	$\omega_d = 0.732$	
Dutch roll requirements	Level 1:	$\varsigma_d > 0.08$	$\varsigma_d\omega_d > 0.10$	$\omega_d > 0.5$	Level 1:	$\varsigma_d > 0.08$	$\varsigma_d\omega_d > 0.15$	$\omega_d > 0.5$
	Level 2:	$\varsigma_d > 0.02$	$\varsigma_d\omega_d > 0.05$	$\omega_d > 0.5$	Level 2:	$\varsigma_d > 0.02$	$\varsigma_d\omega_d > 0.05$	$\omega_d > 0.5$
	Level 3:	$\varsigma_d > 0$	$\omega_d > 0.4$		Level 3:	$\varsigma_d > 0$	$\omega_d > 0.4$	

5. Aperiodic Roll Mode

The aperiodic roll for both the approach phase and the cruise phase is stable due to the negative real eigenvalue. To analyse the flying quality level of the aircraft, it is necessary to analyse the roll time constant (T_r) as can be observed in Table 7. The larger the roll time constant, the more time it takes to achieve a specific roll rate. Table 7 shows that the roll time constant is larger during the cruise condition and also increases when the centre of gravity is shifted aft. During approach the aperiodic roll shows Level 1 flying qualities. Besides that, during cruise the aperiodic roll shows Level 1 flying qualities at the forward centre of gravity location and Level 2 flying qualities at the aft centre of gravity location.

Table 7 Aperiodic roll flying qualities of the Flying-V.

	Approach (Ma = 0.2)		Cruise (Ma = 0.85)	
Forward CG	$T_r = 1.26s$		$T_r = 1.32s$	
Aft CG	$T_r = 1.32s$		$T_r = 1.71s$	
Aperiodic roll requirements	Level 1:	$T_r < 1.4s$	Level 1:	$T_r < 1.4s$
	Level 2:	$T_r < 3.0s$	Level 2:	$T_r < 3.0s$
	Level 3:	$T_r < 10.0s$	Level 3:	$T_r < 10.0s$

6. Spiral Mode

The eigenvalues of the spiral mode show that the spiral is unstable during approach, but stable during cruise. A stable spiral mode automatically implies Level 1 flying qualities. The unstable behaviour of the spiral mode does not necessarily have to be critical as the flying quality level depends on the characteristic time constant for the spiral mode (T_s). The results are shown in Table 8. This table shows that for both the approach and cruise phase, the spiral mode has Level 1 flying qualities.

Table 8 Spiral mode flying qualities of the Flying-V.

	Approach (Ma = 0.2)		Cruise (Ma = 0.85)	
Forward CG	$T_s = 42.6s$		Stable	
Aft CG	$T_s = 79.4s$		Stable	
Spiral requirements	Level 1:	$T_s > 17.3s$	Level 1:	$T_s > 28.9s$
	Level 2:	$T_s > 11.5s$	Level 2:	$T_s > 11.5s$
	Level 3:	$T_s > 7.2s$	Level 3:	$T_s > 7.2s$

C. Handling Qualities

For the handling quality analysis, the Control Anticipation Parameter is considered. The general equation for the Control Anticipation Parameter (CAP) can be observed in Eq. (5), where the parameter T_{θ_2} can be obtained from the second order transfer function shown in Eq. (6).

$$\text{CAP} = \frac{g\omega_{\text{sp}}^2 T_{\theta_2}}{V} \tag{5}$$

$$\frac{q(s)}{\delta_{\text{CS1}}(s)} = \frac{K_q(1 + T_{\theta_2} s)}{s^2 + 2\varsigma_{\text{sp}}\omega_{\text{sp}} + \omega_{\text{sp}}^2} \tag{6}$$

The state-space system obtained from the linearised Flying-V model does not result in a second-order transfer function. Namely, $\dot{q}$ depends on the states: u, w, p, q, and r. Therefore this state-space system is reduced to a system consisting of two states (w and q). The contribution of the other states is significantly smaller compared to these two states. Consequently, the Control Anticipation Parameters for the approach- and cruise phase at the different centre of gravity locations can be observed in Table 9. The results are graphically shown in Fig. 8. The values in Table 9 show that moving the centre of gravity aft results in a decreasing Control Anticipation Parameter. Besides that, the Control Anticipation parameter is lower during approach compared to cruise. This is mainly due to the low airspeed during approach, resulting in less effective control surfaces and a slower response of the Flying-V.

Table 9 Control Anticipation Parameter (CAP) Flying-V.

	Approach (Ma = 0.2)	**Cruise (Ma = 0.85)**
Forward CG	0.16	0.51
Aft CG	0.12	0.22

In Fig. 8 it can be observed that during approach, the Flying-V is on the border of Level 1 handling qualities at the forward centre of gravity and has Level 2 handling qualities at the aft centre of gravity. During cruise, the Flying-V has Level 1 handling qualities at the aft centre of gravity and has Level 2 handling qualities at the forward centre of gravity location. It is clear from the figures that moving the centre of gravity aft results in a lower CAP meaning that the response of the Flying-V becomes more sluggish when moving the centre of gravity aft, which may lead to oversteering. Similar behaviour is also apparent for other types of flying wings, where it is observed that the agility of the aircraft decreases in case the centre of gravity is moved aft [28].

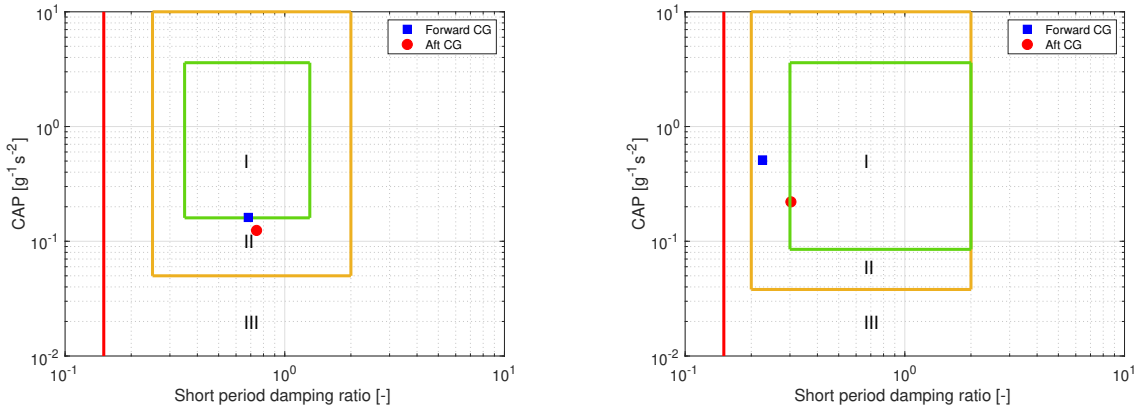

(a) CAP for approach phase.

(b) CAP for cruise phase.

Fig. 8 Control Anticipation Parameter (CAP) analysis.

D. Verification and Validation

In this section, the results obtained from the verification and validation procedure are discussed. First, section III.D.1 elaborates on the verification results. After that, the validation results are shown in section III.D.2.

1. Verification Results

The aerodynamic model is verified by analysing the aerodynamic model results generated by two different researchers using the same set of aerodynamic data points. Each aerodynamic coefficient is a function of the angle of attack, angle of sideslip, roll rate, pitch rate, yaw rate, and control surface deflections ($C_*(\alpha, \beta, p, q, r, \delta_{CS1}, \delta_{CS2}, \delta_{CS1})$). To verify the aerodynamic models, random inputs for each aerodynamic coefficient are determined. Consequently, the aerodynamic coefficients are compared. In case no error is obtained between the coefficients generated by the different researchers, the aerodynamic model is considered verified. This results in the operational range in which the aerodynamic model can be used as shown in Table 10.

Table 10 Verified Operational Range Aerodynamic Model Flying-V

Parameter	α	β	p,q,r	δ_{CS1}, δ_{CS2}, δ_{CS3}
Range	$[-5°; 30°]$	[-20 °; 20 °]	$[-10°/s; 10°/s]$	$[-25°; 25°]$

To verify the linearisation of the equations of motion, the time response of an input on the control surfaces of the nonlinear simulation model is compared with the time response of the linear simulation model. The time responses of an impulse input of 1° on the inboard elevons (pitch control), outboard elevons (roll control), and rudders (yaw control) can be observed in Fig. 9. The time responses show that the linear simulation model is able to approximate the response of the nonlinear simulation model for small deviations from the trim condition. It needs to be noted that large inputs on the control surfaces or large disturbances decrease the fidelity of the linear simulation model.

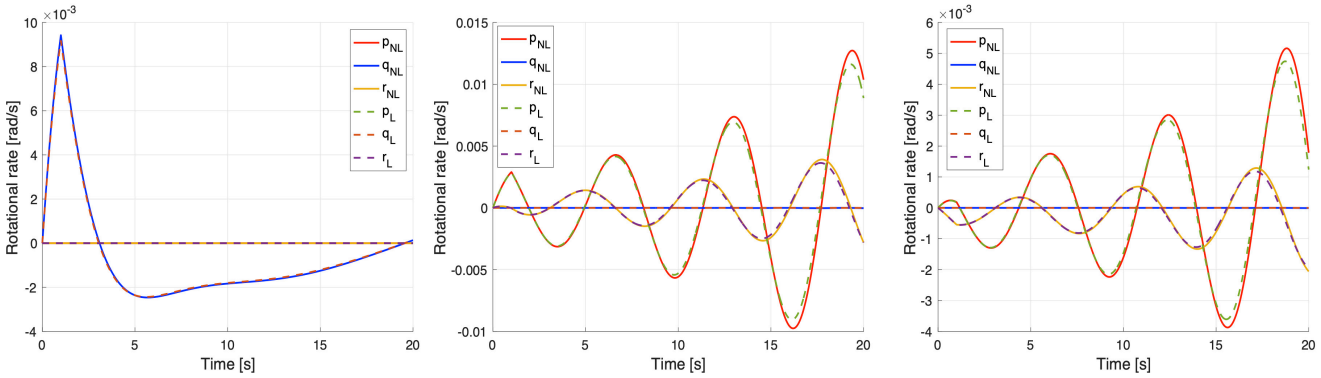

Fig. 9 Comparison between nonlinear simulation model and linearised simulation model.

2. Validation Results

To validate the simulation model of the Flying-V, it is first possible to analyse the thrust conditions during cruise at several centre of gravity locations. During cruise, the thrust setting is on average 124288.7 N. This corresponds to a thrust setting equal to 32.8% of the maximum available thrust. As discussed in section II.B.4, the thrust setting of an aircraft ranges in general between 20% and 30% of the maximum available thrust. Besides that, the thrust setting of the Airbus A350-900 is approximately 33.3%. It is therefore concluded that the thrust setting of the Flying-V coheres with literature, which validates the aerodynamic model used.

Furthermore, after obtaining the eigenvalue results, it is possible to compare the stability of different eigenmodes with literature to validate that the simulation model is able to capture the unstable Dutch roll mode and pitch break tendency for angles of attack larger than 20°. Previous research shows that the Dutch roll mode is unstable during approach conditions. Besides that, moving the centre of gravity forwards leads to an increased damping ratio and natural frequency of the mode [8]. The same conclusion can be drawn at the approach condition from Table 3. However, looking

at the cruise condition, it can be observed that moving the centre of gravity forwards leads to a decreased damping ratio. This is in contrast with previous research [8] and originates from the contribution of the aerodynamic coefficient C_{Y_p} in case the centre of gravity is moved forward. The sign and magnitude of this coefficient mainly depends on the size and location of the winglets of the Flying-V with respect to the centre of gravity location [29, 30]. The coefficient C_{Y_p} is negative for small angles of attack and becomes positive for larger angles of attack [31, 32]. Therefore, a forward shift of the centre of gravity leads to a decreased damping effect of the winglets and therefore results in opposite results of the Dutch roll damping compared to previous research.

Besides the Dutch roll mode, the simulation model has to capture the pitch break tendency for high angles of attack. Figure 5 shows that for angles of attack larger than 20°, C_{m_α} is larger than zero. This implies that for angles of attack larger than 20° pitch break occurs, meaning that the Flying-V becomes statically unstable [13]. This statically unstable behaviour is also discussed in previous research where the longitudinal flight characteristics of the Flying-V are investigated using wind tunnel experiments [11, 13].

IV. Conclusions

After analysing the aerodynamic models obtained from the Vortex Lattice Method (VLM) and wind tunnel experiments (WTE), it is concluded that one single aerodynamic model is not able to capture the unstable Dutch roll and unstable longitudinal behaviour obtained from previous research. Therefore, these aerodynamic models are combined. This combined aerodynamic model is integrated into the flight dynamic simulation model and is able to capture the unstable behaviour shown in previous research. However, the combined aerodynamic model is based on several critical assumptions, such as the assumptions that only the angle of attack makes a non-linear contribution to the force and moment coefficients, and that the relative density factor and the relative moment of inertia of the small-scale model are the same as in the full-scale aircraft, decreasing the fidelity of the model.

Furthermore, the short-period mode is stable and shows Level 1 flying qualities, except for cruise at the forward centre of gravity location where the short-period mode shows Level 2 flying qualities. The low damping ratio of the short period during cruise is due to the high design cruise altitude of the Flying-V. During approach the phugoid mode is unstable, whereas this mode shows Level 1 flying qualities during cruise. Besides that during approach conditions, the Flying-V is longitudinally statically unstable because C_{m_α} is larger than zero. This leads to perturbations in angle of attack being amplified instead of dampened.

Also, the Dutch roll mode is unstable during approach and shows Level 3 flying qualities during cruise at the aft centre of gravity location. The unstable Dutch roll mode indicates that the winglets of the Flying-V are not able to effectively dampen the Dutch roll mode. It is expected that increasing the size of the winglets improves the Dutch roll damping ratio. In case physical design changes are undesired, the Dutch roll damping can also be improved by designing an automatic flight control system that actively stabilises the Dutch roll.

From the control anticipation parameter (CAP) analysis it can be concluded that during approach, the CAP is rated Level 1 at the forward centre of gravity location. At the aft centre of gravity location, the CAP is rated Level 2, resulting in potential oversteering by the pilot. During cruise, the CAP is rated Level 2 at the forward centre of gravity, indicating that the damping ratio of the short period needs to be increased. Besides that, at the aft centre of gravity location, the CAP is rated Level 1 indicating that the pitch output of the Flying-V accurately follows the pitch input by a pilot.

V. Recommendations

With the goal to further improve research on modelling and handling quality assessment of the Flying-V aircraft, future work may include the set of items discussed in this section.

During this research, only the key stability and handling quality requirements for certification and qualification purposes are considered. It is therefore suggested to perform further research on additional requirements necessary for certification and qualification of the Flying-V.

Besides that, it is recommended to conduct further research on flight control systems that can be applied to the Flying-V to stabilise the unstable eigenmodes.

Finally, even though the aerodynamic model designed in this research is able to capture the undesired behaviour of the Flying-V obtained from previous research, several assumptions are made during the construction of the aerodynamic model. To increase the fidelity of the combined aerodynamic model, it is suggested to perform additional research on aerodynamic model identification of the Flying-V.

References

[1] Martinez-Val, R., Perez, E., Puertas, J., and Roa, J., "Optimization of Planform and Cruise Conditions of a Transport Flying Wing," *Proceedings of the Institution of Mechanical Engineers, Part G: Journal of Aerospace Engineering*, Vol. 224, No. 12, 2010, pp. 1243–1251. https://doi.org/10.1243/09544100JAERO812.

[2] Faggiano, F., Vos, R., Baan, M., and Van Dijk, R., "Aerodynamic Design of a Flying V Aircraft," *17th AIAA Aviation Technology, Integration, and Operations Conference*, 2017. https://doi.org/10.2514/6.2017-3589.

[3] Martinez-Val, R., "Flying Wings: A New Paradigm for Civil Aviation?" *Acta Polytechnica Vol. 47 No. 1/2007*, 2007. https://doi.org/10.14311/914.

[4] Okonkwo, P., and Smith, H., "Review of Evolving Trends in Blended Wing Body Aircraft Design," *Progress in Aerospace Sciences*, Vol. 82, 2016, pp. 1–23. https://doi.org/10.1016/j.paerosci.2015.12.002.

[5] Zhenli, C., Zhang, M., Yingchun, C., Weimin, S., Zhaoguang, T., Dong, L., and Zhang, B., "Assessment on Critical Technologies for Conceptual Design of Blended-Wing-Body Civil Aircraft," *Chinese Journal of Aeronautics*, Vol. 32, No. 8, 2019, pp. 1797–1827. https://doi.org/10.1016/j.cja.2019.06.006.

[6] Liebeck, R. H., "Design of the blended wing body subsonic transport," *Journal of aircraft*, Vol. 41, No. 1, 2004, pp. 10–25. https://doi.org/10.2514/1.9084.

[7] Benad, J., "The Flying V, A New Aircraft Configuration for Commercial Passenger Transport," *Deutscher Luft- und Raumfahrtkongress*, 2015. https://doi.org/10.25967/370094.

[8] Cappuyns, T., "Handling Qualities of a Flying V Configuration," http://resolver.tudelft.nl/uuid:69b56494-0731-487a-8e57-cec397452002, 2019.

[9] Humphreys-Jennings, C., Lappas, I., and Sovar, D. M., "Conceptual Design, Flying, and Handling Qualities Assessment of a Blended Wing Body (BWB) Aircraft by Using an Engineering Flight Simulator," *Aerospace*, Vol. 7, No. 5, 2020, p. 51. https://doi.org/10.3390/aerospace7050051.

[10] Ammar, S., Legros, C., and Trépanier, J.-Y., "Conceptual Design, Performance and Stability Analysis of a 200 Passengers Blended Wing Body Aircraft," *Aerospace Science and Technology*, Vol. 71, 2017, pp. 325–336. https://doi.org/10.1016/j.ast.2017.09.037.

[11] Palermo, M., and Vos, R., "Experimental Aerodynamic Analysis of a 4.6%-Scale Flying-V Subsonic Transport," *AIAA Scitech 2020 Forum*, 2020, p. 2228. https://doi.org/10.2514/6.2020-2228.

[12] Viet, R., "Analysis of the Flight Characteristics of a Highly Swept Cranked Flying Wing by Means of an Experimental Test," http://resolver.tudelft.nl/uuid:90de4d9e-70ae-4efc-bd0a-7426a0a669c3, 2019.

[13] Garcia, A.R., "Aerodynamic Model Identification of the Flying V using Wind Tunnel Data," http://resolver.tudelft.nl/uuid:79e01f29-1789-4501-8556-ca2bcf06f3ab, 2019.

[14] CS-25, "Easy Access Rules for Large Aeroplanes (CS-25)," , 2018. Accessed: 23-02-2021.

[15] Perez, R. E., Liu, H. H., and Behdinan, K., "Multidisciplinary Optimization Framework for Control-Configuration Integration in Aircraft Conceptual Design," *Journal of Aircraft*, Vol. 43, No. 6, 2006, pp. 1937–1948. https://doi.org/10.2514/1.22263.

[16] Wahler, N.F.M., "The Impact of Control Allocation on Optimal Control Surface Positioning and Sizing," http://resolver.tudelft.nl/uuid:5e9baf63-8a8f-4c1b-98cd-5aa993938027, 2021.

[17] Cook, M.V., *Flight Dynamics Principles: A Linear Systems Approach to Aircraft Stability and Control*, Butterworth-Heinemann, 2012.

[18] Anonymous, "Military Specifications, Flying Qualities of Piloted Aircraft MIL-F-8785C," , 1980.

[19] Grotens, R., "Nonlinear Flight Control Fault Tolerant Control with Sliding Modes and Control Allocation," http://resolver.tudelft.nl/uuid:29ddf25f-bcc3-47f3-9c26-53da9b6d9301, 2010.

[20] Sieberling, S et al., "Robust Flight Control using Incremental Nonlinear Dynamic Inversion and Angular Acceleration Prediction," *Journal of Guidance, Control, and Dynamics*, Vol. 33, No. 6, 2010, pp. 1732–1742.

[21] Lambert, T., Abdul Razak, N., and Dimitriadis, G., "Vortex Lattice Simulations of Attached and Separated Flows around Flapping Wings," *Aerospace*, Vol. 4, No. 2, 2017, p. 22. https://doi.org/10.3390/aerospace4020022.

[22] Ananda, G. K., Vahora, M., Dantsker, O. D., and Selig, M. S., "Design Methodology for a Dynamically-Scaled General Aviation Aircraft," *35th AIAA Applied Aerodynamics Conference*, 2017, p. 4077. https://doi.org/10.2514/6.2017-4077.

[23] Sun, J. et al., "Aircraft Drag Polar Estimation Based on a Stochastic Hierarchical Model," *8th International Conference on Research in Air Transportation*, 2018.

[24] Murphy, P. et al., "Validation of Methodology for Estimating Aircraft Unsteady Aerodynamic Parameters from Dynamic Wind Tunnel Tests," *AIAA Atmospheric Flight Mechanics Conference and Exhibit*, 2003, p. 5397.

[25] Mulder, J.A., Van Staveren, W.H.J.J., Van der Vaart, J.C., De Weerdt, E., De Visser, C.C., In 't Veld, A.C. and Mooij, E., *Flight Dynamics*, TU Delft, 2013.

[26] Cook, M., and De Castro, H., "The Longitudinal Flying Qualities of a Blended-Wing-Body Civil Transport Aircraft," *The Aeronautical Journal*, Vol. 108, No. 1080, 2004, pp. 75–84.

[27] De Castro, H. V., "Flying and Handling Qualities of a Fly-By-Wire Blended-Wing-Body Civil Transport Aircraft," Ph.D. thesis, Cranfield University, 2003.

[28] Hasan, Y. J., Schwithal, J., Pfeiffer, T., Liersch, C. M., and Looye, G., *Handling Qualities Assessment of a Blended Wing Body Configuration under Uncertainty Considerations*, Deutsche Gesellschaft für Luft-und Raumfahrt-Lilienthal-Oberth eV, 2018.

[29] Finck, R., "USAF (United States Air Force) Stability and Control DATCOM (Data Compendium)," Tech. rep., MC Donnell Aircraft Co St. Louis Mo, 1978.

[30] Toll, T. A., and Queijo, M. J., "Approximate Relations and Charts for Low-Speed Stability Derivatives of Swept Wings," 1948.

[31] Anton, N., Botez, R., and Popescu, D., "New Methodologies for Aircraft Stability Derivatives Determination From its Geometrical Data," 2009, p. 6046.

[32] Ahmad, M., Hussain, Z. L., Shah, S. I. A., and Shams, T. A., "Estimation of Stability Parameters for Wide Body Aircraft Using Computational Techniques," *Applied Sciences*, Vol. 11, No. 5, 2021, p. 2087.

Handling Quality Improvements for the Flying-V Aircraft using Incremental Nonlinear Dynamic Inversion

Simon van Overeem*
Delft University of Technology, The Netherlands, 2629 HS Delft

Considerable growth in the number of passengers and cargo transported by air is predicted. Moreover, aircraft noise and climate impact become increasingly important factors in aircraft design. These existing challenges in aviation boost interest in the design of innovative aircraft configurations. One of these configurations is a V-shaped flying wing named the Flying-V. This work aims at developing a flight control system for the Flying-V that can be used to improve the stability and handling qualities of the aircraft. Prior work shows that the Flying-V is not able to adhere to all stability and handling quality requirements at the forward and aft centre of gravity location during cruise and approach. This paper illustrates how an Incremental Nonlinear Dynamic Inversion flight control system can be used to improve the stability and handling qualities of the aircraft. Furthermore, the robustness of the flight control system is assessed by analysing the effects of aerodynamic uncertainty on the attitude tracking error of the Flying-V. Upon implementation of the flight control system, this research shows that the eigenmodes become stable. Besides that, the flight control system is proved to be robust against aerodynamic uncertainty.

I. Introduction

Over the last fifty years, most commercial aircraft consisted of the traditional tube-and-wing configuration. This conventional design has obtained significant efficiency gains of 100% over the years [1]. However, the Airbus A350 and Boeing 787 represent an aircraft efficiency asymptote. Besides that, the number of passengers and cargo transported by air is predicted to grow considerably [2]. Furthermore, due to the increasing pressure on noise pollution and environmental impact, it is necessary to find a solution that is able to boost the efficiency of aircraft, while reducing noise and environmental impact [3]. One course of action to tackle the existing challenges in aviation is the design of an innovative aircraft configuration. The flying wing is one of the most promising aircraft configurations to overcome the existing challenges in aviation. The flying wing has different settings, such as the Blended-Wing-Body (BWB), C-Wing, and Tail-less aircraft. This type of aircraft has the potential to increase efficiency, resulting in less pollution. Furthermore, it is expected that noise levels during landing and take-off are reduced [3].

The Flying-V is a specific type of flying wing that is tailless, V-shaped, and consists of two cylindrical pressurised cabins located in the leading edge of the wing. The main advantage of the design of a Flying-V aircraft concept compared to conventional tube-and-wing aircraft is the reduction of wetted area and frictional drag. Namely, the Flying-V consists of one structure that integrates the structural function of accommodating payload and aerodynamic function of providing lift [4]. Furthermore, due to the smooth shape of this aircraft, it suffers less from interference drag. Additionally, the reduction of wetted area results in a reduced zero-lift drag [5]. This results in the fact that this type of aircraft can achieve a higher lift-to-drag ratio compared to conventional aircraft, meaning that it has a reduced fuel burn and takeoff weight [6, 7]. Research indicates that the aerodynamic efficiency gains of the Flying-V range between 10% and 25% compared to conventional tube-and-wing aircraft of similar size and weight. Additionally, the location of the engines on top of the wing reduces the noise level [2, 7]. The preliminary design of the Flying-V can be observed in Fig. 1.

Currently, the main Flying-V design challenge is centred on the improvement of the stability and handling qualities of this novel aircraft design for certification and qualification purposes. Previous research is conducted on the stability and handling qualities of the full-size aircraft by designing a six degrees-of-freedom flight dynamic simulation model [8]. This flight dynamic simulation model makes use of an aerodynamic model that combines aerodynamic coefficients obtained from the Vortex Lattice Method with wind tunnel experiments. This combined aerodynamic model is able to capture the undesired behaviour of the Flying-V obtained from previous research, such as the unstable Dutch roll mode and longitudinal unstable behaviour [9–11]. The stability and handling qualities are assessed during cruise and approach conditions at the forward and aft centre of gravity locations obtained from previous research [9]. It is

*Graduate Student, Faculty of Aerospace Engineering at Delft University of Technology, s.vanovereem@student.tudelft.nl

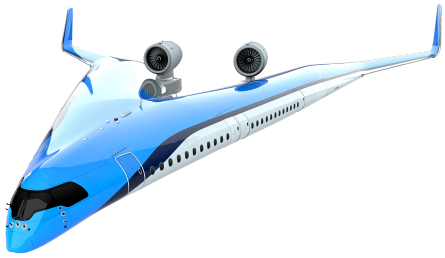

Fig. 1 The Flying-V aircraft.*

concluded that the Flying-V is not able to adhere to all stability and handling qualities during cruise and approach conditions at the forward and aft centre of gravity location. The stability and handling quality assessment is based on the trimmability of the Flying-V, the responses of the eigenmodes, and handling qualities such as the Control Anticipation Parameter (CAP). The analysis performed previously shows that during approach at the forward centre of gravity location, the Flying-V meets the stability and handling qualities the least. At this flight condition, an elevon deflection of 20.2° is required to trim the aircraft. Due to an elevon deflection limit of 25°, this elevon trim deflection reduces the manoeuvrability of the Flying-V. Besides that, the phugoid mode and Dutch roll mode are unstable [8]. To improve the stability and handling qualities of the Flying-V, there is a necessity to design a flight control system. This flight control system is required to cope with the inherent nonlinear behaviour of the aerodynamic model used for the flight dynamic simulation. Furthermore, due to the assumptions made during the design of the flight dynamic simulation model and the uncertainties present in the aerodynamic model, the flight control system has to cope with these model uncertainties to diminish performance degradation [8].

A couple of decades ago, almost all flight control systems for aircraft were designed using classical (linear) control techniques [12]. Even though the systems involved with aircraft control are nonlinear, it is still possible to apply a linear controller to this system by making the key assumption that the linear controller is only applied to a small range within the complete flight envelope [13]. This requires the design of multiple linear controllers to cover the complete flight envelope and construct a gain schedule by interpolating the gains with respect to the flight condition. This procedure is very time consuming, expensive, and is not flexible regarding design changes [14]. Furthermore, during the design of a linear controller, it is necessary to assume that the parameters of the aircraft model are well known, which is not the case for the Flying-V. Therefore, it may exhibit performance degradation or instability [13]. To overcome the shortcomings of linear controllers, several nonlinear control methods have emerged over the past years. One of these nonlinear control methods is known as Incremental Nonlinear Dynamic Inversion (INDI). INDI is a sensor-based control method that requires less model information and can therefore improve the system robustness against model uncertainties [15]. This is especially useful for the control system design of the Flying-V due to the assumptions and uncertainties present in the flight dynamic simulation model.

The contribution of this study to research related to the Flying-V consists of the design of an Incremental Nonlinear Dynamic Inversion (INDI) controller to improve the stability and handling qualities of the Flying-V during approach at the forward centre of gravity location. This flight condition is selected due to the unfavourable stability and handling qualities obtained from previous research [8]. The controller is assessed by first analysing the stability and handling qualities of the controlled aircraft. After that, the robustness of the controller is assessed by analysing the effects of aerodynamic uncertainty on the attitude tracking error of the Flying-V aiming to follow a reference trajectory.

The rest of this paper is structured as follows. Section II elaborates on the Flying-V flight dynamic simulation model and the essential stability and handling qualities obtained from previous research. Besides that, the flight control system design and robustness analysis methodology are discussed. Section III discusses the stability and handling qualities of the controlled Flying-V and shows the robustness of the flight control system. Finally, conclusions are discussed in section IV and recommendations for further research are given in section V.

II. Methodology

In this section, the methodology to design an Incremental Nonlinear Dynamic Inversion (INDI) flight control system is discussed. First of all, section II.A elaborates on the layout of the Flying-V. Secondly, section II.B talks about the dynamic simulation model used for the flight control system design. Furthermore, section II.C shows the essential stability and handling qualities of the Flying-V. Besides that, section II.D develops the methodology for the flight control system design. After that, the robustness assessment is discussed in section II.E. Finally, section II.F elaborates on the assumptions and limitations of the controller design.

A. Flying-V Layout

In Fig. 2* it is possible to observe the general layout of the Flying-V used for the analysis in this research. The figure shows the V-shaped wing planform with engines mounted on top of the aircraft. These engines can be used to control the airspeed. Besides that, the Flying-V consists of a set of inboard elevons (CS1) and outboard elevons (CS2) mounted on each side of the wing. Both elevons can be used for pitch control, whereas only the outboard elevons are used for roll control. Furthermore, due to the tailless design of the aircraft, the rudders (CS3) are integrated into the winglets and can be used for yaw control. The forward centre of gravity is located 29.4 m from the nose of the aircraft. The aft centre of gravity is located 31.7 m from the nose of the aircraft.

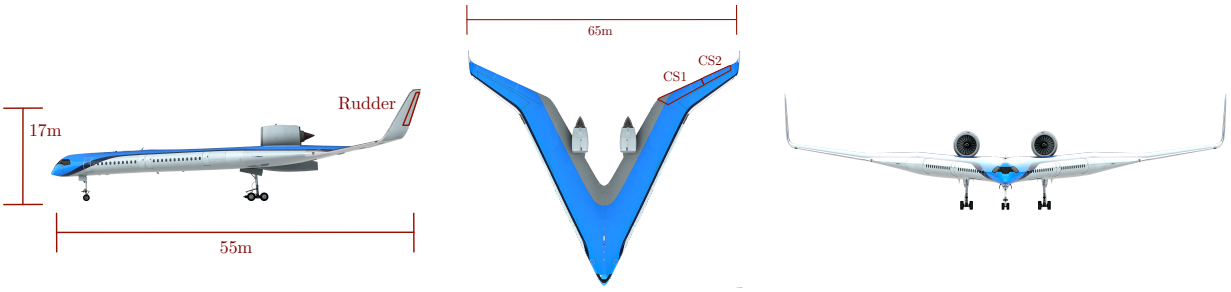

Fig. 2 Flying-V layout.*

B. Flight Dynamic Simulation Model

To develop a flight control system that is able to improve the stability and handling qualities of the Flying-V, a six degrees-of-freedom flight dynamic simulation model is used. The development of this simulation model is discussed in [8]. The simulation model can be used for the cruise condition and approach condition for several centre of gravity locations. Besides that, to estimate the components of the inertia matrix, the lumped mass method is used [8].

Previous research dictates that the undesired behaviour of the Flying-V consists of an unstable Dutch roll mode and longitudinal instability for angles of attack larger than 20°. The unstable Dutch roll is obtained from a stability and handling quality analysis using aerodynamic coefficients obtained from the Vortex Lattice Method [9]. Besides that, the longitudinal unstable behaviour of the aircraft was observed during wind tunnel experiments [11, 16] and captured in an aerodynamic model obtained from these wind tunnel experiments [10]. These aerodynamic models are combined into a single aerodynamic model that is able to capture both the unstable Dutch roll and longitudinal instability for angles of attack larger than 20° for the full-scale aircraft.

C. Stability and Handling Quality analysis

In this subsection, the stability and handling qualities of the Flying-V are discussed. In section II.C.1 the location of the eigenvalues are shown. After that, section II.C.2 shows an assessment of the eigenmodes by comparing the eigenmodes with military standards. Finally, section II.C.3 elaborates on the handling qualities of the Flying-V by analysing the Control Anticipation Parameter.

*https://www.tudelft.nl/lr/flying-v

1. Eigenvalue Analysis

Table 1 shows the eigenvalues obtained from the linearised equations of motion during approach at the forward centre of gravity location [8]. Besides that, the damping ratio and natural frequency of the modes are displayed. This specific flight condition is considered the worst flight condition due to the large elevon deflection required to trim the Flying-V and undesired eigenmodes. Namely, from the eigenvalues shown in Table 1 it can directly be deduced that the phugoid mode and Dutch roll mode are unstable. Also, the spiral mode is unstable, but as is discussed in Section II.C.2 this mode is able to adhere to military standards.

Table 1 Eigenvalues at forward centre of gravity location during approach [8].

Eigenmode	Eigenvalue	Damping ratio	Natural Frequency
Short Period	$-0.47 \pm 0.50i$	0.683	0.681
Phugoid	$4.0 \cdot 10^{-4} \pm 0.16$	$-2.31 \cdot 10^{-3}$	0.161
Dutch roll	$8.1 \cdot 10^{-2} \pm 0.99i$	$-8.14 \cdot 10^{-2}$	0.992
Aperiodic Roll	-0.79	-	-
Spiral	$2.04 \cdot 10^{-2}$	-	-

2. Modes Response Analysis

The flying quality analysis performed for the Flying-V at the forward centre of gravity location during approach is summarised in Table 2 [8, 17]. This table shows that the short period mode had level 1 flying qualities. Besides that, the phugoid mode and Dutch roll mode cannot be rated using these requirements due to the short (unstable) period of the phugoid mode and unstable behaviour of the Dutch roll mode. Finally, the aperiodic roll mode and spiral mode show level 1 flying qualities.

Table 2 Flying-V flying qualities during approach at forward centre of gravity location [8, 17].

Eigenmode	**Values Flying-V**	**Requirements**
Short Period	$\varsigma_{sp} = 6.83 \cdot 10^{-1}$	Level 1: $0.5 < \varsigma_{sp} < 1.3$
		Level 2: $0.35 < \varsigma_{sp} < 2.0$
		Level 3: $\varsigma_{sp} > 0.25$
Phugoid	Unstable but $T_{ph} = 39.0s$	Level 1: $\varsigma_{ph} > 0.04$
		Level 2: $\varsigma_{ph} > 0$
		Level 3: Unstable but $T_{ph} > 55s$
Dutch roll	Unstable	Level 1: $\varsigma_d > 0.08$ $\varsigma_d\omega_d > 0.10$ $\omega_d > 0.5$
		Level 2: $\varsigma_d > 0.02$ $\varsigma_d\omega_d > 0.05$ $\omega_d > 0.5$
		Level 3: $\varsigma_d > 0$ $\omega_d > 0.4$
Aperiodic Roll	$T_r = 1.26s$	Level 1: $T_r < 1.4s$
		Level 2: $T_r < 3.0s$
		Level 3: $T_r < 10.0s$
Spiral	$T_s = 42.6s$	Level 1: $T_s > 17.3s$
		Level 2: $T_s > 11.5s$
		Level 3: $T_s > 7.2s$

3. Handling Quality Analysis

The handling qualities of an aircraft are considered as a description of the adequacy of the short term dynamic response to controls during the execution of a flight task [18]. The handling qualities discussed in this research involve

quantitative handling qualities as these quantitative methods do not require pilot-in-the-loop experiments. The handling quality assessed for this research is the Control Anticipation Parameter (CAP). This is a measure of the manoeuvrability of the aircraft. In case the CAP is too high, the aircraft's response is faster than would be expected by the pilot resulting in understeering. On the other hand, in case the CAP is too low, the aircraft's response is sluggish, which results in oversteering [9]. The Control Anticipation Parameter is equal to 0.16 at the forward centre of gravity location during approach. This is also shown in Fig. 3, where it can be observed that the CAP is at the border of the Level 1 handling qualities region [8].

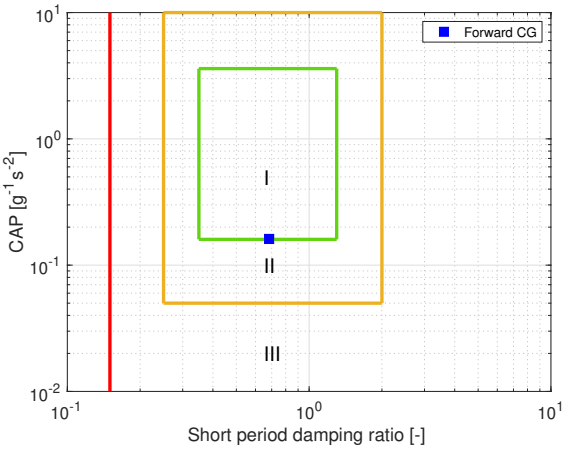

Fig. 3 Control Anticipation Parameter at forward centre of gravity location during cruise [8].

D. INDI Flight Control System Design

In this subsection, the design of the INDI flight control system is discussed. First of all, the INDI derivation is shown in section II.D.1. After that, section II.D.2 elaborates the inner-loop stability augmentation system design. Finally, the outer-loop control augmentation system design is discussed in section II.D.3.

1. INDI Derivation

Incremental Nonlinear Dynamic Inversion (INDI) is a sensor based control method which is derived using an incremental dynamic equation. INDI has reduced model dependency than Nonlinear Dynamic Inversion (NDI) and therefore has an improved robustness of the closed-loop system compared to an NDI controller [19]. One of the differences between an NDI controlled system and INDI controlled system originates from the control input. The NDI controller provides a complete command control input, whereas an INDI controller considers the influence of increments of control commands in the dynamics. These increments in the control commands are provided as a function of the error of the controlled variables [20]. To derive the equations for an INDI controller, it is possible to start with the general equation for a nonlinear system shown in Eq. (1).

$$\dot{\boldsymbol{x}} = \boldsymbol{f}(\boldsymbol{x}, \boldsymbol{u}) \tag{1}$$

Taking the Taylor series expansion of this equation at the current time point, it is possible to linearise the system as shown in Eq. (2).

$$\begin{aligned} \dot{\boldsymbol{x}} &\approx \boldsymbol{f}(\boldsymbol{x}_0, \boldsymbol{u}_0) + \left.\frac{\partial \boldsymbol{f}(\boldsymbol{x}, \boldsymbol{u})}{\partial \boldsymbol{x}}\right|_{\boldsymbol{x}=\boldsymbol{x}_0, \boldsymbol{u}=\boldsymbol{u}_0} (\boldsymbol{x} - \boldsymbol{x}_0) + \left.\frac{\partial \boldsymbol{f}(\boldsymbol{x}, \boldsymbol{u})}{\partial \boldsymbol{u}}\right|_{\boldsymbol{x}=\boldsymbol{x}_0, \boldsymbol{u}=\boldsymbol{u}_0} (\boldsymbol{u} - \boldsymbol{u}_0) \\ &= \dot{\boldsymbol{x}}_0 + \boldsymbol{F}(\boldsymbol{x}_0, \boldsymbol{u}_0)(\boldsymbol{x} - \boldsymbol{x}_0) + \boldsymbol{G}(\boldsymbol{x}_0, \boldsymbol{u}_0)(\boldsymbol{u} - \boldsymbol{u}_0) \end{aligned} \tag{2}$$

Using the time scale separation principle [21], this equation can be further simplified when the system sample rate is considered to be high, resulting in Eq. (3).

$$\dot{\boldsymbol{x}} \approx \dot{\boldsymbol{x}}_0 + \boldsymbol{G}(\boldsymbol{x}_0, \boldsymbol{u}_0)(\boldsymbol{u} - \boldsymbol{u}_0) = \dot{\boldsymbol{x}}_0 + \boldsymbol{G}(\boldsymbol{x}_0, \boldsymbol{u}_0)\Delta\boldsymbol{u} \tag{3}$$

Eq. (3) can consequently be rearranged, where the state derivative ($\dot{\boldsymbol{x}}$) is set as a virtual control input ($\boldsymbol{\nu}$). After implementing INDI, the original nonlinear system becomes a linear integral chain. Therefore, the virtual control input can be designed using a state-feedback linear controller. Eventually, Eq. (4) is obtained.

$$\Delta\boldsymbol{u} = \boldsymbol{G}^{-1}(\boldsymbol{x}_0, \boldsymbol{u}_0)(\boldsymbol{\nu} - \dot{\boldsymbol{x}}_0) \tag{4}$$

This control law results in increments of the control commands, meaning that these changes must be added to the current reference command in order to obtain the full new control command input. This means that the total control command can be obtained using Eq. (5).

$$\boldsymbol{u} = \boldsymbol{u}_0 + \Delta\boldsymbol{u} = \boldsymbol{u}_0 + \boldsymbol{G}^{-1}(\boldsymbol{x}_0, \boldsymbol{u}_0)(\boldsymbol{\nu} - \dot{\boldsymbol{x}}_0) \tag{5}$$

In Eq. (5) it can be observed that the INDI controller does not depend on the exact knowledge of the system dynamics ($\boldsymbol{f}(\boldsymbol{x})$). Instead, the control strategy is merely dependent on the sensor measurements of the time derivative of the state ($\dot{\boldsymbol{x}}_0$) and actuator dynamics measurements ($\boldsymbol{u}_0$). Therefore, the dependency of the closed-loop system has decreased resulting in improved performance in case of model mismatch and model uncertainties. However, it needs to be noted that this controller is not completely independent of the model as changes in the system dynamics are reflected in the derivative of the state vector ($\dot{\boldsymbol{x}}_0$). On the other side, the performance of this controller is expected to be more sensitive to sensor aspects such as noise, bias, and misalignments than an NDI controller [20]. The layout of the closed-loop system including an INDI controller is shown in Fig. 4.

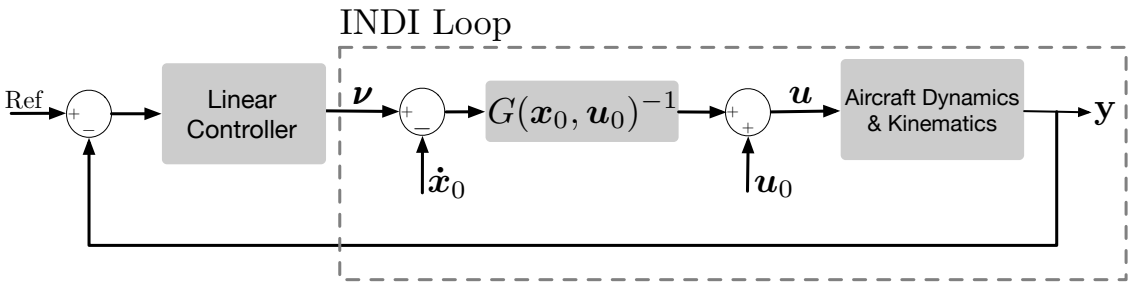

Fig. 4 Block diagram for INDI controller.

2. Stability Augmentation System Design

The stability augmentation system consists of an INDI controller used to control the angular rates and a Proportional-Integral-Derivative (PID) controller to control the airspeed. Due to the slow engine dynamics, it is not possible to control the airspeed using INDI. Therefore, it is decided to use a PID controller to control the airspeed. The angular rate loop is based on the rotational equations of motion as shown in Eq. (6). In this equation, $\boldsymbol{\omega}$ represents the angular rates, $\boldsymbol{J}$ is the inertia matrix, and $\boldsymbol{M}$ represents the moment vector acting on the Flying-V.

$$\dot{\boldsymbol{\omega}} = \boldsymbol{J}^{-1}\boldsymbol{M} - \boldsymbol{J}^{-1}(\boldsymbol{\omega} \times \boldsymbol{J}\boldsymbol{\omega}) \tag{6}$$

Consequently, to obtain the matrix $\boldsymbol{G}(\boldsymbol{x}_0, \boldsymbol{u}_0)$ shown in Eq. (2), it is necessary to differentiate the nonlinear differential equation with respect to the inputs (δ_{CS1}, δ_{CS2}, and δ_{CS3}). After that, the control surface inputs can be calculated. This results in Eq. (7) and Eq. (8), respectively. In Eq. (7) it can be observed that the inboard elevons (δ_{CS1}) are only used for pitch control. Besides that, the outboard elevons (δ_{CS2}) are used for roll-, pitch-, and yaw control. Furthermore, the control surfaces attached to the winglets (δ_{CS3}) are used for roll- and yaw control. Also, ρ is the atmospheric density, V is the total airspeed (which can also be represented as $V = \sqrt{u^2 + v^2 + w^2}$), S is the wing surface area, and $\bar{c}$ is the mean aerodynamic chord. The block diagram of the stability augmentation system is shown in Fig. 5. The actuator dynamics and engine dynamics are modelled using a first-order lag system with a bandwidth of 35.2 rad/s [22] and 5.0 rad/s respectively [23]. Besides that, the saturation values correspond to [-25°, 25°] for the control surfaces [10] and [0 N, $3.79 \cdot 10^5$ N] for the engines [24]. The gains of the stability augmentation system are tuned manually. The

gains are tuned by first increasing the proportional gain such that the Flying-V is able to track a reference angular rate or airspeed. After that, the oscillations are removed by increasing the derivative gain. In case any steady state error is present, this is removed using the integral gain. The gains of the stability augmentation system are shown in Table 3.

$$\boldsymbol{G}_{\omega}(\boldsymbol{x}_0, \boldsymbol{u}_0) = \boldsymbol{J}^{-1}\frac{1}{2}\rho V^2 S\bar{c}\begin{bmatrix} C_{l_{\delta_{\text{CS1}}}} & C_{l_{\delta_{\text{CS2}}}} & C_{l_{\delta_{\text{CS3}}}} \\ C_{m_{\delta_{\text{CS1}}}} & C_{m_{\delta_{\text{CS2}}}} & C_{m_{\delta_{\text{CS3}}}} \\ C_{n_{\delta_{\text{CS1}}}} & C_{n_{\delta_{\text{CS2}}}} & C_{n_{\delta_{\text{CS3}}}} \end{bmatrix} = \boldsymbol{J}^{-1}\frac{1}{2}\rho V^2 S\bar{c}\begin{bmatrix} 0 & C_{l_{\delta_{\text{CS2}}}} & C_{l_{\delta_{\text{CS3}}}} \\ C_{m_{\delta_{\text{CS1}}}} & C_{m_{\delta_{\text{CS2}}}} & 0 \\ 0 & C_{n_{\delta_{\text{CS2}}}} & C_{n_{\delta_{\text{CS3}}}} \end{bmatrix} \tag{7}$$

$$\boldsymbol{u} = \boldsymbol{u}_0 + \frac{2\boldsymbol{J}}{\rho V^2 S\bar{c}}\begin{bmatrix} 0 & C_{l_{\delta_{\text{CS2}}}} & C_{l_{\delta_{\text{CS3}}}} \\ C_{m_{\delta_{\text{CS1}}}} & C_{m_{\delta_{\text{CS2}}}} & 0 \\ 0 & C_{n_{\delta_{\text{CS2}}}} & C_{n_{\delta_{\text{CS3}}}} \end{bmatrix}^{-1}(\boldsymbol{\nu} - \dot{\boldsymbol{\omega}}) \tag{8}$$

$$\boldsymbol{u} = \begin{bmatrix} \delta_{\text{CS1}} \\ \delta_{\text{CS2}} \\ \delta_{\text{CS3}} \end{bmatrix}; \quad \boldsymbol{\nu} = \begin{bmatrix} \nu_p \\ \nu_q \\ \nu_r \end{bmatrix}; \quad \boldsymbol{\omega} = \begin{bmatrix} p \\ q \\ r \end{bmatrix}$$

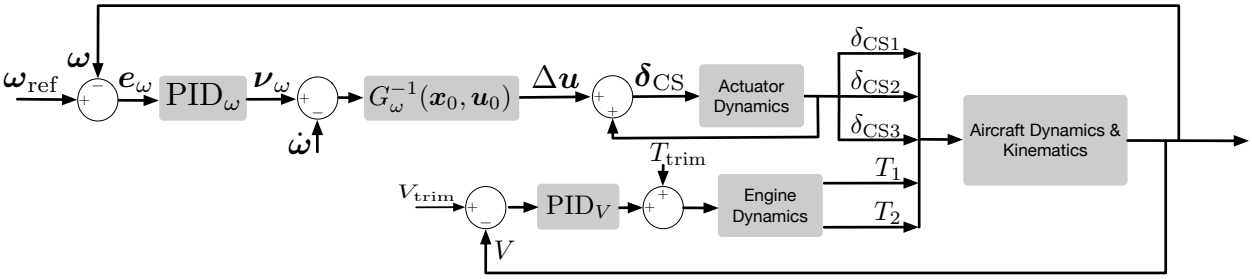

Fig. 5 INDI controller inner-loops.

3. Control Augmentation System Design

The control augmentation outer-loop consists of the control of the roll angle, flight path angle, and sideslip angle. The choice for controlling these variables is obtained from the Airbus A350-900 aircraft, which is used as a reference aircraft for the design of the Flying-V [2, 25]. Besides that, the flight path angle controller can be used to maintain the required flight path angle during approach [8, 17], and keeping the sideslip angle at zero results in coordinated flight [26]. The time-scale separation principle is used to obtain the control augmentation loop around the stability augmentation inner-loops. The principle of time-scale separation implies the use of several loops within the controller to take into account the fast dynamics and slow dynamics of the system. A variable is said to have slow dynamics in case the control effectiveness on the dynamics is low. In case a variable is said to have fast dynamics, the control effectiveness on the dynamics is high. This leads to a control system where the outputs of the slow outer-loop are used as a reference for the fast inner-loop [26].

The relation between the attitude angles and angular rates depends on the kinematic relation shown in Eq. (9). Because there is no model uncertainty nor error in the kinematic equations, this loop is based on Nonlinear Dynamic Inversion (NDI) instead of INDI [22].

$$\underbrace{\begin{bmatrix} \dot{\phi} \\ \dot{\theta} \end{bmatrix}}_{\begin{bmatrix} \nu_\phi & \nu_\theta \end{bmatrix}^T} = \underbrace{\begin{bmatrix} 1 & \sin\phi\tan\theta & \cos\phi\tan\theta \\ 0 & \cos\phi & -\sin\phi \end{bmatrix}}_{\begin{bmatrix} a_\phi(\boldsymbol{x}) & a_\theta(\boldsymbol{x}) \end{bmatrix}^T}\begin{bmatrix} p \\ q \\ r \end{bmatrix} \tag{9}$$

The sideslip dynamic inversion loop can be used to compensate the sideslip angle to perform coordinated turns, whereas the roll angle and flight path angle can be controlled. The sideslip angle can be computed as is shown in Eq. (10). In this equation, β represents the sideslip angle and v is the lateral body velocity component.

$$\beta = \arcsin \frac{v}{V} \tag{10}$$

Taking the derivative of the sideslip angle with respect to time results in Eq. (11). This equation can be rewritten as Eq. (12).

$$\dot{\beta} = \frac{\dot{v}V - v\dot{V}}{V\sqrt{u^2+w^2}} = \frac{\dot{v}}{\sqrt{u^2+w^2}} - \frac{v(u\dot{u}+v\dot{v}+w\dot{w})}{(u^2+v^2+w^2)\sqrt{u^2+w^2}} \tag{11}$$

$$\underbrace{\dot{\beta}}_{\nu_\beta} = \underbrace{\left(\frac{1}{\sqrt{u^2+w^2}}\right)(A_x+A_y+A_z)}_{b_\beta(\boldsymbol{x})} + \underbrace{\begin{bmatrix} \frac{w}{\sqrt{u^2+w^2}} & 0 & \frac{-u}{\sqrt{u^2+w^2}} \end{bmatrix}}_{a_\beta(\boldsymbol{x})} \begin{bmatrix} p \\ q \\ r \end{bmatrix} \tag{12}$$

$$\begin{aligned} A_x &= \frac{uv}{V^2}\left(\frac{F_x}{m} - g\sin\theta\right) \\ A_y &= \left(1 - \frac{v^2}{V^2}\right)\left(\frac{F_y}{m} + g\sin\phi\cos\theta\right) \\ A_z &= -\frac{vw}{V^2}\left(\frac{F_z}{m} + g\cos\phi\cos\theta\right) \end{aligned}$$

Combining Eq. (9) and Eq. (12) results in Eq. (13). To control the flight path angle, another control loop is added to the system including a PID controller that is used for flight path angle control. The gains for the control augmentation system are tuned similarly to the stability augmentation system and are shown in Table 3. Besides that, the block diagram of the control augmentation loop is shown in Fig. 6.

$$\boldsymbol{\omega}_{\text{ref}} = \begin{bmatrix} a_\phi(\boldsymbol{x}) \\ a_\theta(\boldsymbol{x}) \\ a_\beta(\boldsymbol{x}) \end{bmatrix}^{-1} \left(\begin{bmatrix} \nu_\phi \\ \nu_\theta \\ \nu_\beta \end{bmatrix} - \begin{bmatrix} 0 \\ 0 \\ b_\beta(\boldsymbol{x}) \end{bmatrix} \right) \tag{13}$$

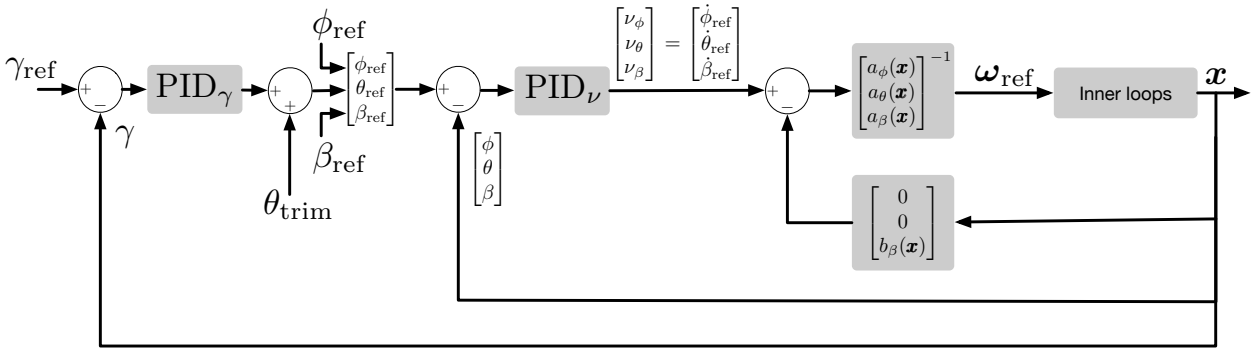

Fig. 6 INDI guidance control loops.

E. Robustness Analysis

Due to the assumptions made during the construction of the aerodynamic model and the inherent uncertainties present in the aerodynamic coefficients obtained from the Vortex Lattice Method and wind tunnel experiments, one of the main components of uncertainty in the simulation model is the aerodynamic model [8]. As is discussed in this section, the INDI controller is able to be linearised under the influence of aerodynamic uncertainties [19]. To demonstrate the influence of aerodynamic uncertainties, the general description for a nonlinear system can be observed in Eq. (1). Adding uncertainties to the system results in Eq. (14), where $\boldsymbol{f}_n(\boldsymbol{x},\boldsymbol{u})$ and $\Delta\boldsymbol{f}(\boldsymbol{x},\boldsymbol{u})$ represent the nominal system and aerodynamic uncertainties respectively. Taking the Taylor series of this equation, it is possible to linearise

Table 3 Controller gains for flight control system.

	PID_ω			PID_V	PID_ν			PID_γ
	p	q	r		ϕ	θ	β	
K_p	1	1	2	50000	1	1	1	1
K_i	0.1	0	0	0	0	0	0	0.2
K_d	0	0	0	30000	1	2	0	0.02

the system under influence of uncertainties as shown in Eq. (15). When the system sample rate is considered to be high this equation can be further simplified using the time scale separation principle. Applying the time scale separation principle results in Eq. (16).

$$\dot{\boldsymbol{x}} = \boldsymbol{f}_n(\boldsymbol{x}, \boldsymbol{u}) + \Delta \boldsymbol{f}(\boldsymbol{x}, \boldsymbol{u}) \tag{14}$$

$$\begin{aligned}\dot{\boldsymbol{x}} &\approx \boldsymbol{f}_n(\boldsymbol{x}_0, \boldsymbol{u}_0) + \Delta \boldsymbol{f}(\boldsymbol{x}_0, \boldsymbol{u}_0) + \left.\frac{\partial \boldsymbol{f}_n(\boldsymbol{x}, \boldsymbol{u}) + \Delta \boldsymbol{f}(\boldsymbol{x}, \boldsymbol{u})}{\partial \boldsymbol{x}}\right|_{\boldsymbol{x}=\boldsymbol{x}_0, \boldsymbol{u}=\boldsymbol{u}_0} (\boldsymbol{x} - \boldsymbol{x}_0) + \left.\frac{\partial \boldsymbol{f}_n(\boldsymbol{x}, \boldsymbol{u}) + \Delta \boldsymbol{f}(\boldsymbol{x}, \boldsymbol{u})}{\partial \boldsymbol{u}}\right|_{\boldsymbol{x}=\boldsymbol{x}_0, \boldsymbol{u}=\boldsymbol{u}_0} (\boldsymbol{u} - \boldsymbol{u}_0) \\ &= \dot{\boldsymbol{x}}_0 + (\boldsymbol{F}_n(\boldsymbol{x}_0, \boldsymbol{u}_0) + \Delta \boldsymbol{F}(\boldsymbol{x}_0, \boldsymbol{u}_0))(\boldsymbol{x} - \boldsymbol{x}_0) + (\boldsymbol{G}_n(\boldsymbol{x}_0, \boldsymbol{u}_0) + \Delta \boldsymbol{G}(\boldsymbol{x}_0, \boldsymbol{u}_0))(\boldsymbol{u} - \boldsymbol{u}_0)\end{aligned} \tag{15}$$

$$\dot{\boldsymbol{x}} \approx \dot{\boldsymbol{x}}_0 + (\boldsymbol{G}_n(\boldsymbol{x}_0, \boldsymbol{u}_0) + \Delta \boldsymbol{G}(\boldsymbol{x}_0, \boldsymbol{u}_0))(\boldsymbol{u} - \boldsymbol{u}_0) = \dot{\boldsymbol{x}}_0 + (\boldsymbol{G}_n(\boldsymbol{x}_0, \boldsymbol{u}_0) + \Delta \boldsymbol{G}(\boldsymbol{x}_0, \boldsymbol{u}_0))\Delta \boldsymbol{u} \tag{16}$$

Eq. (16) shows that an INDI controller subjected to aerodynamic uncertainty does not depend on the system dynamics. Instead, the INDI controller depends on onboard measurements ($\dot{\boldsymbol{x}}_0$) and the control effectiveness matrix ($\boldsymbol{G}_n(\boldsymbol{x}_0, \boldsymbol{u}_0) + \Delta \boldsymbol{G}(\boldsymbol{x}_0, \boldsymbol{u}_0)$). Note that uncertainties applied to the system dynamics are still indirectly reflected in the onboard measurements [27]. Due to the robustness of an INDI controller, it is not required to obtain a very accurate model of the Flying-V. The equation to obtain a specific aerodynamic coefficient C_* is given in Eq. (17). In this equation, C_* represents one of the force or moment coefficients (C_X, C_Y, C_Z, C_L, C_M, C_N). Besides that, this equation shows that sub-coefficient depends on the angle of attack (α), angle of sideslip (β), roll rate (p), pitch rate (q), yaw rate (r), and deflection for the different control surfaces (δ_{CS1}, δ_{CS2}, and δ_{CS3}). To apply aerodynamic uncertainty to the aerodynamic coefficients, Eq. (18) is used. In this equation, $C_*(\Delta)$ represents one of the sub-coefficients, whereas $\hat{C}_*(\Delta)$ represents the sub-coefficient subjected to aerodynamic uncertainty. Besides that, n represents the scaling factor and $N(0, 1)$ represents a normal distribution with a mean equal to zero and a standard deviation equal to one. Previous research dictates a maximum error of 25% during the validation process of the aerodynamic coefficients obtained from the Vortex Lattice Method by comparing these coefficients to aerodynamic coefficients obtained from wind tunnel experiments [9]. Therefore, it is decided to vary the scaling factor in the following range: $\begin{bmatrix}0.0 & 0.05 & 0.10 & 0.15 & 0.20 & 0.25\end{bmatrix}$. The result of this methodology is that aerodynamic uncertainty is applied to each aerodynamic sub-coefficient by adding a normal distribution to the coefficient with a mean equal to zero and standard deviation ranging between 0% and 25% of $C_*(\Delta)$.

$$C_* = C_*(\alpha) + C_*(\alpha, \beta) + C_*(\alpha, p) + C_*(\alpha, q) + C_*(\alpha, r) + C_*(\alpha, \delta_{\text{CS1}}) + C_*(\alpha, \delta_{\text{CS2}}) + C_*(\alpha, \delta_{\text{CS3}}) \tag{17}$$

$$\hat{C}_*(\Delta) = C_*(\Delta)(1 + nN(0, 1)) \tag{18}$$

To analyse the robustness of the flight control system, a reference trajectory is designed for the flight path angle controller and roll angle controller, while maintaining coordinated flight ($\beta_{\text{ref}} = 0$). It is decided to design a 3211 manoeuvre for the flight path angle and roll angle reference trajectory. The magnitude of the 3211 manoeuvre is selected such that actuator saturation is taken into account. Namely, increasing the flight path angle or roll angle demand would result in higher actuator demands than possible due to saturation. The reference trajectories together with the nominal response of the INDI controlled Flying-V are displayed in Fig. 7. Besides that, the control surface deflections are shown in Fig. 8. Consequently, the Root-Mean-Squared Error (RMSE) is determined according to Eq. (19). In this equation,

N represents the total number of timesteps during a simulation run, x_{ref} is the reference state, and x represents the actual state.

$$\text{RMSE} = \sqrt{\frac{1}{N}\sum_{i=0}^{N}(x_{\text{ref}_i} - x_i)^2} \tag{19}$$

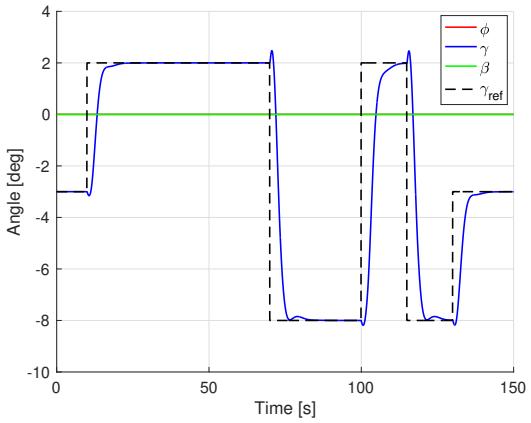

(a) Flight path angle reference trajectory and response.

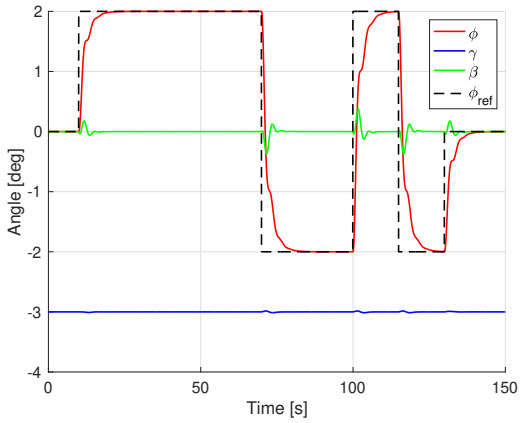

(b) Roll angle reference trajectory and response.

Fig. 7 Reference trajectories and Flying-V response for flight path angle and roll angle.

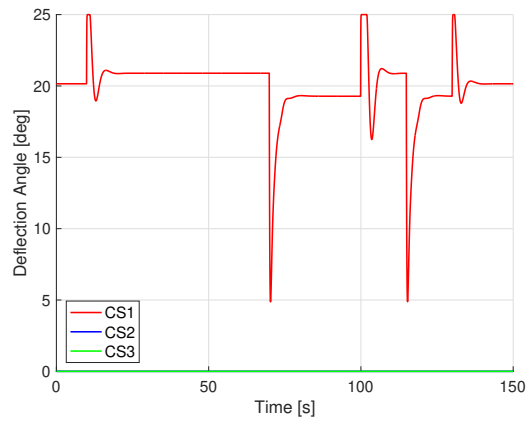

(a) Control surface deflections for flight path angle trajectory.

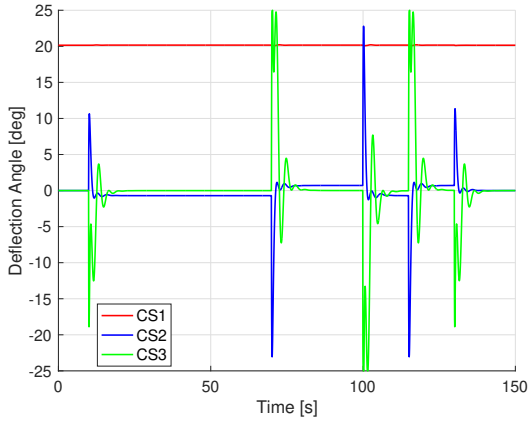

(b) Control surface deflections for roll angle trajectory.

Fig. 8 Control surface deflections for flight path angle and roll angle.

F. Assumptions and Limitations

During the design and assessment of the flight control system, several assumptions and therefore accompanying limitations have to be taken into account.

First of all, during the design of the control system, no sensor dynamics are taken into account. This means that the measurements obtained from the sensors are readily available. Besides that, the measurements are not contaminated with noise and are not biased. The stability of INDI controllers subjected to measurement time delay is an issue. Especially, in case the actuator measurements and the state derivative measurements are not equally delayed. Introducing

measurement time delay to the system results in a reduced stability region for the INDI controlled system [26].

Additionally, it is assumed that the Flying-V experiences a perfect atmosphere that corresponds to the International Standard Atmosphere without any turbulence. In reality, the Flying-V is likely to experience turbulence. Adding turbulence to the system deteriorates the tracking response of the Flying-V. Therefore, additional turbulence increases the RMSE of the tracking task [28].

Finally, when determining the robustness of the INDI controller to aerodynamic uncertainty, previous research dictates a maximum error of 25% between aerodynamic coefficients obtained from the Vortex Lattice Method and wind tunnel experiments [8, 9]. To compare these aerodynamic models it is necessary to assume that the relative density factor and the relative moment of inertia of both models are equal. Because these parameters are different, the actual maximum error between both aerodynamic models likely deviates from the value used in this research.

III. Results

In this section, the results obtained from the stability and handling quality analysis, and robustness assessment of the INDI controlled Flying-V are discussed. Section III.A discusses the stability and handling quality results. Besides that, the robustness results are shown in Section III.B.

A. Stability and Handling Quality Results

In this section, the stability and handling quality results are discussed. In Section III.A.1, the results from the eigenvalue analysis are shown and in Section III.A.2 the handling qualities are discussed.

1. Eigenvalue Results

As discussed in Section II.C, during approach at the forward centre of gravity location, the phugoid mode and Dutch roll mode of the Flying-V are unstable. To stabilise these modes, a stability augmentation system is applied to the aircraft as discussed in Section II.D.2. This section analyses how the eigenmodes of the Flying-V are affected by the application of the phugoid damper and yaw damper to the aircraft. In Fig. 9, the location of the eigenvalues for the uncontrolled and controlled system are displayed. These figures show that application of the stability augmentation system results in a stabilised phugoid mode and Dutch roll mode.

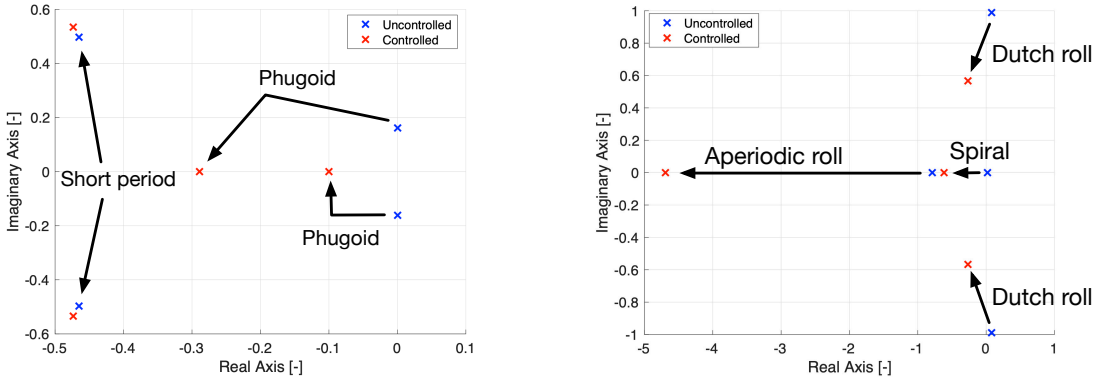

(a) Longitudinal Eigenvalues

(b) Lateral-directional Eigenvalues.

Fig. 9 Eigenvalue shift due to phugoid- and yaw dampers.

2. Modes Response Results

Besides that, the handling qualities of the controlled Flying-V are compared to military standards as shown in Table 4. In this table, the flying quality level of the controlled Flying-V is bold. This table shows that the damping ratio of the short period is equal to $\varsigma_{sp} = 6.63 \cdot 10^{-1}$, resulting in Level 1 handling qualities. Besides that, due to the phugoid damper, the phugoid mode is real and therefore has a damping ratio equal to $\varsigma_{ph} = 1.0$, resulting in Level 1 handling qualities. Furthermore, the application of the yaw damper stabilises the Dutch roll mode resulting in a damping ratio

and natural frequency of $\varsigma_d = 0.42$ and $\omega_d = 0.57$ rad/s. Therefore, the Dutch roll mode is also rated Level 1. Also, the aperiodic roll mode has a characteristic time constant equal to $T_r = 0.21s$, indicating that this mode is rated Level 1. Finally, because the spiral mode is stable, it is rated Level 1.

Table 4 Flying-V flying qualities including a phugoid damper and yaw damper [17].

Eigenmode	Values Flying-V	Requirements		
Short Period	$\varsigma_{sp} = 6.63 \cdot 10^{-1}$	**Level 1:**	**$0.5 < \varsigma_{sp} < 1.3$**	
		Level 2:	$0.35 < \varsigma_{sp} < 2.0$	
		Level 3:	$\varsigma_{sp} > 0.25$	
Phugoid	$\varsigma_{ph} = 1.0$	**Level 1:**	**$\varsigma_{ph} > 0.04$**	
		Level 2:	$\varsigma_{ph} > 0$	
		Level 3:	Unstable but $T_{ph} > 55s$	
Dutch roll	$\varsigma_d = 0.42$ and $\omega_d = 0.57$ rad/s	**Level 1:**	**$\varsigma_d > 0.08$**	**$\varsigma_d\omega_d > 0.10$** **$\omega_d > 0.5$**
		Level 2:	$\varsigma_d > 0.02$	$\varsigma_d\omega_d > 0.05$ $\omega_d > 0.5$
		Level 3:	$\varsigma_d > 0$	$\omega_d > 0.4$
Aperiodic Roll	$T_r = 0.21s$	**Level 1:**	**$T_r < 1.4s$**	
		Level 2:	$T_r < 3.0s$	
		Level 3:	$T_r < 10.0s$	
Spiral	Stable	**Level 1:**	**$T_s > 17.3s$**	
		Level 2:	$T_s > 11.5s$	
		Level 3:	$T_s > 7.2s$	

B. Robustness Results

As discussed in section II.E, the robustness of the flight control system is determined by applying aerodynamic uncertainty to each aerodynamic coefficient. The aerodynamic uncertainty is determined by adding a normal distribution to each aerodynamic coefficient with a mean equal to zero and standard deviation ranging between 0% and 25% of the value of each aerodynamic coefficient. Consequently, 100 runs are performed for each standard deviation. This results in the boxplots shown in Fig. 10 and Fig. 11 for the flight path angle trajectory and roll angle trajectory respectively.

1. Flight Path Angle Robustness

In Fig. 10 the results of the robustness analysis applied to the flight path angle trajectory are shown. Fig. 10a presents the complete boxplots for the flight path angle trajectory, whereas Fig. 10b has zoomed in on the boxplots. In these figures, the RMSE is displayed for each n-factor as discussed in Eq. (18), ranging from 0 to 0.25. Looking at Fig. 10a it is possible to observe an increasing number of outliers with increasing n-factor. These outliers originate from the deflection limits of the control surfaces. In case the effectiveness of the control surfaces is reduced, a larger deflection is required to obtain the same pitch rate demand. However, the control surface deflection limit is equal to 25 degrees. This means that in case the control surface deflection demand is larger than 25 degrees, this control surface deflection demand cannot be achieved, resulting in a larger RMSE. Besides that, Fig. 10b shows that the upper and lower limit of each boxplot tends to increase with increasing aerodynamic uncertainty, while the median remains similar. Even though the upper limit of the boxplot increases, it needs to be noted that the RMSE is still within the same order of magnitude as the nominal case. This indicates that the INDI controller is barely affected by the aerodynamic uncertainty applied to the aerodynamic coefficients.

2. Roll Angle Robustness

In Fig. 11, the results of the robustness applied to the roll angle trajectory are shown. Fig. 11a presents the complete boxplots for the roll angle trajectory, whereas Fig. 11b has zoomed in on the boxplots. Also in these figures, the RMSE is displayed for each n-factor as discussed in Eq. (18), ranging from 0 to 0.25. Also in Fig. 11a it is possible to observe

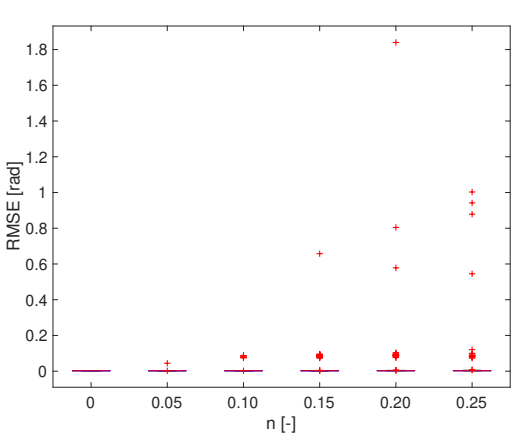

(a) Boxplot for flight path angle trajectory.

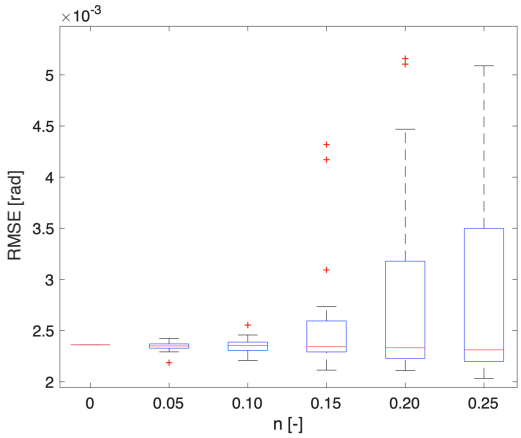

(b) Zoomed boxplot flight path angle.

Fig. 10 Boxplots showing flight path angle tracking error for aerodynamic uncertainty.

several outliers, indicating that these outliers are the results of elevon deflection demands that could not be met. Besides that, Fig. 11b shows similar results as Fig. 10b, where the RMSE increases with increasing n-factor. However, the numbers remain within the same order of magnitude as the nominal case. Also, these results indicate that the INDI controller is barely affected by aerodynamic uncertainty applied to the aerodynamic coefficients.

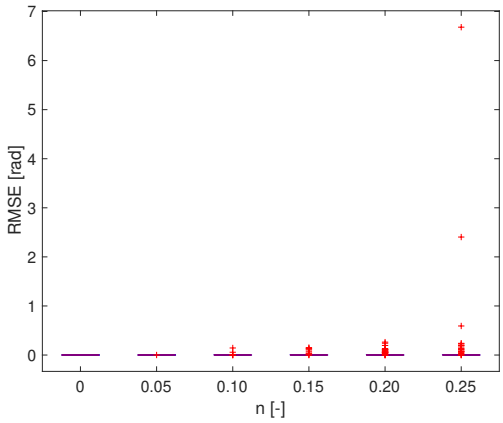

(a) Boxplot for roll angle trajectory.

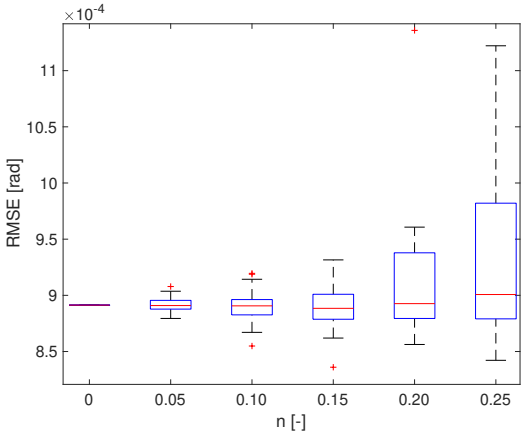

(b) Zoomed boxplot roll angle.

Fig. 11 Boxplots showing roll angle tracking error for aerodynamic uncertainty.

IV. Conclusions

After analysing the stability and handling qualities of the Flying-V, it is concluded that the requirements are met the least during approach conditions at the forward centre of gravity location. Therefore, an Incremental Nonlinear Dynamic Inversion (INDI) controller is applied to the Flying-V that is able to control the roll angle, flight path angle, and sideslip angle. Using this flight control system the eigenvalues of the Flying-V are located on the left half-plane, indicating that the eigenmodes of the aircraft are stable.

Furthermore, the robustness of the flight control system is assessed by analysing the Root-Mean-Square Error (RMSE) of the Flying-V subjected to aerodynamic uncertainty aiming to follow a 3211 reference trajectory. Even though the flight control system proves to be robust in case aerodynamic uncertainty is applied to the Flying-V. The control

surface deflection limits are the only factors limiting the robustness of the flight control system. Namely, excessive control surface deflection demands are required in case the control effectiveness of the control surfaces is decreased. The physical inability of the Flying-V to meet these demands results in an increased RMSE.

Finally, even though previous research indicates that the Flying-V is not able to meet all stability and handling qualities, this research shows that the stability and handling qualities can be improved by designing an INDI controller. Additionally, this controller proves to be robust under the influence of aerodynamic uncertainty. Therefore, this research contributes to the development of the Flying-V by showing that the application of a flight control system is able to improve the stability and handling qualities of the aircraft. Also, due to the robustness of the INDI controller in case of aerodynamic uncertainty, it is possible to start developing a flight control system early in the design phase of the aircraft.

V. Recommendations

With the goal to further improve research on the stability and handling qualities of the Flying-V using an Incremental Nonlinear Dynamic Inversion controller, future work may include the set of items discussed in this section.

During this research, the magnitude of the aerodynamic uncertainty applied to the Flying-V is based on previous research requiring several assumptions to find the maximum aerodynamic uncertainty. It is therefore suggested to perform additional research on the magnitude of the aerodynamic uncertainty to increase the fidelity of the robustness analysis.

Secondly, this research does not analyse the effect of the flight control system on the Control Anticipation Parameter. To perform this analysis, it is necessary to find a lower order equivalent system that translates the pilot input to the pitch rate. For future research, it is therefore suggested to analyse the Control Anticipation Parameter of the controlled Flying-V using a lower order equivalent system.

Besides that, this research only considers aerodynamic uncertainty for the robustness analysis. Therefore, it is suggested to perform additional research on other factors that may affect the stability of the INDI controller such as measurement time delay, sampling frequency, inertia uncertainty, and centre of gravity mismatch.

Furthermore, during this research the outboard elevons and the rudders are used for roll angle control of the Flying-V. Due to the low roll angle that can be achieved without saturating the control surfaces, it is suggested to also incorporate the inboard elevons for roll control in future research.

Finally, this research does not take into account sensor dynamics, nor does it take into account atmospheric effects such as turbulence. To increase the fidelity of the controller analysis, it is suggested to apply these components to the simulation model.

References

[1] Martinez-Val, R., Perez, E., Puertas, J., and Roa, J., "Optimization of Planform and Cruise Conditions of a Transport Flying Wing," *Proceedings of the Institution of Mechanical Engineers, Part G: Journal of Aerospace Engineering*, Vol. 224, No. 12, 2010, pp. 1243–1251. https://doi.org/10.1243/09544100JAERO812.

[2] Faggiano, F., Vos, R., Baan, M., and Van Dijk, R., "Aerodynamic Design of a Flying V Aircraft," *17th AIAA Aviation Technology, Integration, and Operations Conference*, 2017. https://doi.org/10.2514/6.2017-3589.

[3] Martinez-Val, R., "Flying Wings: A New Paradigm for Civil Aviation?" *Acta Polytechnica Vol. 47 No. 1/2007*, 2007. https://doi.org/10.14311/914.

[4] Okonkwo, P., and Smith, H., "Review of Evolving Trends in Blended Wing Body Aircraft Design," *Progress in Aerospace Sciences*, Vol. 82, 2016, pp. 1–23. https://doi.org/10.1016/j.paerosci.2015.12.002.

[5] Zhenli, C., Zhang, M., Yingchun, C., Weimin, S., Zhaoguang, T., Dong, L., and Zhang, B., "Assessment on Critical Technologies for Conceptual Design of Blended-Wing-Body Civil Aircraft," *Chinese Journal of Aeronautics*, Vol. 32, No. 8, 2019, pp. 1797–1827. https://doi.org/10.1016/j.cja.2019.06.006.

[6] Liebeck, R. H., "Design of the blended wing body subsonic transport," *Journal of aircraft*, Vol. 41, No. 1, 2004, pp. 10–25. https://doi.org/10.2514/1.9084.

[7] Benad, J., "The Flying V, A New Aircraft Configuration for Commercial Passenger Transport," *Deutscher Luft- und Raumfahrtkongress*, 2015. https://doi.org/10.25967/370094.

[8] Van Overeem, S. and Wang, X. and Van Kampen, E., "Modelling and Handling Quality Assessment of the Flying-V Aircraft," *AIAA SciTech Forum*, 2022.

[9] Cappuyns, T., "Handling Qualities of a Flying V Configuration," http://resolver.tudelft.nl/uuid:69b56494-0731-487a-8e57-cec397452002, 2019.

[10] Garcia, A.R., "Aerodynamic Model Identification of the Flying V using Wind Tunnel Data," http://resolver.tudelft.nl/uuid:79e01f29-1789-4501-8556-ca2bcf06f3ab, 2019.

[11] Palermo, M., and Vos, R., "Experimental Aerodynamic Analysis of a 4.6%-Scale Flying-V Subsonic Transport," *AIAA Scitech 2020 Forum*, 2020, p. 2228. https://doi.org/10.2514/6.2020-2228.

[12] Balas, G.J., "Flight Control Law Design: An Industry Perspective," *European Journal of Control*, Vol. 9, No. 2-3, 2003, pp. 207–226.

[13] Slotine, J.E. et al., *Applied Nonlinear Control*, Vol. 199, Prentice hall Englewood Cliffs, NJ, 1991.

[14] Adams, R.J. et al., "Robust Flight Control Design using Dynamic Inversion and Structured Singular Value Synthesis," *IEEE Transactions on control systems technology*, Vol. 1, No. 2, 1993, pp. 80–92.

[15] Wang, X. et al., "Stability Analysis for Incremental Nonlinear Dynamic Inversion Control," *Journal of Guidance, Control, and Dynamics*, Vol. 42, No. 5, 2019, pp. 1116–1129.

[16] Viet, R., "Analysis of the Flight Characteristics of a Highly Swept Cranked Flying Wing by Means of an Experimental Test," http://resolver.tudelft.nl/uuid:90de4d9e-70ae-4efc-bd0a-7426a0a669c3, 2019.

[17] Anonymous, "Military Specifications, Flying Qualities of Piloted Aircraft MIL-F-8785C," , 1980.

[18] Cook, M.V., *Flight Dynamics Principles: A Linear Systems Approach to Aircraft Stability and Control*, Butterworth-Heinemann, 2012.

[19] Sieberling, S et al., "Robust Flight Control using Incremental Nonlinear Dynamic Inversion and Angular Acceleration Prediction," *Journal of Guidance, Control, and Dynamics*, Vol. 33, No. 6, 2010, pp. 1732–1742.

[20] Acquatella, P. et al., "Robust Nonlinear Spacecraft Attitude Control using Incremental Nonlinear Dynamic Inversion," *AIAA Guidance, Navigation, and Control Conference*, 2012, p. 4623.

[21] Schumacher, C. et al., "Stability Analysis of a Missile Control System with a Dynamic Inversion Controller," *Journal of Guidance, Control, and Dynamics*, Vol. 21, No. 3, 1998, pp. 508–515.

[22] Matamoros, I., and de Visser, C. C., "Incremental Nonlinear Control Allocation for a Tailless Aircraft with Innovative control Effectors," *2018 AIAA Guidance, Navigation, and Control Conference*, 2018, p. 1116.

[23] Tang, S.H., "Fault-Tolerant Flight Control with Sensor-Based Nonlinear Dynamic Inversion: Application and Evaluation in the SIMONA Research Simulator," http://resolver.tudelft.nl/uuid:c2263beb-602b-4727-9219-43cd11325622, 2014.

[24] European Union Aviation Safety Agency, "Type-Certificate Data Sheet No. E.111 for Trent XWB Series Engines," 2019, p. 7.

[25] Ridcully, M., "A350-900: Flight Deck and Systems Briefing for Pilots," , 2011.

[26] Van 't Veld, R. C., Van Kampen, E., and Chu, Q. P., "Incremental Nonlinear Dynamic Inversion Flight Control: Stability and Robustness Analysis and Improvements," *AIAA Aircraft Flight Control Design Conference*, 2018. https://doi.org/10.2514/6.2018-1127.

[27] Simplício, P.V.M., "Helicopter Nonlinear Flight Control: An Acceleration Measurements-based Approach using Incremental Nonlinear Dynamic Inversion," http://resolver.tudelft.nl/uuid:d2ffe4d1-219e-4965-a6b4-debb900ded4c, 2011.

[28] Wang, X., Van Kampen, E.-J., Chu, Q., and Lu, P., "Stability analysis for incremental nonlinear dynamic inversion control," *Journal of Guidance, Control, and Dynamics*, Vol. 42, No. 5, 2019, pp. 1116–1129. https://doi.org/10.2514/1.G003791.

II

Literature Study

This part has been graded previously.

2

Background

This chapter elaborates on the background information related to the TU Delft Flying-V. To obtain a fundamental background on the current status of the project, section 2.1 displays an overview of the research related to the TU Delft Flying-V that has been conducted. Besides that, the layout of the configuration is discussed in section 2.2.

2.1. Flying-V Research Overview

In 2015, a research paper was published by J. Benad in collaboration with Airbus Hamburg titled: *The Flying-V: A New Aircraft Configuration For Commercial Passenger Transport.* [Benad, J., 2015] This research elaborates on the initial design of a V-shaped aircraft called the Flying-V. During this research, the Flying-V was compared to the performance of the Airbus A350-900. This analysis showed that the Flying-V has the potential to obtain a lift-over-drag increase of 10% and a 2% lower empty weight. Besides that, with his design, Benad was able to reduce the noise level produced by mounting the engines on top of the aircraft. [Benad, J., 2015]

The research performed by Benad was continued by Faggiano on *Aerodynamic Design of a Flying V Aircraft.* [Faggiano, F. et al., 2017] During this research, the aerodynamic design of the aircraft was optimised for cruise conditions. To be more specific, for a Mach number of 0.85, an altitude of 13000m, and a lift coefficient of 0.26. Consequently, this optimised design was compared to the NASA Common Research Model. The TU Delft Flying-V proved to have an aerodynamic efficiency increase of 25% compared to the Common Research Model at this optimisation point. [Faggiano, F. et al., 2017]

In the preparation of a small scale flight test of the TU Delft Flying-V, research was conducted on the flight characteristics of the aircraft. First of all, in the research on *Analysis of the Flight Characteristics of a Highly Swept Cranked Flying Wing by means of an Experimental Test* [Viet, R., 2019], the flight characteristics of the TU Delft Flying-V sub-scale model at approach speed and high angles of attack were investigated using wind tunnel experiments. This resulted in a centre of gravity range for which the aircraft can be trimmed while being statically stable, the optimum centre of gravity was determined, and it was discovered that the aircraft shows unstable behaviour in case the angle of attack is larger than 20°. [Viet, R., 2019] This is endorsed by Palermo in his research titled: *Experimental Aerodynamic Analysis of a 4.6%-Scale Flying-V Subsonic Transport.* [Palermo, M. et al., 2020] In this research, the two control surfaces in the outboard wing are deflected to measure their effects in terms of lift, drag, and pitching moment. Furthermore, this research determines the location of the most forward and aft centre of gravity such that the aircraft can be balanced while being statically stable. Finally, the maximum lift coefficient is determined to be equal to 0.66 in landing conditions. [Palermo, M. et al., 2020] The research from both [Viet, R., 2019] and [Palermo, M. et al., 2020] is combined by Garcia in the research on *Aerodynamic Model Identification of the Flying V from Wind Tunnel Data* [Garcia, A.R., 2019] In this research, an input/output model is generated to estimate the aerodynamic response of the TU Delft Flying-V scale model. Only the steady (static) aerodynamic coefficients are calculated as wind tunnel limitations prevent the identification of dynamic coefficients. Eventually, the

coefficients: C_x, C_z, and C_m are identified with respect to the angle of attack, airspeed and elevon deflections. Furthermore, C_l, C_n, and C_y are identified for specific elevon deflections while assuming zero sideslip. [Garcia, A.R., 2019]

Besides research related to wind tunnel experiments, research on the stability and handling qualities of the TU Delft Flying-V was conducted by Cappuyns in *Handling Qualities of a Flying V Configuration*. [Cappuyns, T., 2019] In this research, the stability and handling qualities of the full-size aircraft are assessed by designing a six Degree-of-Freedom flight dynamics toolbox using aerodynamic coefficients obtained from the Vortex Lattice Method and inertia estimations obtained using a lumped mass method. The stability and handling qualities are assessed using military standards and requirements obtained from the European Aviation Safety Agency (EASA). This research concludes that the Dutch roll mode is unstable and that the lateral directional controllability of the aircraft is limited in the case of One Engine Inoperative (OEI) at low speeds. [Cappuyns, T., 2019] In fig. 2.1 it is possible to observe a timeline displaying relevant research related to the TU Delft Flying-V and how research on modelling and control fits into this framework.

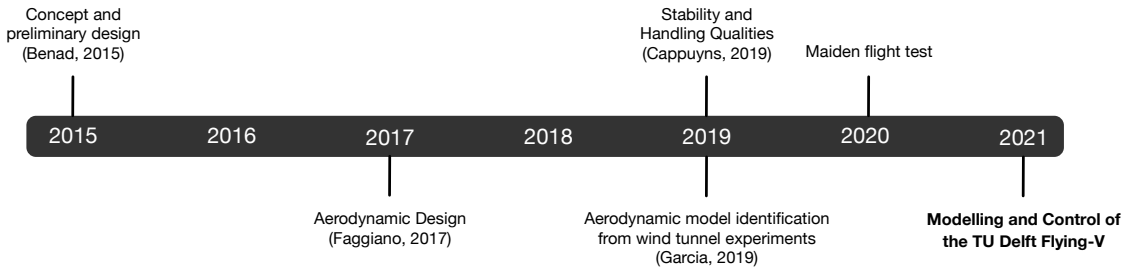

Figure 2.1: Timeline of research related to the TU Delft Flying-V

Besides the assessment of the complete aircraft, also the effects of several aircraft components on the performance have been evaluated. In the research on *Engine Integration of the Flying V: Quantification of Engine Integration Effects using Wind Tunnel Experiments* [Van Empelen, S.A., 2020] the impact of engine integration effects on the low speed performance of the TU Delft Flying-V subscale model is evaluated. With engines integrated on the aircraft, an increased nose down pitching moment is observed between 5° and 12° angle of attack. Between 12.5° and 22.5° angle of attack, an increased nose up pitching moment is observed. Besides that, the change in required control surface deflection for trim due to engine interference is evaluated to be less than +/- 2.5°. The aircraft can be trimmed for maximum climb, level flight, and optimum glide with control surface deflections ranging between -10° and 10°. [Van Empelen, S.A., 2020] Furthermore, the research performed by Johnson on *Effect of Winglet Integration and Rudder Deflection on Flying-V Aerodynamic Characteristics* [Johnson, N.A., 2021] elaborates on the aerodynamic effects of installing the winglet/rudder combination and deflecting the rudder. Furthermore, this research elaborates on the rudder effectiveness for various aileron deflections. From this research, it can be concluded that the effects of the winglet/rudder combination on several aerodynamic characteristics (such as lift and drag) are minimum. With the wing control surfaces at zero deflection, an increase of the angle of attack has a significant effect on the rudder control derivatives (which essentially is the effectiveness) of the side-force, yawing moment, and rolling moment (reductions of 45%, 50%, and 37% respectively for angles of attack ranging between 0° and 20°). [Johnson, N.A., 2021] Also, the research performed by Bourget on *The Effect of Landing Gear Implementation on Flying V Aerodynamics, Stability and Controllability* [Bourget, G., 2020] talks about the consequences of adding landing gear to the TU Delft Flying-V. One of the evaluation criteria for the design of a landing gear is the lateral stability derivatives of the aircraft. Two designs with modified dihedral are considered, one where the main landing gear is shortened from 6m to 5.5m, and another one where the main landing gear is as short as possible. The change in dihedral design does not affect the side force derivatives, but decreases the yawing moment derivatives, while the rolling moment derivative becomes 3.5 times larger compared to an Airbus A350-900. This displays doubts on the controllability of the Dutch roll mode and the roll angle when landing with sideslip. [Bourget, G., 2020] Finally, the research from [Viet, R., 2019] and [Palermo, M. et al., 2020] elaborates on pitch break tendencies at 20° angle of attack. In the research on *Experimental Investigation into the Effect of Aerodynamic Add-ons on the Aerodynamic Characteristics of the Flying V* [Uitert, J.J.D., 2021] three solutions are investigated

to eliminate this unstable pitch break. These solutions consist of the application of trip strips, vortilons, and fences. From this research it can be concluded that the application of trip strips reduces the usable maximum lift coefficient, vortilons have no effect on the unstable pitch break, and fences postpone the unstable pitch break and reduce the absolute value of the pitching moment coefficient. [Uitert, J.J.D., 2021]

2.2. TU Delft Flying-V Layout

The TU Delft Flying-V is an aircraft configuration that features a twin fuselage in a V-shape, connected to the cockpit as can be observed in fig. 2.2[1]. The main benefit of this arrangement is that it is possible to use oval cross-sectional tubular fuselages. These oval cross-sectional tubular fuselages fit a swept back airfoil very efficiently, resulting in a simple and light pressure cabin structure. [Benad, J., 2015, Van Empelen, S.A., 2020] Furthermore, the concept of the TU Delft Flying-V makes it easier for aircraft family design. Due to the relatively straight sections, the design can be easily extruded to generate larger members of the same family. [Van Empelen, S.A., 2020] Furthermore, it can be observed that the engines are located on top of the aircraft. The aircraft consists of a total of four control surfaces on each wing, three elevons located at the trailing edge of the wing and one rudder integrated into the winglet. The most inboard elevon (also indicated by Control Surface 1 or CS1) is used as the main elevator, the centre elevon (also indicated by Control Surface 2 or CS2) provides both lateral and longitudinal control, and the most outboard control surface (also indicated by Control Surface 3 or CS3) mostly provides lateral control. [Palermo, M., 2019] Besides the layout in fig. 2.2 it is possible to observe a set of design parameters in table 2.1.

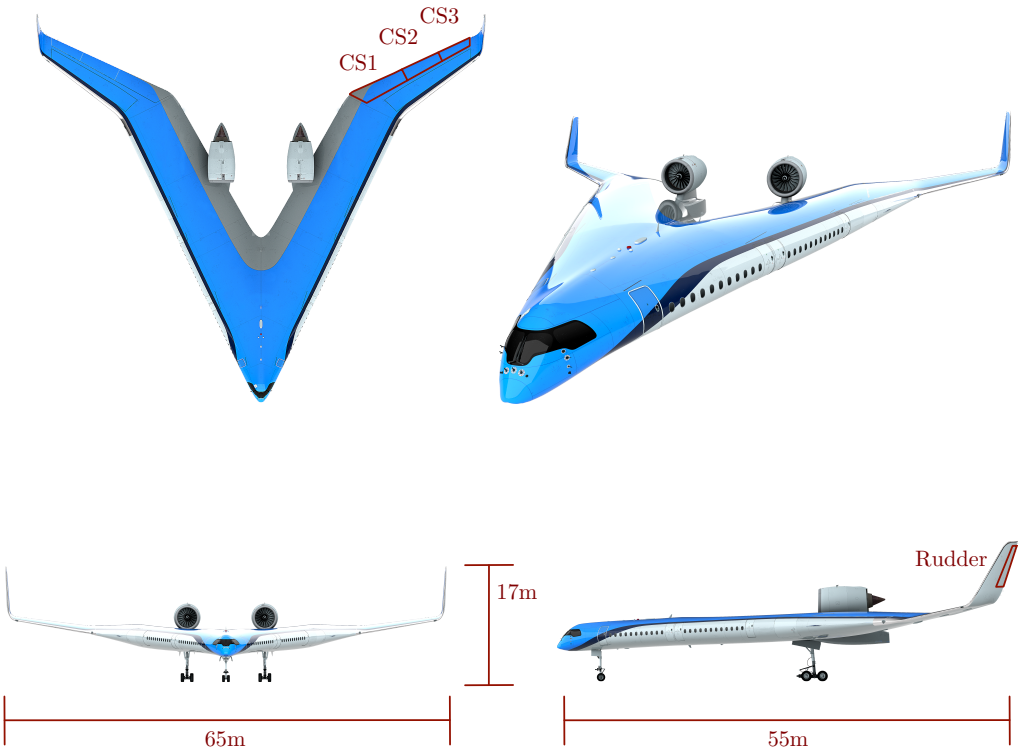

Figure 2.2: TU Delft Flying-V Configuration. [Flying-V Website, 2020]

[1] https://www.tudelft.nl/lr/flying-v (accessed in March 2021)

Table 2.1: Design Parameter for TU Delft Flying-V [Cappuyns, T., 2019]

Parameter	**Value**	**Unit**
Length	55	[m]
Wingspan	65	[m]
Height	17	[m]
Pax	314	[-]
Fuel Capacity	140,000	[l]
Cargo Capacity	160	[m^3]
Design Mach Number	0.85	[-]
Cruise Altitude	43,000	[ft]

3

Stability and Handling Qualities Analysis

In chapter 2 an overview is given on the research related to the TU Delft Flying-V. Furthermore, the layout of the aircraft including design parameters is displayed. Therefore, in this chapter it is possible to gain more knowledge about the stability and handling qualities of the aircraft by answering the first sub-question obtained from chapter 1:

> What are the stability and handling qualities of the Flying-V?

In this chapter, section 3.1 elaborates on the longitudinal stability and handling qualities of the aircraft. Furthermore, section 3.2 continues on the lateral-directional stability and handling qualities of the aircraft. Additionally, the control surface layout is discussed in section 3.3. After that, the assessment criteria for the stability and handling qualities are defined in section 3.4. Finally, section 3.5 concludes this chapter.

3.1. Longitudinal Stability and Handling Qualities

In this section the longitudinal stability and handling qualities of the TU Delft Flying-V are discussed. In section 3.1.1 the static longitudinal handling qualities are discussed and section 3.1.2 elaborates on the dynamic longitudinal stability and handling qualities.

3.1.1. Static Longitudinal Stability and Handling Qualities

The longitudinal stability of an aircraft is connected to the location of the centre of gravity with respect to the neutral point. [Jansen, Q.J.M., 2015] The neutral point of an aircraft is defined as the location where a disturbance does not result in a stable response nor an unstable response. Because the TU Delft Flying-V does not have an empennage, the aerodynamic centre of the main wing, which is the location where the aerodynamic moment does not change with the angle of attack, intersects with the neutral point. [De Castro, H. V., 2003] In case the neutral point is located aft of the centre of gravity the aircraft is stable and in case the neutral point is located forward this results in an unstable aircraft. If the centre of gravity is located at the neutral point, the aircraft keeps its disturbed state and is called neutrally stable. [Mulder, J.A. et al., 2013] To find a measure for the stability of an aircraft, the static stability is defined as shown in eq. (3.1). In this equation, the static margin (SM) is given as the distance between the location of the neutral point (x_{np}) and the centre of gravity (x_{cg}). The equation is made non-dimensional by dividing the distance over the Mean Aerodynamic Chord (MAC or $\bar{c}$).

$$\text{SM} = \frac{(x_{\text{np}} - x_{\text{cg}})}{\bar{c}} \tag{3.1}$$

In case the static margin is negative, this results in a longitudinally statically unstable aircraft. Therefore, typical values of the static margin for a transport aircraft range between 5% and 15%. However, it needs to be noted that the manoeuvrability of the aircraft decreases with increasing static margin. [Jansen, Q.J.M., 2015] An aircraft is longitudinally stable if the change in pitching moment with increasing angle of attack is negative ($C_{m_\alpha} < 0$). In case this parameter is positive, the aircraft will pitch further up with an increasing angle of attack resulting in an unstable configuration. The aircraft is trimmed in case the total pitching moment equals zero.

Regarding the TU Delft Flying-V, a static stability analysis has been conducted for several flight conditions. First of all, an analysis has been performed on the flight characteristics of the TU Delft Flying-V at approach speed and high angles of attack. [Viet, R., 2019] According to this research the aircraft becomes statically unstable at an angle of attack equal to 20° due to the slope of the moment coefficient derivative with respect to the angle of attack becoming positive at 20° angle of attack ($C_{m_\alpha} > 0$ for $\alpha > 20°$). [Palermo, M. et al., 2020, Viet, R., 2019] In order to trim the aircraft for an angle of attack ranging between -2° and 28° the optimum location of the centre of gravity is found to be at 1.365m behind the nose of the aircraft, resulting in a static margin of 9%. [Viet, R., 2019] According to a rule of thumb mentioned in *Analysis of the flight characteristics of a highly swept cranked flying wing by means of an experimental test* [Viet, R., 2019] a static margin ranging between 5%-15% provides sufficient stability with enough control authority for the control surfaces to trim the aircraft at high angles of attack. Besides this research, another analysis is performed in *Experimental Aerodynamic Analysis of a 4.6%-Scale Flying-V Subsonic Transport* [Palermo, M. et al., 2020] on the aerodynamic characteristics of the TU Delft Flying-V to obtain the most forward and aft centre of gravity locations and to determine whether the aircraft is statically stable. According to this research, the location of the aerodynamic centre ranges between 1.32m and 1.37m (for an angle of attack of -10° - 0°) and between 1.37m and 1.39m (for an angle of attack of 0° - 10°). This is in accordance with [Viet, R., 2019], where the average location of the aerodynamic centre for angles of attack ranging between 0° and 20° equals 1.422m. According to [Palermo, M. et al., 2020], the optimum centre of gravity location to attain maximum lift in trimmed conditions with an ultimate static stability margin of 4.4% equals 1.336m.

The research on the static stability performed by both [Viet, R., 2019] and [Palermo, M. et al., 2020] is combined in the research conducted on *Aerodynamic Model Identification of the Flying-V using Wind Tunnel Data* [Garcia, A.R., 2019] on the development of an input/output model based on splines to estimate the aerodynamic response of the TU Delft Flying-V using wind tunnel experiments as shown in fig. 3.1.

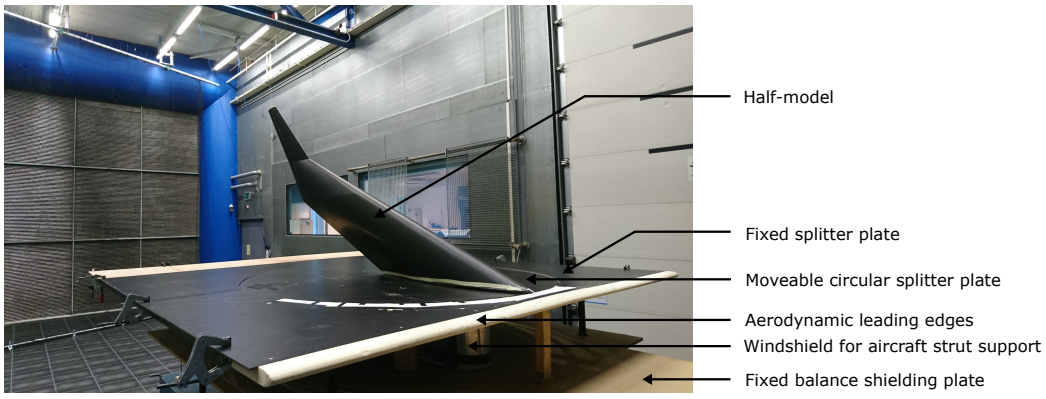

Figure 3.1: Wind tunnel setup for experiments TU Delft Flying-V. [Viet, R., 2019]

By changing a set of independent variables (angle of attack, airspeed, and deflection of the three control surfaces) this results in the identification of the longitudinal force and moment coefficients (C_x, C_z and C_m) and their derivatives with respect to the independent variables. The test campaign only considered the static tests and during the tests, the engine and winglets were not analysed. It is assumed that the altitude of the scale model and full scale model are equal which means that the study focuses on low altitude characteristics of the aircraft. Furthermore, geometric differences were not taken into account and it is expected that the use of a half model and manufacturing inaccuracies also

cause discrepancies. The measurements are considered accurate for angles of attack ranging between -10° and 30°. The aft centre of gravity location is limited by the location of the aerodynamic centre and is determined to be equal to 1.4m from the nose of the aircraft. The forward centre of gravity location is limited by the ability to trim the aircraft (thus the maximum control surface deflection) and is determined to be equal to 1.32m from the nose of the aircraft. Using the forward and aft centre of gravity locations, and earlier research, the optimal location of the centre of gravity is estimated to be equal to 1.36m. This leads to a model of the TU Delft Flying-V aircraft that can be trimmed for the proposed centre of gravity range (1.32m - 1.4m) for airspeeds ranging between 17 m/s - 30 m/s and an angle of attack up to 20°.

3.1.2. Dynamic Longitudinal Stability and Handling Qualities

The fact that an aircraft is statically stable does not automatically impose dynamic stability on the system. [Jansen, Q.J.M., 2015] The longitudinal dynamic stability can be assessed using the symmetric equations of motion in state-space form. From the eigenvalues of this system it is possible to deduce that the disturbed motion is the sum of a relatively slow oscillation (the phugoid mode) and an oscillation with a much shorter period (the short period mode). The longitudinal dynamic stability properties of a BWB aircraft are not radically different compared to that of a conventional aircraft. [De Castro, H. V., 2003] For this reason, it is possible to use the eigenvalues to assess the stability of the aircraft. Besides that, using the eigenvalues it is possible to determine the period, time to damp to half the amplitude, undamped natural frequency, and damping ratio for both oscillations. [Mulder, J.A. et al., 2013]

Currently, the research performed on the dynamic stability of the TU Delft Flying-V is limited. The experiments performed by [Viet, R., 2019], [Palermo, M. et al., 2020], and [Garcia, A.R., 2019] only consider the static conditions of the aircraft due to the limited capabilities of the half model inside the wind tunnel. However, the research performed by [Cappuyns, T., 2019] concludes that the Phugoid motion has a damping ratio of $\zeta_{\text{ph}} = 0.03$ during cruise conditions and $\zeta_{\text{ph}} = 0.08$ during approach conditions, meaning that the aircraft has a positively damped, stable phugoid. Furthermore, regarding the short period motion, the aircraft obtains its worst damping ratio at the most forward centre of gravity position equal to $\zeta_{\text{sp}} = 0.27$. In case the centre of gravity is located at the most aft position, the damping ratio during cruise conditions is equal to $\zeta_{\text{sp}} = 0.33$ and the damping ratio during approach conditions is equal to $\zeta_{\text{sp}} = 0.79$. From the flight test of the small scale model, it was concluded that the aircraft has sufficient control authority to provide the required pitch during take-off.[1] Moreover, using a simplified study, it is determined that the pitch damping coefficient (C_{m_q}) is negative as long as the centre of pressure is located behind the centre of gravity. [Garcia, A.R., 2019] Currently research is done on the design of a complete dynamic model of the TU Delft Flying-V using data from the maiden test flight. Soon this dynamic model can be used in this thesis for the assessment of the dynamic stability of the aircraft.

3.2. Lateral-Directional Stability and Handling Qualities

In this section the lateral-directional stability and handling qualities of the TU Delft Flying-V are discussed. In section 3.2.1 the static lateral-directional handling qualities are discussed and section 3.2.2 elaborates on the dynamic lateral-directional stability and handling qualities.

3.2.1. Static Lateral-Directional Stability and Handling Qualities

The lateral static stability of an aircraft is concerned with the ability to return to a wings-level equilibrium position in case of a roll disturbance. The condition for an aircraft to be laterally stable is that the rolling moment due to a positive disturbance must be negative ($C_{l_\beta} < 0$). [De Castro, H. V., 2003] This can be explained as follows, in case a disturbance causes a positive roll angle, the aircraft starts sideslipping to the right due to the gravity component along the right wing. A negative C_{l_β} would therefore cause a rolling moment returning the aircraft to its equilibrium position. [Mulder, J.A. et al., 2013]

[1] https://www.tudelft.nl/en/2020/tu-delft/successful-maiden-flight-for-the-tu-delft-flying-v (accessed in January 2021)

The directional static stability is concerned with the aircraft's ability to yaw in the direction of the wind (like a weathercock). An aircraft is directionally stable in case $C_{n_\beta} > 0$ which results in a positive moment to reduce the sideslip angle. The directional stability is also highly dependent on the centre of gravity location. Namely, the orthogonal distance between the vertical stability surface and the centre of gravity determines the length of the moment arm and also influences whether the aircraft is directionally statically stable. [De Castro, H. V., 2003]

A wind tunnel test campaign is performed to develop an input/output model to estimate the aerodynamic response of the TU Delft Flying-V. The identification of the lateral-directional parameters (C_y, C_l, and C_n) is performed under the assumption of zero sideslip ($\beta = 0$). Due to this assumption, this effectively means that the lateral-directional coefficients could only be identified for specific elevon deflections with zero sideslip. After identification, the lateral force coefficient (C_y) is left out of the study due to large uncertainties. Furthermore, it was identified that a positive deflection of the control surfaces (right elevon up and left elevon down) leads to a positive rolling moment and a negative yawing moment due to the difference in drag for both wings. This adverse yaw effect can be fixed using differential aileron deflection. [Garcia, A.R., 2019]

3.2.2. Dynamic Lateral-Directional Stability and Handling Qualities

To analyse the lateral-directional dynamic stability it is possible to identify two aperiodic motions and one periodic motion. The aperiodic motions represent the aperiodic roll which is damped primarily due to the rolling moment generated by the wing in case of a roll disturbance ($C_{l_p} < 0$) and the spiral motion for which the aircraft enters into a sideslipping turn with an increasing roll angle and decreasing radius. The periodic motion is the Dutch roll, for which the aircraft sideslips, yaws, and rolls. Using the eigenvalues obtained from the linearised system it is possible to obtain the time to damp to half the amplitude for the aperiodic motions and the period, time to damp to half amplitude, undamped natural frequency, and damping ratio for the periodic motion. [Mulder, J.A. et al., 2013]

The research performed by [Cappuyns, T., 2019] elaborates on the eigenvalues for each of the eigenmodes of the aircraft. First of all, the spiral mode shows stable behaviour in the cruise condition. The only unstable spiral mode was obtained during approach conditions with the centre of gravity located at the forward limit. However, as will be discussed in section 3.4, the time to double bank angle is equal to 10 times the minimum value set by requirements. Therefore, this motion can be considered stable. Besides that, the Dutch roll motion is assessed. From the eigenvalue analysis it can be concluded that the Dutch roll mode is unstable for the TU Delft Flying-V except for the condition where the aircraft is flying in cruise conditions with the centre of gravity located at the forward limit. [Cappuyns, T., 2019] This is in coherence with the maiden test flight, where it was concluded that the aircraft shows too much Dutch roll, resulting in a heavy landing.[2] Finally, after analysing the aperiodic roll mode, it can be concluded that the eigenvalue with the smallest magnitude is equal to $\lambda_{\text{ar}} = -0.7$. Furthermore, no time constants were found that surpassed the recommended maximum values as will be discussed in section 3.4.

3.3. Control Surface Layout

In this section, the design methodology to obtain the size of the control surfaces of the aircraft is discussed. The design methodology can be found in literature on the aerodynamic design of the aircraft. In section 3.3.1 the design of the elevons are discussed. After that, section 3.3.2 elaborates on the design of the rudders.

3.3.1. Elevon Control Surface Design

The design of the elevons of the aircraft is performed using a comparative analysis with respect to the Airbus A350-900. The horizontal tail volume of this aircraft is equal to $2.74 \cdot 10^3$ m^3. The elevons of the Flying-V are consequently sized to have a similar value compared to the Airbus A350-900. For this analysis, the most aft centre of gravity is taken, resulting in a horizontal tail volume of $3.18 \cdot 10^3$

[2] https://www.tudelft.nl/en/2020/tu-delft/successful-maiden-flight-for-the-tu-delft-flying-v (accessed in January 2021)

m^3. This means that the horizontal tail volume of the Flying-V is 16% larger compared to the Airbus A350-900.

3.3.2. Rudder Control Surface Design

In general the rudder has to accomplish three different tasks. First of all, the rudder has to satisfy the static and dynamic stability functions as displayed in section 3.2. Secondly, the rudder has to be able to control the aircraft in any flight condition. Thirdly, the rudder has to be able to trim the aircraft in each different flight condition. The research performed by [Faggiano, F. et al., 2017] transforms these tasks into three different requirements. The first requirement states that static directional stability shall be guaranteed. This requirement is met in case $C_{n_\beta} > 0$. Dynamic stability requirements are not defined in this research, therefore it is suggested to add yaw dampers to reduce the Dutch roll mode. Secondly, the control force shall balance the yawing moment generated by the engine operating at a high thrust setting in case one engine is inoperative during take-off. To satisfy this requirement, the aircraft has to be able to guarantee zero sideslip at the most aft centre of gravity location with a maximum rudder deflection of 20° to allow for additional manoeuvring within the rudder deflection limits. Thirdly, the aircraft shall be able to land with maximum crosswind, when the wind speed is equal to 20% of the take-off velocity. This corresponds to an angle of sideslip of 11.5° with a maximum rudder deflection of 20°. Aileron deflection impact (such as adverse yaw) was not taken into account. [Faggiano, F. et al., 2017]

In case no vertical control surface is added to the design of the TU Delft Flying-V, the aircraft is directionally statically unstable due to a negative C_{n_β} coefficient. Taking the three requirements into account, this results in a vertical control surface area of $13m^2$. Besides that, it turns out that the most critical requirement for the design is not the one engine inoperative condition, but the static directional stability requirement. [Faggiano, F. et al., 2017] This is different from conventional aircraft design, where the most critical requirements are the one engine inoperative condition and landing during crosswind. [Nicolosi, F. et al., 2017]

3.4. Stability and Handling Qualities Assessment

This section elaborates on the assessment of the stability and handling qualities of the aircraft. In section 3.4.1 the assessment criteria are defined. After that section 3.4.2 discusses the requirements obtained from civil aviation authorities. Finally, section 3.4.3 displays the criteria from military standards.

3.4.1. Assessment Criteria

The stability of an aircraft is characterised by the ability to return to a steady state position in case a disturbance or pilot input is applied. In case the aircraft has the ability to return to a steady state, the aircraft is considered stable. However, in case an aircraft diverges from the steady state after applying an input, the aircraft is considered unstable. The handling qualities of an aircraft are considered as a description of the adequacy of the short term dynamic response to controls during the execution of a flight task. [Cook, M.V., 2012] Therefore, the aircraft must demonstrate adequate control authority to maintain steady, straight, horizontal flight. Besides that, the aircraft must be able to safely manoeuvre from one steady state to another one. Furthermore, the aircraft must have the ability to be trimmed in a certain flight condition. Finally, the cockpit control forces should be acceptable. [Roskam, J., 1986] To guarantee a safe flight of the TU Delft Flying-V, it is necessary to identify the key elements regarding stability and handling qualities of the aircraft. Therefore, it is possible to look at civil certification authorities (such as EASA or FAA) or military standards to identify a set of key specifications on stability and handling qualities of the aircraft. However, the requirements from aviation authorities are often not specific and therefore difficult to use during the design and evaluation of the aircraft. As an example, it is possible to look at the Acceptable Means of Compliance for EASA CS25.181 (Dynamic stability) [CS-25, 2018].

Any combined lateral-directional oscillations ('Dutch roll') occurring between 1.13 VSR and maximum allowable speed appropriate to the configuration of the aeroplane must be positively damped with controls

free, and must be controllable with normal use of the primary controls without requiring exceptional pilot skill.

From this quote it can be concluded that it is difficult to identify the exact requirements of the Dutch roll mode. Therefore, it can be concluded that making use of only the specifications from civil aviation authorities is insufficient for the assessment of the stability and handling qualities of the TU Delft Flying-V. [Wahler, N.F.M., 2021] The requirements for civil aircraft are mainly concerned with safety, while specific requirements related to stability, control, and handling qualities are relatively relaxed. The requirements set by military documents are specified in much more detail. Using these comprehensive and demanding requirements, the aircraft will undoubtedly also meet the civil requirements. [Cook, M.V., 2012] From *Flight Dynamics Principles* [Cook, M.V., 2012] it is possible to obtain DEF-STAN 00-970 and MIL-F-8785C requirements for military aircraft that can be used to assess the performance of the TU Delft Flying-V. To assess the stability and handling qualities of the TU Delft Flying-V for a complete set of flight conditions, it is decided to divide the mission profile into several flight phases and perform an assessment for each flight phase as was done in *A Multidisciplinary Optimization Framework for Control-Configuration Integration in Aircraft Conceptual Design.* [Perez, R.E. et al., 2006] This research elaborates on an integrated control-configured aircraft design sizing framework that takes into account the dynamic characteristics and automatic control capabilities at the early conceptual stage. [Perez, R.E. et al., 2006] The different flight phases and the different stability and handling qualities assessment criteria can be observed in fig. 3.2. To limit the scope of this research, the most crucial in-flight phases of the mission profile are taken into account. Therefore the cruise phase and the approach phase are considered for this research. It is decided to focus on the cruise phase as an aircraft spends most of its time in air in cruise. Besides that, after an aircraft takes-off, it has to approach (and land) at some point, resulting in the approach phase considered crucial. It is decided to not focus on the climb phase, as climbing is a choice and not a direct necessity. For each of these flight phases, several criteria are defined as indicated by the numbers in fig. 3.2. The criteria defined in fig. 3.2 are also displayed in table 3.1. In this table, it can be observed that for both the cruise phase and approach phase, the criteria that correspond to either of the phases are given a checkmark. Furthermore, each cell is given a different colour. In this table, green corresponds to criteria that will be evaluated in this research, orange corresponds to criteria that will only be evaluated in case it is executable and time restrictions allow for proper evaluation, and red corresponds to criteria that will not be evaluated. Section 3.4.2 elaborates on each of the different criteria.

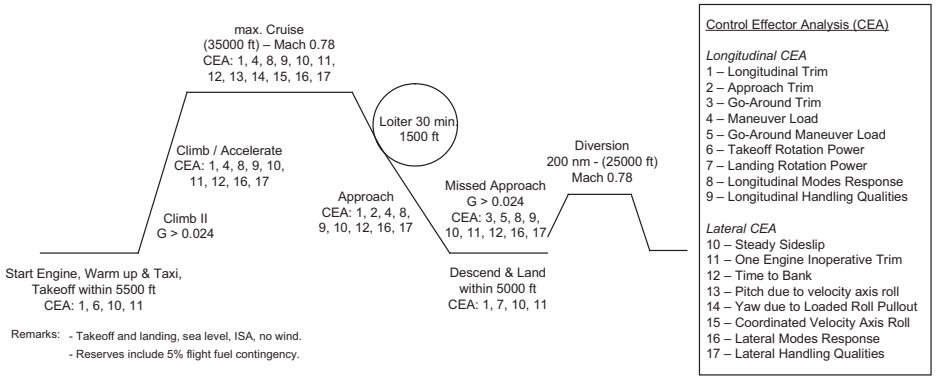

Figure 3.2: Mission Profile and Stability and Handling Qualities Criteria Considered. [Perez, R.E. et al., 2006]

Flight Phase:	**1**	**2**	**3**	**4**	**5**	**6**	**7**	**8**	**9**	**10**	**11**	**12**	**13**	**14**	**15**	**16**	**17**
Cruise Phase	✓			✓				✓	✓	✓	✓	✓	✓	✓	✓	✓	✓
Approach Phase	✓	✓		✓				✓	✓	✓		✓				✓	✓

Table 3.1: Stability and Handling Quality Criteria per Flight Phase

3.4.2. Civil Aviation Authority Requirements

In this section, the different requirements as can be observed in fig. 3.2 are discussed.

Longitudinal Trim (Number 1)

The first criterion is the longitudinal trim condition. This condition requires the aircraft to have the ability to be trimmed to maintain steady 1-g level flight for the cruise-, and approach condition. This has to be demonstrated for the most forward and most aft centre of gravity position. This is mainly demanding for low speeds. [Perez, R.E. et al., 2006]

Approach Trim (Number 2)

The second criterion is the approach trim condition. This condition requires the aircraft to have the ability to be trimmed to maintain steady 1-g level flight for the approach condition with landing gear extended. [CS-25, 2018] Currently, insufficient research as been conducted on the influence of extended landing gear on the aerodynamic coefficients of the TU Delft Flying-V. Therefore, this criterion is not considered for evaluation.

Go-Around Trim (Number 3)

This criterion is not required for either the cruise phase nor the approach phase and is therefore not evaluated.

Manoeuvre Load (Number 4)

The control surfaces should be able to achieve load factors between the maximum and minimum operational limits in a pull-up from a dive over the flight envelope for the cruise-, and approach condition. [Perez, R.E. et al., 2006] This essentially means that using the control surfaces it should be possible to achieve the minimum load factor of -1-g and maximum load factor of 2-g. [CS-25, 2018] This scenario is critical for the maximum take-off weight and forward centre of gravity position. [Perez, R.E. et al., 2006] The limiting factor of this criterion is the size and maximum deflection of the control surfaces. Therefore, this criterion is only assessed in case time restrictions allow.

Go-Around Manoeuvre Load (Number 5)

This criterion is not required for either the cruise phase nor the approach phase and is therefore not evaluated.

Take-off Rotation Power (Number 6)

This criterion is not required for either the cruise phase nor the approach phase and is therefore not evaluated.

Landing Rotation Power (Number 7)

This criterion is not required for either the cruise phase nor the approach phase and is therefore not evaluated.

Longitudinal Modes Response (Number 8)

The longitudinal modes of an aircraft consist of the short period mode and the phugoid mode. As discussed in section 3.4.1, requirements obtained from civil certification authorities do not provide quantitative assessment criteria. Therefore, military standards are used for these criteria as is discussed in section 3.4.3.

Longitudinal Handling Qualities (Number 9)

The main focus of the longitudinal handling qualities involve quantitative handling qualities. The reason for analysing quantitative methods is that it does not require involvement of a pilot-in-the-loop. However, it needs to be noted that potential future pilot-in-the-loop experiments are taken into account while analysing the handling qualities. The first criteria that can be investigated is the stability margins and open-loop responses of the aircraft. Even though stability margins can only be used for linear systems and therefore do not guarantee stability or robustness for a nonlinear system, it is possible to linearise the system and determine the stability margins for a small region around the equilibrium. [Miller, C., 2011] Besides that, it is possible to analyse Gibson's criteria. [Gibson, J.C., 1999] These criteria can be used to evaluate the short period mode and consist of the dropback ratio, flight path delay, maximum pitch rate value, time to reach the first peak, and time to reach steady state. [Tang, S.H., 2014, Van 't Veld, R.C., 2016] Other methods mainly involve pilot-in-the-loop criteria such as analysing the bandwidth, Maximum Unnoticeable Added Dynamics (MUAD), and the Neal-Smith Criterion. [Miller, C., 2011]

Steady Sideslip (Number 10)

For the steady sideslip the lateral control surfaces should have the ability to provide sufficient roll and yaw power to perform a steady sideslip manoeuvre at a 10° sideslip angle. This yields for the cruise-, and approach condition. [Perez, R.E. et al., 2006] For this criterion, the limiting factor is the size and maximum deflection of the control surfaces. Therefore, this criterion is only assessed in case time restrictions allow.

One Engine Inoperative Trim (Number 11)

For the One Engine Inoperative (OEI) Trim, the control surfaces should provide sufficient roll and yaw to maintain a steady straight flight with a 5 degree bank angle in case of an engine failure. This yields for the cruise-, and approach condition. This requirement is most demanding at low airspeeds, especially during take-off due to the larger weight and higher inertial parameters. [Perez, R.E. et al., 2006] Mainly at low airspeeds, the limiting factor is the size and maximum deflection of the control surfaces to provide sufficient control authority. Therefore, this criterion is only assessed in case time restrictions allow.

Time to Bank (Number 12)

The time to bank defines the time it takes to reach a bank angle of 30°. [Anonymous, 1980, Perez, R.E. et al., 2006] This yields for the cruise-, and approach condition. For this criterion, the limiting factor is the size and maximum deflection of the control surfaces. Therefore, this criterion is only assessed in case time restrictions allow.

Pitch due to Velocity Axis Roll (Number 13)

In this case, the elevons of the aircraft have to provide sufficient nose-down pitch authority to compensate for the nose-up moment as a result of inertia cross-coupling during roll manoeuvres. This yields for the cruise condition. [Perez, R.E. et al., 2006] Inertia coupling results when a disturbance along one axis of the aircraft causes a disturbance along another axis of the aircraft. This is mainly the case for high speed aircraft with a high-density fuselage and short, thin wings. It is not expected that this phenomenon is apparent for the TU Delft Flying-V. Therefore, this criterion is only considered in case it becomes apparent from simulation results. [Hurt, H. H., 1965]

Yaw due to Loaded Roll Pullout (Number 14)

In this case, the rudders have to be able to provide adequate control authority to counteract the yawing moment as a result of inertia coupling during a rolling pullout manoeuvre. This yields for the cruise condition. [Perez, R.E. et al., 2006] This manoeuvre can be used to recover the aircraft from a diving condition after stall or spin. [Bunge, R. et al.] This is more evident for high manoeuvrable aircraft compared to transport aircraft. Therefore, this criterion is only considered in case it becomes apparent from simulation results.

Coordinated Velocity Axis Roll (Number 15)

The elevons and the rudders have to provide sufficient control power to be able to maintain zero sideslip when performing a coordinated stability-axis roll. This yields for the cruise condition. [Perez, R.E. et al., 2006] This phenomenon is also likely only present for high manoeuvrable aircraft. [Hurt, H. H., 1965] Therefore, this criterion is only considered in case it becomes apparent from simulation results.

Lateral Modes Response (Number 16)

The lateral modes of an aircraft consist of the aperiodic roll mode, spiral mode, and Dutch roll mode. As discussed in section 3.4.1, requirements obtained from civil certification authorities do not provide quantitative assessment criteria. Therefore, military standards are used for these criteria as is discussed in section 3.4.3.

Lateral Handling Qualities (Number 17)

For the lateral handling qualities, the main focus will be on the analysis of the open-loop stability margins of the aircraft. As is discussed for the longitudinal handling qualities of number 9.

3.4.3. Military Requirements

As mentioned before, civil aviation authorities do not provide quantifiable requirements for the longitudinal- and lateral modes of an aircraft. For this reason, this section elaborates on the use of military (quantifiable) requirements to assess the classical modes of an aircraft. Therefore, it is first necessary to identify the aircraft class, category, and prevailing flight condition. After that, the longitudinal modes responses and handling qualities are discussed and the lateral-directional handling qualities and modes responses are discussed.

Aircraft Identification

Before it is possible to select the key flight requirements it is necessary to identify the aircraft type (class) and the prevailing flight condition (flight phase). From military requirements it is possible to select four different types of aircraft classes that can be used to identify the aircraft types as shown in table 3.2. [Cook, M.V., 2012]

Class I	Small light aircraft (MTOM $<$ 6000 kg)
Class II	Medium weight, low to medium manoeuvrability aircraft (6000 kg $<$ MTOM $<$ 30000 kg)
Class III	Large, heavy, low to medium manoeuvrability aircraft (MTOM $>$ 30000 kg)
Class IV	High manoeuvrability aircraft (e.g. aerobatic or fighter)

Table 3.2: Aircraft class identification. [Cook, M.V., 2012]

After analysing the aircraft class, it is necessary to identify the flight phase the aircraft is prominently in. The different flight phases can be observed in table 3.3. Besides that, to categorise which flight phase belongs to which flight phase category, table 3.4 shows how different flight phases translate to flight phase categories (according to DEF-STAN 00-970). [Cook, M.V., 2012]

Category A	Non-terminal flight phases that require rapid manoeuvring, precision tracking, or precise flight path control.
Category B	Non-terminal flight phases that require gradual manoeuvring, less precise tracking and accurate flight path control.
Category C	Terminal flight phases that require gradual manoeuvring and precision flight path control.

Table 3.3: Aircraft flight phase identification. [Cook, M.V., 2012]

Flight phase category	*Flight phase*
A	Air-to-air combat
	Ground attack
	Weapon delivery/launch
	Reconnaissance
	In-flight refuel (receiver)
	Terrain following
	Maritime search
	Aerobatics
	Close formation flying
B	Climb
	Cruise
	Loiter
	In-flight refuel (tanker)
	Descent
	Aerial delivery
C	Takeoff
	Approach
	Overshoot
	Landing

Table 3.4: Flight phase category to flight phase. [Cook, M.V., 2012]

To identify the ability of the aircraft to complete the mission for which it is designed, three levels of flying qualities can be defined that indicate the severity of the pilot workload during the execution of a specific flight phase. These levels are displayed in table 3.5. [Cook, M.V., 2012]

Level 1	Flying qualities clearly adequate for the mission flight phase.
Level 2	Flying qualities adequate to accomplish the mission flight phase, but with an increase in pilot workload and, or, degradation in mission effectiveness.
Level 3	Degraded flying qualities, but such that the aircraft can be controlled, inadequate mission effectiveness and high, or, limiting, pilot workload.

Table 3.5: Aircraft levels of flying qualities [Cook, M.V., 2012]

The design of the TU Delft Flying-V is similar to that of the Airbus A350[3]. For this reason, the aircraft can be classified as a Class III aircraft. Besides that, from table 3.3 and table 3.4 it can be deduced that the aircraft should be able to adhere the requirements that are linked to flight phase category B and C. In the following sections, the different stability margins and handling qualities are discussed for the TU Delft Flying-V.

3.4.4. Longitudinal Dynamic Stability and Handling Qualities Requirements

In this section, the longitudinal dynamic stability and handling qualities are discussed. This is done by first elaborating on the short period pitching oscillation and after that on the phugoid oscillation.

Short Period Pitching Oscillation

The short period motion is an oscillating pitch rate response. This motion is fast and is the transient response of an elevator input. Therefore, to have a sufficient tracking of a reference signal, the short period must be well damped to reach a steady state pitch condition quickly. [Grotens, R., 2010] To assess the stability of the short period oscillation, fig. A.1 and fig. A.2 can be used. These figures correspond to flight phase B and C respectively. The boundaries of each flying quality level are equal to specific values of the Control Anticipation Parameter (CAP). The CAP is a quantifiable measure to

[3] https://www.tudelft.nl/lr/flying-v

assess the pilot's ability to anticipate on the ultimate response of the aircraft. [Cook, M.V., 2012] The CAP is defined as shown in eq. (3.2). In this equation, $\omega^2_{n_{sp}}$ represents the undamped natural frequency of the short period mode, n_α is the gust- or load-factor-sensitivity of the aircraft, g is the gravitational acceleration, T_{θ_2} can normally be obtained from the short period reduced pitch rate transfer function, and V represents the airspeed. [Cook, M.V., 2012] The definition of the CAP can be considered as follows, in case the CAP is too high, the aircraft's response is faster than would be expected by the pilot resulting in understeering. On the other hand, in case the CAP is too low, the aircraft's response is sluggish resulting in oversteering. [Cappuyns, T., 2019]

$$\text{CAP} = \frac{\omega^2_{n_{sp}}}{n_\alpha} = \frac{g\omega^2_{n_{sp}} T_{\theta_2}}{V} \tag{3.2}$$

The limits of stability of the short period mode are also quantified in terms of the maximum and minimum values of the damping ratio for each flight phase category and level of flying qualities. These are displayed in table A.1.

Taking into account the required CAP and damping ratio for specific handling qualities levels, this results in fig. A.3, these figures combine the requirements set in fig. A.1, fig. A.2, and table A.1. [Roskam, J., 1995]

Phugoid

The phugoid is a slow pitch angle response. During a phugoid motion, the aircraft follows a sinusoidal path, while interchanging potential energy with kinetic energy. [Grotens, R., 2010] In general, the phugoid dynamics are considered acceptable in case the mode is stable and the damping ratio adheres to the limits displayed in table A.2. [Cook, M.V., 2012]

3.4.5. Lateral-Directional Dynamic Stability and Handling Qualities Requirements

In this section, the lateral-directional dynamic stability and handling qualities are discussed. This is done by first elaborating on the aperiodic roll mode, after that on the spiral mode, and finally on the Dutch roll mode.

Aperiodic Roll Mode

This represents the quick response of the roll rate to a control input. In case the control input is removed, the roll rate should return to zero. [Grotens, R., 2010] The limiting acceptable time constants for the roll mode are displayed in table A.3.

Spiral Mode

The spiral mode is a slowly developing turning flight when the aircraft spirals down. In case this motion is stable, the aircraft returns to wings level flight after a roll disturbance. In case this motion is unstable, the roll angle slowly increases. [Grotens, R., 2010] In case the spiral mode is stable, it is always acceptable irrespective of its time constant. This time constant is dependent on lateral static stability, meaning that the maximum level of stability is determined by the maximum acceptable roll control force. Because this mode generally involves slow dynamic behaviour, it is not a very critical mode, unless the mode is very unstable. For this reason, the minimum acceptable degrees of instability are quantified in terms of the time to double bank angle (T_2) during an uncontrolled departure from straight and level flight. This is shown in table A.4. [Cook, M.V., 2012]

Dutch Roll Mode

The Dutch roll is a yawing and simultaneously rolling motion which originates from a side slip deviation that induces a yawing motion. Aerodynamic coupling results into rolling of the aircraft. The vertical tail surface of a conventional aircraft has the largest contribution in dampening the motion. [Grotens,

R., 2010] The Dutch roll mode can be considered as a short period mode and has therefore an important influence on lateral-directional handling qualities. For this reason, the damping and frequency requirements are displayed in table A.5. [Cook, M.V., 2012]

3.5. Stability and Handling Quality Analysis Conclusion

From chapter 1 it is possible to obtain the first sub-question, namely:

> What are the stability and handling qualities of the Flying-V?

To answer this sub-question, it is first necessary to obtain information on the stability and handling quality characteristics of the TU Delft Flying-V. Results from research using wind tunnel experiments applied to a scaled half-model of the TU Delft Flying-V show that the aircraft is statically longitudinally stable for angles of attack up to 20° with the centre of gravity between 1.32m - 1.4m from the nose of the aircraft. Besides that, research on the dynamic stability of the aircraft shows that the Dutch roll is unstable except for the cruise condition with the centre of gravity located at the forward limit.

Secondly, it is necessary to develop stability and handling assessment criteria. The stability and handling quality analysis will be performed for the cruise and approach phase. For each phase, the essential stability and handling quality criteria are selected to be evaluated. These criteria include trimmability of the aircraft, analysis of the dynamic modes, and handling quality assessment such as stability margins and open loop responses.

After analysing the stability and handling quality characteristics and defining criteria to assess these characteristics, it is possible to develop a simulation model that can be used for the analysis. This will be discussed in chapter 4.

4

Simulation Model Design

In this chapter different elements required to obtain a simulation model are discussed. Therefore this chapter aims to answer the second sub-question:

> How can a simulation model of the TU Delft Flying-V aircraft be obtained?

In section 4.1, an overview is given of the different techniques that can be used to simulate aircraft. Furthermore, in section 4.2 different reference frames are defined that can be used during the simulation of the aircraft. After that, section 4.3 elaborates on the assumptions that will be made during the design of the simulation model. The equations of motion and kinematic equations are derived in section 4.4 and section 4.5 respectively. In addition, section 4.6 discusses the determination of the aerodynamic forces and moments acting on the aircraft. Section 4.7 elaborates on verification and validation and the model limitations are discussed in section 4.8. Finally, section 4.9 concludes this chapter.

4.1. Aircraft Simulation Techniques Overview

Aircraft simulation models can be applied to a variety of research areas. First of all, it is possible to use simulation models for flight crew training research. Furthermore, human-machine interface research can be conducted. Besides that, research related to aircraft and equipment design, development, test, and evaluation can be performed. Finally, it is also possible to use simulation models for licensing, certification, and accident investigations. [Baarspul, M., 1990] Especially for research related to aircraft stability and handling qualities, it is necessary to reproduce the behaviour of the aircraft in flight as close as possible. Therefore the basis of any simulation model related to this type of research is a set of dynamic mathematical models of the aerodynamic, propulsion, and inertia characteristics of the aircraft. The aerodynamic model can be obtained by applying system identification techniques to data from theoretical analysis, wind tunnel measurements, and flight tests. [Baarspul, M., 1990]

Traditional theoretical analysis methods make use of data sheets, linear aerodynamic theory, and empirical relations. Continuing on these methods, currently theoretical analysis is also performed using Computational Fluid Dynamics (CFD). Using off-the-shelf CFD tools it is possible to determine aircraft static stability derivatives. Furthermore, to predict dynamic aerodynamic derivatives it is required to apply a time-dependent prescribed motion capability to the solver and specific manoeuvres that adequately excite the desired aerodynamic modes. [Dean, J. et al., 2008]

Theoretical parameter estimation is mainly used during the preliminary design stage. The accuracy of the coefficients can be improved using wind tunnel testing. [Chauhan, R.K. et al., 2017] Wind tunnel experiments are used to test small scale models of the aircraft. Wind tunnel testing is a time consuming and expensive process. Furthermore, proper modelling of the full-scale vehicle is prevented due to blockage, scaling, and Reynolds-number effects together with support interference issues. [Dean, J. et al., 2008]

Flight test data analysis obtained from flight tests can be considered as the most accurate method

to determine stability and control characteristics. [Dean, J. et al., 2008] It is therefore an inherent part of aircraft development and the evaluation of aircraft performance, stability, and control. The aerodynamic characteristics from flight data can be used to better understand theoretical predictions and wind tunnel test results, and to generate more accurate mathematical models of aircraft aerodynamics for aircraft simulation, control system design and evaluation, and dynamic analysis. [Morelli, E.A. and Klein, V., 2005] To obtain the parameters that define the aerodynamic characteristics, flight-test manoeuvres are executed by applying a designed input to the control surfaces of the aircraft. These inputs are perturbations from the nominal or trim control surface deflections. Consequently, various forms of least-squares fitting can be applied to the data to obtain the desired parameters. [Morelli, E.A., 2009]

4.2. Frames of Reference

Before it is possible to construct a set of equations of motion, it is first necessary to construct several reference frames. The reference frames used during this research are the Vehicle-carried normal Earth reference frame ($\mathcal{E}$-frame), the Body-fixed reference frame ($\mathcal{B}$-frame), and the Aerodynamic reference frame ($\mathcal{A}$-frame). In section 4.2.1 the Vehicle-carried normal Earth reference frame is discussed. After that, section 4.2.2 elaborates on the Body-fixed reference frame. Finally, section 4.2.3 discusses the Aerodynamic reference frame.

4.2.1. Vehicle-carried normal Earth reference frame

The Vehicle-carried normal Earth reference frame can be observed in fig. 4.1. [Mulder, J.A. et al., 2013] The location of the origin of this frame is the centre of gravity of the aircraft. The $X_\mathcal{E}Y_\mathcal{E}$ plane is tangential to the surface of the Earth. The $X_\mathcal{E}$-axis is directed to the north and the $Y_\mathcal{E}$-axis is directed 90 degrees to the right of the $X_\mathcal{E}$-axis. In case it is assumed that the Earth is spherical, the $Z_\mathcal{E}$-axis is pointed in the direction of the centre of the Earth. [Mulder, J.A. et al., 2013]

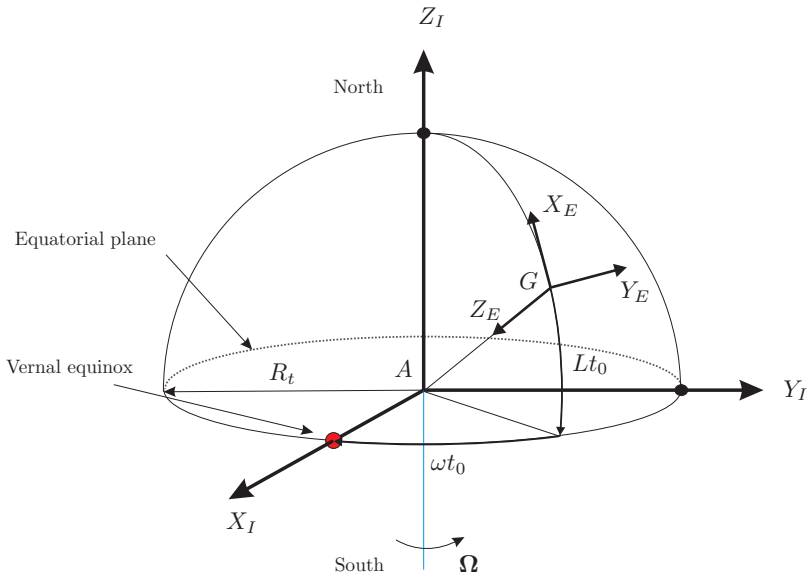

Figure 4.1: Vehicle-carried normal Earth reference frame. [Mulder, J.A. et al., 2013]

4.2.2. Body-fixed reference frame

In fig. 4.2 it is possible to observe the Body-fixed reference frame of the TU Delft Flying-V. [Cappuyns, T., 2019] This is a right-handed coordinate system with the origin located at the centre of mass of the aircraft. This frame remains fixed to the aircraft. The $X_\mathcal{B}$-axis is located in the plane of symmetry and points forward. The $Z_\mathcal{B}$-axis is also located in the symmetry plane and points downwards. Finally, the $Y_\mathcal{B}$-axis completes the right-handed coordinate system and points perpendicular to both the $X_\mathcal{B}$-

axis and the $Z_{\mathcal{B}}$-axis. [Mulder, J.A. et al., 2013] Figure 4.2 also indicates the positive moments and rotational rates around each axis. Where l and p represent the roll moment and roll rate respectively, m and q represent the pitch moment and pitch rate respectively, and n and r represent the yaw moment and yaw rate respectively.

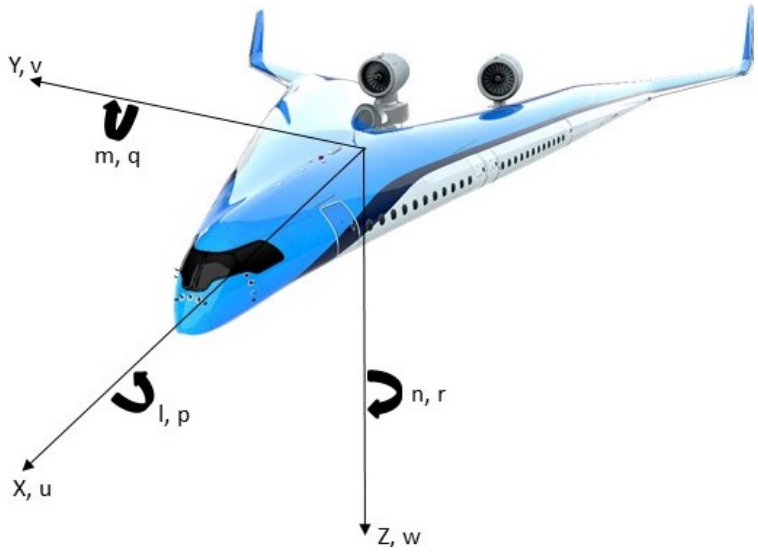

Figure 4.2: Body-fixed reference frame. [Cappuyns, T., 2019]

4.2.3. Aerodynamic Reference Frame

The aerodynamic reference frame is coupled to the aerodynamic velocity of the aircraft (${}^{\mathcal{A}}\boldsymbol{v}$), which is defined as the velocity of the centre of gravity relative to the undisturbed air. The origin of this frame is equal to the origin of the body-fixed reference frame. The $X_{\mathcal{A}}$ axis points into the direction of the aerodynamic velocity (${}^{\mathcal{A}}\boldsymbol{v}$), the $Z_{\mathcal{A}}$ is in the symmetry plane of the aircraft, and $Y_{\mathcal{A}}$ is directed perpendicular to $X_{\mathcal{A}}Z_{\mathcal{A}}$ plane to complete the right-handed coordinate system. In fig. 4.3 it is possible to observe the aerodynamic reference frame relative to the body-fixed reference frame. In this figure α represents the aerodynamic angle of attack and β represents the aerodynamic angle of sideslip. [Mulder, J.A. et al., 2013]

4.3. Assumptions

The following assumptions are made during the construction of the equations of motion [Cappuyns, T., 2019]:

- The aircraft is a rigid body and has a constant mass.
- The Earth is flat and non-rotating.
- There is zero wind and a perfect atmosphere.
- The resultant thrust lies in the symmetry plane (not for OEI).
- The gravitational acceleration is constant.

The forces acting on the aircraft consist of gravity, propulsion forces, and aerodynamic forces. It is assumed that the distributed forces can be replaced with point forces that generate moments around the centre of gravity. [Cappuyns, T., 2019] It needs to be noted that due to the flat and non-rotating Earth assumption, the vehicle-carried normal Earth reference frame is similar to an inertial reference frame. [Mulder, J.A. et al., 2013]

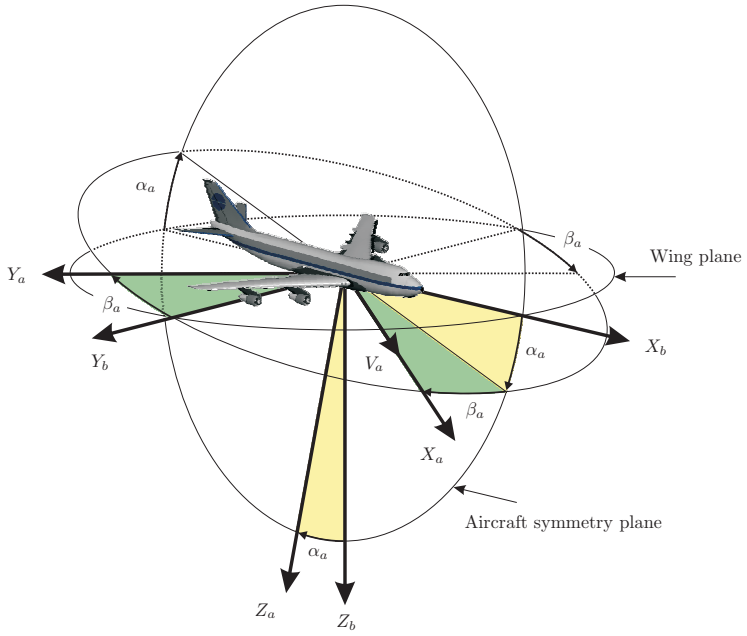

Figure 4.3: Aerodynamic reference frame. [Mulder, J.A. et al., 2013]

4.4. Equations of Motion

In this section, the derivation of the equations of motion is discussed. First, section 4.4.1 elaborates on the position equations of motion. After that, section 4.4.2 displays the attitude equations of motion. The complete set of equations of motion are shown in section 4.4.3. Finally, section 4.4.4, section 4.4.5, and section 4.4.6 elaborate on different components of the equations of motion.

4.4.1. Position Equations of Motion

To design a simulation model of the aircraft it is first necessary to find an equation that relates the external forces and moments to the (angular) acceleration of the aircraft. Starting with the external forces, it can be observed from Newton's second law in eq. (4.1) that the acceleration of the aircraft displayed in $\mathcal{E}$-frame components (${}^{\mathcal{E}}\dot{\boldsymbol{v}}$) is equal to the external forces (F_{ext}) over the mass (m).

$$ {}^{\mathcal{E}}\dot{\boldsymbol{v}} = \frac{\boldsymbol{F}_{\text{ext}}}{m} \tag{4.1} $$

To transform this equation to the body-fixed reference frame, the transport theorem can be used as stated in eq. (4.2). In this equation, ${}^{\mathcal{B}}\dot{\boldsymbol{v}}$ represents the acceleration of the aircraft in $\mathcal{B}$-frame components, ${}^{\mathcal{B}}\boldsymbol{\omega}_{\mathcal{B}/\mathcal{E}}$ represents the angular velocity of the $\mathcal{B}$-frame with respect to the $\mathcal{E}$-frame displayed in $\mathcal{B}$-frame components $\left(\begin{bmatrix} p & q & r \end{bmatrix}^T\right)$ and ${}^{\mathcal{B}}\boldsymbol{v}$ is the velocity of the aircraft in $\mathcal{B}$-frame components $\left(\begin{bmatrix} u & v & w \end{bmatrix}^T\right)$.

$$ {}^{\mathcal{E}}\dot{\boldsymbol{v}} = {}^{\mathcal{B}}\dot{\boldsymbol{v}} + {}^{\mathcal{B}}\boldsymbol{\omega}_{\mathcal{B}/\mathcal{E}} \times {}^{\mathcal{B}}\boldsymbol{v} \tag{4.2} $$

Substituting eq. (4.2) into eq. (4.1) results into eq. (4.3).

$$ \begin{bmatrix} \dot{u} + qw - rv \\ \dot{v} + ru - pw \\ \dot{w} + pv - qu \end{bmatrix} = \frac{\boldsymbol{F}_{\text{ext}}}{m} \tag{4.3} $$

Consequently, the forces acting on the aircraft consist of the gravity force and the aerodynamic forces. The force of gravity can be displayed as: ${}^{\mathcal{E}}\boldsymbol{F}_{\text{grav}} = \begin{bmatrix} 0 & 0 & mg \end{bmatrix}^T$ where g represents the gravitational acceleration. This force is given in $\mathcal{E}$-frame components. To transform the force of gravity

to $\mathcal{B}$-frame components, the transformation matrix $[\mathcal{BE}]$ (as discussed in section 4.4.4) can be used as shown in eq. (4.4).

$$ {}^{\mathcal{B}}\boldsymbol{F}_{\text{grav}} = [\mathcal{BE}]\,{}^{\mathcal{E}}\boldsymbol{F}_{\text{grav}} = \begin{bmatrix} -\sin\theta \\ \sin\phi\cos\theta \\ \cos\phi\cos\theta \end{bmatrix} mg \tag{4.4} $$

Furthermore, the forces acting on the aircraft consist of the aerodynamic forces including engine forces (${}^{\mathcal{B}}\boldsymbol{F}_{\text{aero}}$). These forces are assumed to be present in the $\mathcal{B}$-frame and can therefore be used directly. Therefore, eq. (4.3) can be written as eq. (4.5) to obtain the position equations of motion.

$$ {}^{\mathcal{B}}\dot{\boldsymbol{v}} = \begin{bmatrix} -\sin\theta \\ \sin\phi\cos\theta \\ \cos\phi\cos\theta \end{bmatrix} g + \frac{{}^{\mathcal{B}}\boldsymbol{F}_{\text{aero}}}{m} - \begin{bmatrix} qw - rv \\ ru - pw \\ pv - qu \end{bmatrix} = \frac{{}^{\mathcal{B}}\boldsymbol{F}_{\text{grav}}}{m} + \frac{{}^{\mathcal{B}}\boldsymbol{F}_{\text{aero}}}{m} - {}^{\mathcal{B}}\Omega_{\mathcal{B}/\mathcal{E}}\,{}^{\mathcal{B}}\boldsymbol{v} \tag{4.5} $$

After integration it is possible to obtain the velocity in the $\mathcal{B}$-frame (${}^{\mathcal{B}}\boldsymbol{v}$). Consequently, to obtain the velocity in the $\mathcal{E}$-frame, the transformation matrix $[\mathcal{EB}]$ can be used which transforms the $\mathcal{B}$-frame to the $\mathcal{E}$-frame (as discussed in section 4.4.4). This can be observed in eq. (4.6).

$$ {}^{\mathcal{E}}\boldsymbol{v} = \begin{bmatrix} V_N \\ V_E \\ V_D \end{bmatrix} = [\mathcal{EB}]\,{}^{\mathcal{B}}\boldsymbol{v} \tag{4.6} $$

Integrating the velocity components in the $\mathcal{E}$-frame results in the position of the aircraft in $\mathcal{E}$-frame components.

4.4.2. Attitude Equations of Motion

To obtain the attitude equations of motion, it is necessary to start with the fact that a moment acting on a body in an inertial reference frame results in a change in angular momentum as seen in eq. (4.7). In this equation, ${}^{\mathcal{E}}\boldsymbol{H}$ represents the angular momentum in $\mathcal{E}$-frame components and $\boldsymbol{M}$ represents the moment acting on the aircraft.

$$ {}^{\mathcal{E}}\dot{\boldsymbol{H}} = \boldsymbol{M} \tag{4.7} $$

Using the transport theorem, this results in the change in angular momentum displayed in $\mathcal{B}$-frame components as shown in eq. (4.8).

$$ {}^{\mathcal{B}}\dot{\boldsymbol{H}} + {}^{\mathcal{B}}\boldsymbol{\omega}_{\mathcal{B}/\mathcal{E}} \times {}^{\mathcal{B}}\boldsymbol{H} = \boldsymbol{M} \tag{4.8} $$

Furthermore, it needs to be noted that angular momentum is formulated as: ${}^{\mathcal{B}}\boldsymbol{H} = I\,{}^{\mathcal{B}}\boldsymbol{\omega}_{\mathcal{B}/\mathcal{E}}$, where I represents the inertia matrix displayed in section 4.4.6. Because a rigid body is assumed with a constant mass, the time derivative of the angular momentum can be displayed as: ${}^{\mathcal{B}}\dot{\boldsymbol{H}} = I\,{}^{\mathcal{B}}\dot{\boldsymbol{\omega}}_{\mathcal{B}/\mathcal{E}}$. Therefore eq. (4.8) can be written as shown in eq. (4.9).

$$ I\,{}^{\mathcal{B}}\dot{\boldsymbol{\omega}}_{\mathcal{B}/\mathcal{E}} + {}^{\mathcal{B}}\boldsymbol{\omega}_{\mathcal{B}/\mathcal{E}} \times I\,{}^{\mathcal{B}}\boldsymbol{\omega}_{\mathcal{B}/\mathcal{E}} = \boldsymbol{M} \tag{4.9} $$

There are two types of forces acting on the aircraft that can cause moments. First of all, the force of gravity. However, this force acts on the centre of gravity resulting in zero moment. Furthermore, the aerodynamic forces are able to generate moments acting on the aircraft and are displayed as: ${}^{\mathcal{B}}\boldsymbol{M}_{\text{aero}}$. Therefore, the attitude equations of motion can be written as shown in eq. (4.10). In this equation, ${}^{\mathcal{B}}\Omega_{\mathcal{B}/\mathcal{E}}$ represents the angular velocity matrix as is discussed in section 4.4.5.

$$ {}^{\mathcal{B}}\dot{\boldsymbol{\omega}}_{\mathcal{B}/\mathcal{E}} = I^{-1}\,{}^{\mathcal{B}}\boldsymbol{M}_{\text{aero}} - I^{-1}\,{}^{\mathcal{B}}\Omega_{\mathcal{B}/\mathcal{E}} I\,{}^{\mathcal{B}}\boldsymbol{\omega}_{\mathcal{B}/\mathcal{E}} \tag{4.10} $$

4.4.3. Complete Set of Equations of Motion

In eq. (4.11) it is possible to find the complete set of equations of motion in matrix form.

$$\begin{bmatrix} {}^{\mathcal{B}}\dot{\boldsymbol{v}} \\ {}^{\mathcal{B}}\dot{\boldsymbol{\omega}}_{\mathcal{B}/\mathcal{E}} \end{bmatrix} = \begin{bmatrix} -{}^{\mathcal{B}}\Omega_{\mathcal{B}/\mathcal{E}} & 0 \\ 0 & -I^{-1}{}^{\mathcal{B}}\Omega_{\mathcal{B}/\mathcal{E}} I \end{bmatrix} \begin{bmatrix} {}^{\mathcal{B}}\boldsymbol{v} \\ {}^{\mathcal{B}}\boldsymbol{\omega}_{\mathcal{B}/\mathcal{E}} \end{bmatrix} + \begin{bmatrix} \frac{{}^{\mathcal{B}}\boldsymbol{F}_{\text{grav}}}{m} + \frac{{}^{\mathcal{B}}\boldsymbol{F}_{\text{aero}}}{m} \\ I^{-1}{}^{\mathcal{B}}\boldsymbol{M}_{\text{aero}} \end{bmatrix} \tag{4.11}$$

4.4.4. Normal Earth to Body Fixed Reference Frame Transformation

In eq. (4.12) it is possible to observe the transformation matrix that transforms the normal earth reference frame to the body fixed reference frame. In this equation ϕ represents the roll angle, θ represents the pitch angle, and ψ represents the yaw angle.

$$[\mathcal{BE}] = \begin{bmatrix} \cos\psi\cos\theta & \sin\psi\cos\theta & -\sin\theta \\ \cos\psi\sin\theta\sin\phi - \sin\psi\cos\phi & \sin\psi\sin\theta\sin\phi + \cos\psi\cos\phi & \cos\theta\sin\phi \\ \cos\psi\sin\theta\cos\phi + \sin\psi\sin\phi & \sin\psi\sin\theta\cos\phi - cos\psi\sin\phi & \cos\theta\cos\phi \end{bmatrix} \tag{4.12}$$

4.4.5. Angular Velocity Matrix

The angular velocity matrix can be observed in eq. (4.13).

$${}^{\mathcal{B}}\Omega_{\mathcal{B}/\mathcal{E}} = \begin{bmatrix} 0 & -r & q \\ r & 0 & -p \\ -q & p & 0 \end{bmatrix} \tag{4.13}$$

4.4.6. Inertia Matrix

The inertia matrix can be observed in eq. (4.14). The coefficients I_{xy} and I_{yz} can be set to zero as the TU Delft Flying-V is assumed to be a mass-symmetrical vehicle. [Cappuyns, T., 2019]

$$I = \begin{bmatrix} I_{xx} & -I_{xy} & -I_{xz} \\ -I_{xy} & I_{yy} & -I_{yz} \\ -I_{xz} & -I_{yz} & I_{zz} \end{bmatrix} \tag{4.14}$$

Inertia Estimation

To estimate the inertia of the TU Delft Flying-V, [Cappuyns, T., 2019] makes use of a lumped mass model. The general idea of this method is to consider the power plant and landing gear as point masses. The rest of the aircraft is divided in lumped masses placed at half chord locations. The lumped masses are divided over point masses equally spaced from the root of the wing to the tip. The spacing is considered to be good enough such that the Moment of Inertia around each specific point mass is negligible (meaning that the Steiner Theorem can be use to obtain the Moment of Inertia of the aircraft). [Cappuyns, T., 2019] The resulting principle axes moments of inertia can be observed in table 4.1.

Table 4.1: Moments of Inertia for TU Delft Flying-V. [Cappuyns, T., 2019]

Inertia	MTOW	Empty Weight	Unit
I_{xx}	3.9641	1.2275	$[\cdot 10^7 \text{kgm}^2]$
I_{yy}	2.7619	1.0504	$[\cdot 10^7 \text{kgm}^2]$
I_{zz}	6.5822	2.1437	$[\cdot 10^7 \text{kgm}^2]$

4.5. Euler Kinematics

To obtain the Euler angles from the rotational rates in the body fixed reference frame ($\boldsymbol{\omega}_b$) it is possible to use eq. (4.15). In this equation, ϕ represents the roll angle, θ is the pitch angle, and ψ is the yaw angle.

$$\begin{bmatrix} \dot{\phi} \\ \dot{\theta} \\ \dot{\psi} \end{bmatrix} = \begin{bmatrix} 1 & \sin\phi\tan\theta & \cos\phi\tan\theta \\ 0 & \cos\phi & -\sin\phi \\ 0 & \frac{\sin\phi}{\cos\theta} & \frac{\cos\phi}{\cos\theta} \end{bmatrix} \begin{bmatrix} p \\ q \\ r \end{bmatrix}_{\mathcal{B}} \tag{4.15}$$

4.6. Aerodynamic Model

In this section the different sources that can be used to obtain several aerodynamic coefficients to construct the aerodynamic forces and moments are discussed. In section 4.6.1 the Vortex Lattice Method is discussed. After that, section 4.6.2 elaborates on the wind tunnel experiments that have been performed. Finally, section 4.6.3 talks about the flight test experiments performed to obtain the aerodynamic coefficients.

4.6.1. Vortex Lattice Method

The geometry defined in previous work is used to obtain the aerodynamic coefficients using Odilila, which is a Vortex Lattice Method. The aircraft geometry is first translated into BlackSwan, which transforms this parametric model into a strip model that can be used for inertia estimations and a panel model that can be used for aerodynamic estimations. [Cappuyns, T., 2019]

Using Odilila, it is possible to compute the lift and induced drag of the aircraft, while omitting the thickness and viscosity. Furthermore, Odilila also takes into account the taper, twist, camber, control surfaces, high lift devices, and nacelles. The output of Odilila consists of the aerodynamic coefficients for specific Mach numbers. [Cappuyns, T., 2019] The panel method of Odilila for the TU Delft Flying-V can be observed in fig. 4.4.

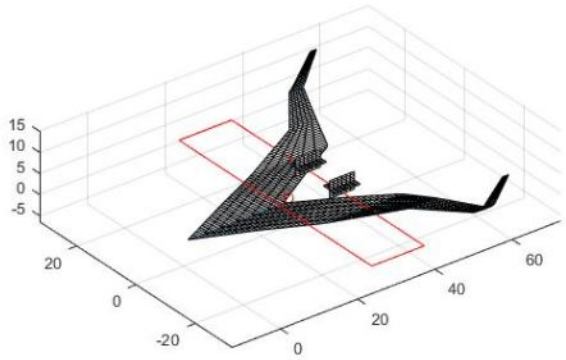

Figure 4.4: Odilila panel method for TU Delft Flying-V [Cappuyns, T., 2019]

To validate the aerodynamic model, the lift coefficient and pitching moment coefficient were compared with the wind tunnel tests performed by [Palermo, M. et al., 2020]. It needs to be noted that the model in the wind tunnel tests consists of a half-span model without winglets added to the wing planform. [Cappuyns, T., 2019] Furthermore, it needs to be noted that the wing planform designed by [Cappuyns, T., 2019] only consists of two elevons, whereas the design used for the wind tunnel experiments consists of three elevons. The results can be observed in fig. 4.5. It is possible to observe that up to an angle of attack of 10° the slope of both lift curves is equal, but starts to diverge afterwards. However, the moment curve starts with an offset and converges for angles of attack larger than 10°. Finally, it needs to be noted that the wind tunnel experiments are performed with a free stream velocity of 20 m/s and Reynolds number of $1 \cdot 10^6$, while the results from Odilila are obtained for a velocity of 250 m/s and Reynolds number of $6.5 \cdot 10^6$.

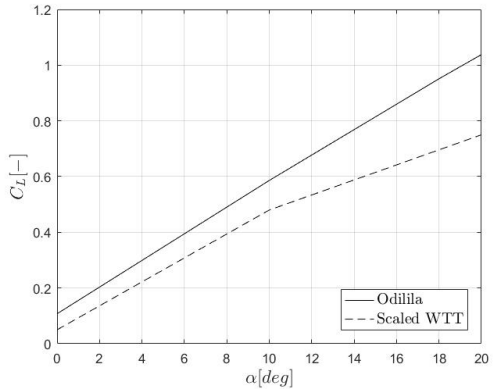

(a) Lift coefficient comparison between Odilila and wind tunnel experiment. [Cappuyns, T., 2019]

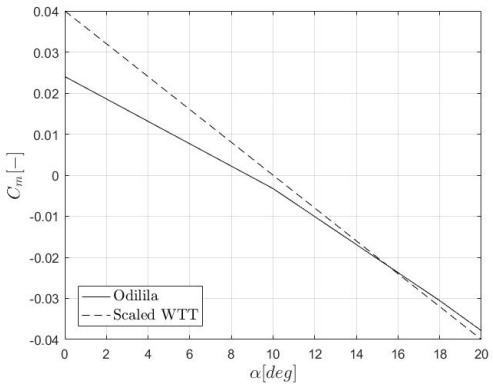

(b) Moment coefficient comparison between Odilila and wind tunnel experiment. [Cappuyns, T., 2019]

Figure 4.5: Odilila Validation

4.6.2. Wind Tunnel Experiments

As mentioned before, [Garcia, A.R., 2019] makes use of wind tunnel experiments for a 4.6% scaled half model of the TU Delft Flying-V. During this research, several independent variables (the angle of attack, wind speed, and elevon deflections) are altered to determine the aerodynamic coefficients (dependent variables). During the identification process, it is assumed that the independent variables are not contaminated with noise, while the dependent variables are contaminated with uniformly distributed noise. During the experiments at high angles of attack, vibrations occurred that affected the accuracy of the measurements. To make sure that the right coefficients are calculated, four runs were performed for each angle of attack. Two at an airspeed of 18m/s and two at an airspeed of 20m/s. For this reason, the measurements are considered accurate enough for angles of attack ranging from -10° up to 30°. The regions for which the aerodynamic coefficients are valid can be observed in fig. 4.6. Outside this convex full, unmodeled effects might occur, decreasing the validity of the aerodynamic model. [Garcia, A.R., 2019]

The different polynomial models to obtain the aerodynamic coefficients can be observed in eq. (6.2). Due to high uncertainties, the lateral force coefficient (C_Y) could not be used for analysis. [Garcia, A.R., 2019] Therefore, the lateral-directional force and moment coefficients only involve C_Z, C_l, and C_n as seen below.

$$
\begin{aligned}
C_X &= C_{X_0} + C_{X_\alpha}\alpha + C_{X_{\alpha^2}}\alpha^2 + C_{X_{\alpha^3}}\alpha^3 + C_{X_{\alpha^4}}\alpha^4 + C_{X_{\delta_1}}\delta_1 + C_{X_{\delta_2}}\delta_2 + C_{X_{\delta_3}}\delta_3 \\
&\quad + C_{X_{\delta_1^2}}\delta_1^2 + C_{X_{\delta_2^2}}\delta_2^2 + C_{X_{\hat{V}}}\hat{V} + C_{X_{\hat{V}^2}}\hat{V}^2 \\
C_Z &= C_{Z_0} + C_{Z_\alpha}\alpha + C_{Z_{\alpha^2}}\alpha^2 + C_{Z_{\alpha^3}}\alpha^3 + C_{Z_{\delta_1}}\delta_1 + C_{Z_{\delta_2}}\delta_2 + C_{Z_{\delta_3}}\delta_3 + C_{Z_{\hat{V}}}\hat{V} \\
C_l &= C_{l_0} + C_{l_\alpha}\alpha + C_{l_{\alpha^2}}\alpha^2 + C_{l_{\alpha^3}}\alpha^3 + C_{l_{\alpha^4}}\alpha^4 C_{l_{\delta_1}}\delta_1 + C_{l_{\delta_2}}\delta_2 + C_{l_{\delta_3}}\delta_3 + C_{l_{\hat{V}}}\hat{V} \\
C_m &= C_{m_0} + C_{m_\alpha}\alpha + C_{m_{\alpha^2}}\alpha^2 + C_{m_{\alpha^3}}\alpha^3 + C_{m_{\alpha^4}}\alpha^4 + C_{m_{\delta_1}}\delta_1 + C_{m_{\delta_2}}\delta_2 + C_{m_{\delta_3}}\delta_3 \\
&\quad + C_{m_{\delta_1^2}}\delta_1^2 + C_{m_{\delta_2^2}}\delta_2^2 + C_{m_{\delta_1\delta_2}}\delta_1\delta_2 + C_{m_{\alpha\delta_1^2}}\alpha\delta_1^2 + C_{m_{\alpha\delta_2^2}}\alpha\delta_2^2 + C_{m_{\alpha^2\delta_1}}\alpha^2\delta_1 \\
&\quad + C_{m_{\alpha^2\delta_2}}\alpha^2\delta_2 + C_{m_{\hat{V}}}\hat{V} + C_{m_{\hat{V}\delta_1}}\hat{V}\delta_1 \\
C_n &= C_{n_0} + C_{n_\alpha}\alpha + C_{n_{\alpha^2}}\alpha^2 + C_{n_{\alpha^3}}\alpha^3 + C_{n_{\alpha^4}}\alpha^4 + C_{n_{\delta_1}}\delta_1 + C_{n_{\delta_2}}\delta_2 + C_{n_{\delta_1^2}}\delta_1^2 + C_{n_{\delta_2^2}}\delta_2^2 \\
&\quad + C_{n_{\hat{V}}}\hat{V}
\end{aligned}
\tag{4.16}
$$

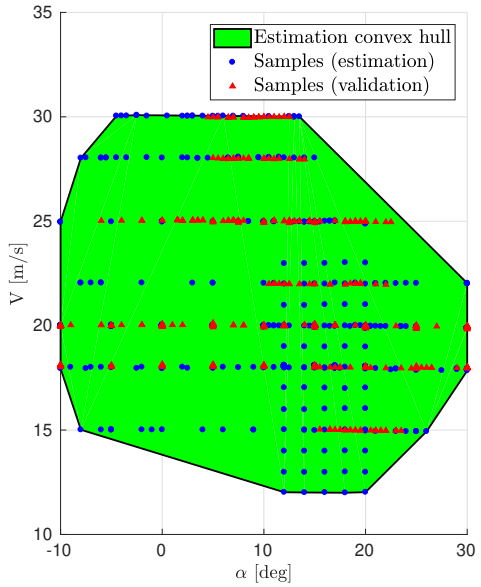

(a) Convex hull for angle of attack versus airspeed. [Garcia, A.R., 2019]

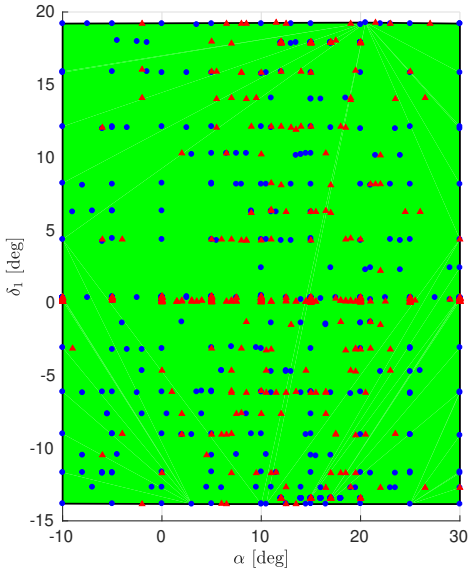

(b) Convex hull for angle of attack versus elevator deflection. [Garcia, A.R., 2019]

Figure 4.6: Convex hulls.

4.6.3. Flight Test Experiments

After performing the maiden flight test of the TU Delft Flying-V, Alberto Garcia [Garcia, A.R., 2021] has worked on a system identification implementation of the flight data to obtain the forces and moments acting on the aircraft. An impression of the flight test is shown in fig. 4.7.

Figure 4.7: Flight test impression. [Flying-V Website, 2020]

Before diving into the model, it is necessary to note that the model consists of some uncertainties:

- First of all, the model is based on a single flight test in which no specific manoeuvres for aerodynamic identification could be performed.
- The model for the pitching moment (C_m) has a lower quality compared to the rest of the coefficients due to higher noise present in the measurements. The aircraft has to fly at least once more to get a better estimate.
- There might be a shift in angle of attack, which will change the moment coefficients in case this is true. In fig. 4.8 it is possible to observe the comparison of the lift coefficient of the maiden flight test with the wind tunnel tests performed by [Garcia, A.R., 2019]. It can be observed that the

slope is exactly the same, however, the result from the maiden test flight is shifted with respect to the wind tunnel data. Besides that, looking at the curve from the drag coefficient, it can be observed that the drag is higher for the maiden flight test. This is due to induced drag from nacelles, pylons, landing gear, cooling ducts etc.

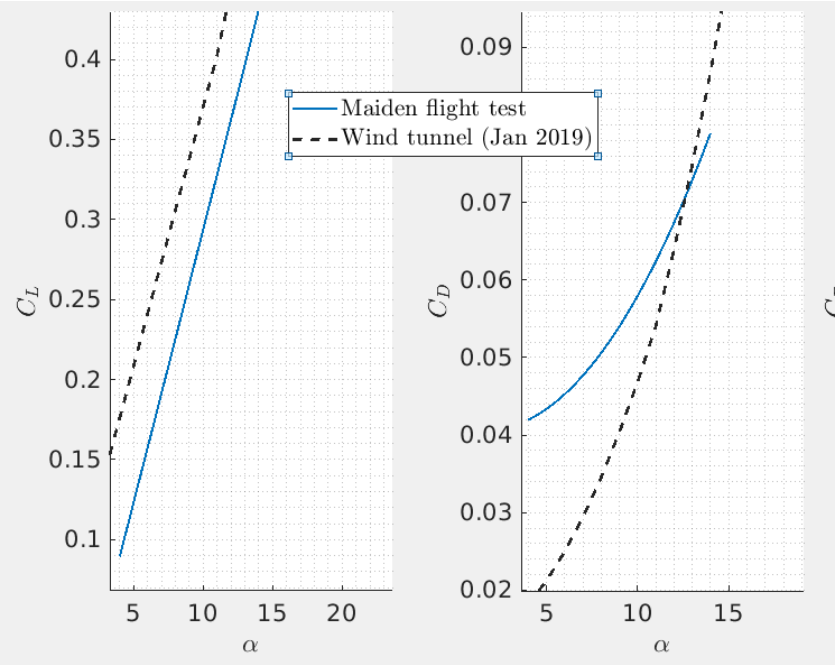

Figure 4.8: Lift and drag polars from wind tunnel test and maiden flight test. [Garcia, A.R., 2021]

The inputs of the model consist of the airspeed (V), the angle of attack (α), the angle of sideslip (β), the dimensionless roll rate ($\hat{p} = \frac{pb}{2V}$ with b equal to the span), the dimensionless pitch rate ($\hat{q} = \frac{qc}{2V}$ with c equal to the span), the dimensionless yaw rate ($\hat{r} = \frac{rb}{2V}$ with b equal to the span), the dimensionless pitch input (δ_e ranges between [-1,1]), the dimensionless roll input (δ_a ranges between [-1,1]), the dimensionless yaw input (δ_r ranges between [-1,1]), the advance ratio ($J = \frac{V}{nD}$ with n the rotational speed of the engine blades in revolutions per second and D the diameter of the engine), and the angular velocity of the engine blades (ω_{eng}). The output of the model consists of the aerodynamic coefficients in the body fixed reference frame.

It needs to be noted that the pilot stick inputs (ranging between [-1,1]) are used as control surface deflections (shown in table 4.2). The maximum down and maximum up deflection of different control surfaces can be observed in table 4.2. The controls used during the flight test consisted of elevon deflections for pitch and roll, and rudder deflections for yaw. The control authority for a pitch input is equal to 80% on the elevons, the control authority for a roll input is 50% on the elevons, and the control authority for a yaw input is 100% on the rudders. This essentially means that e.g. a pitch input of 1 corresponds to 80% of the maximum down deflection and an input of -1 corresponds to 80% of the maximum up deflection.

Table 4.2: Control Surface Deflections. [Garcia, A.R., 2021]

Control Surface	Maximum Down Deflection	Maximum Up Deflection
CS 1	18 degrees	-25 degrees
CS 2	25 degrees	-25 degrees
CS 3	25 degrees	-25 degrees
Rudders	27 degrees	-29 degrees

It needs to be noted that during the flight test, only small deflections of the control surfaces were used. Therefore, this model can be used for the ranges displayed in table 4.3.

Table 4.3: Flight Test Model Limitations. [Garcia, A.R., 2021]

Parameter	Maximum Value	Minimum Value	Unit
Pitch Deflection	$3.2399 \cdot 10^{-1}$	$-3.1511 \cdot 10^{-1}$	[-]
Roll Deflection	$3.6608 \cdot 10^{-1}$	$-4.5057 \cdot 10^{-1}$	[-]
Yaw Deflection	$2.6202 \cdot 10^{-1}$	$-2.4529 \cdot 10^{-1}$	[-]
$\hat{p}$	$3.0364 \cdot 10^{-3}$	$-2.6807 \cdot 10^{-3}$	[-]
$\hat{q}$	$6.1234 \cdot 10^{-5}$	$-6.1123 \cdot 10^{-5}$	[-]
$\hat{r}$	$1.4888 \cdot 10^{-3}$	$-7.1897 \cdot 10^{-4}$	[-]
α	$2.2014 \cdot 10^{-1}$	$8.0387 \cdot 10^{-3}$	[rad]
β	$1.3819 \cdot 10^{-1}$	$-1.0600 \cdot 10^{-1}$	[rad]

After the different inputs it is possible several regressors as can be observed in eq. (4.17).

$$\begin{aligned} q_{\text{inf}} &= \frac{1}{2}\rho V^2 \\ \text{bias} &= 1 \\ V &= \frac{V}{V_{\text{ref}}} \\ J_{m_1} &= J^{-1} \\ J_{m_2} &= J^{-2} \\ \omega_{\text{eng}_r} &= \omega_{\text{eng}}\hat{r} \\ \omega_{\text{eng}_{rq}} &= \frac{\omega_{\text{eng}_r}}{q_{\text{inf}}} \\ \alpha_q &= \alpha\hat{q} \\ \omega_{\text{eng}_q} &= \omega_{\text{eng}}\hat{q} \\ \alpha_{J_{m_2}} &= \alpha J_{m_2} \\ \alpha_{\delta_e} &= \alpha\delta_e \end{aligned} \tag{4.17}$$

The equations used to obtain the aerodynamic force and moment coefficients can consequently be observed in eq. (4.18).

$$\begin{aligned} C_X &= C_{X_{J_{m_1}}} J_{m_1} - C_{X_{J_{m_2}}} J_{m_2} + C_{X_\alpha}\alpha + C_{X_{\alpha^2}}\alpha^2 + C_{X_\beta}\beta - C_{X_{\text{bias}}}\text{bias} \\ C_Y &= C_{Y_V} V - C_{Y_\beta}\beta - C_{Y_{\text{bias}}}\text{bias} + C_{Y_{\delta_a}}\delta_a - C_{Y_{\delta_r}}\delta_r - C_{Y_{\hat{p}}}\hat{p} + C_{Y_{\hat{r}}}\hat{r} \\ C_Z &= C_{Z_\alpha}\alpha + C_{Z_{\text{bias}}}\text{bias} - C_{Z_{\delta_e}}\delta_e - C_{Z_{\hat{q}}}\hat{q} \\ C_m &= C_{m_{J_{m_2}}} J_{m_2} - C_{m_V} V - C_{m_\alpha}\alpha + C_{m_{\text{bias}}}\text{bias} - C_{m_{\delta_e}}\delta_e + C_{m_{\omega_{\text{eng}_{rq}}}}\omega_{\text{eng}_{rq}} + C_{m_{\hat{q}}}\hat{q} - C_{m_{\hat{r}}}\hat{r} \\ C_l &= C_{l_{\alpha q}}\alpha q - C_{l_{\alpha\beta}}\alpha\beta - C_{l_{\beta^2}}\beta^2 - C_{l_\beta}\beta - C_{l_{\text{bias}}}\text{bias} + C_{l_{\delta_a}}\delta_a - C_{l_{\delta_r}}\delta_r - C_{l_{\hat{p}}}\hat{p} + C_{l_{\hat{r}}}\hat{r} \\ C_n &= C_{n_\beta}\beta - C_{n_{\text{bias}}}\text{bias} + C_{n_{\delta_a}}\delta_a - C_{n_{\delta_r}}\delta_r - C_{n_{\hat{p}}}\hat{p} - C_{n_{\hat{r}}}\hat{r} \end{aligned} \tag{4.18}$$

4.6.4. Aerodynamic Model Selection

Based on section 4.6.1, section 4.6.2, and section 4.6.3 it is possible to deduce that there are three sources that can be used to obtain the aerodynamic model. None of the aerodynamic sources is perfect, meaning that it is necessary to find a solution to make a well-considered choice for the aerodynamic model that will be used. To make a well-considered choice, the choice for the aerodynamic model depends on three different criteria:

- The ability of the model to catch the aircraft's instabilities.
- The availability of the most important aerodynamic coefficients.

- The accuracy of the coefficients.

Starting with the ability to catch the aircraft's instabilities, the goal of this research is to assess and where necessary improve the stability and handling qualities of the TU Delft Flying-V. From literature, it can concluded that the main instabilities of the aircraft consist of the pitch break for angles of attack larger than 20 degrees and the unstable Dutch roll during approach. Therefore, it is essential that the aerodynamic model is able to capture this behaviour. The model obtained from the Vortex Lattice Method does show the unstable roll, however, because this is a linear model it does not show the pitch break behaviour. Secondly, the wind tunnel model does show the pitch break behaviour but does not show unstable Dutch roll due to the limited lateral-directional system identification. Thirdly, during the flight test, the aircraft experienced unstable Dutch roll. It is therefore expected that this is phenomenon can be captured with this model. Due to the small fidelity range of the model it is not expected that this model is able to correctly capture the pitch break. The second and third criteria are summarised in table 4.4 and table 4.5. In these tables it is possible to observe the value and uncertainty of several aerodynamic coefficients obtained from the Vortex Lattice Method (VLM), Wind Tunnel Experiments (WTE), and Flight Test Experiments (FTE). The most important aerodynamic coefficients are given the colour green. The selection of these coefficients is based on the fact that these coefficients are expected to have the largest influence on stability of the aircraft's eigenmodes. The C_{Z_q} coefficient is coloured orange as this coefficient is expected to influence the stability, but to have a minor effect compared to the green coefficients. The uncertainty of the VLM method is obtained by comparing the moment coefficient gradient and the lift coefficient gradient relative to the angle of attack of the VLM method with wind tunnel experiments. The uncertainty of the wind tunnel experiments is obtained during the system identification process, which was done by adding white noise to the process. The uncertainty of the flight test experiment is unknown. The green coloured aerodynamic coefficients are shortly discussed:

- C_{X_u}: The sign of this coefficient depends on the flight path angle. This explains the discrepancies between the different methods.
- C_{Z_u}: The sign of this coefficient is generally negative. However, the coefficients obtained are positive.
- C_{m_u}: The sign of this coefficient is generally close to zero. This is also the case for the coefficients in the table.
- C_{l_p}: The sign of this coefficient is generally smaller than zero. This is also the case for the coefficients in the table. This coefficient could not be obtained from the WTE.
- C_{n_p}: This coefficient is generally larger than zero. This is also the case for the coefficients in the table. This coefficient could not be obtained from the WTE.
- C_{Z_q}: This coefficient is generally smaller than zero. This is not the case for the VLM model, but is the case for the FTE model.
- C_{m_q}: This coefficient is generally smaller than zero. This is also the case for the coefficients in the table. This coefficient could not be obtained from the WTE.
- C_{l_r}: This coefficient is generally larger than zero. This is also the case for the coefficients in the table. This coefficient could not be obtained from the WTE.
- C_{n_r}: This coefficient is generally smaller than zero. This is only the case for the coefficient of the VLM method. This coefficient could not be obtained from the WTE.
- C_{X_α}: The sign of this coefficient depends on the angle of attack. In general it is negative for negative angles of attack and positive for positive angles of attack.
- C_{Z_α}: This coefficient is in general smaller than zero. This is also the case for the coefficients of the WTE and FTE.
- C_{m_α}: This coefficient is in general smaller than zero. This is also the case for the coefficients in the table.

- C_{Y_β}: This coefficient is in general smaller than zero. This is also the case for the coefficients in the table. This coefficient could not be obtained from the WTE.
- C_{l_β}: This coefficient is in general smaller than zero. This is also the case for the coefficients in the table. This coefficient could not be obtained from the WTE.
- C_{n_β}: This coefficient is in general larger than zero. This is also the case for the coefficients in the table. This coefficient could not be obtained from the WTE.

Based on the aforementioned criteria it is possible to conclude that the VLM model is able to model unstable Dutch roll, the WTE model is able to model pitch break, and the FTE is expected to be able to model unstable Dutch roll. Furthermore, both the VLM model and the FTE model have a value for all important coefficients, whereas the WTE model only has a value for static longitudinal coefficients. Finally, the uncertainty of the VLM model is large, the uncertainty of the WTE model is small, and the uncertainty of the FTE model is unknown. Finally, it is decided to couple the VLM model and WTE model such that it is possible to obtain an aerodynamic model that is able to capture the unstable behaviour with known uncertainty bounds.

4.7. Verification and Validation

This section elaborates on the verification and validation methods that can be used to guarantee correct results from the simulation model of the aircraft. First, section 4.7.1 elaborates on the verification of the aircraft. After that section 4.7.2 elaborates on the validation of the aircraft.

4.7.1. Verification

To verify the simulation model of the aircraft, it is necessary to check whether no computational errors are made. Based on the research performed by [Cappuyns, T., 2019], it is consequently possible to verify the correctness of the model by removal of all forces except for gravity. In this case, the aircraft is treated as a point mass and for a specific altitude it is possible to assess the different velocity- and acceleration components for several different reference frames. Besides that, several other features can be assessed to verify the model. First of all, the load factor for a coordinated turn with bank angle ϕ is equal to: $n_z = \frac{1}{\cos\phi}$. After initialising a specific bank angle, it is possible to verify that the load factor corresponds to the correct value. Besides that, [Cappuyns, T., 2019] initiates a rate one turn, which is defined as a 360° turn completed in 2 minutes. This turn is initiated to demonstrate that the Euler yaw angle increases linearly from 0° to 360°.

4.7.2. Validation

Ideally, validation of the simulation model of an aircraft is accomplished by comparison of accurately predicted aerodynamic responses of the aircraft from the simulation model with experimental tests. [Murphy, P. et al., 2003] The same holds for the TU Delft Flying-V aircraft. Ideally, the simulation model in this research is validated using data obtained from a flight test. There are two reasons why it seems unreasonable to make use of flight test data from the maiden flight test for validation purposes. First of all, the flight test involves a small scale model, whereas the simulation model considers a full scale model. Therefore, it is necessary to apply dynamic scaling to one of the models. This is however not possible, because the mass distribution of the full scale model and small scale model is different, resulting in the fact that it is not possible to apply a scaling factor to one of the models. Garcia, A.R. [2019] Besides that, Reynolds number effects will be present due to discrepancies between the airflow over the small scale model and full scale model. Garcia, A.R. [2019] For these two reasons, using the flight test data for validation purposes is considered unreliable.

	u			p			q			r		
$C_{X_{...}}$	VLM	$1.519 \cdot 10^{-3}$	25%	VLM	$-2.233 \cdot 10^{-2}$	25%	VLM	$1.121 \cdot 10^{-2}$	25%	VLM	$-1.514 \cdot 10^{-3}$	25%
	WTE	$8.727 \cdot 10^{-3}$	$\pm 3.708 \cdot 10^{-4}$	WTE	–	–	WTE	–	–	WTE	–	–
	FTE	$-1.781 \cdot 10^{-2}$	*TBD*	FTE	–	–	FTE	–	–	FTE	–	–
$C_{Y_{...}}$	VLM	0	25%	VLM	$-2.272 \cdot 10^{-1}$	25%	VLM	$5.285 \cdot 10^{-17}$	25%	VLM	$-2.306 \cdot 10^{-1}$	25%
	WTE	–	–	WTE	–	–	WTE	–	–	WTE	–	–
	FTE	$2.561 \cdot 10^{-3}$	*TBD*	FTE	$-0.2152 \cdot 10^{0}$	*TBD*	FTE	–	–	FTE	-0.2051	*TBD*
$C_{Z_{...}}$	VLM	$2.533 \cdot 10^{-2}$	25%	VLM	$2.584 \cdot 10^{-3}$	25%	VLM	$8.573 \cdot 10^{-1}$	25%	VLM	$4.023 \cdot 10^{-3}$	25%
	WTE	$3.747 \cdot 10^{-2}$	$\pm 7.564 \cdot 10^{-3}$	WTE	–	–	WTE	–	–	WTE	–	–
	FTE	$7.041 \cdot 10^{-2}$	*TBD*	FTE	–	–	FTE	-9.411	*TBD*	FTE	–	–
$C_{l_{...}}$	VLM	0	25%	VLM	$-1.691 \cdot 10^{0}$	25%	VLM	$-2.157 \cdot 10^{-15}$	25%	VLM	$3.625 \cdot 10^{-1}$	25%
	WTE	$-3.036 \cdot 10^{-3}$	$\pm 5.311 \cdot 10^{-4}$	WTE	–	–	WTE	–	–	WTE	–	–
	FTE	–	–	FTE	$-9.372 \cdot 10^{-2}$	*TBD*	FTE	$-1.155 \cdot 10^{-1}$	*TBD*	FTE	$4.765 \cdot 10^{-2}$	*TBD*
$C_{m_{...}}$	VLM	$-1.082 \cdot 10^{-2}$	25%	VLM	$-4.123 \cdot 10^{-3}$	25%	VLM	$-1.055 \cdot 10^{0}$	25%	VLM	$-4.722 \cdot 10^{-3}$	25%
	WTE	$8.071 \cdot 10^{-3}$	$\pm 3.664 \cdot 10^{-3}$	WTE	–	–	WTE	–	–	WTE	–	–
	FTE	$4.941 \cdot 10^{-3}$	*TBD*	FTE	–	–	FTE	$-2.135 \cdot 10^{0}$	*TBD*	FTE	–	–
$C_{n_{...}}$	VLM	0	25%	VLM	$2.381 \cdot 10^{-1}$	25%	VLM	$-2.137 \cdot 10^{-16}$	25%	VLM	$-2.470 \cdot 10^{-1}$	25%
	WTE	$-1.075 \cdot 10^{-3}$	$\pm 2.293 \cdot 10^{-4}$	WTE	–	–	WTE	–	–	WTE	–	–
	FTE	–	–	FTE	$3.767 \cdot 10^{-2}$	*TBD*	FTE	–	–	FTE	$9.269 \cdot 10^{-3}$	*TBD*

Table 4.4: Aerodynamic coefficients

	α			β		
$C_{X_{...}}$	VLM	$4.645 \cdot 10^{-2}$	25%	VLM	$-1.364 \cdot 10^{-3}$	25%
	WTE	$4.288 \cdot 10^{-2}$	$\pm 2.662 \cdot 10^{-3}$	WTE	–	–
	FTE	$1.804 \cdot 10^{-2}$	TBD	FTE	–	–
$C_{Y_{...}}$	VLM	$-1.517 \cdot 10^{-16}$	25%	VLM	$-2.259 \cdot 10^{-1}$	25%
	WTE	–	–	WTE	–	–
	FTE	–	–	FTE	$-2.832 \cdot 10^{-1}$	TBD
$C_{Z_{...}}$	VLM	$2.881 \cdot 10^{0}$	25%	VLM	$9.024 \cdot 10^{-4}$	25%
	WTE	$-1.943 \cdot 10^{0}$	$\pm 1.564 \cdot 10^{-2}$	WTE	–	–
	FTE	$-1.258 \cdot 10^{0}$	TBD	FTE	–	–
$C_{l_{...}}$	VLM	$-2.142 \cdot 10^{-15}$	25%	VLM	$-3.945 \cdot 10^{-1}$	25%
	WTE	$1.842 \cdot 10^{-1}$	$\pm 1.895 \cdot 10^{-3}$	WTE	–	–
	FTE	–	–	FTE	$-3.346 \cdot 10^{-2}$	TBD
$C_{m_{...}}$	VLM	$-1.890 \cdot 10^{-1}$	25%	VLM	$-2.117 \cdot 10^{-3}$	25%
	WTE	$-1.069 \cdot 10^{-1}$	$\pm 5.938 \cdot 10^{-3}$	WTE	–	–
	FTE	$-6.018 \cdot 10^{-2}$	TBD	FTE	–	–
$C_{n_{...}}$	VLM	$-3.101 \cdot 10^{-16}$	25%	VLM	$1.744 \cdot 10^{-1}$	25%
	WTE	$5.085 \cdot 10^{-5}$	$\pm 4.599 \cdot 10^{-4}$	WTE	–	–
	FTE	–	–	FTE	$2.968 \cdot 10^{-2}$	TBD

Table 4.5: Aerodynamic coefficients

4.8. Model Limitations

In this section, the model limitations of the simulation model are discussed. In section 4.8.1, the model limitations based on the assumptions are discussed. After that, section 4.8.2 elaborates on the model limitations for each of the aerodynamic models that can be used.

4.8.1. Model Limitations Based on Assumptions

The assumptions presented in section 4.3 result in several limitations of the simulation model. First of all, the aircraft is assumed to be a rigid body with a constant mass. In reality, the aircraft is likely to deform during the flight and is therefore not a rigid body. Changes in mass (distribution) due to e.g. fuel burn and transport of fuel to different parts of the aircraft are neither taken into account. These effects introduce changed inertia properties of the aircraft and may therefore influence the dynamics. Eventually, aeroelastic deformation that occurs during flight and the change in mass (distribution) may result in discrepancies between the dynamic behaviour of the simulation model and the dynamic behaviour of the real aircraft.

In case the duration of the flight is short, the influence of the Earth's curvature and angular velocity is negligible. Therefore, the Earth can assumed to be flat and the coriolis acceleration and centripetal acceleration can be neglected. In case the time-span of the flight is large (in the order of hours), this introduces large errors that influence the accuracy of the simulation. [Mulder, J.A. et al., 2013]

Due to the no wind assumption with perfect atmosphere, the undisturbed air is at rest relative to the Earth's surface and the atmospheric conditions correspond to the International Standard Atmosphere. In reality, there will always be wind, which results in the fact that the kinematic velocity of the vehicle is different from the aerodynamic velocity. Wind conditions result in changing aerodynamic forces and moments acting on the aircraft, influencing the dynamic response of the aircraft.

Due to the assumption that the resultant thrust lies in the symmetry plane of the aircraft (not in case OEI), the thrust only influences the aerodynamic forces in the x-direction and z-direction and the pitch moment of the body fixed reference frame. In reality, the thrust will also influence the other force and moment components, resulting in a different aerodynamic load acting on the aircraft compared to the simulation model.

Because the Earth is not perfectly spherical with a constant mass distribution, the gravity vector is not constant with respect to different locations on Earth. In reality, the gravity vector changes in direction and magnitude throughout the flight of the aircraft resulting in changing dynamic responses.

4.8.2. Model Limitations Based on Aerodynamic Model

For the Vortex Lattice Method, the aerodynamic data is linearised, meaning that this model is not able to accurately display the corners of the flight envelope due to nonlinearities. This also means that deviation from the linearisation points results in inaccurate estimations. Besides that, frictional drag [Lambert, T. et al., 2017], ground effect, impressibility, and aeroelasticity effects are not taken into account. Furthermore, there is no compressible drag prediction in the VLM resulting that the stability and control derivatives are accurate for $M < M_{\text{cruise}}$. Also, the atmospheric model does not include wing, turbulence, nor wind shear. Finally, the landing gear and fairing are not modelled. [Cappuyns, T., 2019]

For the wind tunnel model, it is necessary to take into account that only the half-span clean wing configuration is modelled without landing gear, fairing, nor engines. This results in limited fidelity of this model with respect to the full aircraft configuration. Furthermore, no winglets including rudders are added to the wind tunnel model. For this reason, using this model limits the user to accurately simulate the lateral-directional dynamics of the aircraft. Besides that, as shown in section 4.6.2, the model is only valid for angles of attack ranging between -10° and 30° for airspeeds ranging between roughly 12.5 m/s and 30 m/s with control surface deflections between -14° and 19°. Outside these ranges, no measurements were taken during the construction of the aerodynamic model meaning that extrapolating outside this convex hull results in new, unmodeled effects that affect the validity of the model. [Garcia, A.R., 2019]

Finally, the main limitation of the flight test model is the fact that no specific manoeuvres were performed for the aerodynamic identification process. Therefore, the uncertainty of the different com-

ponents of the flight test model is higher compared to the wind tunnel model, and the quality of the pitching moment is lower due to noisy measurements. Even though this model represents the most complete and accurate representation of the aircraft aerodynamics, the uncertainties present in the model drastically limit the extent to which this model can be used. [Garcia, A.R., 2021]

4.9. Simulation Model Design Conclusion

From chapter 1 it is possible to obtain the second sub-question, namely:

> How can a simulation model of the TU Delft Flying-V aircraft be obtained?

To answer this sub-question, it is first necessary to understand the specific elements of a simulation model of the TU Delft Flying-V. For this reason, the equations of motion are derived and three aerodynamic models are discussed. These include an aerodynamic model of the full scale aircraft obtained from the Vortex Lattice Method, an aerodynamic model of the small scale aircraft from Wind Tunnel Experiments, and an aerodynamic model of the small scale aircraft from a flight test experiment. It is determined to combine the aerodynamic models from the Vortex Lattice Method and Wind Tunnel Experiments such that the instabilities obtained from literature are captured in the simulation model.

Secondly, it is necessary to identify the uncertainty sources of the simulation model. These uncertainty sources originate from assumptions made, such as a rigid body with constant mass, flat Earth, no wind and perfect atmosphere, and resultant thrust in symmetry plane. Other uncertainties arise from each of the aerodynamic models. Namely, for the Vortex Lattice Method the aerodynamic data is linearised. Besides that, for the wind tunnel model, only static, longitudinal aerodynamic coefficients could be taken into account. Finally, for the flight test model, no specific aerodynamic manoeuvres were performed resulting in high uncertainty.

Thirdly, it is necessary to determine the validity of the simulation model. In general this is done by comparison of the simulation model with flight test data. However, due to scaling effects and Reynolds number effects this method is considered unreliable for validation.

After developing a simulation model and assessing the stability and handling qualities it is possible to design a flight control system to improve the aerodynamic characteristics of the TU Delft Flying-V. This is discussed in chapter 5.

5

Flight Control System Design

This chapter elaborates on the design of the flight control system. Therefore this chapter aims to answer the third sub-question:

> How do the stability and handling qualities of the Flying-V aircraft change after applying a flight control system?

In section 5.1 several requirements are displayed for the control system. Besides that, section 5.2 gives an overview of different flight control systems that can be applied to the TU Delft Flying-V. After that, section 5.3 elaborates on the Proportional-Integral-Derivative Controller, and section 5.4 discusses the nonlinear controller. Additionally, section 5.5 elaborates on the assessment of the flight control system. Finally, section 5.6 concludes this chapter.

5.1. Flight Control System Requirements

Before it is possible to develop a flight control system that can be applied to the simulation model, it is necessary to define a set of requirements the control system needs to satisfy. First of all, from the stability and handling quality analysis performed in chapter 3, the TU Delft Flying-V contains several stability issues. Besides that, several essential stability and handling quality requirements are identified from both civil certification authorities as well as military standards. Therefore the flight control system shall be able to make the aircraft adhere to the key stability and handling quality requirements from civil certification authorities and military standards.

Secondly, the equations of motion and aerodynamic models described in chapter 4 consist of several nonlinear components. To prevent degradation of the controller, the flight control system shall be able to cope with the inherent nonlinear behaviour of the aircraft.

As mentioned in chapter 4, the simulation model that will be designed consists of several assumptions such as rigid body and zero wind. Furthermore, three different sources (Vortex Lattice Method, wind tunnel test, and flight test) can be used to obtain the aerodynamic coefficients used in the equations of motion. Each of these sources consists of its own limitations and inaccuracies. This introduces uncertainties into the simulation model of the TU Delft Flying-V. Consequently, in case the flight control system developed for the simulation model is applied to the real aircraft, this leads to performance degradation of the control system. In order to diminish the performance degradation due to model uncertainties, the flight control system shall be able to cope with these model uncertainties.

5.2. Flight Control System Overview

A couple of decades ago, almost all Flight Control Systems (FCS) for aircraft were designed using classical (linear) control techniques. [Balas, G.J., 2003] Even though the systems involved with aircraft control are nonlinear, it is still possible to apply a linear controller to this system by making the

key assumption that the linear controller is only applied to a small range within the complete flight envelope. [Slotine, J.E. et al., 1991] This requires the design of multiple linear controllers to cover the complete flight envelope and construct a gain schedule by interpolating the gains with respect to the flight condition. This procedure is very time consuming, expensive, and is not flexible regarding design changes. [Adams, R.J. et al., 1993] Furthermore, during the design of a linear controller, it is necessary to assume that the parameters of the aircraft model are well known, which is not always the case. In case a linear controller is based on inaccurate model parameters, it may exhibit performance degradation or instability. [Slotine, J.E. et al., 1991]

To overcome the shortcomings of linear controllers, several nonlinear control methods have emerged over the past years. One of the most popular of these control methodologies is known as Feedback Linearisation (FL). The theory of feedback linearisation originates from research performed by Brockett and Krener on the extension of linear control studies to the nonlinear case. [Brockett, R.W., 1978, Krener, A.J., 1999] Feedback Linearisation makes use of an accurate model of the system to entirely or partially cancel nonlinearities using feedback and exact state transformations. These transformations transform the nonlinear system dynamics into a linear system over the desired region of interest. Consequently, it is possible to apply conventional linear control techniques to achieve the desired closed-loop dynamics. [Acquatella, P. et al., 2012]

In the aerospace field, FL is commonly referred to as Nonlinear Dynamic Inversion (NDI). Using NDI it is no longer necessary to divide the flight envelope into multiple sections and use gain-scheduling to make the aircraft controllable over the complete flight envelope. Instead, due to the cancellation of the nonlinear dynamics it is possible to use a single linear controller for the complete flight envelope. The disadvantage of NDI-based control laws is the necessity for accurate knowledge of the nonlinear system dynamics. [Acquatella, P. et al., 2012] This requirement is almost impossible to meet in reality due to model simplifications, computational errors, and external disturbances. [Wang, X. et al., 2019] In an attempt to increase the robustness of the NDI controller, the controller is combined with linear robust control techniques such as structural singular value (μ) analysis [Reiner, J. et al., 1996] and $\mathcal{H}_\infty$ synthesis. [Spillman, M. et al., 1996] However, these control techniques often treat known nonlinear time-varying dynamics as uncertainties. This results in control systems that are either marginal or very conservative in performance and stability robustness. [Hodel, A. et al., 2008].

Incremental Nonlinear Dynamic Inversion (INDI) is a sensor-based control method. Therefore, this control method requires less model information and can therefore improve the system robustness against model uncertainties. [Wang, X. et al., 2019] This is especially useful for the control system design of the TU Delft Flying-V. As discussed in section 4.8, the aerodynamic coefficients contain a certain degree of uncertainty resulting in a simulation model including these uncertainties as well. The development of INDI started in the late nineties [Smith, P., 1998] and was previously referred to as Simplified NDI [Smith, P., 1998] and Modified NDI. [Bacon, B.J. et al., 2001] Furthermore, there are several examples of INDI being applied to aerospace vehicles. [Acquatella, P. et al., 2012, Kumtepe. Y., 2020, Van 't Veld, R.C., 2016]

5.3. Proportional-Integral-Derivative Controller

One of the most conventional linear controllers is the Proportional-Integral-Derivative (PID) controller. This controller takes the state error as an input and defines a system input that consists of a linear combination of the error (e) multiplied with a proportional gain (K_P), the integral of the error multiplied with an integral gain (K_I), and the derivative of the error multiplied with a derivative gain (K_D). This can be observed in eq. (5.1). In this equation, $u(t)$ represents the system input. [Karssies H.J., 2020]

$$u(t) = K_P e(t) + K_I \int e(t) + K_D \frac{de(t)}{dt} \tag{5.1}$$

The PID controller is not only able to track a reference signal taking into account the error, it is also able to anticipate on changes in the reference signal using the derivative of the error. Furthermore, it is able to account for any residual error using the integral term. Finally, a PID controller does not require a detailed model of the system and is applicable to both first and second order systems. [Karssies H.J., 2020]

5.4. Nonlinear Controller

Before it is possible to elaborate on the design of an INDI controller, it is necessary to first understand the working principles of an NDI controller, which is discussed in section 5.4.1. After that, the INDI controller is discussed in section 5.4.2. In section 5.4.3 the controller performance under uncertainties of both NDI and INDI is discussed. Finally, section 5.4.4 elaborates on the time-scale separation principle.

5.4.1. Nonlinear Dynamic Inversion (NDI)

NDI is a nonlinear control technique based on the algebraic transformation of nonlinear system dynamics into a, fully or partial, linear system. [Van 't Veld, R.C., 2016] This essentially means that the nonlinear system is inverted into a linear structure using state feedback, meaning that it is possible to apply a linear controller. To invert the nonlinear system, it is necessary to assume that the model of the system is exactly known, and that the complete and accurate knowledge about the state of the system can be obtained. [Acquatella, P. et al., 2012] In this subsection, NDI is first applied through a system in the companion form. After that, NDI applied through input-output linearisation for Single input Single Output (SISO) and Multiple input Multiple Output (MIMO) is discussed.

NDI for Systems in Companion Form

The principle of NDI is most easily demonstrated using a Single Input Single Output (SISO) system in companion form. A system is in the companion form if the system dynamics are represented by eq. (5.2). In this equation, $x^{(n)}$ represents the n$^{\text{th}}$ time derivative of x, $\boldsymbol{x} = \begin{bmatrix} x & \dot{x} & \dots & x^{n-1} \end{bmatrix}^T$ is the state vector, and u represents a scalar control input. Furthermore, the functions $a(\boldsymbol{x})$ and $b(\boldsymbol{x})$ are nonlinear functions that only depend on the state vector. The system can also be presented in a state-space representation as can be observed in eq. (5.3) (where $x = x_1$, $\dot{x} = x_2$ etc.). [Slotine, J.E. et al., 1991, Van 't Veld, R.C., 2016]

$$x^{(n)} = b(\boldsymbol{x}) + a(\boldsymbol{x})u \tag{5.2}$$

$$\frac{d}{dt}\begin{bmatrix} x_1 \\ \vdots \\ x_{n-1} \\ x_n \end{bmatrix} = \begin{bmatrix} x_2 \\ \vdots \\ x_n \\ b(\boldsymbol{x}) + a(\boldsymbol{x})u \end{bmatrix} \tag{5.3}$$

The nonlinearities of the system can consequently be cancelled by solving for control input (u) using the virtual control input (ν) as can be observed in eq. (5.4). Implementing this into eq. (5.3), this results in linear input-state relation as is shown in eq. (5.5). [Van 't Veld, R.C., 2016]

$$u = a^{-1}(\boldsymbol{x})[\nu - b(\boldsymbol{x})] \tag{5.4}$$

$$\frac{d}{dt}\begin{bmatrix} x_1 \\ x_2 \\ \vdots \\ x_{n-1} \\ x_n \end{bmatrix} = \begin{bmatrix} 0 & 1 & 0 & \cdots & 0 \\ 0 & 0 & 1 & \cdots & 0 \\ \vdots & \vdots & \vdots & \ddots & \vdots \\ 0 & 0 & 0 & \cdots & 1 \\ 0 & 0 & 0 & \cdots & 0 \end{bmatrix} \begin{bmatrix} x_1 \\ x_2 \\ \vdots \\ x_{n-1} \\ x_n \end{bmatrix} + \begin{bmatrix} 0 \\ 0 \\ \vdots \\ 0 \\ 1 \end{bmatrix} \nu = \begin{bmatrix} x_2 \\ x_3 \\ \vdots \\ x_n \\ \nu \end{bmatrix} \tag{5.5}$$

After that, it is possible to replace the virtual control input by a state feedback control law as can be observed in eq. (5.6). This control law can be used to relocate the poles of the closed-loop system to the left-half complex plane for stable behaviour. Besides that, it is possible to apply exponentially convergent tracking for a task with a desired output $x_d(t)$ and tracking error $e(t) = x(t) - x_d(t)$ using the control law displayed in eq. (5.7). In this equation $x_d^{(n)}$ can be added as a feedforward term to increase controller performance. [Slotine, J.E. et al., 1991, Van 't Veld, R.C., 2016]

$$\nu = -k_0 x - k_1 x_1 - \cdots - k_{n-1} x^{(n-1)} \tag{5.6}$$

$$\nu = x_d^{(n)} - k_0 e - k_1 \dot{e} - \cdots - k_{n-1} e^{(n-1)} \tag{5.7}$$

In summary, the implementation of an NDI controller requires the functions $a^{-1}(\boldsymbol{x})$ and $b(\boldsymbol{x})$ to be evaluated for the current state. Furthermore, it is necessary to design a linear controller that computes a virtual input based on the difference between a reference state and the measured state. [Slotine, J.E. et al., 1991] Besides that, the implementation of NDI using a companion matrix is not directly applicable to all systems. [Van 't Veld, R.C., 2016] Therefore, input-output linearisation is discussed next.

NDI using Input-Output Linearisation for SISO Systems

The basic concept of input-output linearisation is the differentation of the output function (y) until the control input (u) appears. [Slotine, J.E. et al., 1991] This starts with the system shown in eq. (5.8).

$$\begin{aligned} \dot{\boldsymbol{x}} &= \boldsymbol{f}(\boldsymbol{x}) + \boldsymbol{g}(\boldsymbol{x})u \\ y &= h(\boldsymbol{x}) \end{aligned} \tag{5.8}$$

To perform the input-output linearisation, it is necessary to introduce the Lie derivative of $h(\boldsymbol{x})$ with respect to $\boldsymbol{f}(\boldsymbol{x})$, and the Lie derivative of $h(\boldsymbol{x})$ with respect to $\boldsymbol{g}(\boldsymbol{x})$. The Lie derivatives can be observed in eq. (5.9) and eq. (5.10) respectively. In these equations, $\nabla h(\boldsymbol{x})$ represents the gradient of $h(\boldsymbol{x})$. Besides that, the r^{th}-order Lie derivative of $h(\boldsymbol{x})$ is defined as $L_{\boldsymbol{f}}^r h(\boldsymbol{x}) = L_{\boldsymbol{f}}[L_{\boldsymbol{f}}^{r-1} h(\boldsymbol{x})]$ and $L_{\boldsymbol{g}}^r h(\boldsymbol{x}) = L_{\boldsymbol{g}}[L_{\boldsymbol{g}}^{r-1} h(\boldsymbol{x})]$ for $\boldsymbol{f}(\boldsymbol{x})$ and $\boldsymbol{g}(\boldsymbol{x})$ respectively.

$$L_{\boldsymbol{f}} h(\boldsymbol{x}) = \nabla h(\boldsymbol{x}) \cdot \boldsymbol{f}(\boldsymbol{x}) \tag{5.9}$$

$$L_{\boldsymbol{g}} h(\boldsymbol{x}) = \nabla h(\boldsymbol{x}) \cdot \boldsymbol{g}(\boldsymbol{x}) \tag{5.10}$$

If $L_{\boldsymbol{g}} h(\boldsymbol{x}) \neq 0$ for any $\boldsymbol{x}$, it is possible to obtain a control input as shown in eq. (5.11). Note that there is a linear relation between the output (y) and the input (u) via $\dot{y} = \nu$.

$$u = \frac{1}{L_{\boldsymbol{g}} h(\boldsymbol{x})} (\nu - L_{\boldsymbol{f}} h(\boldsymbol{x})) \tag{5.11}$$

In case $L_{\boldsymbol{g}} h(\boldsymbol{x}) = 0$ for all $\boldsymbol{x}$, then the output is differentiated again up until the control input (u) appears. This is shown in eq. (5.12) resulting in a control input as shown in eq. (5.13).

$$y^{(i)} = L_{\boldsymbol{f}}^i h(\boldsymbol{x}) + L_{\boldsymbol{g}} L_{\boldsymbol{f}}^{i-1} h(\boldsymbol{x}) u \tag{5.12}$$

$$u = \frac{1}{L_{\boldsymbol{g}} L_{\boldsymbol{f}}^{i-1} h(\boldsymbol{x})} (\nu - L_{\boldsymbol{f}}^i h(\boldsymbol{x})) \tag{5.13}$$

The number of differentiations (r) until an explicit relation between the input and the output can be found is defined as the relative degree. For any system of order n, the maximum number of differentiations required to find this relation cannot be larger than n, meaning that $r \leq n$. In case $r < n$, a part of the system is unobservable withing the input-output linearisation. These unobservable dynamics can be reffered to as internal dynamics and do not explicitly depend on u and can therefore not be controlled. [Van 't Veld, R.C., 2016] Therefore, the internal dynamics have to be stable in order for the NDI controller to be effective. In case $r = n$ the system does not have any internal dynamics. [Slotine, J.E. et al., 1991]

NDI using Input-Output Linearisation for MIMO Systems

In eq. (5.14) it is possible to observe a general Multiple Input Multiple Output (MIMO) system where the number of input is equal to the number of outputs to prevent control allocation problems. [Acquatella, P. et al., 2012]

$$\begin{aligned} \dot{\boldsymbol{x}} &= \boldsymbol{f}(\boldsymbol{x}) + G(\boldsymbol{x})\boldsymbol{u} \\ \boldsymbol{y} &= \boldsymbol{h}(\boldsymbol{x}) \end{aligned} \tag{5.14}$$

In this equation $\boldsymbol{x}$ represents the state vector, $\boldsymbol{u}$ represents the control input vector of length m, $\boldsymbol{y}$ is the system output vector of length m, $\boldsymbol{f}$ and $\mathbf{h}$ are vectors, and G is a matrix of size $m \times m$. The elements of the output vector $\boldsymbol{y}$ are often selected as the parameters that need to be controlled. These are most of the time directly related to the physical states of the system. [Acquatella, P. et al., 2012] Again, it is necessary to differentiate the output equation up until the point there is a specific relation between the output vector ($\boldsymbol{y}$) and the control input vector ($\boldsymbol{u}$). Starting with eq. (5.14) it is possible to define the general equation for the specific components of the output equation with relative degree r_j as can be observed in eq. (5.15).

$$\boldsymbol{y}^{(i)} = L_{\boldsymbol{f}}^{i}\boldsymbol{h}(\boldsymbol{x}) + L_G L_{\boldsymbol{f}}^{i-1}\boldsymbol{h}(\boldsymbol{x})\boldsymbol{u} \tag{5.15}$$

Considering a system where the output vector is equal to the state vector as shown in eq. (5.16) it is possible to obtain a relation between the output and the input using eq. (5.17).

$$\boldsymbol{y} = \boldsymbol{x} \tag{5.16}$$

$$\begin{aligned} \dot{\boldsymbol{y}} &= \dot{\boldsymbol{x}} \\ \dot{\boldsymbol{y}} &= \boldsymbol{f}(\boldsymbol{x}) + G(\boldsymbol{x})\boldsymbol{u} \end{aligned} \tag{5.17}$$

If matrix $G(\boldsymbol{x})$ is non-singular (meaning that the matrix is invertible), the nonlinearities of the system can be cancelled by designing a control input $\boldsymbol{u}$ that is able to cancel the nonlinear system dynamics as is shown in eq. (5.18). In this equation, $\boldsymbol{\nu}$ represents the virtual input.

$$\boldsymbol{u} = G(\boldsymbol{x})^{-1}\left(\boldsymbol{\nu} - \boldsymbol{f}(\boldsymbol{x})\right) \tag{5.18}$$

This results in a linear relation between the virtual input and the output of the system, for this reason, the virtual input can consequently be designed using linear control techniques. The layout of the closed-loop system including an NDI controller can be observed in fig. 5.1.

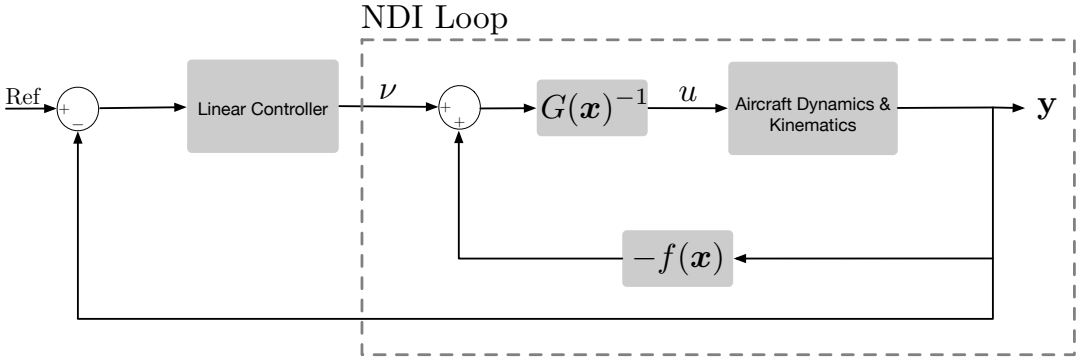

Figure 5.1: NDI Controller

Finally, it can be concluded that the use of NDI control techniques is fundamentally different from first order approximations based on Jacobian linearisation at specific operational points (section 5.3).

The NDI controller requires full state feedback and for the design of a proper controller, it is necessary to have accurate knowledge about the system model. Any uncertainties present in the model results in errors during the linearisation, meaning that the system may not be completely linearised. [Chu, Q.P. et al., 2019-2020]

5.4.2. Incremental Nonlinear Dynamic Inversion

The concept of Incremental Nonlinear Dynamic Inversion (INDI) essentially consists of the application of NDI to a system expressed in an incremental form to improve the robustness of the closed-loop system compared to an NDI controller. This is obtained by reducing the controller's dependency on the model and exact knowledge of the system dynamics. The difference between an NDI controlled system and INDI controlled system originates from the control input. The NDI controller provides a complete command control input, whereas an INDI controller considers the influence of increments of control commands in the dynamics. These increments in the control commands are provided as a function of the error of the control variables. [Acquatella, P. et al., 2012] To derive the equations for an INDI controller, it is possible to start with the general equation for a nonlinear system shown in eq. (5.19).

$$\dot{\boldsymbol{x}} = \boldsymbol{f}(\boldsymbol{x}, \boldsymbol{u}) \tag{5.19}$$

Taking the Taylor series expansion of this equation at the current time point, it is possible linearise the system as shown in eq. (5.20).

$$\begin{aligned} \dot{\boldsymbol{x}} &\approx \boldsymbol{f}(\boldsymbol{x}_0, \boldsymbol{u}_0) + \left.\frac{\partial \boldsymbol{f}(\boldsymbol{x}, \boldsymbol{u})}{\partial \boldsymbol{x}}\right|_{\boldsymbol{x}=\boldsymbol{x}_0, \boldsymbol{u}=\boldsymbol{u}_0} (\boldsymbol{x} - \boldsymbol{x}_0) + \left.\frac{\partial \boldsymbol{f}(\boldsymbol{x}, \boldsymbol{u})}{\partial \boldsymbol{u}}\right|_{\boldsymbol{x}=\boldsymbol{x}_0, \boldsymbol{u}=\boldsymbol{u}_0} (\boldsymbol{u} - \boldsymbol{u}_0) \\ &= \dot{\boldsymbol{x}}_0 + F(\boldsymbol{x}_0, \boldsymbol{u}_0)(\boldsymbol{x} - \boldsymbol{x}_0) + G(\boldsymbol{x}_0, \boldsymbol{u}_0)(\boldsymbol{u} - \boldsymbol{u}_0) \end{aligned} \tag{5.20}$$

Using the time scale separation principle, this equation can be further simplified when the system sample rate is considered to be high, resulting in eq. (5.21).

$$\dot{\boldsymbol{x}} \approx \dot{\boldsymbol{x}}_0 + G(\boldsymbol{x}_0, \boldsymbol{u}_0)(\boldsymbol{u} - \boldsymbol{u}_0) = \dot{\boldsymbol{x}}_0 + G(\boldsymbol{x}_0, \boldsymbol{u}_0)\Delta\boldsymbol{u} \tag{5.21}$$

This can be rewritten as an NDI controller in the incremental form resulting in eq. (5.22).

$$\Delta\boldsymbol{u} = G^{-1}(\boldsymbol{x}_0, \boldsymbol{u}_0)(\boldsymbol{\nu} - \dot{\boldsymbol{x}}_0) \tag{5.22}$$

This control law results in increments of the control commands, meaning that these changes must be added to the current reference command in order to obtain the full new control command input. This means that the total control command can be obtained using eq. (5.23).

$$\boldsymbol{u} = \boldsymbol{u}_0 + \Delta\boldsymbol{u} = \boldsymbol{u}_0 + G^{-1}(\boldsymbol{x}_0, \boldsymbol{u}_0)(\boldsymbol{\nu} - \dot{\boldsymbol{x}}_0) \tag{5.23}$$

In eq. (5.23) it can be observed that the INDI controller does not depend on the exact knowledge of the system dynamics ($\boldsymbol{f}(\boldsymbol{x})$). Instead, the control strategy is merely dependent on the sensor measurements of $\dot{\boldsymbol{x}}_0$ and $\boldsymbol{u}_0$. Therefore, the dependency of the closed-loop system has decreased resulting in improved performance in case of model mismatch and model uncertainties. However, it needs to be noted that this controller is not completely independent of the model as changes in the system dynamics are reflected in the derivative of the state vector ($\dot{\boldsymbol{x}}_0$). On the other side, the performance of this controller is expected to be more dependent on sensor aspects such as noise, bias, and misalignments than an NDI controller. [Acquatella, P. et al., 2012] The layout of the closed-loop system including an INDI controller can be observed in fig. 5.2.

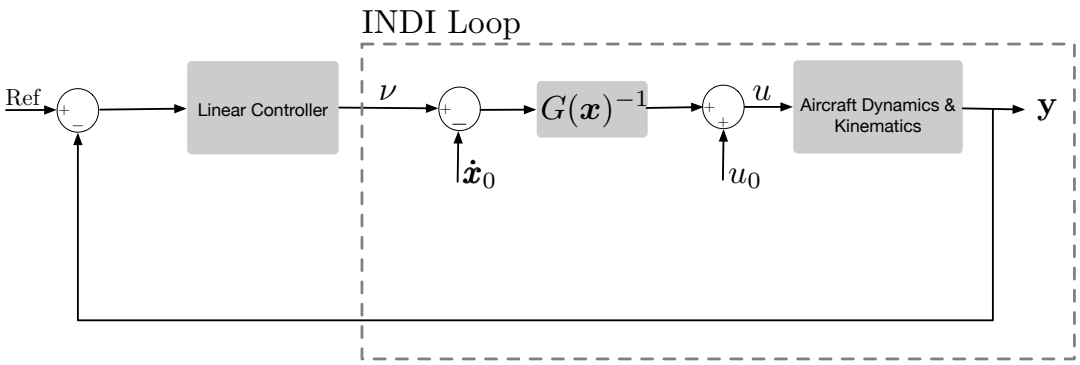

Figure 5.2: INDI Controller

5.4.3. Controller Performance with Model Uncertainties

The main argument for using an INDI controller is the increased robustness to model uncertainties compared to NDI. Therefore the difference between model uncertainty effects are assessed for both an NDI controller (section 5.4.3) and an INDI controller (section 5.4.3). Only model uncertainties are taken into account, so uncertainties with respect to sensor measurements and dynamics are not evaluated. Furthermore, instantaneous control surface deflections are assumed. [Sieberling, S et al., 2010, Van 't Veld, R.C., 2016]

NDI Controller with Model Uncertainties

In eq. (5.24) it is possible to observed the system response for a system controlled by a nominal NDI controller (therefore subscript n). From this equation, it can be clearly observed that the closed-loop response of the controlled system is linear with $\dot{\boldsymbol{x}} = \boldsymbol{\nu}$.

$$\begin{aligned} \dot{\boldsymbol{x}} &= \boldsymbol{f}_n(\boldsymbol{x}) + G_n(\boldsymbol{x})\boldsymbol{u} \\ \boldsymbol{u} &= G_n(\boldsymbol{x})^{-1}\left(\boldsymbol{\nu} - \boldsymbol{f}_n(\boldsymbol{x})\right) \\ \dot{\boldsymbol{x}} &= \boldsymbol{\nu} \end{aligned} \tag{5.24}$$

However, in reality, the system is not perfect and contains model uncertainties as can be observed in eq. (5.25). From this response it is clear that multiple nonlinear terms remain in the system response. [Sieberling, S et al., 2010]

$$\begin{aligned} \dot{\boldsymbol{x}} &= \boldsymbol{f}_n(\boldsymbol{x}) + \Delta\boldsymbol{f}(\boldsymbol{x}) + G_n(\boldsymbol{x})\boldsymbol{u} + \Delta G(\boldsymbol{x})\boldsymbol{u} \\ \dot{\boldsymbol{x}} &= \boldsymbol{f}_n(\boldsymbol{x}) + \Delta\boldsymbol{f}(\boldsymbol{x}) + G_n(\boldsymbol{x})G_n(\boldsymbol{x})^{-1}\left(\boldsymbol{\nu} - \boldsymbol{f}_n(\boldsymbol{x})\right) + \Delta G(\boldsymbol{x})G_n(\boldsymbol{x})^{-1}\left(\boldsymbol{\nu} - \boldsymbol{f}_n(\boldsymbol{x})\right) \\ \dot{\boldsymbol{x}} &= \left(I + \Delta G(\boldsymbol{x})G_n(\boldsymbol{x})^{-1}\right)\boldsymbol{\nu} + \Delta\boldsymbol{f}(\boldsymbol{x}) - \Delta G(\boldsymbol{x})G_n(\boldsymbol{x})^{-1}\boldsymbol{f}_n(\boldsymbol{x}) \end{aligned} \tag{5.25}$$

INDI Controller with Model Uncertainties

The same procedure can be followed for a system controlled by an INDI controller. In eq. (5.26) it is possible to observe that the nominal system is linear with $\dot{\boldsymbol{x}} = \boldsymbol{\nu}$.

$$\begin{aligned} \dot{\boldsymbol{x}} &= \dot{\boldsymbol{x}}_0 + G_n(\boldsymbol{x}_0, \boldsymbol{u}_0)\Delta\boldsymbol{u} \\ \Delta\boldsymbol{u} &= G_n^{-1}(\boldsymbol{x}_0, \boldsymbol{u}_0)(\boldsymbol{\nu} - \dot{\boldsymbol{x}}_0) \\ \dot{\boldsymbol{x}} &= \boldsymbol{\nu} \end{aligned} \tag{5.26}$$

However, in reality, the system is not perfect and contains model uncertainties as can be observed in eq. (5.27). [Sieberling, S et al., 2010]

$$\begin{aligned}\dot{\boldsymbol{x}} &= \dot{\boldsymbol{x}}_0 + G_n(\boldsymbol{x}_0, \boldsymbol{u}_0)\Delta\boldsymbol{u} + \Delta G(\boldsymbol{x}_0, \boldsymbol{u}_0)\Delta\boldsymbol{u} \\ \dot{\boldsymbol{x}} &= \dot{\boldsymbol{x}}_0 + G_n(\boldsymbol{x}_0, \boldsymbol{u}_0)G_n^{-1}(\boldsymbol{x}_0, \boldsymbol{u}_0)\left(\boldsymbol{\nu} - \dot{\boldsymbol{x}}_0\right) + \dot{\boldsymbol{x}}_0 + \Delta G(\boldsymbol{x}_0, \boldsymbol{u}_0)G_n^{-1}(\boldsymbol{x}_0, \boldsymbol{u}_0)\left(\boldsymbol{\nu} - \dot{\boldsymbol{x}}_0\right) \\ \dot{\boldsymbol{x}} &= \left(I + \Delta G(\boldsymbol{x}_0, \boldsymbol{u}_0)G_n^{-1}(\boldsymbol{x}_0, \boldsymbol{u}_0)\right)\boldsymbol{\nu} - \Delta G(\boldsymbol{x}_0, \boldsymbol{u}_0)G_n^{-1}(\boldsymbol{x}_0, \boldsymbol{u}_0)\dot{\boldsymbol{x}}_0\end{aligned} \tag{5.27}$$

When small sampling time and ideal sensor measurements are assumed, the new state derivative and the current state derivative are approximately equal according to: $\dot{\boldsymbol{x}} \approx \dot{\boldsymbol{x}}_0$. Using this assumption it is possible to simplify eq. (5.27) according to eq. (5.28). From this equation it is possible to conclude that for an INDI controller, the system response including perturbations is approximately equal to the nominal system response.

$$\begin{gathered}\left(I + \Delta G(\boldsymbol{x}_0, \boldsymbol{u}_0)G_n^{-1}(\boldsymbol{x}_0, \boldsymbol{u}_0)\right)\boldsymbol{\nu} \approx \Delta G(\boldsymbol{x}_0, \boldsymbol{u}_0)G_n^{-1}(\boldsymbol{x}_0, \boldsymbol{u}_0)\dot{\boldsymbol{x}}_0 \\ \dot{\boldsymbol{x}} \approx \boldsymbol{\nu}\end{gathered} \tag{5.28}$$

5.4.4. Time-Scale Separation

The principle of time-scale separation implies the use of several loops within the controller to take into account fast dynamics and slow dynamics of the system. A variable is said to have slow dynamics in case the control effectiveness on the dynamics is low. In case a variable is said to have fast dynamics, the control effectiveness on the dynamics is high. [Chu, Q.P. et al., 2019-2020] This essentially leads to a control system where the outputs of the slow outer loop are used as inputs for the fast inner loop. Considering an aircraft using four different control inputs namely: aileron deflections, elevator deflections, rudder deflections, and thrust input, it is possible to identify the order of a system relating the inputs to the dynamics of a variable as shown in fig. 5.3. In this figure, it can be observed that it takes a specific number of integrations to link an input to a specific variable.

In this figure it is possible to observe that it takes two integration steps to link the effect of an elevator input (δ_e) to the pitch rate (q), while it takes three integration steps to link an elevator input (δ_e) to the pitch angle (θ). This essentially means that the dynamic response of the pitch rate is faster to an elevator input compared to the pitch rate. For this reason, the principle of time-scale separation suggests that the variables dictating the slow dynamics are assumed constant in the fast, inner loops. Besides that, the variables that dictate the fast dynamics are assumed to achieve their commands instantaneously. [Van 't Veld, R.C., 2016] In theory, the time-scale separation principle could result in stability problems. However, the closed-loop stability of the system can be guaranteed if the frequency of the inner-loop dynamics is sufficiently large. [Schumacher, C. et al., 1998]

The main advantage of using time-scale separation is the reduction of mathematical complexity, while it is still possible to perform unbiased tracking by the closed-loop system. [Van 't Veld, R.C., 2016]

5.5. Flight Control System Assessment

To assess the flight control system it is first necessary to determine the specific control mode that is used for the assessment. In general, there are three different types of control modes that can be used for the assessment: pilot-in-the-loop, passenger-in-the-loop, and fully automatic. Currently, no operational TU Delft Flying-V simulator or aircraft is available to perform human-in-the-loop experiments. Therefore, the fully automatic control mode is used for the assessments. For this control mode, the control inputs are developed pre-flight and run using the simulation model and the experimental flight control system. [Van 't Veld, R.C., 2016] Section 5.5.1 elaborates on quantitative methods to assess the performance of the flight control system based on the research performed by [Van 't Veld, R.C., 2016]. Besides that, in section 5.5.2 the robustness of the flight control system is discussed.

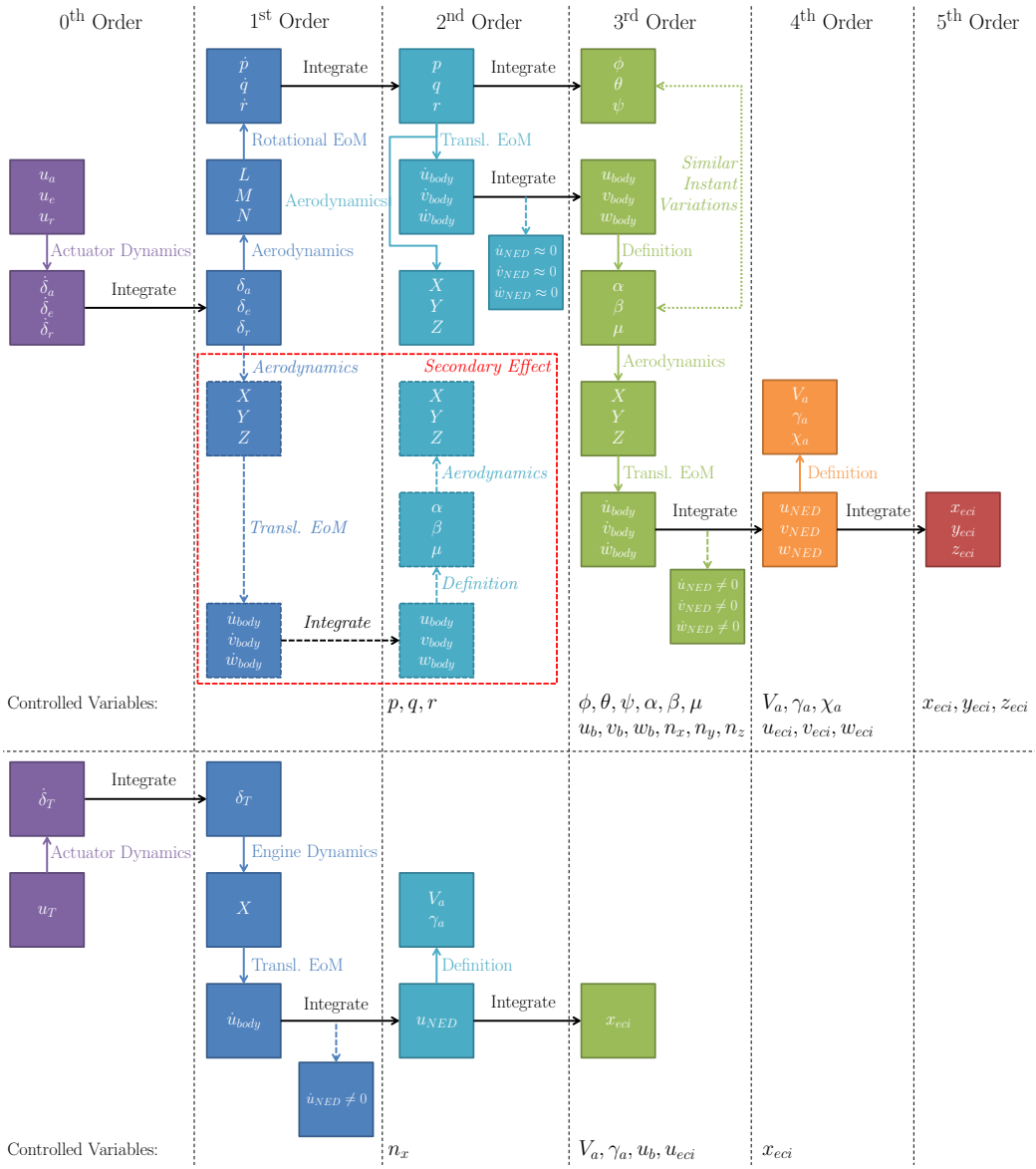

Figure 5.3: Time-Scale Separation. [Van 't Veld, R.C., 2016]

5.5.1. Performance Assessment Criteria

In this subsection, the performance assessment criteria for the flight control system are defined. First, an assessment method including the closed-loop eigenvalues is defined, after that, the gain and phase margin are discussed.

Closed-loop Eigenvalues

In case the closed-loop nonlinear control system is linearised around a local point, it is possible to assess the eigenvalues at this local point and determine whether the closed-loop system is stable. Besides that, using the eigenvalues of the system it is possible to determine the natural frequency and the damping ratio of the specific eigenmotion. [Van 't Veld, R.C., 2016]

Gain and Phase Margin

As mentioned in section 3.4.2 it is possible to analyse the gain and phase margin of the open-loop aircraft by linearising the equations of motion around a specific equilibrium point and assuming that in the region surrounding this point, the dynamics are linear.

5.5.2. Robustness Assessment Criteria

In this subsection, the robustness criteria are discussed, starting with the aerodynamic uncertainty. After that, time delay is discussed. Finally, the sampling frequency is discussed.

Aerodynamic Uncertainties

As mentioned before, one of the main components of uncertainty is the aerodynamic model used. The research performed by [Simplício, P.V.M., 2011] presents an aerodynamic uncertainty analysis method, where the nominal control performance is compared with the control performance under aerodynamic uncertainty. The uncertainty introduced is generated by adding a normally distributed error terms to specific aerodynamic coefficients. Consequently, the Root Mean Square error is determined to compare the performance of the controller including uncertainty with the nominal condition. [Simplício, P.V.M., 2011]

Time Delay

Another aspect that needs to be taken to assess the robustness of the control system is the time delay between a specific command given by the control system and the deflection of the actuators. The time delay originates from the transmission time between the control system and the actuator and can be estimated to be equal to 100 ms. [Padfield, G.D., 2008] Depending on operation frequency of the control system, this can result in several delayed samples between the computation of the control command and the deflection of the control surface. Also taking into account the rate limits of the actuators, the caused delays may lead to severe performance degradation of the control system. [Simplício, P.V.M., 2011]

Sampling Frequency

The final aspect that needs to be considered is changing the sampling frequency of the control system. Namely, decreasing the sampling frequency of the control system results in less required computational effort. However, an inherent assumption of INDI is a high sampling rate, resulting in the assumption that $\boldsymbol{x} \approx \boldsymbol{x}_0$. In case the sampling frequency is too low, this may result in performance degradation of the control system. [Simplício, P.V.M., 2011]

5.6. Flight Control System Design Conclusion

From chapter 1 it is possible to obtain the third sub-question, namely:

> How do the stability and handling qualities of the Flying-V aircraft change after applying a flight control system?

To answer this sub-question, it is first necessary to determine what types of flight control systems are applicable to the aircraft and can contribute to the stability and handling qualities performance of the aircraft. To determine the applicability of a flight control system to the TU Delft Flying-V, it is determined that the flight control system must be able to make the aircraft adhere to the essential stability and handling qualities. Besides that, the flight control system must be able to cope with the inherent nonlinear behaviour of the aircraft. Thirdly, the controller must be able to cope with model uncertainties. In the past, mainly linear control techniques were used. This type of controller requires the linearisation of the system and is only valid for a small range within the complete flight envelope. One of the most widely used linear controllers is the Proportional-Integral-Derivative (PID) controller. To overcome the shortcomings of linear controllers, nonlinear control techniques have been developed. One of these techniques is Incremental Nonlinear Dynamic Inversion (INDI). This is a sensor-based control method that requires less model information and can therefore improve the system robustness against model uncertainties. For this research it is decided to apply both a PID and INDI controller to the TU Delft Flying-V and compare both controllers.

Secondly, it is necessary to determine how these two different flight control systems can be compared. This is done by defining several assessment criteria. These assessment criteria can be divided into performance assessment criteria and robustness assessment criteria. Performance assessment criteria consists of an analysis of the closed loop eigenvalues of the system to determine stability. Besides that the gain and phase margin are assessed. Robustness assessment criteria consist of introducing aerodynamic uncertainties, introducing time delay, and changing the sampling frequency to analyse how the root mean square error of each control system changes.

III

Additional Derivations and Results

6

Simulation Model Design

6.1. Simulation Model Overview

The simulation model of the Flying-V consists of one main simulation file and several functions defined in external files that can be called by the main simulation file. The files required to run a simulation of the Flying-V are listed below:

- `Flying_V_Simulation.m`
- `FV_reset.HQ.json`
- `VLM_WTE_AeroData.HQ.json`
- `coeff.m`
- `TRIM.m`
- `EOM.m`
- `Linear_model.m`
- `RK4.m`

This section gives an overview of the main purpose and functions of each file required for the simulation of the Flying-V.

6.1.1. Flying_V_Simulation.m

This is the main simulation file of the Flying-V simulation model. This file is used to call the functions and data defined in different files and uses this to run the simulation. To run a simulation of the Flying-V, the following steps are chronologically executed:

1. The aerodynamic data obtained from the Vortex Lattice Method and Wind Tunnel Experiments is called.
2. The geometric properties such as the wing surface area and moment of inertia are defined. Besides that, the user is able to choose between the cruise and approach condition.
3. The initial flight conditions are determined by trimming the Flying-V.
4. The initial flight conditions are used to construct a state space matrix obtained from the linearised set of equations of motion.
5. The nonlinear and linear simulation is executed for a specific time defined by the user.
6. The time responses of the Flying-V are plotted.

6.1.2. FV_reset.HQ.json

This data file is obtained from Airbus and contains aerodynamic data of the Flying-V for Mach 0.2 (approach), 0.3 (approach), and 0.85 (cruise). Airbus has used the Vortex Lattice Method to generate this aerodynamic data. For this research only Mach 0.2 and Mach 0.85 are considered. Mach 0.3 is not considered as Mach 0.2 considers lower airspeed. This involves decreased effectiveness of the control surfaces and is therefore considered a more critical flight condition for analysis. The aerodynamic data consists of tables that display the aerodynamic coefficients for several angles of attack, angles of sideslip, rotational rates, and control surface deflections. The aerodynamic coefficients for a specific flight condition can be obtained by interpolating between different data points.

6.1.3. VLM_WTE_AeroData.HQ.json

This data file is created by combining the aerodynamic data obtained from Airbus with aerodynamic data obtained from Wind Tunnel Experiments at TU Delft. This data file has the same structure as `VLM_WTE_AeroData.HQ.json`. This combination of two sources of aerodynamic data is performed to design an aerodynamic model that is able to capture the nonlinear longitudinal behaviour of the Flying-V obtained from previous research. [Garcia, A.R., 2019, Palermo, M. et al., 2020, Viet, R., 2019]

6.1.4. coeff.m

This file contains a function that takes the current flight condition and uses the aerodynamic data obtained from `FV_reset.HQ.json` and `VLM_WTE_AeroData.HQ.json`. Consequently, the current flight condition is used to obtain the aerodynamic coefficients (C_x, C_y, C_z, C_l, C_m, C_n) that can be used to calculate the forces and moments acting on the Flying-V.

6.1.5. TRIM.m

This file contains a function that calculates the trim condition of the Flying-V. The trim function uses the horizontal body velocity component (u), vertical body velocity component (w), pitch angle (θ), control surface deflection of the inboard and outboard elevon (δ_{CS1} and δ_{CS2}), and thrust setting (T) to trim the aircraft. The aircraft is trimmed for steady and symmetric flight. Therefore, the rudder deflections are set to zero.

6.1.6. EOM.m

This file contains a function that takes the current aircraft state and the aerodynamic coefficients obtained from `coeff.m` to calculate the state derivatives using a set of nonlinear equations of motion.

6.1.7. Linear_model.m

This file contains a function that takes the trimmed flight condition and uses this flight condition to obtain the partial derivatives of the nonlinear equations of motion, with respect to the states. These partial derivatives are consequently written in a state space form. The state space is used for linear simulations and eigenvalue analysis.

6.1.8. RK4.m

This file contains a function that takes the current aircraft state and uses this state together with the nonlinear set of equations of motion for integration. The integration method used for this research is a Runge-Kutte integration. It is decided to use this implicit integration method to guarantee stability of the integration.

6.2. Simulation Model Settings

The simulation of the Flying-V requires the definition of several parameters that depend on the geometry and flight conditions of the Flying-V. The parameters defined by the geometry of the aircraft are shown in table 6.1. In this table, S represents the wing surface area, c is the mean aerodynamic chord, and b is the span. Besides that, T_{dy} represents the vertical distance between the engines of the Flying-V and the centre of gravity. Also, T_{dz} is the horizontal distance between the engines and the line of symmetry. In fig. 6.1 the location of the engines is displayed. [Rubio Pascual, B., 2018] Furthermore, the moments of inertia are displayed in table 6.1. Finally, three several centre of gravity positions are defined (p_{ref} and p_{cg}). The centre of gravity is defined from the nose of the aircraft, where the forward centre of gravity position is equal to 29.372 m (corresponding to 45% MAC), the aft centre of gravity location is equal to 31.714 m (corresponding to 57.5% MAC). Finally, 32.18268 m corresponds to the reference position around which the aerodynamic model is defined (p_{ref}).

Table 6.1: Geometric parameter Flying-V

$S = 883.3$ m^2	$I_{xx} = 3.9641 \cdot 10^7$ kg m^2
$c = 18.73851$ m	$I_{yy} = 2.7619 \cdot 10^7$ kg m^2
$b = 65.0$ m	$I_{zz} = 2.7619 \cdot 10^7$ kg m^2
$T_{dy} = 0.8$ m	$I_{xz} = 0$ kg m^2
$T_{dz} = 5.7$ m	$p_{\text{ref}} = 32.18268$ m
$p_{\text{cg}} = [29.372$ m; 31.714 m$]$	

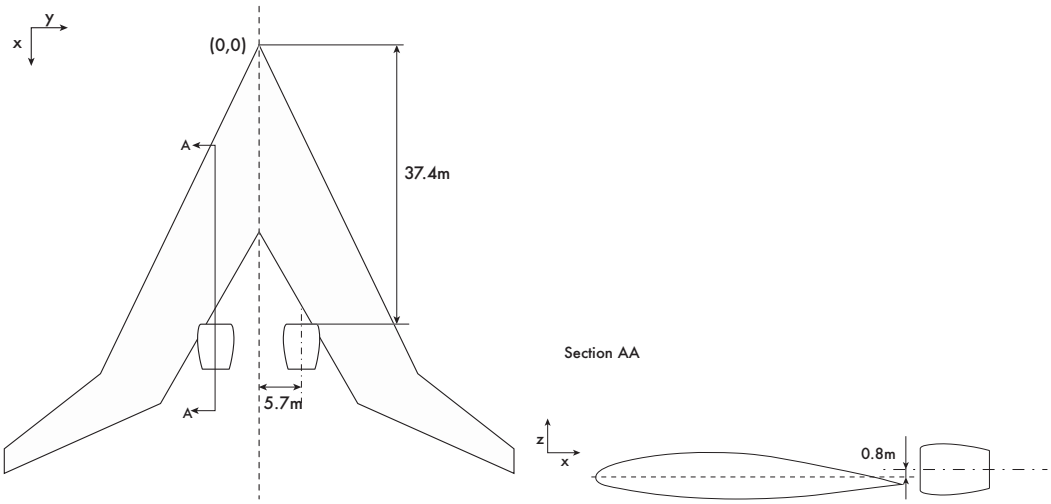

Figure 6.1: Engine Location Flying-V. [Rubio Pascual, B., 2018]

It is possible to identify two different flight conditions for which the Flying-V can be simulated. Namely, the aircraft can be simulated for approach conditions and for cruise conditions. The flight conditions for both cruise and approach can be observed in table 6.2. It is possible to observe that approach takes place at sea level conditions whereas the cruise condition corresponds to an altitude of 13 km.

Table 6.2: Flight conditions Flying-V

Approach Condition	**Cruise Condition**
Ma $= 0.2$	Ma $= 0.85$
$\rho = 1.225$ kg/m^3	$\rho = 0.265483$ kg/m^3
$a_{\text{mach}} = 343$ m/s	$a_{\text{mach}} = 295$ m/s
mass $= 210{,}000$ kg	mass $= 240{,}000$ kg

6.3. Aerodynamic Model

From previous research it is determined that the Flying-V experiences two types of undesired aerodynamic behaviour, namely pitch break for angles of attack larger than 20 degrees and unstable Dutch roll for specific combinations of the centre of gravity location and flight condition. [Cappuyns, T., 2019, Palermo, M. et al., 2020, Viet, R., 2019] Currently, it is possible to obtain an aerodynamic model based on aerodynamic data from:

- The Vortex Lattice Method
- Wind Tunnel Experiments
- Flight Test Experiments

Based on the trade-off made in part II, it is possible to identify that the unstable Dutch roll behaviour can be obtained from an aerodynamic model using the Vortex Lattice Method (VLM), whereas the unstable pitch break behaviour can be obtained from Wind Tunnel Experiments (WTE). Therefore, it is decided to combine the data obtained from the Vortex Lattice Method and Wind Tunnel Experiments into one aerodynamic model that captures the undesired aerodynamic behaviour mentioned in literature. [Cappuyns, T., 2019, Garcia, A.R., 2019, Viet, R., 2019]

Both aerodynamic models also consist of a number of differences. Namely, the aerodynamic model obtained from the VLM method involves the full size aircraft including two elevons and one rudder on each side of the wing. On the other hand, the aerodynamic model obtained from the WTE experiments involves a small scale model of the aircraft, including three elevons and one rudder on each side of the wing.

The VLM model is stored in a json file called `FV_reset.HQ.json`. This file is obtained from Airbus and contains the aerodynamic coefficients for the approach and cruise condition, for angles of attack ranging between 0° and 15°. Each coefficient can be written as shown in eq. (6.1). In this equation, C_* represents a specific coefficient (C_X, C_Y, C_Z, C_l, C_m, or C_n). Besides that $C_*(\cdot)$ represents the contribution of a specific parameter to the aerodynamic coefficient. Finally, $p^* = p\frac{c}{\hat{V}}$, $q^* = q\frac{c}{\hat{V}}$, and $r^* = r\frac{c}{\hat{V}}$. The coefficients can be obtained from the file by interpolating or extrapolating between/outside the data points.

$$C_* = C_*(\alpha) + C_*(\beta) + C_*(p^*) + C_*(q^*) + C_*(r^*) + C_*(\delta_{\text{CS1}}) + C_*(\delta_{\text{CS2}}) + C_*(\delta_{\text{CS3}}) \tag{6.1}$$

The WTE model can be obtained from the set of equations shown in eq. (6.2). Due to high uncertainties, the lateral force coefficient (C_Y) cannot be used. [Garcia, A.R., 2019]

$$\begin{aligned}
C_X &= C_{X_0} + C_{X_\alpha}\alpha + C_{X_{\alpha^2}}\alpha^2 + C_{X_{\alpha^3}}\alpha^3 + C_{X_{\alpha^4}}\alpha^4 + C_{X_{\delta_{\text{CS1}}}}\delta_{\text{CS1}} + C_{X_{\delta_{\text{CS2}}}}\delta_{\text{CS2}} + C_{X_{\delta_{\text{CS3}}}}\delta_{\text{CS3}} \\
&\quad + C_{X_{\delta^2_{\text{CS1}}}}\delta^2_{\text{CS1}} + C_{X_{\delta^2_{\text{CS2}}}}\delta^2_{\text{CS2}} + C_{X_{\hat{V}}}\hat{V} + C_{X_{\hat{V}^2}}\hat{V}^2 \\
C_Z &= C_{Z_0} + C_{Z_\alpha}\alpha + C_{Z_{\alpha^2}}\alpha^2 + C_{Z_{\alpha^3}}\alpha^3 + C_{Z_{\delta_{\text{CS1}}}}\delta_{\text{CS1}} + C_{Z_{\delta_{\text{CS2}}}}\delta_{\text{CS2}} + C_{Z_{\delta_{\text{CS3}}}}\delta_{\text{CS3}} + C_{Z_{\hat{V}}}\hat{V} \\
C_l &= C_{l_0} + C_{l_\alpha}\alpha + C_{l_{\alpha^2}}\alpha^2 + C_{l_{\alpha^3}}\alpha^3 + C_{l_{\alpha^4}}\alpha^4 C_{l_{\delta_{\text{CS1}}}}\delta_{\text{CS1}} + C_{l_{\delta_{\text{CS2}}}}\delta_{\text{CS2}} + C_{l_{\delta_{\text{CS3}}}}\delta_{\text{CS3}} + C_{l_{\hat{V}}}\hat{V} \\
C_m &= C_{m_0} + C_{m_\alpha}\alpha + C_{m_{\alpha^2}}\alpha^2 + C_{m_{\alpha^3}}\alpha^3 + C_{m_{\alpha^4}}\alpha^4 + C_{m_{\delta_{\text{CS1}}}}\delta_{\text{CS1}} + C_{m_{\delta_{\text{CS2}}}}\delta_{\text{CS2}} + C_{m_{\delta_{\text{CS3}}}}\delta_{\text{CS3}} \\
&\quad + C_{m_{\delta^2_{\text{CS1}}}}\delta^2_{\text{CS1}} + C_{m_{\delta^2_{\text{CS2}}}}\delta^2_{\text{CS2}} + C_{m_{\delta_{\text{CS1}}\delta_{\text{CS2}}}}\delta_{\text{CS1}}\delta_{\text{CS2}} + C_{m_{\alpha\delta^2_{\text{CS1}}}}\alpha\delta^2_{\text{CS1}} + C_{m_{\alpha\delta^2_{\text{CS2}}}}\alpha\delta^2_{\text{CS2}} + C_{m_{\alpha^2\delta_{\text{CS1}}}}\alpha^2\delta_{\text{CS1}} \\
&\quad + C_{m_{\alpha^2\delta_{\text{CS2}}}}\alpha^2\delta_{\text{CS2}} + C_{m_{\hat{V}}}\hat{V} + C_{m_{\hat{V}\delta_{\text{CS1}}}}\hat{V}\delta_{\text{CS1}} \\
C_n &= C_{n_0} + C_{n_\alpha}\alpha + C_{n_{\alpha^2}}\alpha^2 + C_{n_{\alpha^3}}\alpha^3 + C_{n_{\alpha^4}}\alpha^4 + C_{n_{\delta_{\text{CS1}}}}\delta_{\text{CS1}} + C_{n_{\delta_{\text{CS2}}}}\delta_{\text{CS2}} + C_{n_{\delta^2_{\text{CS1}}}}\delta^2_{\text{CS1}} + C_{n_{\delta^2_{\text{CS2}}}}\delta^2_{\text{CS2}} \\
&\quad + C_{n_{\hat{V}}}\hat{V}
\end{aligned} \tag{6.2}$$

To combine the VLM aerodynamic model and the WTE aerodynamic model, the VLM model is used as the baseline model. This means that the Flying-V model used for this analysis consists

of an inboard elevon, outboard elevon, and rudder integrated into the winglet. After that, elements from the WTE model are implemented into the VLM model, such that the combined model is able to capture the unstable Dutch roll and longitudinal instability obtained from previous research. [Cappuyns, T., 2019, Palermo, M. et al., 2020, Viet, R., 2019] Therefore, this research combines the coefficients that are relevant for modelling the longitudinal instability (C_X, C_Z, and C_m). For the remaining coefficients (C_Y, C_l, and C_n), the coefficients obtained from the VLM model are used. Besides that, the aerodynamic coefficients are determined for the approach- and cruise condition (Ma = 0.2 and Ma = 0.85 respectively) for angles of attack ranging between $-5°$ and $30°$. Additionally, due to the significant difference in control surface layout between the two models, deflections are kept equal to zero. Essentially, this means that the aerodynamic model combination entails combining the contribution of the angle of attack to the coefficients: C_X, C_Z, and C_m.

Both aerodynamic models operate in different airspeed regimes due to the difference in aircraft size. Therefore it is necessary to scale the airspeed according to Dynamic or Froude scaling. This scaling method can be used for scaled aircraft models that are capable of simulating the relative motions of a larger full-scale aircraft. [Ananda, G.K. et al., 2017] After scaling the airspeed, it is possible to compare the aerodynamic coefficients for different angles of attack as shown in Fig. 6.2.

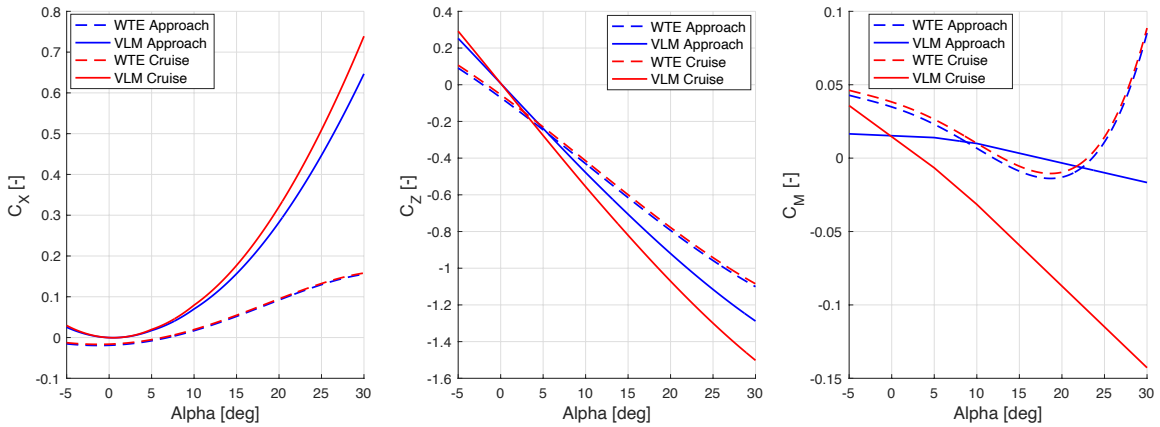

Figure 6.2: Aerodynamic model curves from VLM and WTE for approach and cruise phase.

This figure shows that the aerodynamic coefficients of the VLM and WTE are of the same magnitude, but that the VLM model is not able to capture the longitudinal instability that becomes apparent at 20 degrees angle of attack. Therefore, the WTE curves are vertically translated to match the VLM curve at $\alpha = 15°$ and put together. The discontinuity that originates from this operation is resolved by interpolating the datapoints using the shape-preserving piecewise cubic interpolating polynomial function "pchip". This function makes use of splines, where each spline is a third-degree polynomial with specified derivatives at the interpolation points[1]. This results in a combined aerodynamic model, where the coefficients for angles of attack ranging between -5° up to 15° are obtained from the VLM model and the coefficients for angles of attack ranging between 15° up to 30° are obtained from the WTE model. Based on the aerodynamic model obtained from the combination of the VLM model and WTE model, it can be concluded that the aerodynamic model does not contain any lift induced drag (C_{D_0}), decreasing the fidelity of the model. Due to limited analysis on the lift induced drag of a full scale model of the Flying-V it is decided to use the lift induced drag from the Airbus A350-900 (the aircraft used as a reference for the design of the Flying-V) and add this to the aerodynamic model of the Flying-V. This results into a lift induced drag of 0.027 during cruise and 0.057 during approach. [Sun, J. et al., 2018] The combined aerodynamic model is shown in Fig. 6.3, where it is visible that the longitudinal unstable behaviour is captured by the combined aerodynamic model.

Because the combined aerodynamic model only captures the contribution of the angle of attack to the coefficients C_X, C_Z, and C_m a separate file is created with the same layout of `FV_reset.HQ.json`. This new file called `VLM_WTE_AeroData.HQ.json` can be used in combination with `FV_reset.HQ.json` to obtain a complete aerodynamic model of the Flying-V that includes the nonlinear pitch break be-

[1] https://www.mathworks.com/help/matlab/ref/pchip.html#bvjbz1m-2

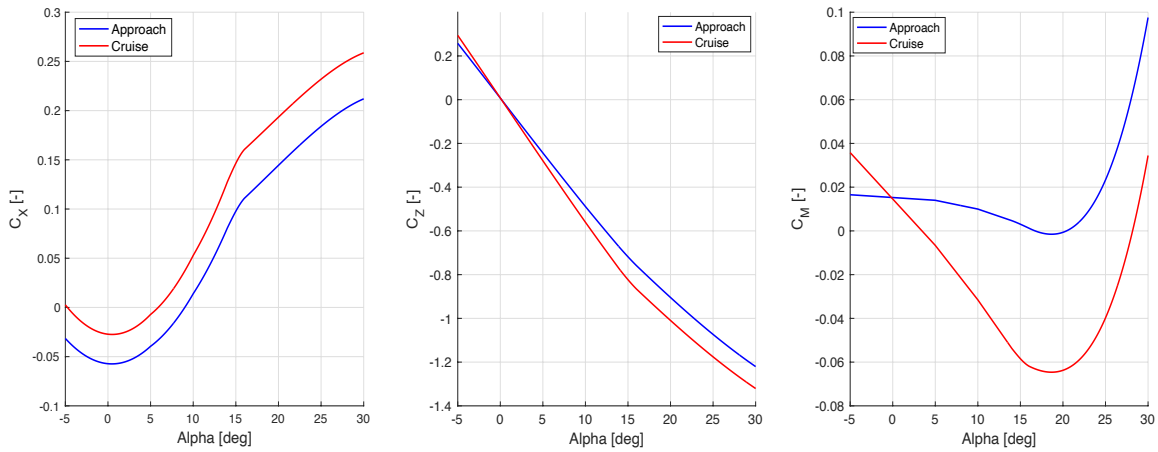

Figure 6.3: Aerodynamic model obtained from combining VLM with WTE.

haviour obtained from previous research.

6.4. Nonlinear Equations of Motion

The nonlinear set of equations of motion can be observed in eq. (6.3). The set of nonlinear equations of motion show how the derivative of each state can be obtained. In this equation, $I^* = I_{xx}I_{zz} - I_{xz}^2$. Besides that F_x, F_y, F_z, M_x, M_y, and M_z represent the forces and moments acting on the Flying-V in the x-, y-, and z-direction respectively.

$$
\begin{aligned}
\dot{x} &= (u\cos(\theta) + (v\sin(\phi) + w\cos(\phi))\sin(\theta))\cos(\psi) - (v\cos(\phi) - w\sin(\phi))\sin(\psi) \\
\dot{y} &= (u\cos(\theta) + (v\sin(\phi) + w\cos(\phi))\sin(\theta))\sin(\psi) + (v\cos(\phi) - w\sin(\phi))\cos(\psi) \\
\dot{z} &= -u\sin(\theta) + (v\sin(\phi) + w\cos(\phi))\cos(\theta) \\
\dot{u} &= vr - wq - g\sin(\theta) + \frac{F_x}{m} \\
\dot{v} &= wp - ur + g\sin(\phi)\cos(\theta) + \frac{F_y}{m} \\
\dot{w} &= uq - vp + g\cos(\phi)\cos(\theta) + \frac{F_z}{m} \\
\dot{p} &= \frac{I_{zz}}{I^*}M_x + \frac{I_{xz}}{I^*}M_z + \frac{(I_{xx} - I_{yy} + I_{zz})I_{xz}}{I^*}pq + \frac{((I_{yy} - I_{zz})I_{zz} - I_{xz}^2)}{I^*}qr \\
\dot{q} &= \frac{M_y}{I_{yy}} + \frac{(r^2 - p^2)I_{xz}}{I_{yy}} + \frac{(I_{zz} - I_{xx})}{I_{yy}}pr \\
\dot{r} &= \frac{I_{xz}}{I^*}M_x + \frac{I_{xx}}{I^*}M_z + \frac{((I_{xx} - I_{yy})I_{xx} + I_{xz}^2)}{I^*}pq + \frac{(-I_{xx} + I_{yy} - I_{zz})I_{xz}}{I^*}qr \\
\dot{\phi} &= p + \sin(\phi)\tan(\theta)q + \cos(\phi)\tan(\theta)r \\
\dot{\theta} &= \cos(\phi)q - \sin(\phi)r \\
\dot{\psi} &= \frac{\sin(\phi)}{\cos(\theta)}q + \frac{\cos(\phi)}{\cos(\theta)}r
\end{aligned}
\tag{6.3}
$$

The forces and moments consist of several components as can be observed in eq. (6.4). In this set of equations, the aerodynamic forces can be recognised by the subscript "aero" and are displayed in the body reference frame. Besides that, contributions of the thrust force and moments can be observed. Finally, it is also necessary to add a component that takes into account the contribution of a centre of gravity shift to the moments around the y-axis and z-axis. [Sieberling, S et al., 2010]

$$\begin{aligned}
F_x &= F_{x_{\text{aero}}} + T_1 + T_2 \\
F_y &= F_{y_{\text{aero}}} \\
F_z &= F_{z_{\text{aero}}} \\
M_x &= M_{x_{\text{aero}}} \\
M_y &= M_{y_{\text{aero}}} - (T_1 + T_2)T_{\text{dy}} + F_{z_{\text{aero}}}(p_{\text{ref}} - p_{\text{cg}}) \\
M_z &= M_{z_{\text{aero}}} + T_1 T_{\text{dz}} - T_2 T_{\text{dz}} - F_{y_{\text{aero}}}(p_{\text{ref}} - p_{\text{cg}})
\end{aligned} \tag{6.4}$$

6.5. State Space Model

To obtain the state space model, it is necessary to linearise the nonlinear set of equations of motion around the trim conditions of the aircraft. After linearisation it is possible to obtain the state-space model of aircraft, which can be used to obtain the eigenvalues of the system.

To fill the A-matrix of the state space system, it is necessary to obtain the derivative of each nonlinear equation of motion with respect to each state. To fill the B-matrix of the state space system, it is necessary to obtain the derivative of each nonlinear equation of motion with respect to each input. This is also shown in eq. (6.5). In this equation, $\boldsymbol{x}$ represents the state vector ($\begin{bmatrix} x & y & z & u & v & w & p & q & r & \phi & \theta & \psi \end{bmatrix}^T$). Furthermore, $\boldsymbol{u}$ represents the input vector ($\begin{bmatrix} \delta_{\text{CS1}} & \delta_{\text{CS2}} & \delta_{\text{CS3}} & T_1 & T_2 \end{bmatrix}^T$).

$$\dot{\boldsymbol{x}} = A\boldsymbol{x} + B\boldsymbol{u} = \left(\frac{\partial \dot{\boldsymbol{x}}}{\partial \boldsymbol{x}}\right)_{\text{trim}} \boldsymbol{x} + \left(\frac{\partial \dot{\boldsymbol{x}}}{\partial \boldsymbol{u}}\right)_{\text{trim}} \boldsymbol{u} \tag{6.5}$$

The linearisation of the main part of the equations of motion is relatively simple. To give an example: $\frac{\partial \dot{x}}{\partial u} = \cos(\theta)\cos(\psi)$. The main challenge entails the derivative of the forces and moments with respect to each of the states and inputs. To give an illustration on how to obtain the derivatives of the force and moment coefficients with respect to the states and inputs, the derivative of the forces in the x-direction (F_x) with respect to the forward velocity components (u) is given. To obtain the complete state space system, the reader is referred to the file: `Linear_model.m`. This file contains the complete linearisation of the equations of motion including sufficient explanation.

The forces in the x-direction can be obtained using eq. (6.6). In this equation, ${}^{\mathcal{A}}F_*$ represents a force in the Airbus-aerodynamic frame. This frame is similar to an ordinary aerodynamic frame, with the difference that the force in the x-direction points backwards (the drag force) and the force in the z-direction points upwards (the lift force). These two forces are therefore multiplied with -1 to convert them to the general aerodynamic frame.

$$\begin{aligned}
{}^{\mathcal{B}}F_x &= {}^{\mathcal{A}}F_x \cos(\alpha)\cos(\beta) - {}^{\mathcal{A}}F_y \sin(\beta)\cos(\alpha) - {}^{\mathcal{A}}F_z \sin(\alpha) + T_1 + T_2 \\
{}^{\mathcal{A}}F_x &= -C_x \frac{1}{2}\rho V^2 S \\
{}^{\mathcal{A}}F_y &= C_y \frac{1}{2}\rho V^2 S \\
{}^{\mathcal{A}}F_z &= -C_z \frac{1}{2}\rho V^2 S
\end{aligned} \tag{6.6}$$

Consequently, the derivative of the forces with respect to the x-direction is shown in eq. (6.7).

$$\begin{aligned}
\frac{\partial {}^{\mathcal{B}}F_x}{\partial u} = {} & \frac{\partial {}^{\mathcal{A}}F_x}{\partial u}\cos(\alpha)\cos(\beta) + {}^{\mathcal{A}}F_x \frac{\partial(\cos(\alpha)\cos(\beta))}{\partial u} \\
& - \frac{\partial {}^{\mathcal{A}}F_y}{\partial u}\sin(\beta)\cos(\alpha) - {}^{\mathcal{A}}F_y \frac{\partial(\sin(\beta)\cos(\alpha))}{\partial u} - \frac{\partial {}^{\mathcal{A}}F_z}{\partial u}\sin(\alpha) - {}^{\mathcal{A}}F_z \frac{\partial \sin(\alpha)}{\partial u}
\end{aligned} \tag{6.7}$$

The derivatives shown in eq. (6.7) are consequently equal to:

$$
\begin{aligned}
\frac{\partial^{\mathcal{A}} F_x}{\partial u} &= -\frac{1}{2}\rho S\left(\frac{\partial C_x}{\partial u}V^2 + C_x\frac{\partial V^2}{\partial u}\right) = -\frac{1}{2}\rho S\left(\frac{\partial C_x}{\partial u}V^2 + C_x 2u\right)\\
\frac{\partial(\cos(\alpha)\cos(\beta))}{\partial u} &= \frac{(v^2+w^2)}{(u^2+v^2+w^2)^{\frac{3}{2}}}\\
\frac{\partial^{\mathcal{A}} F_y}{\partial u} &= \frac{1}{2}\rho S\left(\frac{\partial C_y}{\partial u}V^2 + C_y 2u\right)\\
\frac{\partial(\sin(\beta)\cos(\alpha))}{\partial u} &= \frac{(-u^4 v + v^3 w^2 + v w^4)}{((u^2+v^2+w^2)(u^2+w^2))^{\frac{3}{2}}}\\
\frac{\partial^{\mathcal{A}} F_z}{\partial u} &= \frac{1}{2}\rho S\left(\frac{\partial C_z}{\partial u}V^2 + C_z 2u\right)\\
\frac{\partial \sin(\alpha)}{\partial u} &= \frac{-uw}{(u^2+w^2)^{\frac{3}{2}}}
\end{aligned}
\tag{6.8}
$$

As mentioned in section 6.3, the aerodynamic coefficients are not a function of u. Therefore, it is necessary to obtain the derivative of the aerodynamic coefficients using eq. (6.9).

$$
\begin{aligned}
\frac{\partial C_*}{\partial u} &= \frac{\partial C_*(\alpha)}{\partial \alpha}\frac{\partial \alpha}{\partial u} + \frac{\partial C_*(\beta)}{\partial \beta}\frac{\partial \beta}{\partial u} + \frac{\partial C_*(p^*)}{\partial p^*}\frac{\partial p^*}{\partial u} + \frac{\partial C_*(q^*)}{\partial q^*}\frac{\partial q^*}{\partial u} + \frac{\partial C_*(r^*)}{\partial r^*}\frac{\partial r^*}{\partial u}\\
&+ \frac{\partial C_*(\delta_{\mathrm{CS1}})}{\partial \delta_{\mathrm{CS1}}}\frac{\partial \delta_{\mathrm{CS1}}}{\partial u} + \frac{\partial C_*(\delta_{\mathrm{CS2}})}{\partial \delta_{\mathrm{CS2}}}\frac{\partial \delta_{\mathrm{CS2}}}{\partial u} + \frac{\partial C_*(\delta_{\mathrm{CS3}})}{\partial \delta_{\mathrm{CS3}}}\frac{\partial \delta_{\mathrm{CS3}}}{\partial u}\\
&= \frac{\partial C_*(\alpha)}{\partial \alpha}\frac{\partial \alpha}{\partial u} + \frac{\partial C_*(\beta)}{\partial \beta}\frac{\partial \beta}{\partial u} = \frac{\partial C_*(\alpha)}{\partial \alpha}\frac{-w}{u^2+w^2} + \frac{\partial C_*(\beta)}{\partial \beta}\frac{-uv}{V^2\sqrt{u^2+w^2}}
\end{aligned}
\tag{6.9}
$$

The derivatives $\frac{\partial C_*(\alpha)}{\partial \alpha}$ and $\frac{\partial C_*(\beta)}{\partial \beta}$ are obtained using numerical differentiation between the datapoints of the aerodynamic model. A similar derivation can be obtained for the different forces and moments with respect to the states and inputs in order to obtain the state space system.

6.6. Trim Function

To define the initial conditions of the Flying-V it is necessary to trim the aircraft. During approach it is required to trim the aircraft for a steady, symmetric flight with a flight path angle of -3°. During cruise, it is required to trim the aircraft for a steady, symmetric, horizontal flight. The trim algorith takes five inputs, namely the forward velocity component (u), the vertical velocity component (w), the pitch angle (θ), the control surface deflections of the inboard and outboard elevons ($\delta_{\mathrm{CS1}}/\delta_{\mathrm{CS2}}$), and the total thrust setting (T). The trim algorithm aims at minimising the cost function shown in eq. (6.10). In this equation, W_* represents the weight of each parameter of the cost function. The weights are determined iteratively and shown in table 6.3. Besides that, $\dot{u}$, $\dot{w}$, and $\dot{q}$ are the time derivatives of the forward velocity component, horizontal velocity component, and pitch rate respectively. Furthermore, V represents the airspeed, a represents the speed of sound, and γ is the flight path angle. Consequently, the trim algorithm minimises the cost function using "fminsearch". This algorithm can be used to find the minimum of unconstrained multivariable functions using the Nelder-Mead simplex algorithm[2]. The trim algorithm has three different stopping criteria. First of all, the trim algorithm stops in case the current function value differs by less than 10^{-9} from the previous function value. Besides that, the trim algorithm stops in case the current inputs differ from the previous inputs by less than 10^{-9}. In case these two criteria are not met, the trim algorithm stops in case the maximum number of trim function evaluations exceeds 1,000,000.

$$
J(\dot{u},\dot{w},\dot{q},V,\gamma) = W_u\dot{u}^2 + W_w\dot{w}^2 + W_q\dot{q}^2 + W_V\left(\frac{V-V_{\mathrm{ref}}}{a}\right)^2 + W_\gamma(\gamma-\gamma_{\mathrm{ref}}) \tag{6.10}
$$

[2] https://www.mathworks.com/help/matlab/ref/fminsearch.html

Table 6.3: Weights for cost function.

Parameter	W_u	W_w	W_q	W_V	W_γ
Weight	100	1	100	100	1

6.7. Integration Method

To obtain the states discussed in section 6.4 it is necessary to integrate the differential equations displayed in eq. (6.3). To perform the integration it is necessary to make use of a numerical integration method. In general it is possible to distinguish two types of integration methods, namely explicit integration methods and implicit integration methods. Explicit integration methods make use of the current and previous states and derivatives, whereas implicit integration methods also make use of the predicted state derivatives. Explicit integration are known to break down earlier for stiff systems or large time steps. To guarantee stability of the integration it is therefore decided to integrate the dynamic- and kinematic equations using the Runge-Kutte (RK4) method and is shown in eq. (6.11).

$$\begin{aligned} k_1 &= \Delta t \boldsymbol{f}(\boldsymbol{x}_i, \boldsymbol{u}_i) \\ k_2 &= \Delta t \boldsymbol{f}(\boldsymbol{x}_i + \frac{k_1}{2}, \boldsymbol{u}_i) \\ k_3 &= \Delta t \boldsymbol{f}(\boldsymbol{x}_i + \frac{k_2}{2}, \boldsymbol{u}_i) \\ k_4 &= \Delta t \boldsymbol{f}(\boldsymbol{x}_i + k_3, \boldsymbol{u}_i) \\ \boldsymbol{x}_{i+1} &= \boldsymbol{x}_i + \frac{1}{6}(k_1 + 2k_2 + 2k_3 + k_4) \end{aligned} \tag{6.11}$$

7

Dutch Roll Mode Analysis

As discussed in part I, the damping ratio of the Dutch roll mode during cruise is negative at the forward centre of gravity location and positive at the aft centre of gravity location. This implies that the Dutch roll mode is stable during cruise at the aft centre of gravity location and unstable during cruise at the forward centre of gravity location. This is in contrast with previous research that describes that the damping ratio has to decrease when moving the centre of gravity aft [Cappuyns, T., 2019, Hasan et al., 2018]. This chapter elaborates on the Dutch roll mode

7.1. Centre of Gravity Shift

As mentioned before, the centre of gravity shift is applied by adding an external moment to the equations of motion as shown in eq. (7.1) [Sieberling, S et al., 2010]. This equation shows that the moment due to a centre of gravity shift can be obtained by first subtracting the centre of gravity position ($\boldsymbol{p}_{\text{cg}}$) from the reference position around which the aerodynamic forces and moments are calculated ($\boldsymbol{p}_{\text{ref}}$). Consequently, a cross product with the aerodynamic forces results in the moment induced by the centre of gravity shift.

$$^{\mathcal{B}}\boldsymbol{M}_{\text{cg}} = (\boldsymbol{p}_{\text{ref}} - \boldsymbol{p}_{\text{cg}}) \times {}^{\mathcal{B}}\boldsymbol{F}_{\text{aero}} \tag{7.1}$$

Because it is assumed that the centre of gravity only acts along the x-axis of the body frame, the external moment acting on the system due to a centre of gravity shift is equal to eq. (7.2). This equation shows that the centre of gravity shift results in a moment an additional moment around the y-axis and z-axis. Using the body fixed reference frame, both p_{ref_x} and p_{cg_x} are negative numbers. Therefore, eq. (7.2) can also be written as eq. (7.3).

$$^{\mathcal{B}}\boldsymbol{M}_{\text{cg}} = \begin{bmatrix} 0 & -(p_{\text{ref}_x} - p_{\text{cg}_x})^{\mathcal{B}}F_{\text{aero}_z} & (p_{\text{ref}_x} - p_{\text{cg}_x})^{\mathcal{B}}F_{\text{aero}_y} \end{bmatrix}^T \tag{7.2}$$

$$^{\mathcal{B}}\boldsymbol{M}_{\text{cg}} = \begin{bmatrix} 0 & (|p_{\text{ref}_x}| - |p_{\text{cg}_x}|)^{\mathcal{B}}F_{\text{aero}_z} & -(|p_{\text{ref}_x}| - |p_{\text{cg}_x}|)^{\mathcal{B}}F_{\text{aero}_y} \end{bmatrix}^T \tag{7.3}$$

To obtain a state space model, the derivative of each equation of motion is obtained with respect to each state (as discussed in section 6.5). Due to the centre of gravity shift it is also necessary to take this additional moment ($^{\mathcal{B}}\boldsymbol{M}_{\text{cg}}$) into account when linearising the equations of motion. The Dutch roll mode mainly involves a lateral-directional motion. Therefore, only the linearisation of the moments around the z-axis are considered as shown in eq. (7.4). Some of the equations shown in eq. (7.4) are equal to zero because the forces and moment do not depend on this specific state.

$$
\begin{aligned}
\frac{\partial M_z}{\partial y} &= \left(\frac{\partial M_z}{\partial y}\right)_{\text{aero}} - (|p_{\text{ref}_x}| - |p_{\text{cg}_x}|)\left(\frac{\partial F_{\text{aero}_y}}{\partial y}\right) = 0 \\
\frac{\partial M_z}{\partial v} &= \left(\frac{\partial M_z}{\partial \beta}\frac{\partial \beta}{\partial v}\right)_{\text{aero}} - (|p_{\text{ref}_x}| - |p_{\text{cg}_x}|)\left(\frac{\partial F_{\text{aero}_y}}{\partial \beta}\frac{\partial \beta}{\partial v}\right) \\
\frac{\partial M_z}{\partial p} &= \left(\frac{\partial M_z}{\partial p}\right)_{\text{aero}} - (|p_{\text{ref}_x}| - |p_{\text{cg}_x}|)\left(\frac{\partial F_{\text{aero}_y}}{\partial p}\right) \\
\frac{\partial M_z}{\partial r} &= \left(\frac{\partial M_z}{\partial r}\right)_{\text{aero}} - (|p_{\text{ref}_x}| - |p_{\text{cg}_x}|)\left(\frac{\partial F_{\text{aero}_y}}{\partial r}\right) \\
\frac{\partial M_z}{\partial \phi} &= \left(\frac{\partial M_z}{\partial \phi}\right)_{\text{aero}} - (|p_{\text{ref}_x}| - |p_{\text{cg}_x}|)\left(\frac{\partial F_{\text{aero}_y}}{\partial \phi}\right) = 0 \\
\frac{\partial M_z}{\partial \psi} &= \left(\frac{\partial M_z}{\partial \psi}\right)_{\text{aero}} - (|p_{\text{ref}_x}| - |p_{\text{cg}_x}|)\left(\frac{\partial F_{\text{aero}_y}}{\partial \psi}\right) = 0
\end{aligned}
\tag{7.4}
$$

Looking at eq. (7.4) it is possible to identify six different aerodynamic coefficients that are directly related to the centre of gravity shift, namely: C_{n_β}, C_{y_β}, C_{n_p}, C_{y_p}, C_{n_r}, and C_{y_r}.

7.2. Aerodynamic Coefficient Analysis

After determining the aerodynamic coefficients directly related to the centre of gravity shift, it is necessary to analyse the behaviour of each aerodynamic coefficient with respect to the angle of attack and how these coefficients affect $\frac{\partial M_z}{\partial v}$, $\frac{\partial M_z}{\partial p}$, and $\frac{\partial M_z}{\partial r}$. Before the analysis is performed, it is necessary to mention that the angle of attack increases in case the centre of gravity is moved forward. In section 7.2.1 - section 7.2.6 the effect of an increased angle of attack is discussed for each aerodynamic coefficient. After that section 7.2.7 elaborates on the coefficients that have the largest contribution on the Dutch roll mode.

7.2.1. C_{n_β}

The coefficient C_{n_β} represents the generated yawing moment due to a change in angle of sideslip. In case of a general aircraft, the vertical tailplane has the largest contribution to this coefficient. Namely, in case an aircraft experiences a sideslip angle, the vertical tail surface generates a force in the negative y-direction, resulting in a positive yawing moment that turns the aircraft into the wind. To obtain this weathervane stability it is thus desired to have a positive C_{n_β} [Mulder, J.A. et al., 2013]. It can be observed in table 7.1 that with increasing angle of attack, C_{n_β} decreases. At 15° angle of attack, the coefficient is even negative. This indicates that the Flying-V does not possess weathervane stability for larger angles of attack.

Table 7.1: Coefficient C_{n_β} for different angles of attack.

α [deg]	0	5	10	15
C_{n_β} [-]	0.0037	0.00226	0.0008	-0.00062

7.2.2. C_{y_β}

As already mentioned in section 7.2.1, the vertical tail of a conventional aircraft generates a force in the negative y-direction in case of a sideslip angle. The change in sideforce with sideslip angle is represented by the coefficient C_{y_β}. In general, it is desired for the coefficient C_{y_β} to be negative such that weathervane stability is obtained [Mulder, J.A. et al., 2013]. Table 7.2 shows that the coefficient C_{y_β} remains negative for increasing angle of attack. However, the magnitude of the coefficient decreases with increasing angle of attack. This implies a smaller tendency to obtain weathervane stability for the Flying-V.

Table 7.2: Coefficient C_{y_β} for different angles of attack.

α [deg]	0	5	10	15
C_{y_β} [-]	-0.0044	-0.0042	-0.00393	-0.00362

7.2.3. C_{n_p}

The coefficient C_{n_p} represent the yawing moment generated due to a change in roll rate. For conventional aircraft, this coefficient is negative. Namely, in case an aircraft achieves a positive roll rate, the down-going wing experiences a larger angle of attack. On the other hand, the up-going wing experiences a smaller angle of attack. This results in the fact that the down-going wing's lift component will point slightly forwards, whereas the up-going wing's lift component points slightly backwards. This results into a negative yawing moment. The fact that C_{n_p} is negative is the reason for Dutch roll [Mulder, J.A. et al., 2013]. Table 7.3 shows that C_{n_p} is positive for smaller angles of attack but becomes negative with increasing angle of attack. This essentially means that the Flying-V has a larger Dutch roll tendency for larger angles of attack.

Table 7.3: Coefficient C_{n_p} for different angles of attack.

α [deg]	0	5	10	15
C_{n_p} [-]	0.43928	-0.11459	-0.6673	-1.21465

7.2.4. C_{y_p}

The coefficient C_{y_p} represents the sideforce generated due to a change in roll rate. For conventional aircraft, the main contributing factor is the vertical tailplane. Namely, in case an aircraft obtains a positive roll rate, the tail experiences an angle of attack, resulting in a negative sideforce. Therfore, the coefficient C_{y_p} is generally negative [Mulder, J.A. et al., 2013]. Looking at table 7.4, it is possible to observe that C_{y_p} is negative for smaller angles of attack, but becomes positive for larger angles of attack.

Table 7.4: Coefficient C_{y_p} for different angles of attack.

α [deg]	0	5	10	15
C_{y_p} [-]	-0.4354	-0.03677	0.36207	0.7581

7.2.5. C_{n_r}

The coefficient C_{n_r} represents the yaw moment generated due to a change in yaw rate. For conventional aircraft, the vertical tailplane is the main contributor to this coefficient. In case the aircraft obtains a yaw rate, the vertical tailplane experiences an angle of attack, resulting in a positive sideforce. This positive sideforce results in a negative yaw moment. Therefore, the coefficient C_{n_r} is generally negative [Mulder, J.A. et al., 2013]. Table 7.5 shows that for smaller angle of attack, the coefficient C_{n_r} is negative, whereas the magnitude of this coefficient becomes smaller for larger angles of attack.

7.2.6. C_{y_r}

The coefficient C_{y_r} represents the sideforce generated due to a change in yaw rate. For conventional aircraft, this coefficient is positive, as a positive yaw rate results in an angle of attack experienced by the vertical tail. Consequently, this results in a sideforce pointed in the positive y-direction [Mulder, J.A. et al., 2013]. Looking at table 7.6, the coefficient C_{y_r} is positive and increasingly positive for larger angles of attack.

Table 7.5: Coefficient C_{n_r} for different angles of attack.

α [deg]	0	5	10	15
C_{n_r} [-]	-0.25959	-0.22829	-0.19525	-0.1607

Table 7.6: Coefficient C_{y_r} for different angles of attack.

α [deg]	0	5	10	15
C_{y_r} [-]	0.23438	0.27424	0.31197	0.34727

7.2.7. Dutch Roll Mode Analysis

In general it is concluded that shifting the centre of gravity forwards (increasing the angle of attack) leads to a reduced lateral-directional stability. Namely, increasing the angle of attack leads to a smaller or even negative C_{n_β}, implying no weathervane stability for larger angles of attack. Furthermore, C_{n_p} becomes increasingly negative for larger angles of attack, leading to a larger Dutch roll increasing the risk of instabilities. The main component of interest for the analysis of the Dutch roll mode is $\frac{\partial M_z}{\partial p}$. The equation for the determination of $\frac{\partial M_z}{\partial p}$ is shown in eq. (7.5).

$$\frac{\partial M_z}{\partial p} = C_{n_p}\frac{1}{2}\rho V^2 Sc - C_{y_p}\frac{1}{2}\rho V^2 S(p_{\text{ref}} - p_{\text{cg}}) \tag{7.5}$$

Looking at C_{n_p} for several angles of attack in table 7.3, it is shown that this coefficient is negative for zero angle of attack and becomes increasingly negative for larger angle of attack. A more negative C_{n_p} increases the yawing of the aircraft while rolling, increasing the movement of the Dutch roll and decreasing the stability. This means that moving the centre of gravity forward (increasing the angle of attack) results in a more negative C_{n_p}, decreasing the stability of the Dutch roll.

Besides that, there is the second component, namely C_{y_p}. This coefficient for several angles of attack is shown in table 7.4. For conventional aircraft, the vertical tailplane is the only contributor to this coefficient and this coefficient is generally negative. For the Flying-V, this coefficient is negative at zero angle of attack and becomes positive for larger angles of attack. During the cruise and approach condition, this coefficient is positive. Therefore, this coefficient makes $\frac{\partial M_z}{\partial p}$ more negative at the forward centre of gravity location (due to the larger moment arm and larger positive value of C_{y_p}), decreasing the stability even further.

Eventually this component results in the fact that moving the centre of gravity forwards leads to an eigenvalue shift to the right. In case of the cruise condition this leads to an unstable Dutch roll mode at the forward centre of gravity location, whereas the Dutch roll mode is stable at the aft centre of gravity location.

7.3. Dutch Roll Mode Improvement

To improve the behaviour of the Dutch roll mode at the forward centre of gravity location, it is necessary to find a solution that decreases the magnitude of $\frac{\partial M_z}{\partial p}$. Therefore it is necessary to look at the coefficients C_{n_p} and C_{y_p}. The behaviour of the coefficient C_{n_p} coheres with expected results. Changing this coefficient would require a redesign of the wing and is therefore not considered. Therefore, the coefficient C_{y_p} is analysed. The trend of C_{y_p} being negative for smaller angles of attack and being positive for larger angles of attack can also be found in literature [Ahmad et al., 2021, Anton et al., 2009]. To determine C_{y_p} it is possible to use eq. (7.6) [Finck, 1978, Toll and Queijo, 1948]. This equation shows that C_{y_p} consists of contributions of the main wing ($(C_{y_p})_w$) and the vertical tail surface ($(C_{y_p})_v$). In case of the Flying-V, the vertical tail surface is represented by the winglets.

$$C_{y_p} = (C_{y_p})_w + (C_{y_p})_v \tag{7.6}$$

The contribution of the main wing can be observed in eq. (7.7). This equations shows that the contribution of the wing depends on the lift coefficient (C_L), the aspect ratio (A), and the sweep angle (Λ). This equation shows that a positive C_L results in a positive contribution to C_{y_p}. Besides that,

increasing the aspect ratio increases the magnitude of C_{y_p}. Finally, increasing the wing sweep, increases the magnitude of C_{y_p}.

$$\left(C_{y_p}\right)_w = C_L \frac{A + \cos\Lambda}{A + 4\cos\Lambda} \tan\Lambda \tag{7.7}$$

The contribution of the vertical tail can be observed in eq. (7.8). In this equation, z_p represents the vertical distance of the vertical-tail centre of pressure location above or below the centre of gravity location. Besides that, z can be obtained using eq. (7.9). Each component is also shown in fig. 7.1.

$$\left(C_{y_p}\right)_v = \frac{2z - z_p}{b} \left(C_{y_\beta}\right)_v \tag{7.8}$$

$$z = z_p \cos\alpha - l_p \sin\alpha \tag{7.9}$$

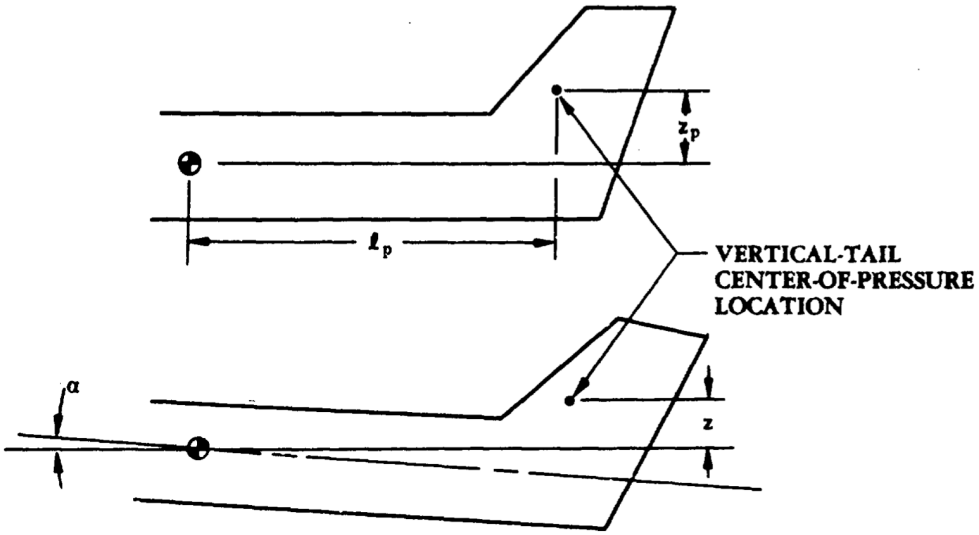

Figure 7.1: Parameter for estimation of C_{Y_p} [Finck, 1978]

To improve the Dutch roll behaviour of the Flying-V, the goal is to keep C_{y_p} negative as long as possible. This result can be obtained by decreasing the aspect ratio or the sweep angle of the Flying-V. However, the effect of changing these components is relatively small. A large effect is redesigning the winglets such that the distance z_p increases. The winglets can also be placed more forward such that l_p is reduced, and the wing span can be decreased. However, these effect of increasing the distance z_p results in the largest effect.

8

Conclusions and Recommendations

This chapter concludes the thesis by answering the research questions. Furthermore, the recommendations for future research are treated.

8.1. Answers to Research Questions

1. **What are the stability and handling qualities of the Flying-V?**

   (a) **How can the stability and handling qualities of the Flying-V be assessed?**
   A literature study has established that stability is defined as the ability to return to a steady state position in case a disturbance or pilot input is applied. Besides that, handling qualities of an aircraft are considered as a description of the adequacy of the short term dynamic response to controls during the execution of a flight task. For this assessment, it is determined to only focus on the most crucial in-flight phases of the mission profile of an aircraft: the cruise- and approach phase. During these flight phases, it is decided to focus the assessment on the trimmability of the Flying-V, the responses of the eigenmodes, and the Control Anticipation Parameter (CAP). It is possible to obtain these stability and handling quality requirements from civil certification authorities (such as EASA or FAA) or military standards. The requirements for civil aircraft are mainly concerned with safety, while specific requirements related to stability, control, and handling qualities are relatively relaxed. The requirements set by military documents are specified in much more detail. Therefore, it is decided to base the assessment on military standards, as these comprehensive and demanding requirements undoubtedly also make sure that the Flying-V meets the civil requirements.

   (b) **What are the stability and handling quality characteristics of the Flying-V?**
   The stability and handling qualities of the Flying-V are assessed during the cruise- and approach phase at the forward and aft centre of gravity location. Previous research dictates that the Flying-V is longitudinally statically stable up to an angle of attack of 20°. In case the angle of attack is further increased, pitch break occurs meaning that the slope of the pitch moment coefficient derivative with respect to the angle of attack becomes positive ($C_{m_\alpha} > 0$ for $\alpha > 20°$). Besides that, previous research concludes that the Dutch roll mode is unstable. After developing a flight dynamic simulation model, the stability and handling qualities are assessed. The Flying-V can be trimmed at each flight condition. However, during approach at the forward centre of gravity location, control surface deflections reach 20.2°, decreasing the manoeuvrability of the aircraft. Besides that, all eigenmodes are rated either Level 1 or Level 2 based on military standards. Except for the phugoid mode and Dutch roll mode during the approach phase. At this flight condition, both modes are unstable and therefore are worse than Level 3 handling qualities. Finally, to adhere to the CAP requirements, it is concluded that the Flying-V requires a faster response to pilot inputs during the approach phase at the aft centre of gravity location, whereas the short period damping ratio needs be increased during the cruise phase at the forward centre of gravity location.

2. **How can a simulation model of the Flying-V aircraft be obtained?**

   (a) **What are the specific elements of a simulation model of the Flying-V?**
   To define the dynamic equations that describe the behaviour of the Flying-V, it is necessary to obtain an aerodynamic model of the aircraft. Previous research using wind tunnel experiments (WTE) indicates that the Flying-V is longitudinally unstable for angles of attack larger than 20°. During these experiments a 1/22 small-scale half-span model of the Flying-V is used. Besides that, research using the Vortex Lattice Method (VLM) concludes that the Dutch roll mode is unstable during the approach phase. The VLM research makes use of a full-scale model of the Flying-V. To design a simulation model that captures the undesired behaviour from previous research, it is necessary to combine the aerodynamic models obtained from WTE and VLM into a single aerodynamic model. Therefore, the VLM aerodynamic model is used as the baseline model for angles of attack ranging between -5° and 15° and the WTE aerodynamic model is added for angles of attack ranging between 15° and 30° to capture the longitudinal unstable behaviour. Due to the significant difference in control surface layout between the two models, control surface deflections are kept equal to zero. Consequently, the WTE aerodynamic model is scaled up using Dynamic or Froude scaling, vertically translated to match the VLM aerodynamic model at an angle of attack of 15°, and smoothened to resolve the discontinuity in slope. This results in an aerodynamic model that captures both the unstable Dutch roll and the longitudinal unstable behaviour of the Flying-V.

   (b) **What uncertainty sources are present in the simulation model of the Flying-V?**
   During the construction of the dynamic simulation model several sources of uncertainty are present that may affect the validity of the simulation model. The main uncertainty sources are present in the aerodynamic model used for the simulation. First of all, during the construction of the combined aerodynamic model, it is assumed that only the angle of attack makes a non-linear contribution to the force and moment coefficients. In reality, it is likely that other components (such as the control surfaces) also show nonlinear behaviour at high angles of attack. Therefore, this forms a source of uncertainty of the simulation model. Secondly, Dynamic or Froude scaling is applied to scale the WTE aerodynamic model. To apply this scaling method, the relative density factor and the relative moment of inertia of the small-scale model must be the same as in the full-scale aircraft. This is not the case for the Flying-V and therefore results in inaccuracies of the combined aerodynamic model. Moreover, because the VLM model is used as the baseline model, the combined aerodynamic model of the Flying-V does not contain zero-lift drag. It is not possible to obtain an accurate estimate of the zero-lift drag from the WTE model due to scaling. Zero-lift drag is therefore added to the combined aerodynamic model using data obtained from the Airbus A350-900 (which is used as a reference aircraft for the design of the Flying-V), even though previous research dictates that the shape of a flying wing results in less zero-lift drag.

   (c) **What is the validity of the simulation model of the Flying-V?**
   To validate the simulation model of the Flying-V, the thrust conditions during cruise at several centre of gravity locations are analysed. It is determined that during cruise, the thrust setting is on average equal to 32.8% of the maximum available thrust. Literature describes that the thrust setting of an aircraft during cruise ranges between 20% and 30% of the maximum allowable thrust. Besides that, the thrust setting of the Airbus A350-900 is approximately 33.3%. This indicates that the aerodynamic model used for the simulation model results in thrust setting that is in accordance with literature. Besides that, analysing the eigenmodes for several centre of gravity locations shows that during cruise conditions, the Dutch roll mode damping ratio decreases when moving the centre of gravity forwards. This discrepancy with previous research originates from a decreased damping effect of the winglets due to a forward centre of gravity shift, leading to a decreased damping ratio of the Dutch roll mode. Finally, the aerodynamic model designed based on the WTE model and VLM model shows that for angles of attack larger than 20°, the pitch moment coefficient slope is positive. This is in coherence with wind tunnel experiments that show this longitudinally statically unstable behaviour of the Flying-V.

3. **How do the stability and handling qualities of the Flying-V aircraft change after applying a flight control system?**

   (a) **What types of flight control systems are applicable to the aircraft and can contribute to improved stability and handling qualities of the aircraft?**
   The flight control system that is applied to the Flying-V needs to adhere to several requirements. First of all, from the stability and handling quality analysis, it is determined that the Flying-V contains several stability issues. Therefore, the flight control system has to be able to make the Flying-V adhere to the key stability and handling quality requirements. Secondly, the equations of motion and aerodynamic model consist of several nonlinear components. To prevent degradation of the controller, the flight control system has to be able to cope with the inherent nonlinear behaviour of the aircraft. Finally, the simulation model designed consists of several assumptions and limitations, introducing uncertainties. Consequently, to diminish the performance degradation due to model uncertainties, the flight control system shall be able to cope with these model uncertainties. Based on these requirements it is determined to develop an Incremental Nonlinear Dynamic Inversion (INDI) flight control system for the Flying-V. This is a sensor-based control method, requiring less model information and therefore improves the system robustness against model uncertainties. Due to the uncertainties present in the aerodynamic model, the application of INDI diminishes performance degradation.

   (b) **How does the performance of the aircraft change using a flight control system?**
   To analyse the stability and handling qualities of the Flying-V after application of the flight control system, the effect of the phugoid damper and yaw damper on the eigenvalues is analysed. Due to the flight control system, both eigenmodes are stabilised. After comparing the eigenmodes with military standards, all eigenmodes are rated Level 1 handling qualities during approach at the forward centre of gravity location. Besides that, the robustness of the flight control system to aerodynamic uncertainty is assessed using the attitude tracking error of the Flying-V aiming to follow a reference trajectory. This research shows that increasing the aerodynamic uncertainty results in more and larger outliers of the attitude tracking error. These outliers originate from the deflection limits of the control surfaces. In case the effectiveness of the control surfaces is reduced due to aerodynamic uncertainty, a larger deflection is required to obtain the same attitude rate demand. However, the control surface deflection limit is equal to 25 degrees. This means that in case the control surface deflection demand is larger than 25 degrees, this control surface deflection demand cannot be achieved, resulting in a larger attitude tracking error.

4. **What kind of design changes can further improve the stability and handling qualities of the aircraft?**

   - **How can additional requirements on the flight control system design improve the stability and handling qualities?**
   During this research, the gains of the flight control system have been tuned manually. Even though the system is able to track the reference trajectory, the tracking behaviour of the Flying-V can be improved. Therefore it is recommended to define a set of requirements related to the handling qualities of the aircraft and a set of requirements related to the attitude tracking behaviour such as rise time, overshoot, and settling time. Using these requirements it is possible to design an optimisation algorithm that is able to tune the gains such that these requirements are met, improving the performance of the flight control system.
   - **How can additional requirements on the aircraft aerodynamic design and control surface layout design improve the stability and handling qualities?**
   First of all, to improve the unstable behaviour of the Dutch roll mode at the forward centre of gravity location, it is necessary to find a solution that decreases the magnitude of the moment around the z-axis due to a rolling motion of the Flying-V. There are several parameters that affect the magnitude of this moment. First of all, the aspect ratio or sweep angle of the Flying-V can be decreased. However, the effect of these components is relatively small. It is found that redesigning the winglets has the largest effect on the magnitude of the moment around the z-axis. To be more specific, it is suggested to increase the size of the winglets

such that the distance between the centre of pressure of the winglets and centre of gravity of the aircraft is increased. It is expected that this results in a decreased magnitude of the moment around the z-axis due to a rolling motion and therefore a stable Dutch roll mode. Secondly, after analysing the roll manoeuvrability of the Flying-V, it is noticed that using only the outboard elevons for roll control results in a maximum achievable roll angle of 2° without saturating the control surfaces. To achieve higher roll angles, it is suggested to use both the inboard and outboard elevons for roll control.

8.2. Contribution to research related to the Flying-V

This section puts the observations and conclusions made in this thesis into perspective of the development of the Flying-V. As mentioned earlier, the development of the Flying-V offers the opportunity to overcome the existing challenges in aviation. However, previous research and experiments also show that the Flying-V consists of its own challenges such as an unstable Dutch roll mode and pitch break tendencies for larger angles of attack. This research contributes to the development of the Flying-V by combining the results obtained from these different previous studies into one dynamic simulation model. Using this simulation model it is not only possible to assess the key stability and handling qualities defined by certification authorities, as was done in this research. The development of this simulation model also opens up the possibility to do follow-up research on additional stability and handling qualities to take the next step towards certification and qualification of the Flying-V.

Upon analysis of the stability and handling qualities of the Flying-V during the cruise phase and approach phase at the forward and aft centre of gravity location. It is found that the Flying-V is not always able to satisfy the stability and handling quality requirements. This research shows that the stability and handling qualities can be improved by designing an Incremental Nonlinear Dynamic Inversion flight control system. Additionally, this flight control system is applied to the Flying-V aiming to execute a tracking task under the influence of aerodynamic uncertainty. It is concluded that aerodynamic uncertainty has a negligible effect on the tracking error. Namely, the tracking error is mainly affected by the control surface deflection limits. Therefore, this research also contributes to the development of the Flying-V by showing that not only iteration on the aerodynamic design but also the application of a flight control system is able to improve the stability and handling qualities of the aircraft. Because this type of flight control system is negligibly affected by aerodynamic uncertainty, it is possible to start developing a flight control system early in the design phase.

8.3. Recommendations

With the goal to further improve research related to the Flying-V aircraft, this section discusses the recommendations for future research. First of all, section 8.3.1 discusses the recommendations related to research involving the stability and handling quality assessment. Secondly, section 8.3.2 elaborates on recommendations related to research involving the Incremental Nonlinear Dynamic Inversion flight control system.

8.3.1. Recommendations for stability and handling quality analysis

With the goal to further improve research on modelling and handling quality assessment of the Flying-V aircraft, future work may include the set of items discussed in this section.

During this research, only the key stability and handling quality requirements for certification and qualification purposes are considered. It is therefore suggested to perform further research on additional requirements necessary for certification and qualification of the Flying-V.

Besides that, even though the aerodynamic model designed in this research is able to capture the undesired behaviour of the Flying-V obtained from previous research, several assumptions are made during the construction of the aerodynamic model. To increase the fidelity of the combined aerodynamic model, it is suggested to perform additional research on aerodynamic model identification of the Flying-V.

8.3.2. Recommendations for Incremental Nonlinear Dynamic Inversion control system design

With the goal to further improve research on the stability and handling qualities of the Flying-V using an Incremental Nonlinear Dynamic Inversion controller, future work may include the set of items discussed in this section.

During this research, the magnitude of the aerodynamic uncertainty applied to the Flying-V is based on previous research requiring several assumptions to find the maximum aerodynamic uncertainty. It is therefore suggested to perform additional research on the magnitude of the aerodynamic uncertainty to increase the fidelity of the robustness analysis.

Secondly, this research does not analyse the effect of the flight control system on the Control Anticipation Parameter. To perform this analysis, it is necessary to find a lower order equivalent system that translates the pilot input to the pitch rate. For future research, it is therefore suggested to analyse the Control Anticipation Parameter of the controlled Flying-V using a lower order equivalent system.

Besides that, this research only considers aerodynamic uncertainty for the robustness analysis. Therefore, it is suggested to perform additional research on other factors that may affect the stability of the INDI controller such as measurement time delay, sampling frequency, inertia uncertainty, and centre of gravity mismatch.

Furthermore, during this research the outboard elevons and the rudders are used for roll angle control of the Flying-V. Due to the low roll angle that can be achieved without saturating the control surfaces, it is suggested to also incorporate the inboard elevons for roll control in future research.

Finally, this research does not take into account sensor dynamics, nor does it take into account atmospheric effects such as turbulence. To increase the fidelity of the controller analysis, it is suggested to apply these components to the simulation model.

Bibliography

Acquatella, P. et al. Robust Nonlinear Spacecraft Attitude Control using Incremental Nonlinear Dynamic Inversion. In *AIAA Guidance, Navigation, and Control Conference*, page 4623, 2012.

Adams, R.J. et al. Robust Flight Control Design using Dynamic Inversion and Structured Singular Value Synthesis. *IEEE Transactions on control systems technology*, 1(2):80–92, 1993.

Muhammad Ahmad, Zukhruf Liaqat Hussain, Syed Irtiza Ali Shah, and Taimur Ali Shams. Estimation of stability parameters for wide body aircraft using computational techniques. *Applied Sciences*, 11 (5):2087, 2021.

Ammar, S. et al. Conceptual Design, Performance and Stability Analysis of a 200 Passengers Blended Wing Body Aircraft. *Aerospace Science and Technology*, 71:325–336, 2017.

Ananda, G.K. et al. Design Methodology for a Dynamically-Scaled General Aviation Aircraft. In *35th AIAA Applied Aerodynamics Conference*, page 4077, 2017.

Anonymous. Military Specifications, Flying Qualities of Piloted Aircraft MIL-F-8785C, 1980.

Nicoleta Anton, Ruxandra Botez, and Dumitru Popescu. New methodologies for aircraft stability derivatives determination from its geometrical data. In *AIAA atmospheric flight mechanics conference*, page 6046, 2009.

Baarspul, M. A Review of Flight Simulation Techniques. *Progress in Aerospace Sciences*, 27(1):1–120, 1990.

Bacon, B.J. et al. Reconfigurable NDI Controller Using Inertial Sensor Failure Detection & Isolation. *IEEE Transactions on Aerospace and Electronic Systems*, 37(4):1373–1383, 2001.

Balas, G.J. Flight Control Law Design: An Industry Perspective. *European Journal of Control*, 9(2-3): 207–226, 2003.

Benad, J. The Flying V, A New Aircraft Configuration for Commercial Passenger Transport. *Deutscher Luft- und Raumfahrtkongress*, 2015.

Bourget, G. The Effect of LandingGear Implementation on Flying V Aerodynamics, Stability and Controllability, 2020.

Brockett, R.W. Feedback Invariants for Nonlinear Systems. *IFAC Proceedings Volumes*, 11(1):1115–1120, 1978.

Bunge, R. et al. Minimal Altitude Loss Pullout Maneuvers. In *2018 AIAA Guidance, Navigation, and Control Conference*, page 1339.

Cappuyns, T. Handling Qualities of a Flying V Configuration, 2019.

Chauhan, R.K. et al. Review of Aerodynamic Parameter Estimation Techniques. In *2017 International Conference on Infocom Technologies and Unmanned Systems (Trends and Future Directions)(ICTUS)*, pages 864–869. IEEE, 2017.

Chu, Q.P. et al. *Spacecraft Attitude Dynamics and Control: AE4313 Course Notes*. TU Delft, 2019-2020.

Cook, M.V. *Flight Dynamics Principles: A Linear Systems Approach to Aircraft Stability and Control*. Butterworth-Heinemann, 2012.

CS-25. Easy Access Rules for Large Aeroplanes (CS-25), 2018. Accessed: 23-02-2021.

De Castro, H. V. *Flying and Handling Qualities of a Fly-By-Wire Blended-Wing-Body Civil Transport Aircraft*. PhD thesis, Cranfield University, 2003.

Dean, J. et al. Aircraft Stability and Control Characteristics Determined by System Identification of CFD Simulations. In *AIAA Atmospheric Flight Mechanics Conference and Exhibit*, page 6378, 2008.

Faggiano, F. et al. Aerodynamic Design of a Flying V Aircraft. *17th AIAA Aviation Technology, Integration, and Operations Conference*, 2017.

RD Finck. Usaf (united states air force) stability and control datcom (data compendium). Technical report, MCDONNELL AIRCRAFT CO ST LOUIS MO, 1978.

Flying-V Website. Successful maiden flight for the TU Delft Flying-V. https://www.tudelft.nl/en/2020/tu-delft/successful-maiden-flight-for-the-tu-delft-flying-v, 2020. Accessed: 16-12-2020.

Garcia, A.R. Aerodynamic Model Identification of the Flying V using Wind Tunnel Data, 2019.

Garcia, A.R. Personal Communication. 2021.

Gibson, J.C. Development of a Design Methodology for Handling Qualities Excellence in Fly by Wire Aircraft. 1999.

Grotens, R. Nonlinear Flight Control Fault Tolerant Control with Sliding Modes and Control Allocation, 2010.

Yasim J Hasan, Jana Schwithal, Till Pfeiffer, Carsten M Liersch, and Gertjan Looye. *Handling Qualities Assessment of a Blended Wing Body Configuration under Uncertainty Considerations*. Deutsche Gesellschaft für Luft-und Raumfahrt-Lilienthal-Oberth eV, 2018.

Hodel, A. et al. Stability Metrics for Simulation and Flight-software Assessment and Monitoring of Adaptive Control Assist Compensators. pages 1–25, 2008.

Humphreys-Jennings, C. et al. Conceptual Design, Flying, and Handling Qualities Assessment of a Blended Wing Body (BWB) Aircraft by Using an Engineering Flight Simulator. *Aerospace*, 7(5):51, 2020.

Hurt, H. H. *Aerodynamics for Naval Aviators*. Office of the Chief of Naval Operations, Aviation Training Division, 1965.

Jansen, Q.J.M. Relaxed Static Stability Performance Assessment on Conventional and Unconventional Aircraft Configurations, 2015.

Johnson, N.A. Effect of Winglet Integration and Rudder Deflection on Flying-V Aerodynamic Characteristics, 2021.

Karssies H.J. XINCA on the TU Delft Quadplane, 2020.

Krener, A.J. Feedback Linearization. In *Mathematical control theory*, pages 66–98. Springer, 1999.

Kumtepe. Y. Flight Control Design Using Hybrid Incremental Nonlinear Dynamic Inversion, 2020.

Lambert, T. et al. Vortex Lattice Simulations of Attached and Separated Flows around Flapping Wings. *Aerospace*, 4(2):22, 2017.

Robert H Liebeck. Design of the blended wing body subsonic transport. *Journal of aircraft*, 41(1): 10–25, 2004. doi: 10.2514/1.9084.

R. Martinez-Val, E. Perez, J. Puertas, and J. Roa. Optimization of Planform and Cruise Conditions of a Transport Flying Wing. *Proceedings of the Institution of Mechanical Engineers, Part G: Journal of Aerospace Engineering*, 224(12):1243–1251, 2010. doi: 10.1243/09544100JAERO812.

Martinez-Val, R. Flying Wings: A New Paradigm for Civil Aviation? *Acta Polytechnica Vol. 47 No. 1/2007*, 2007.

Miller, C. Nonlinear Dynamic Inversion Baseline Control Law: Flight-Test Results for the Full-Scale Advanced Systems Testbed F/A-18 Airplane. In *AIAA Guidance, Navigation, and Control Conference*, page 6468, 2011.

Morelli, E.A. Flight-test Experiment Design for Characterizing Stability and Control of Hypersonic Vehicles. *Journal of Guidance, Control, and Dynamics*, 32(3):949–959, 2009.

Morelli, E.A. and Klein, V. Application of System Identification to Aircraft at NASA Langley Research Center. *Journal of Aircraft*, 42(1):12–25, 2005.

Mulder, J.A. et al. *Flight Dynamics*. TU Delft, 2013.

Murphy, P. et al. Validation of Methodology for Estimating Aircraft Unsteady Aerodynamic Parameters from Dynamic Wind Tunnel Tests. In *AIAA Atmospheric Flight Mechanics Conference and Exhibit*, page 5397, 2003.

Nicolosi, F. et al. A Comprehensive Review of Vertical Tail Design. *Aircraft Engineering and Aerospace Technology*, 2017.

P. Okonkwo and H. Smith. Review of evolving trends in blended wing body aircraft design. *Progress in Aerospace Sciences*, 82:1–23, 2016. doi: 10.1016/j.paerosci.2015.12.002.

Padfield, G.D. *Helicopter Flight Dynamics*. Wiley Online Library, 2008.

Palermo, M. The Longitudinal Static Stability and Control Characteristics of a Flying V Scaled Model, 2019.

Palermo, M. et al. Experimental Aerodynamic Analysis of a 4.6%-Scale Flying-V Subsonic Transport. In *AIAA Scitech 2020 Forum*, page 2228, 2020.

Perez, R.E. et al. Multidisciplinary Optimization Framework for Control-Configuration Integration in Aircraft Conceptual Design. *Journal of Aircraft*, 43(6):1937–1948, 2006.

Reiner, J. et al. Flight Control Design using Robust Dynamic Inversion and Time-scale Separation. *Automatica*, 32(11):1493–1504, 1996.

Roskam, J. *Determination of Stability, Control and Performance Characteristics: FAR and Military Requirements*. DARcorporation, 1986.

Roskam, J. *Airplane Flight Dynamics and Automatic Flight Controls*. DARcorporation, 1995.

Rubio Pascual, B. Engine-Airframe Integration for the Flying-V, 2018.

Schumacher, C. et al. Stability Analysis of a Missile Control System with a Dynamic Inversion Controller. *Journal of Guidance, Control, and Dynamics*, 21(3):508–515, 1998.

Sieberling, S et al. Robust Flight Control using Incremental Nonlinear Dynamic Inversion and Angular Acceleration Prediction. *Journal of Guidance, Control, and Dynamics*, 33(6):1732–1742, 2010.

Simplício, P.V.M. Helicopter Nonlinear Flight Control: An Acceleration Measurements-based Approach using Incremental Nonlinear Dynamic Inversion, 2011.

Slotine, J.E. et al. *Applied Nonlinear Control*, volume 199. Prentice hall Englewood Cliffs, NJ, 1991.

Smith, P. A Simplified Approach to Nonlinear Dynamic Inversion Based Flight Control. In *23rd Atmospheric Flight Mechanics Conference*, page 4461, 1998.

Spillman, M. et al. A Robust Gain-Scheduling Example Using Linear Parametervarying Feedback. *IFAC Proceedings Volumes*, 29(1):3615–3620, 1996.

Sun, J. et al. Aircraft Drag Polar Estimation Based on a Stochastic Hierarchical Model. In *8th International Conference on Research in Air Transportation*, 2018.

Tang, S.H. Fault-Tolerant Flight Control with Sensor-Based Nonlinear Dynamic Inversion: Application and Evaluation in the SIMONA Research Simulator, 2014.

Thomas A Toll and Manuel J Queijo. Approximate relations and charts for low-speed stability derivatives of swept wings. 1948.

Uitert, J.J.D. Experimental Investigation into the Effect of Aerodynamic Add-ons on the Aerodynamic Characteristics of the Flying V, 2021.

Van Empelen, S.A. Engine Integration of the Flying V: Quantification of Engine Integration Effects using Wind Tunnel Experiments, 2020.

Van 't Veld, R.C. Incremental Nonlinear Dynamic Inversion Flight Control: Stability and Robustness Analysis and Improvements, 2016.

Viet, R. Analysis of the Flight Characteristics of a Highly Swept Cranked Flying Wing by Means of an Experimental Test, 2019.

Wahler, N.F.M. The Impact of Control Allocation on Optimal Control Surface Positioning and Sizing, 2021.

Wang, X. et al. Stability Analysis for Incremental Nonlinear Dynamic Inversion Control. *Journal of Guidance, Control, and Dynamics*, 42(5):1116–1129, 2019.

CHEN Zhenli, Minghui Zhang, CHEN Yingchun, SANG Weimin, TAN Zhaoguang, LI Dong, and Binqian Zhang. Assessment on critical technologies for conceptual design of blended-wing-body civil aircraft. *Chinese Journal of Aeronautics*, 32(8):1797–1827, 2019. doi: 10.1016/j.cja.2019.06.006.

A

Appendix A

A.1. Short Period Mode Handling Qualities Requirements

Table A.1: Short period mode damping [Cook, M.V., 2012]

	Level 1		Level 2		Level 3
Flight phase	ς_s min	ς_s max	ς_s min	ς_s max	ς_s min
CAT A	0.35	1.30	0.25	2.00	0.10
CAT B	0.30	2.00	0.20	2.00	0.10
CAT C	0.50	1.30	0.35	2.00	0.25

A.2. Phugoid Mode Handling Qualities Requirements

Table A.2: Phugoid damping ratio. [Cook, M.V., 2012]

Level of flying qualities	Minimum ς_p
1	0.04
2	0
3	Unstable, period $T_p > 55s$

A.3. Roll Mode Handling Qualities Requirements

Table A.3: Roll mode time constant [Cook, M.V., 2012]

		Maximum value of T_r (seconds)		
Aircraft class	*Flight phase category*	*Level 1*	*Level 2*	*Level 3*
I, IV	A, C	1.0	1.4	10.0
II, III	A, C	1.4	3.0	10.0
I, II, III, IV	B	1.4	3.0	10.0

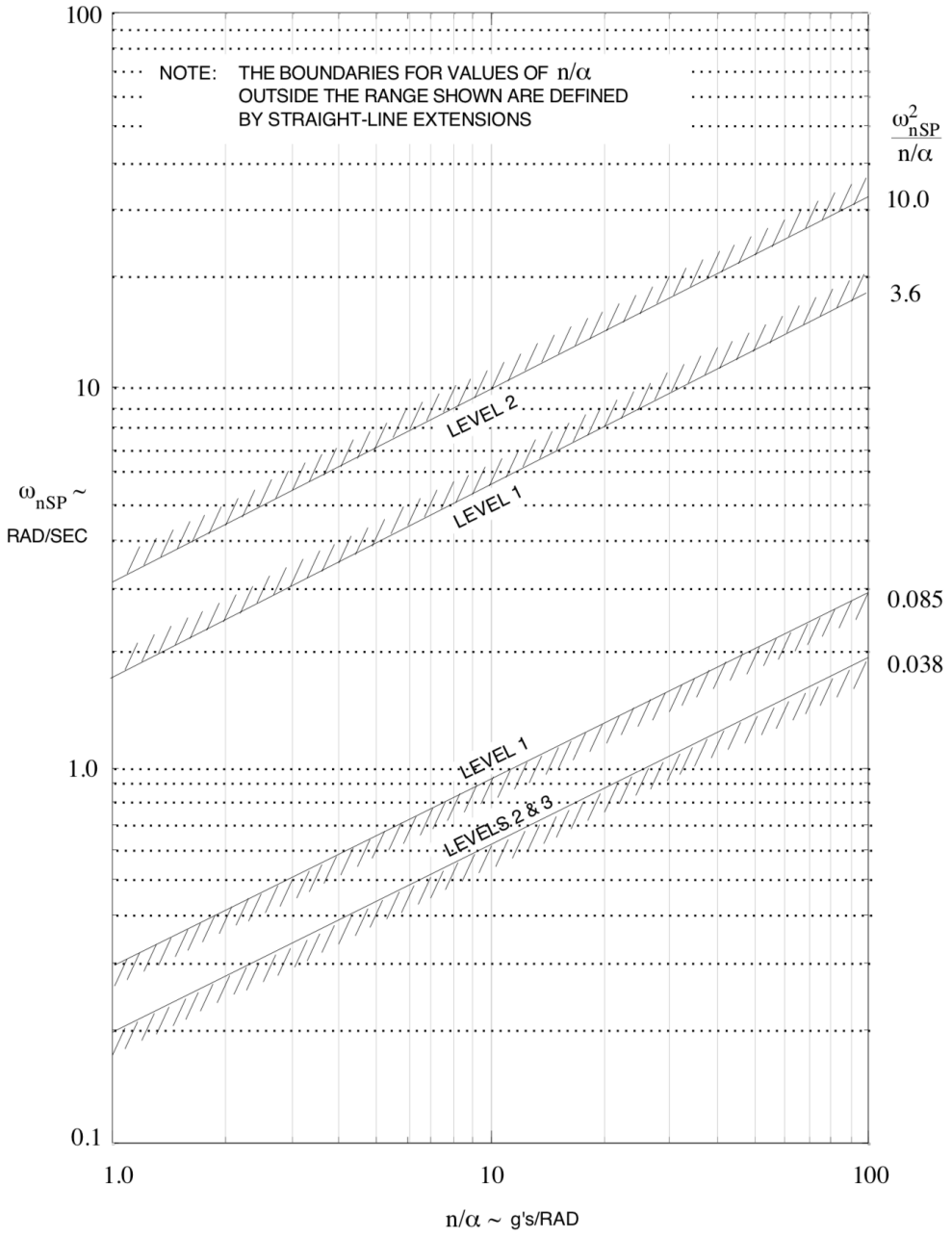

Figure A.1: MIL-F-8785C for Flight Phase B

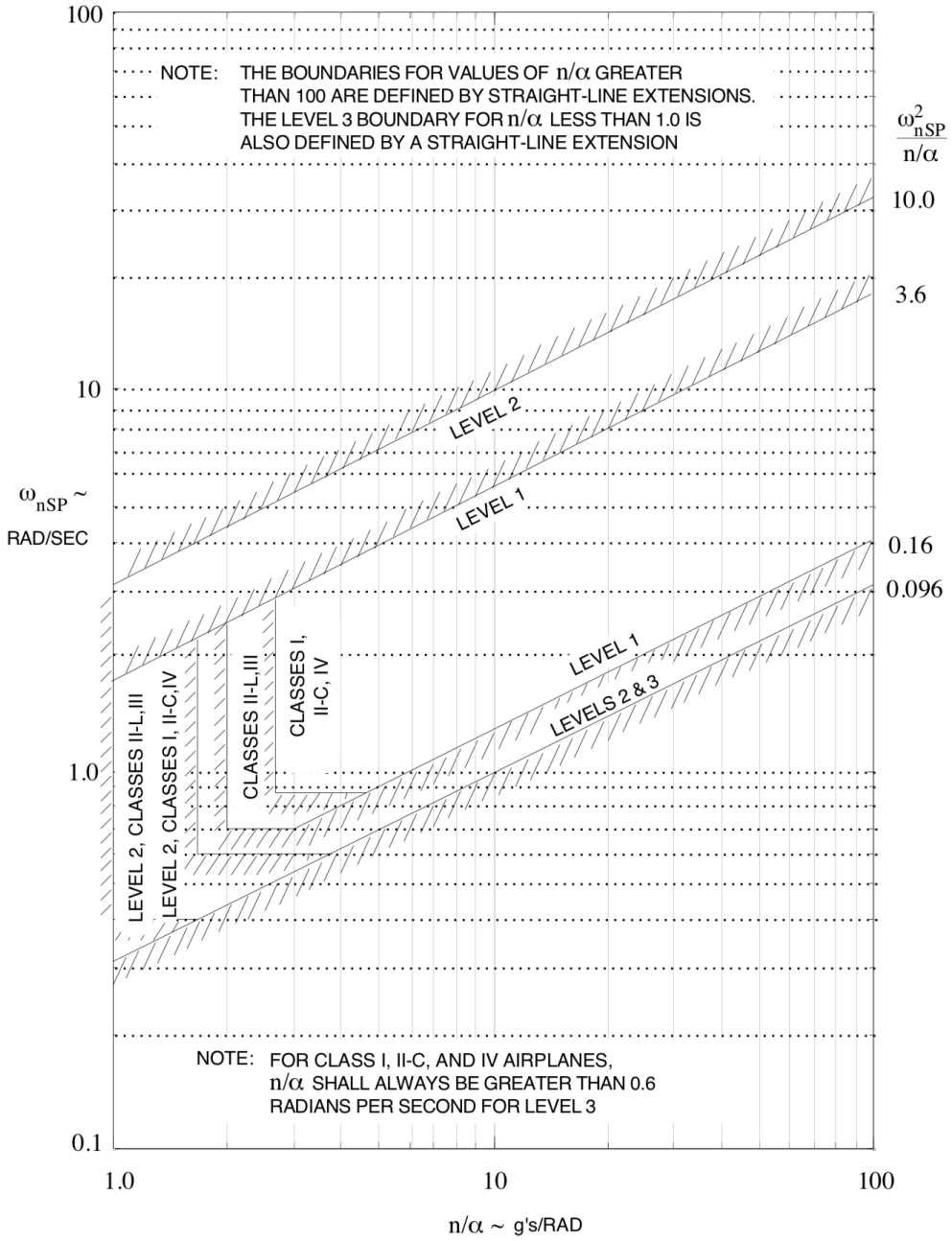

Figure A.2: MIL-F-8785C for Flight Phase C

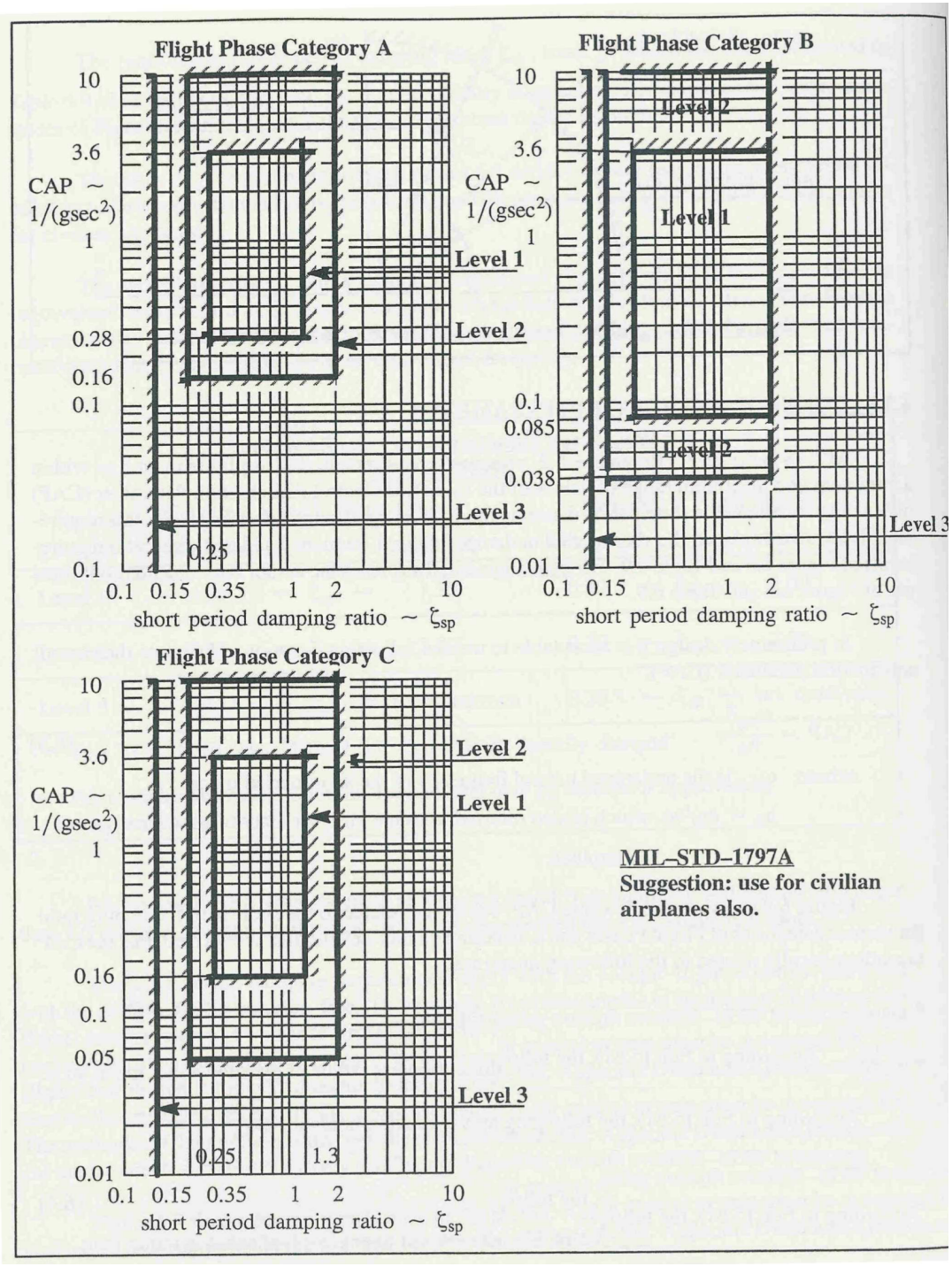

Figure A.3: Control Anticipation Parameter and short period damping ratio requirements. [Roskam, J., 1995]

A.4. Spiral Mode Handling Qualities Requirements

Table A.4: Spiral mode time constant [Anonymous, 1980, Cook, M.V., 2012]

	Maximum value of T_2 (seconds)		
Flight phase category	*Level 1*	*Level 2*	*Level 3*
A, C	12	8	5
B	20	8	5

A.5. Dutch Roll Mode Handling Qualities Requirements

Table A.5: Dutch roll frequency and damping [Cook, M.V., 2012]

		Minimum values							
		Level 1			*Level 2*			*Level 3*	
Aircraft class	*Flight phase*	ς_d	$\varsigma_d\omega_d$	ω_d	ς_d	$\varsigma_d\omega_d$	ω_d	ς_d	ω_d
I, IV	CAT A	0.19	0.35	1.0	0.02	0.05	0.5	0	0.4
II, III	CAT A	0.19	0.35	0.5	0.02	0.05	0.5	0	0.4
All	CAT B	0.08	0.15	0.5	0.02	0.05	0.5	0	0.4
I, IV	CAT C	0.08	0.15	1.0	0.02	0.05	0.5	0	0.4
II, III	CAT C	0.08	0.10	0.5	0.02	0.05	0.5	0	0.4

B

Appendix B

B.1. Longitudinal Static Coefficients based on System Identification

Table 5.3: Coefficients of the polynomial model for C_X

Parameter	Value ± confidence bounds
C_{X0}	$-2.029 \cdot 10^{-2} \pm (8.556 \cdot 10^{-4})$
$C_{X\alpha}$	$4.288 \cdot 10^{-2} \pm (2.662 \cdot 10^{-3})$
$C_{X\alpha^2}$	$9.792 \cdot 10^{-1} \pm (2.227 \cdot 10^{-3})$
$C_{X\alpha^3}$	$-1.617 \cdot 10^{-2} \pm (7.731 \cdot 10^{-2})$
$C_{X\alpha^4}$	$-1.519 \pm (1.639 \cdot 10^{-1})$
$C_{X\delta_1}$	$1.060 \cdot 10^{-2} \pm (6.473 \cdot 10^{-4})$
$C_{X\delta_2}$	$7.162 \cdot 10^{-3} \pm (1.193 \cdot 10^{-3})$
$C_{X\delta_3}$	$6.893 \cdot 10^{-4} \pm (1.294 \cdot 10^{-4})$
$C_{X\delta_1^2}$	$-3.928 \cdot 10^{-2} \pm (2.945 \cdot 10^{-3})$
$C_{X\delta_2^2}$	$-2.047 \cdot 10^{-2} \pm (4.027 \cdot 10^{-3})$
$C_{X\hat{V}}$	$8.727 \cdot 10^{-3} \pm (3.708 \cdot 10^{-4})$
$C_{X\hat{V}^2}$	$-3.075 \cdot 10^{-3} \pm (3.318 \cdot 10^{-4})$

Figure B.1: Table for C_X taken from [Garcia, A.R., 2019]

B.2. Lateral-Directional Static Coefficients based on System Identification

Table 5.6: Coefficients of the polynomial model for C_m

Parameter	Value ± confidence bounds
C_{m0}	$3.361 \cdot 10^{-2} \pm (2.788 \cdot 10^{-3})$
$C_{m\alpha}$	$-1.069 \cdot 10^{-1} \pm (5.938 \cdot 10^{-3})$
$C_{m\alpha^2}$	$-2.883 \cdot 10^{-1} \pm (6.506 \cdot 10^{-3})$
$C_{m\alpha^3}$	$-8.492 \cdot 10^{-1} \pm (1.839 \cdot 10^{-1})$
$C_{m\alpha^4}$	$4.088 \pm (3.731 \cdot 10^{-1})$
$C_{m\delta_1}$	$-1.482 \cdot 10^{-1} \pm (2.139 \cdot 10^{-3})$
$C_{m\delta_2}$	$-1.092 \cdot 10^{-1} \pm (1.433 \cdot 10^{-3})$
$C_{m\delta_3}$	$-6.377 \cdot 10^{-2} \pm (3.673 \cdot 10^{-3})$
$C_{m\delta_1^2}$	$1.039 \cdot 10^{-1} \pm (1.608 \cdot 10^{-2})$
$C_{m\delta_2^2}$	$3.400 \cdot 10^{-2} \pm (1.127 \cdot 10^{-2})$
$C_{m\delta_1\delta_2}$	$6.120 \cdot 10^{-2} \pm (1.248 \cdot 10^{-2})$
$C_{m\alpha\delta_1^2}$	$-5.459 \cdot 10^{-1} \pm (5.529 \cdot 10^{-2})$
$C_{m\alpha\delta_2^2}$	$-2.125 \cdot 10^{-1} \pm (4.211 \cdot 10^{-2})$
$C_{m\alpha^2\delta_1}$	$1.729 \cdot 10^{-1} \pm (4.450 \cdot 10^{-2})$
$C_{m\alpha^2\delta_2}$	$1.775 \cdot 10^{-1} \pm (3.443 \cdot 10^{-2})$
$C_{m\hat{V}}$	$8.071 \cdot 10^{-3} \pm (3.664 \cdot 10^{-3})$
$C_{m\hat{V}\delta_1}$	$2.203 \cdot 10^{-3} \pm (4.492 \cdot 10^{-4})$

Figure B.2: Table for C_m taken from [Garcia, A.R., 2019]

Table 5.4: Coefficients of the polynomial model for C_Z

Parameter	Value ± confidence bounds
C_{Z0}	$-7.583 \cdot 10^{-2} \pm (5.310 \cdot 10^{-3})$
$C_{Z\alpha}$	$-1.943 \pm (1.564 \cdot 10^{-2})$
$C_{Z\alpha^2}$	$-1.026 \pm (1.288 \cdot 10^{-1})$
$C_{Z\alpha^3}$	$1.866 \pm (2.343 \cdot 10^{-1})$
$C_{Z\delta_1}$	$-1.353 \cdot 10^{-1} \pm (5.239 \cdot 10^{-3})$
$C_{Z\delta_2}$	$-8.462 \cdot 10^{-2} \pm (6.915 \cdot 10^{-3})$
$C_{Z\delta_3}$	$-5.012 \cdot 10^{-3} \pm (7.192 \cdot 10^{-4})$
$C_{Z\hat{V}}$	$3.747 \cdot 10^{-2} \pm (7.564 \cdot 10^{-3})$

Figure B.3: Table for C_Z taken from [Garcia, A.R., 2019]

Table 5.5: Coefficients of the polynomial model for C_l

Parameter	Value ± confidence bounds
C_{l0}	$3.584 \cdot 10^{-3} \pm (4.866 \cdot 10^{-4})$
$C_{l\alpha}$	$1.842 \cdot 10^{-1} \pm (1.895 \cdot 10^{-3})$
$C_{l\alpha^2}$	$-1.543 \cdot 10^{-2} \pm (4.737 \cdot 10^{-4})$
$C_{l\alpha^3}$	$3.215 \cdot 10^{-1} \pm (4.315 \cdot 10^{-2})$
$C_{l\alpha^4}$	$-8.141 \cdot 10^{-1} \pm (8.337 \cdot 10^{-2})$
$C_{l\delta_1}$	$1.842 \cdot 10^{-2} \pm (2.649 \cdot 10^{-4})$
$C_{l\delta_2}$	$1.450 \cdot 10^{-2} \pm (3.125 \cdot 10^{-4})$
$C_{l\delta_3}$	$9.893 \cdot 10^{-3} \pm (5.844 \cdot 10^{-4})$
$C_{l\hat{V}}$	$-3.036 \cdot 10^{-3} \pm (5.311 \cdot 10^{-4})$

Figure B.4: Table for C_l taken from [Garcia, A.R., 2019]

Table 5.7: Coefficients of the polynomial model for C_n

Parameter	Value ± confidence bounds
C_{n0}	$2.636 \cdot 10^{-3} \pm (2.609 \cdot 10^{-4})$
$C_{n\alpha}$	$5.085 \cdot 10^{-5} \pm (4.599 \cdot 10^{-4})$
$C_{n\alpha^2}$	$9.565 \cdot 10^{-3} \pm (5.479 \cdot 10^{-4})$
$C_{n\alpha^3}$	$-2.732 \cdot 10^{-1} \pm (1.304 \cdot 10^{-2})$
$C_{n\alpha^4}$	$2.324 \cdot 10^{-1} \pm (2.823 \cdot 10^{-2})$
$C_{n\delta_1}$	$-1.097 \cdot 10^{-3} \pm (1.224 \cdot 10^{-4})$
$C_{n\delta_2}$	$-1.311 \cdot 10^{-3} \pm (2.030 \cdot 10^{-4})$
$C_{n\delta_1^2}$	$-6.060 \cdot 10^{-3} \pm (8.422 \cdot 10^{-4})$
$C_{n\delta_2^2}$	$-5.544 \cdot 10^{-3} \pm (6.520 \cdot 10^{-4})$
$C_{n\hat{V}}$	$-1.075 \cdot 10^{-3} \pm (2.293 \cdot 10^{-4})$

Figure B.5: Table for C_n taken from [Garcia, A.R., 2019]

C

Appendix C

In this appendix the longitudinal and lateral-directional coefficients for the preliminary analysis are displayed. Table C.1 shows the longitudinal coefficients, whereas the lateral-directional coefficients are shown in table C.2.

Table C.1: Longitudinal aerodynamic coefficients for the Cessna Ce500 'Citation'

$V = 59.9$ m/s	$m = 4547.8$ kg	$\overline{c} = 2.022$m
$S = 24.2$ m^2	$l_h = 5.5$ m	$\mu_c = 102.7$
$K_Y^2 = 0.980$	$x_{\text{cg}} = 0.30\overline{c}$	
$C_{X_0} = 0$	$C_{Z_0} = -1.1360$	
$C_{X_u} = -0.2199$	$C_{Z_u} = -2.2720$	$C_{m_u} = 0$
$C_{X_\alpha} = 0.4653$	$C_{Z_\alpha} = -5.1600$	$C_{m_\alpha} = -0.4300$
$C_{X_{\dot{\alpha}}} = 0$	$C_{Z_{\dot{\alpha}}} = -1.4300$	$C_{m_{\dot{\alpha}}} = -3.7000$
$C_{X_q} = 0$	$C_{Z_q} = -3.8600$	$C_{m_q} = -7.0400$
$C_{X_\delta} = 0$	$C_{Z_\delta} = -0.6238$	$C_{m_\delta} = -1.5530$

Table C.2: Lateral-directional aerodynamic coefficients for the Cessna Ce500 'Citation'

$b = 13.36$ m	$\mu_b = 15.5$	$K_Z^2 = 0.37$
$C_L = 1.1360$	$K_X^2 = 0.012$	$K_{XY} = 0.002$
$C_{Y_\beta} = -0.9896$	$C_{l_\beta} = -0.0772$	$C_{n_\beta} = 0.1638$
$C_{Y_p} = -0.0870$	$C_{l_p} = -0.3444$	$C_{n_p} = -0.0108$
$C_{Y_r} = 0.4300$	$C_{l_r} = 0.2800$	$C_{n_r} = -0.1930$
$C_{Y_{\delta_a}} = 0$	$C_{l_{\delta_a}} = -0.2349$	$C_{n_{\delta_a}} = 0.0286$
$C_{Y_{\delta_r}} = 0.3037$	$C_{l_{\delta_r}} = 0.0286$	$C_{n_{\delta_r}} = -0.1261$